WITS UNIVERSITY

The synthesis of carbon dots for possible use as a carbon monoxide sensor in polymer electrolyte membrane fuel cells

Master of Science in the field of chemistry (by dissertation)

Prepared by

NIKIWE KHOZA

Student number: 719086

Supervisors:

Prof. Neil. J. Coville and Dr. Manoko. S. Maubane-Nkadimeng

Submitted to

School of Chemistry, University of the Witwatersrand, Johannesburg, South Africa

Declaration

I declare that this Master of Science dissertation is my own, unaided work. It is being submitted for the Degree of Master of Science at the University of the Witwatersrand, Johannesburg. It has not been submitted before for any degree or examination at any other University.

_____

(Signature of candidate)

19th day of March 2021 at Braamfotein

Abstract

Carbon monoxide (CO) poisoning is one of the main factors retarding the advancement of the commercialisation of polymer electrolyte membrane (PEM) fuel cells because it drastically decreases the efficiency of the fuel cell through the poisoning of Pt. To date, carbon dots (CDs) have not been explored for sensing CO for this application. CDs are carbon nanomaterials of less than 10 nm diameter and with unique photoluminescence properties. Herein, we investigate the synthesis of CDs for possible use as CO sensors in PEM fuel cells. To develop a synthesis method, three reagents were investigated as carbon precursors for the CDs synthesis namely, sucrose, chitosan and polyethylene glycol (PEG). Furthermore, use of three different heat sources was investigated for the hydrothermal synthesis of CDs namely, the autoclave, the microwave and the reflux methods. PEG was found to be the best precursor for CDs synthesis and the autoclave method was favoured because it is a more facile and reliable synthesis method. Hence, the synthesis of CDs was investigated further through the synthesis of CDs made from PEG using the autoclave method while varying other reaction parameters.

The variation of the PEG (1) precursor concentration, (2) precursor molecular mass and (3) the reaction time were all found to have no significant effect on the chemical nature and size of CDs. It was found that long reaction times, beyond 4 hours, produced carbon nanospheres (CNSs) as by-products. The production of CNSs as by-products was found to prevail when water was used as a solvent. The variation of the solvent used was found to have a huge impact on the particle size and chemical nature of the resulting CDs, the size, quantum yield (%QY) and whether the CDs made were short- or long-wavelength CDs. Solvents with higher boiling points produced smaller CDs. Solvents with high relative polarity were found to yield CDs with a high %QY. Short-wavelength emitting CDs were favoured using solvents with non-hydrogen bonding properties, low boiling point, low relative polarity and low molecular weight. In general, the %QY was found to correlate with the particle size of the synthesised CDs with exceptions where aggregation induced emission was at play. The most photoluminescent synthesised CDs had a %QY of 15% (2.04 nm sized CDs) and 18% (1.83 nm sized CDs) from reaction time studies (3 hours) and a molecular mass study (PEG_{6000}), respectively.

Preliminary tests on CDs were conducted as proof of concept, where CDs were successfully incorporated into a filter paper to produce a highly photoluminescent paper-based sensing device. Changes in photoluminescence (PL) were monitored on the paper using a UV-lamp.

Exposure to Pt switched off the PL of the CDs/paper-based sensor and no PL change was observed upon CO exposure to pure CDs. In conclusion, the preliminary results indicate a proof of concept approach to produce a sensing device using CDs that can be tailored for CO detection, that requires further study.

Dedication

To my mother, Nwamalachi Grace Khoza, "Mama, we made it!"

Acknowledgment

I would like to extend my most sincere appreciation to my supervisor, Prof Neil Coville. Thank you for granting me the opportunity to complete my MSc under your supervision, its truly a pleasure. Moreover, thank you for your unwavering support, supervision, and motivation. This journey has been long and filled with ups and downs, yet you have remained constant and had faith in me throughout, for that, I am truly thankful.

I would also like to thank Dr Manoko Maubane-Nkadimeng, AKA Dr Manox for going the extra mile with supervising my MSc -going through presentation slides and speech around midnight to ensure that everything is in order is one of the highlights of her dedication.

This work would not be possible without the financial support received from the DSI/NRF Centre of Excellence in Strong Materials. Thus, I would like to thank them and hope that they keep funding other aspiring postgraduate candidates.

I would also like to thank the Microscopy and Microanalysis Unit (MMU) at Wits University, specifically Dr Manox, Dr Zikhona, Dr Ella for the training they gave me as well as their sheer kindness and cooperation when I visited them for TEM grids and the likes. I would also like to thank Dr Osuntokun (from North-West University) and CSIR (specifically Ms Rikhotso) for their assistance with characterising the synthesized materials.

I would also like to thank the CATMAT group for being my family and support structure during my journey. I am thankful for the socialising that we did be it at birthday parties, funerals, braais, conferences, Christmas parties and PIG hangouts – we surely had lots of fun! I would also like to thank the CATMAT group for grilling me at presentations, your questions and comments did not only prepare for bigger audiences at conferences/symposiums but also assisted me in surfacing valuable insights from this project.

I would also like to thank Masego Molefe, my MSc journey would have not been the same without you going through it with me. I would like to thank Sheila for being my designated Grammarly. A special thanks to Dr Osuntokun, Victor Mashindi, Puledi Mphago, Ashla Mothiba, Crystaline Dliwayo, Comfort Mbazima, Sibusiso Makonjwa and Grace Khoza for being an amazing support structure at various points in my MSc journey. Finally, I would like to thank everyone (named above or not) who had an impact on my MSc journey. Thank you for playing a role in one of my greatest achievements yet.

Presentations

1. "*One-step synthesis of photoluminescent carbon dots from chitosan*" **Poster presentation** at the 16th Frontiers of Electron Microscopy in Materials Science International Conference; Indaba Hotel and Conference Centre, Fourways, Johannesburg, 10 -15 September 2017
2. "*One-step synthesis of photoluminescent carbon dots from chitosan*" **Poster presentation** at 7th Annual Gauteng Nanoscience Young Researchers' symposium (2017 SANi-NYRS); Tshwane University of Technology, Pretoria West Campus, Johannesburg, 20 October 2017
3. "*One-step synthesis of photoluminescent carbon dots from chitosan*" **Poster presentation** at the 8th Cross Faculty Postgraduate Symposium; University of the Witwatersrand, School of Public Health Auditorium, Education campus, 27th St Andrews Road, Parktown, Johannesburg, 25 - 26 October 2017
4. "*Synthesis of carbon dots for use as carbon monoxide sensors in Fuel cells*" **Poster presentation** at the 28th annual conference of the Catalysis Society of South Africa (CATSA); Kwa Maritane Bush Lodge, Pilanesberg, North-West, 19 - 22 November 2017
5. "*Synthesis of carbon dots for use as carbon monoxide sensors in Fuel cells*" **Oral presentation** at the Annual CoE-SM/AMSEN Student Presentation Workshop; Senate Room, Solomon Mahlangu House, University of the Witwatersrand, Johannesburg, 4 April 2018
6. "*Synthesis of carbon dots for use as carbon monoxide sensors in Fuel cells*" **Oral presentation** at the 9th Cross Faculty Postgraduate Symposium; University of the Witwatersrand, New Commerce Building, Braamfontein West Campus, Johannesburg, 29 - 30 October 2018
7. "*Synthesis of highly photoluminescent CDs from PEG for use as carbon monoxide sensors in Fuel cells*" **Oral presentation** at the 8th Annual Gauteng Nanosciences Young Researchers Symposium (2018 SANi-NYRS), Vaal University of Technology,
8. "*Synthesis of highly photoluminescent CDs from PEG for use as carbon monoxide sensors in Fuel cells*" **Oral presentation** at NANOSMAT- AFRICA 2018, Cape Town, 19 - 23 November 2018
9. "*Synthesis of highly photoluminescent CDs from PEG for use as carbon monoxide sensors in Fuel cells*" **Poster presentation**; MSSA-2018 Workshop, University of the Witwatersrand, Johannesburg, 3 - 5 December 2018

Table of Contents

Declaration ii
Abstract iii
Dedication v
Acknowledgment vi
Presentations vii
Table of Contents viii
List of Abbreviations xi
List of Figures xii
List of Tables xvi
1 Synopsis 1
1.1 Motivation 1
1.2 Organisation of dissertation 2
2 Literature review 4
2.1 Background 4
2.2 Fuel cells 5
2.2.1 Types of fuel cells 5
2.2.2 Carbon monoxide (CO) poisoning 10
2.2.3 CO sensors 12
2.3 Carbon dots 14
2.3.1 CDs overview 14
2.3.2 CDs' optical properties 17
2.3.3 CDs in sensing 35
2.4 Characterisation of carbon nanodots (CDs) 38
3 Experimental procedure 40
3.1 Introduction 40
3.2 Development of the synthesis method of highly photo luminescent CDs 40
3.2.1 Sucrose 40
3.2.2 Chitosan 41
3.2.3 PEG 41

3.3 Hydrothermal synthesis of highly photo luminescent CDs using PEG: A paramedic study…….. 42
3.3.1 Variation of volume percentage of $\boldsymbol{PEG400}$ to water 42
3.3.2 Variation of reaction time 42
3.3.3 Variation of solvent used during synthesis 42
3.3.4 Variation of molecular weight of the PEG precursor 42
3.4 Characterization 43
3.4.1 TEM 43
3.4.2 PL and UV-vis spectra 43
3.4.3 FTIR spectra.....43
3.4.4 Quantum yield measurements.....43
3.4.5 %By-product determination.....44
4 Development of the synthesis method to make highly photoluminescent CDs 46
4.1 Introduction 46
4.2 Results and discussion.....48
4.1.1 CDs from sucrose.....49
4.1.2 CDs from Chitosan 60
4.1.3 CDs from PEG_{400} 69
4.2 Conclusion.....78
4.2.1 Methods.....78
4.2.2 Precursors.....79
4.2.3 Summary 79
5 Hydrothermal synthesis of highly photo luminescent CDs using PEG: A paramedic study ……..81
5.1 Introduction 81
5.2 Results and discussion.....83
5.2.1 Variation of volume percentage of $\boldsymbol{PEG400}$ to water 83
5.2.2 Variation of reaction time 91
5.2.3 Variation of solvent used during synthesis 98
5.2.4 Variation of molecular weight of the PEG precursor 112
5.3 Conclusion.....120
6 Sensing ability of CDs: Preliminary testing and proof of concept 122
6.1 Introduction 122
6.2 Preliminary results.....122

6.3 Conclusion.....125
7 Conclusion and Future work.....126
7.1 Conclusion.....126
7.2 Future Work.....129
References.....130
Appendix: Supplementary Information.....155

List of Abbreviations

Abbreviation	Description
%QY	Quantum yield
0D	Zero-dimension
1D	One-dimension
2D	Two-dimensional
3D	Three-dimension
AFC	Alkaline fuel cell
AIE	Aggregation induced emission
AIQ	Aggregation induced quenching
CDs	Carbon dots
CEE	Crosslink-enhanced emission effect
CNDs	Carbon nanodots
CNS	Carbon nanospheres
CO	Carbon monoxide
DCM	Dichloromethane
DMFC	Direct methanol fuel cell
DMSO	Dimethyl sulfoxide
DOX	Anticancer drug doxorubicin
EMF	Electromotive force
FRET	Fluorescence resonance energy transfer
FRET	Forster resonance energy transfer
FTIR	Fourier transform infrared
GQDs	Graphene quantum dots
HPS	Hexaphenylsilole
HR-TEM	High-resolution transmission electron microscopy
IFE	Inner filter effect
IR	Infrared spectroscopy
LEDs	Light emitting diodes
MCFCs	Molten carbonate fuel cells
PAFC	Phosphoric acid fuel cells
PDs	Polymer dots
PEG	Polyethylene glycol
PEM	Polymer electrolyte membrane
PEMFC	Polymer electrolyte (or proton exchange membrane) fuel cell
PET	Photo-induced electron transfer
PL	Photoluminescence
PSS	Polystyrene sulfonate
SOFCs	Solid oxide fuel cells
SWCNT	Single-walled carbon nanotubes
T	Transition
TBAP	Tetrabutylammonium perchlorate
TEM	Transmission electron microscopy
XPS	X-ray photoelectron spectroscopy
XRD	X-ray diffraction

List of Figures

Figure 2-1: Fuel cell. As depicted, the fuel cell processes a flow of electrons (electricity, power) from electrochemical reaction of hydrogen (anode) and oxygen (cathode). Water and heat are produced as by-products. 4

Figure 2-2: A schematic representation of the processing of fuel in a fuel stack system [19] 13

Figure 2-3: The three different types of CDs (a) graphene quantum dots (GQDs), (b) carbon nanodots (CNDs) and (c) polymer dots (PDs) (modified from (Zhu et al., 2015) (Zhu et al., 2013) 15

Figure 2-4: Illustrates the attainance of naturally occuring CDs from honey....15

Figure 2-5: Shows CDs in the centre (with a carbon core and functional groups wiggling on the surface), the appealing properties of CDs (PL is photoluminescence and D/A stands for donor/acceptor) and a fields where CDs can be applied....16

Figure 2-6: Schematic representation of the discrete vibrational energy levels of quantum dots versus the Continuum vibrational energy levels of bulk semi-conductors. Also, illustrates the bag-gap dependency of quantum on their particle and emphasis the blue to red-shift of the emitted light that accompanies the particle size increase of quantum dots 18

Figure 2-7: Effect of reduced dimensionality. Electrons are confined in a semiconductor (red) with a smaller band gap than the cladding semiconductor (blue). The confinement changes the density of states, depicted as D(E). Ec is the conduction-band edge of a 3D....19

Figure 2-8: Energy diagram of CDs....22

Figure 2-9: Absorption and emission spectra of rhodamine 6G with ~25 nm Stokes shift....23

Figure 2-10: Absorption and emission spectra of typical quantum dots with large Stokes shift 23

Figure 2-11: Representation of PDs (the PDs always contain CPDs and NCPDs), and the relationship between NCPDs and other CDs. 27

Figure 2-12: Illustration of the three routes that lead CEE effect of the non-conjugated linear polymers....27

Figure 2-13: The demonstration the AIQ and AIE effects of Pyrelene and hexaphenylsilole, respectively, by gradually increasing the fraction of water (a poor solvent) by Mei et. al....29

Figure 2-14: Illustration on restriction of intramolecular motion....30

Figure 2-15: The two approaches for carbon dots synthesis namely top-down and bottom-up approach....31

Figure 2-16: A schematic of the CDs/DOX for FRET mechanism for drug tracking and delivery. CDs acts as both a drug carrier and a donor and DOX acts as an acceptor. When DOX is released from the CDs surface, the FRET between CDs and DOX is terminated, recovering the short wavelength 34

Figure 2-17: A schematic illustration of the synthetic route of NH2-C-dots, Br-coated C-dots, and polymer dots. DMSO and PMDETA dimethyl sulfoxide and penta-methyl-diethyl-enetriamine, respectively, and were used as primers 35

Figure 2-18: Illustrated Fe^{3+} concentration dependent PL quenching of CDs. Whereby CDs PL intensity decreases with increasing Fe^{3+} concentration 36

Figure 2-19: Illustration of the AA sensor based on the off–on fluorescent probe of CDs adjusted with Fe^{3+} 38

Figure 3-1: Schematic representation of the reflux method set-up 41

Figure 3-2: Illustration of the %by-product calculation 45

Figure 4-1: The carbon precursors investigated for the synthesis of CDs 47

Figure 4-2: The reactors investigated for the synthesis of CDs 48

Figure 4-3: Schematic diagram showing the synthesis of CDs from three different precursors 49

Figure 4-4: TEM images and corresponding particle size distribution curves of Sucrose-CDs synthesised using (a) autoclave, (b) microwave and (c) reflux, respectively. 50

Figure 4-5: (a) UV-Vis absorption and PL spectra of Sucrose-CDs at 350 nm excitation wavelength. PL spectra of (b) autoclave, (c) microwave and (d) reflux synthesised Sucrose--CDs, respectively, at various excitation wavelengths 52

Figure 4-6: The excitation wavelength vs emission peak position (black) and the excitation wavelength vs emission peak intensity(blue) of (a) autoclave, (b) microwave, and (C) reflux synthesised Sucrose-CDs, respectively. 54

Figure 4-7: Particle size of sucrose synthesised CDs versus their optimal PL emission and the corresponding excitation wavelength 56

Figure 4-8: FTIR spectra of Sucrose-CDs synthesised via reflux, microwave, autoclave and the FTIR spectra of Sucrose respectively 58

Figure 4-9: TEM images and corresponding particle size distribution curves of Chitosan-CDs synthesised using (a) autoclave, (b) microwave and (c) reflux methods, respectively. 61

Figure 4-10: (a) UV-Vis absorption and PL spectra of Chitosan-CDs/nanoparticles at 350 nm excitation wavelength. PL spectra of products produced from (b) autoclave, (c) microwave and (d) reflux synthesised Chitosan-CDs/nanoparticles, respectively, at various excitation wavelengths 63

Figure 4-11: The excitation wavelength vs emission peak position (black) and the excitation wavelength vs emission peak intensity(blue) of (a) autoclave, (b) microwave, and (C) reflux synthesised Chitosan-CDs, respectively. 66

Figure 4-12: FTIR spectra of Chitosan-CDs/nanoparticles synthesised via reflux, microwave, autoclave and the FTIR spectra of Chitosan respectively 68

Figure 4-13: TEM images and corresponding particle size distribution curves of PEG-CDs synthesised using (a) autoclave, (b) microwave and (c) reflux, respectively 70

Figure 4-14: UV-Vis absorption and PL spectra of PEG-CDs at 350nm excitation wavelength. PL spectra of (b) autoclave, (c) microwave and (d) reflux synthesised PEG-CDs, respectively, at various excitation wavelengths 72

Figure 4-15: The excitation wavelength vs emission peak position (black) and the excitation wavelength vs emission peak intensity (blue) of (a) autoclave, (b) microwave, and (C) reflux synthesised PEG-CDs, respectively. 74

Figure 4-16: Particle size of PEG synthesised CDs versus their optimal PL emission and the corresponding excitation wavelength 76

Figure 4-17: FTIR spectra of PEG-CDs synthesised via reflux, microwave, autoclave and the FTIR spectra of Sucrose respectively 77

Figure 5-1: Schematic showing how PEG-CDs synthesis using different reaction conditions 82

Figure 5-2: TEM images and corresponding particle size distribution curve of PEG-CDs synthesised with (a)25vol%, (b)33vol%, (c)50vol%, (d)67vol%, (e)75vol% and (F)100vol% of the PEG400 precursor was mixed with water, respectively 85

Figure 5-3: FTIR spectra of PEG-CD synthesised using various PEG% starting materials ... 87

Figure 5-4: UV-Vis absorption and fluorescence spectra of CDs synthesised using various PEG_{400} to water volume ratios at 350 nm excitation wavelength 88

Figure 5-5: Vol%PEG / water ratio of the starting material versus particle size of resulting PEG-CDs 90

Figure 5-6: TEM images and corresponding particle size distribution curve of PEG-CDs synthesised at (a) 1 h (b) 2 hrs , (c) 3 hrs, (d) 4 hrs, (e) 5 hrs and (F) 12 hrs of reaction time, respectively 92

Figure 5-7: UV-Vis absorption and fluorescence spectra of various PEG-CDs synthesised after various reaction time, recorded using 350 nm excitation wavelength. 93

Figure 5-8: General course of reaction: step 1 is the heating up of the reaction to the desired rection temperature, step 2 is the synthesis (the duration of step 2 is generally noted as the reaction time) and lastly step 3 is the cooling of the reaction. 94

Figure 5-9: FTIR spectra of PEG CDs synthesised at various reaction times 96

Figure 5-10: The quantum yield of CDs synthesised after reaction times 98

Figure 5-11: TEM images and corresponding particle size distribution curve of PEG-CDs synthesised using different solvent namely (a) ethylene glycol, (b) dichloromethane, (c) 2-butanol, (d) acetonitrile and (e) chloroform, respectively 101

Figure 5-12: Particle size vs boiling point of solvent used. The size of the sphere correlates to the particle size of the CDs 103

Figure 5-13: TEM image and corresponding particle size distribution of CDs synthesised by Chen et al., CDs-w, CDs-m, CDs-d were synthesised using water, methanol and dimethylformamide respectively. 104

Figure 5-14: UV-Vis absorption and fluorescence spectra of various PEG-CDs synthesised using various solvents, recorded using 350 nm excitation wavelength 105

Figure 5-15: FTIR spectra of PEG CDs synthesised using various solvents..... 108

Figure 5-16: Particle size distribution and quantum yield at various reaction times..... 109

Figure 5-17: HR-TEM images and corresponding particle size distribution curve of PEG-CDs synthesised using PEG of different molecular weights as starting material namely a PEG with MW of (a) 1500 g/mol, (b) 4000 g/mol, (c) 6000 g/mol, (d) 10 000 g/mol, (e) 12 000 g/m, and (f) 35 000 g/mol, respectively 114

Figure 5-18: UV-Vis absorption and fluorescence spectra of various PEG-CDs synthesised using PEG precursors of various molecular weight..... 116

Figure 5-19: FTIR spectra of PEG CDs synthesised using various PEG molecular weights 117

Figure 5-20: The molecular mass of the PEG precursor versus the quantum yield of the resulting CDs 118

Figure 6-1: Schematic representation of the sensing ability testing of the synthesised CD .. 124

Figure S1: TEM image of the reflux and chitosan synthesised sample that was not reproducible…… 128

Figure S2: TEM image of CDs sample with CNS expressed as by-product. CDs have particle sizes of 1-10nm, while the expressed CNS are relatively bigger at 20 – 40 nm…… 129

Figure S3: The vol% of the PEG precursor to water (solvent) ratio versus the particle size of the resulting CDs…… 130

Figure S4: Particle size of CDs synthesised after various reaction times……..130

Figure S5: The course of the ‘ramp-only’ reaction…… 131

Figure S6: TEM image of CDs sample synthesised with ramping only…… 132

Figure S7: FTIR spectra the PEG precursor and the CDs sample synthesised after ramping only…… 132

Figure S8: The quantum yield of CDs synthesised after reaction times with a trend line … 133

Figure S9: The particle size of the CDs against solvent used during synthesis…… 133

Figure S10: The molecular mass of the PEG precursor versus the particle size of the resulting CDs…… 134

Figure S11: high magnification HR-TEM image of CDs synthesised from PEG12000 and corresponding d-spacing plot…… 134

List of Tables

Table 2-1: Comparison of fuel cell technologies 8

Table 2-2: Summary of the advantages and disadvantages of different synthesis methods 33

Table 4-1: The physical state and % yield of the CDs 49

Table 4-2: UV-Vis and PL emission peaks of Sucrose-CDs, with corresponding spectral assignments and particle size of the CDs. 53

Table 4-3: The strongest PL emission at varying excitation wavelengths with the corresponding excitation wavelength and size of the sucrose- CDs sample 55

Table 4-4: Fluorescence %QY of the sucrose synthesised CDs 59

Table 4-5: UV-Vis and PL emission peaks of chitosan-CDs, with corresponding spectral assignments and particle size of the CDs 64

Table 4-6: Fluorescence %QY of the chitosan synthesised CDs 69

Table 4-7: UV-Vis and PL emission peaks of PEG-CDs, with corresponding spectral assignments and particle of the CDs 73

Table 4-8: UV-Vis and PL emission peaks of PEG-CDs, with corresponding spectral assignments and particle size of the CDs 75

Table 4-9: Fluorescence %QY of the sucrose synthesised CDs 78

Table 5-1: The volume ratio of $PEG400$ to water used during synthesised and corresponding particle size of the produced CDs 84

Table 5-2: Particle sizes of vol%PEG-CDs and corresponding fluorescence quantum 89

Table 5-3: The %by-product observed on TEM images 89

Table 5-4: The particle of CDs synthesised after various reaction times 91

Table 5-5: Particle sizes PEG-CDs and correponding fluorescence quantum of CDs synthesised after various reaction times 97

Table 5-6: Some of the properties of the solvents used in making PEG_{400} CDs 99

Table 5-7: The solvent used during synthesis and the particle size of the synthesised CDs . 100

Table 5-8: Correlation Matrix of the properties of the solvent used during synthesis and the particle size of the resulting PEG-CDs 102

Table 5-9: UV-Vis and PL emission peaks of PEG-CDs, with corresponding spectral assignments and particle of the PEG-CDs synthesised using various solvents 105

Table 5-10: Classification of CDs synthesised using varying solvent based on the PL maxima wavelength they exhibit at an excitation wavelength of 350 nm 106

Table 5-11: The correlation matrix of the properties of the solvent used during synthesis and the emission wavelength of the resulting PEG-CDs at 350 nm excitation wavelength 107

Table 5-12: Corresponding particle sizes and fluorescence quantum yield % as the synthesis solvent was varied as starting conditions 109

Table 5-13: The correlation matrix of the particle size of violet CDs and their %QY 110

Table 5-14: The correlation matrix of the properties of the solvent used during synthesis and the properties of the resulting PEG-CDs 111

Table 5-15: The molecular weight of the PEG precursor and the particle size of the synthesised CDs 113

Table 5-16: Corresponding particle sizes and fluorescence quantum yield % as the PEG molecular weight was varied as a starting condition 118

Table 5-17: Summary of results of Zhang *et al., and* Fan *et al.,* 119

1 Synopsis

1.1 Motivation

About a decade ago, carbon nanomaterials of less than 10 nm in size were discovered as by-products during the synthesis of multi-wall carbon nanotubes (MWCNT) and were later named carbon nanodots (CDs). During their discovery, CDs were serendipity etched out of relatively larger carbon nanomaterials, MWCNT, of 130-250 nm sizes. [1] To date, CDs have been shown to be highly photoluminescent, an excellent electron donor and acceptor. Most importantly, CDs are inherently non-toxic to humans (biocompatible) because their structure is primarily comprised of the organic element carbon. In addition, CDs are decorated with functional groups (such as hydroxyls, carboxylic acids and amino groups) on their surface which allow for tuning of the properties of CDs (to make CDs more suitable for the application of interest) through modification of the surface. As a result of the above appealing properties, CDs have been applied in various fields such as biomedicine, catalysis, optronics, and sensing. CDs have been successfully used as a probe for the sensing of a vast number of analytes (for example Cu^{2+}, Fe^{3+}, DNA and vitamin C) through the monitoring of their PL in response to the presence of the analyte. However, CDs have not been explored in sensing carbon monoxide (CO) for application in polymer electrolyte membrane (PEM) fuel cells. [1]–[3]

PEM fuel cells are currently being developed for portable, stationery and transportation applications. Their development was inspired by their ability to produce electricity from the electrochemical reaction of hydrogen and oxygen. With only water and heat as the by-products, PEM fuel cells are highly environmentally friendly. As such, PEM fuel cells can be used in place of fossil fuel for the generation of power and used in place of combustion engines for propulsion of vehicles. [3] Pure hydrogen is highly explosive thus, as a safety measure, pure hydrogen gas cannot be packaged into the PEM fuel cell. Therefore, to drive the PEM fuel cells, hydrogen is formed on site, through the reformation of fuels such as methane and natural gas. The major drawback of fuel reformation is that CO is always produced as a by-product, which consequently reduces the durability of the fuel cell. This happens because CO preferentially and irreversibly binds to the anode platinum catalyst of the fuel cell, and in doing so inhibits the binding and catalytic splitting of hydrogen which results in the deterioration of the efficiency of the fuel cell over time. [3]–[6]

To combat this, a CO cleaner (carbon monoxide preferential oxidizing reactor, referred to as the PROX reactor) has been integrated into fuel cells. [7], [8] However, for the CO cleaner to be efficient and selective to CO, the presence and amount of CO must be known. This necessitates the incorporation of a CO sensor to regulate the function of the CO cleaner. [9] There has been a considerable amount of research done in search of this CO sensor, however to date, the reported CO sensors have one or two of the following obstacles: (a) expensive (b) poor compatibility with the humid and reducing environment of the fuel cells (c) poor CO selectivity- cross sensitive to hydrogen, methane, NOx and/or components present in the fuel stream (d) poor CO sensitivity. [4], [7], [8], [10] Thus, the search of a novel CO sensor for application in fuel cells is still at large and this study joins on search by exploring photoluminescent CDs which have been highlighted as good sensing candidates.

The aim of the project is to develop a C-dots based CO sensor for application in PEM fuel cells. To achieve this, we oath to undertake the following objectives:

i. Develop synthesis method for CDs
ii. Optimise synthesis of 1-10 nm CDs
iii. Modify the CDs by chemical procedures (i.e. Synthesise Pt/ CDs materials for sensor testing)
iv. Test and optimise CO sensing of CDs for PEM fuel cell

1.2 Organisation of dissertation

Chapter 1: Gives a brief introduction to the study and elaborates the motivation, aim, and objectives of the project.

Chapter 2*:* Details the background of the development of fuel cells, outlines the types of fuel cells, presents the advantages and shortcomings of fuel cells and discloses the potential of CDs in combating the shortcoming of fuel cells.

Chapter 3*:* Details the experimental procedure and characterisation of the CDs. Moreover, the materials and apparatus used for this work are stated and described.

Chapter 4*:* Explores the synthesis of CDs from various precursors using various reactors to development a synthesis method which yields CDs with ideal properties for use as a sensor for application in PEM fuel cells.

Chapter 5*:* The effect of various reaction parameters on the synthesis highly photoluminescent CDs using the precursor and reactors couple method identified in the previous chapter.

Chapter 6: This chapter details the preliminary testing of the CO sensing ability of the synthesised CDs.

Chapter 7*:* Summaries the findings of the study (The synthesis of carbon dots for possible use as a CO sensor in polymer electrolyte membrane fuel cells).

2 Literature review

2.1 Background

Being non-renewable resources, fossil fuels such as coal and crude oil are depleting, yet they are still the main source of power generation. This global scarcity crisis, together with the pursuit of reduction of greenhouse gas emissions, inspired the development of fuel cells. Fuel cells produce electricity (power) when hydrogen and oxygen electrochemically react to form water. They operate silently and in doing so reduce noise and air pollution. Also, fuel cells can be coupled to other systems which can harvest their by-products and put them to good use. For instance, a 1 kW fuel cell stack has been used in the Gemini program as an auxiliary power source for an aircraft and to supply astronauts with clean drinking water. The heat generated in the reaction can be collected for use as a heating system (an alternative to geysers and heaters). Considering that water and heat are the only by-products, this emission-free technology of producing electricity is environmentally friendly with extra credit of being a clean, quiet and highly efficient technology. A fuel cell is depicted below in Figure 2-1. [6], [11]

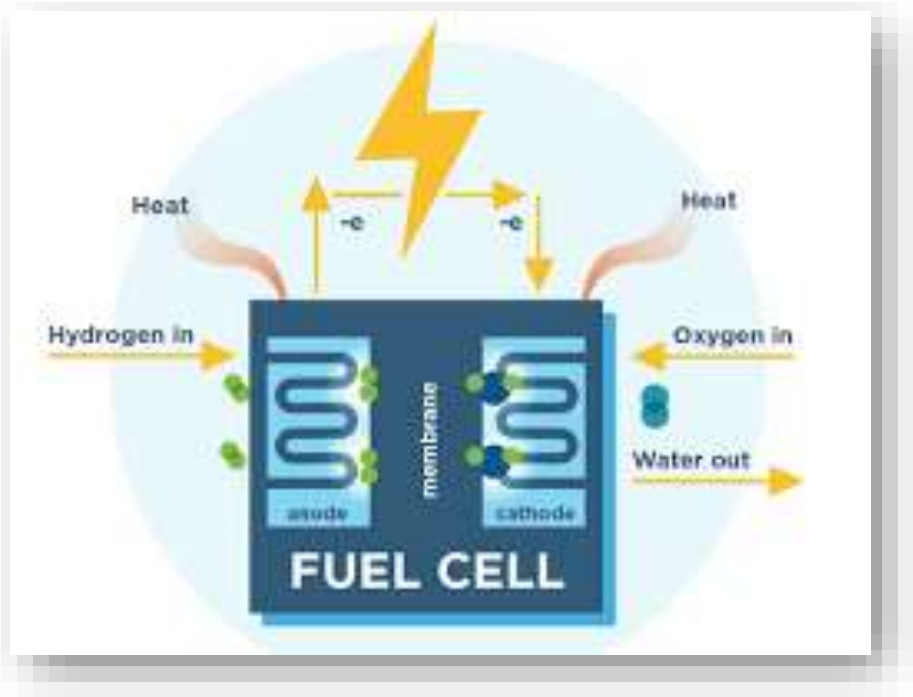

Figure 2-1: Fuel cell. As depicted, the fuel cell processes a flow of electrons (electricity, power) from electrochemical reaction of hydrogen (anode) and oxygen (cathode). Water and heat are produced as by-products. [12]

The selling point for fuel cells as power generators over other renewable resource technologies (e.g. solar cells, windmills and water turbines) is that fuel cells exhibit all the following benefits: highly efficient, durable, reliable, flexible and can be easily scaled and maintained. Thus, a significant reduction in the use of fossil fuels worldwide will be better realised through the global application of fuel cells as well as other green power generation systems. Other than the disadvantage of fuel cells operating with an expensive metal (platinum) as the anode catalyst, the major drawback with the use of fuel cells is that they are susceptible to carbon monoxide (CO) poisoning. [4], [6], [11], [13]

2.2 Fuel cells

2.2.1 Types of fuel cells

It is important to state the major difference between batteries and fuel cells: the process of electricity production and the composition of batteries and fuel cells are similar, the major difference is that batteries are energy storage devices whereas in fuel cells, power is continuously generated as long as fuel is supplied. There are several types of fuel cells- broadly classed into two major types based on their operating temperature. They are referred to as high- and low-temperature fuel cells, respectively. They can be further classified according to the type of electrolyte material used. A low-temperature fuel cell can be as an alkaline fuel cell (AFC), a polymer electrolyte (or proton exchange membrane) fuel cell (PEMFC), a phosphoric acid fuel cells (PAFC) and a direct methanol fuel cell (DMFC). It is worth mentioning that the DMFC fuel cell is the only fuel cell whereby methanol is directly fed to the anode (fuel is usually converted to hydrogen first) and for this reason, as an exception, DMFCs are classed according to the fuel they use rather than the type of electrolyte material used. High temperature (600 - 1000 ℃) fuel cells are solid oxide fuel cells (SOFCs) and molten carbonate fuel cells (MCFCs). These different types of fuel cells have different properties and in turn, have different capabilities. They are also distinctly suited for different applications. [13]

2.2.1.1 High temperature fuel cells

SOFCs use a strong, nonporous ceramic powder as an electrolyte. There are two types of SOFCs; one uses an array of long tubes and the other uses a compressed disc. Tubular SOFCs designs are close to commercialisation. On the other hand, MCFCs use an electrolyte consisting of a molten carbonate salt mixture suspended in a porous, chemically inert matrix. MCFCs of 10 kW to 2 MW have been tested with a variety of fuels and are primary targeted for electric

utility applications. Both these high-temperature fuel cells can be combined to give heat and power for regionalized stationary power systems and in heavy vehicle transportation such as trains and boats. [13]

2.2.1.2 Low temperature fuel cells

To date, PAFCs are the most commercially advanced systems. The major drive in their commercialisation is their simple construction; their electrochemical, chemical and thermal stability; and the low volatility of their electrolyte (at 150 - 200 ℃ operational temperatures). PAFCs have been applied in combined heat and power for regionalized stationary power systems. They have been installed around the world in about 19 nations in hospitals, nursing homes, office buildings, schools, etc. Phosphoric acid is the ideal acid in acidic fuel cells due to its high stability. In early developments, dilute phosphoric acid was used to prevent corrosion of the cell's material, but recently with the advancement of strong material research concentrated phosphoric acid is used. [13]

In DMFCs, the anode catalyst draws hydrogen from liquid methanol. This fuel cell has low efficiency (about 40%) due to the poor ability of the proton exchange membrane to block and keep methanol on the anode side of the membrane. The water content of the membrane assists the proton movement in the fuel cell. As both methanol and water have similar polarities and thus both methanol and water permeate across the membrane and into the cathode side of the cell by electro-osmotic drag and diffusion. In the cathode side, methanol oxidation interferes with oxygen reduction. This results in mixed potentials, and ultimately a decrease in cell performance. Thus, research on optimising the membrane's exclusivity for methanol is a priority. The attractive feature of these fuel cells is their low range operational temperature (49 - 88℃), which is useful in small electronic devices such as cellular phones and laptops. [13]

AFCs have the highest efficiency (about 70%) of all the fuel cells. The major drawback of its application is that it only works with very pure gasses (highly pure gasses are expensive and/or sometimes difficult to access). Nevertheless, this was the second fuel cell to be used in space: it was used in the Apollo spacecraft for power generation and to supply astronauts with clean drinking water. NASA opted to use the AFC over the DMFC (first to be used in space) because, at the time, the DMFC used polystyrene sulfonate (PSS) polymer which was unstable. The use of the Nafion® membrane was a major breakthrough in the field of PEMFC. [13], [4]

Like the DMFC, the PEMFC also utilises a proton exchange membrane. However, the fuel used (including methanol) is reformed to produce hydrogen which is then fed to the anode. PEMFCs operate at low temperatures of about 80℃ - 120℃ (**Table 2-1**) and they exhibit a high power density. Table 2-1 is the comparison fuel cell technologies put together by U.S. Department of Energy. [14] The most fascinating and distinctive feature of PEMCFs is their ability to vary the output quickly to meet shifts in power demand. This makes them suitable for automobiles (in light-duty vehicles, displacing the internal combustion engine) where the quick start-up is necessary. PEMFCs can also be used as small energy storage devices (to replace rechargeable batteries) and in the residential stationary power market. Our interest is on PEMFCs with respect to their application in propulsion. [13], [15]

Table 2-1: Comparison of fuel cell technologies. [14]

Fuel Cell Type	Common Electrolyte	Operating Temperature	Typical Stack Size	Electrical Efficiency (LHV)	Applications	Advantages	Challenges
Polymer electrolyte membrane (PEM)	Perfluorosulfonic acid	<120°C	<1 kW–100 kW	60% direct H_2; 40% reformed fuel	Backup power Portable power Distributed generation Transportation Specialty vehicles	Solid electrolyte reduces corrosion and electrolyte management problems Low temperature Quick start-up and load following	Expensive catalysts Sensitive to fuel impurities
Alkaline (AFC)	Aqueous potassium hydroxide soaked in a porous matrix, or alkaline polymer membrane	<100°C	1–100 kW	60%	Military Space Backup power Transportation	Wider range of stable materials allows lower cost components Low temperature Quick start-up	Sensitive to CO_2 in fuel and air Electrolyte management (aqueous) Electrolyte conductivity (polymer)

Fuel Cell Type	Common Electrolyte	Operating Temperature	Typical Stack Size	Electrical Efficiency (LHV)	Applications	Advantages	Challenges
Phosphoric acid (PAFC)	Phosphoric acid soaked in a porous matrix or imbibed in a polymer membrane	150°–200°C	5–400 kW, 100 kW module (liquid PAFC) <10 kW (polymer membrane)	40% [d]	Distributed generation	Suitable for CHP Increased tolerance to fuel impurities	Expensive catalysts Long start-up time Sulfur sensitivity
Molten carbonate (MCFC)	Molten lithium, sodium, and/or potassium carbonates, soaked in a porous matrix	600°–700°C	300 kW–3 MW, 300 kW module	50% [e]	Electric utility Distributed generation	High efficiency Fuel flexibility Suitable for CHP Hybrid/gas turbine cycle	High temperature corrosion and breakdown of cell components Long start-up time Low power density
Solid oxide (SOFC)	Yttria stabilized zirconia	500°–1,000°C	1 kW–2 MW	60% [f]	Auxiliary power Electric utility Distributed generation	High efficiency Fuel flexibility Solid electrolyte Suitable for CHP Hybrid/gas turbine cycle	High temperature corrosion and breakdown of cell components Long start-up time Limited number of shutdowns

2.2.2 Carbon monoxide (CO) poisoning

The Pt catalyst is at the heart of a fuel cell as it catalyses the anode reaction whereby H_2, the fuel, is split into H^+ and electrons (two of each per hydrogen molecule). The products of the anode reaction permeate through the polymer electrolyte membrane into the cathode whereby they react with oxygen to form water. The Gibbs free energy of the overall reaction is -237 kJ/mol; for standard conditions at 25℃, the equilibrium cell voltage is 1.23 V. Thus electricity is produced. [13]

The ideal PEM fuel is hydrogen, however, due to size, weight, cost and technical limitations it is difficult with covert technology to store enough quantity and quality of hydrogen gas. Thus, the bulk hydrogen is produced on site and on demand by external fuel (methanol, natural gas, gasoline and propane) reforming. Further, reforming fuels to produce reformate gas always produce some CO. However, the major drawback of this process is that the fuel cell efficiency can be deteriorated by CO poisoning. CO poisoning occurs through CO preferentially and irreversibly binding to the active sites of the anode Pt catalyst, and this precludes the essential hydrogen gas binding reaction. [10], [13], [16]

Depending on the type of reformer used, operating conditions and fuel, the reformate gas from the reformer contains 3 - 10% CO. The residual CO is further converted to more hydrogen and carbon dioxide through the water gas shift reaction - thereafter only 0.5 - 1% CO remains on the reformate gas (with hydrogen around 40 - 75 %). The sorption force of CO onto the anode Pt catalyst is very strong, which is a problem because the performance of the fuel cell falls when only a small amount CO (about 1% CO in bulk hydrogen stream) is present. Thus, a CO clean-up step is necessary to reduce or nullify the CO concentration in the reformate gas. There are two approaches that have been undertaken to save the fuel cell from CO poisoning, namely catalyst alloying and fuel reforming. [13], [17]

2.2.2.1 Catalyst alloying

Utilising Pt alloy catalysts to catalyse the anode reaction has proven to be a promising manner to mitigate CO poisoning. Quite several metals have been mixed with Pt and investigated for this purpose, including Sn, Ru, Mo, Fe and Co. Even though all previously mentioned metals form Pt alloys which exhibit higher CO tolerance compared to pure Pt, the Pt-Ru alloy is a

more novel approach to solving the problem. [17], [18] The CO tolerance capacity of a Pt-Ru alloy catalyst can be improved by incorporation of a third metal to the bimetallic catalysts. Indeed, carbon supported ternary Pt-Ru-M (M= Sn, Au, Ag, W, Os or Rh) catalysts have been investigated. Only incorporation of W (forming Pt-Ru-W) improved the CO tolerance significantly with electro-oxidation of hydrogen being twice that of Pt-Ru catalyst in the presence of 1% CO. [17], [18]

It has also been suggested that catalyst alloying improves CO tolerance through a ligand effect and/or a bi-functional effect. Ligand effects occur when the promoter changes the electronic properties of Pt and in doing so decreases the sorption force of CO onto Pt. A bi-functional effect occurs when the promoter forms one of the necessary reactive intermediates. In the case of Pt-Ru, both mechanisms are at play in improving CO tolerance. Ru acts as the promoter and in a bi-functional effect, oxygen-containing species form on Ru sites and facilitate oxidation of CO to carbon dioxide. [5]

Catalyst alloying has a disadvantage of using expensive noble metals as promoters which may further hinder the commercialisation of PEMFC due to cost. Another concern is that Ru is not entirely stable at very high over-potentials and this worsens as the catalyst ages. Also, even though alloy catalysts are tolerant to CO poisoning, CO molecules are not being effectively eliminated from the cell system. As such over time, the CO levels and coverage (on a catalyst) will rise and CO poisoning will eventually occur. This poses durability problems for PEMFCs. [10]

2.2.2.2 Fuel reforming

While more CO-tolerant fuel cell catalysts are being developed, efforts in developing a catalyst to selectively remove the 0.5-1% CO from the H_2-rich reformate prior to reaching the fuel cell are continuing. Several procedures are currently applied and are still under investigation: catalytic methanation Pd-membrane technology and CO preferential oxidation. [17] A Pd alloy membrane features a system whereby the hydrogen-rich reformate gas is fed through the membrane which only allows the passage of hydrogen to the anode Pt catalyst. This membrane can be very effective in the removal of CO from a hydrogen-rich reformate gas. However, this technique requires large pressure differences and relatively high temperatures which reduce the efficiency of the system. [13], [16]

On the other hand, catalytic methanation entails reacting CO with hydrogen which forms methane and water. Methanation requires stringent conditions to be effectively used as a CO clean-up system in fuel cell because the CO_2 present in the hydrogen-rich reformate gas may react with the produced water through a reverse-gas-shift reaction, thereby undesirably producing CO. Furthermore, the amount of hydrogen necessary to carry out the methanation reaction is three times that of CO resulting in a decrease in efficiency of the system. [13], [16], [17]

CO selective oxidation can occur in one of two ways. Firstly, there is hydrogen peroxide bleeding whereby H_2O_2 in the anode humidifier mitigates CO in the hydrogen-rich reformate gas. It was suggested that CO mitigation appears to provide by an unintended O_2 bleed produced by decomposing of H_2O_2 in the humidifier rather that H_2O_2 vapours transported from the humidifier to the anode. [13], [16] Secondly, the hydrogen-rich reformate gas is mixed with air or oxygen (which selectively oxidises CO) either before the fuel is fed into the cell or within the stack. [17] This process may be supplemented using a CO preferential oxidation (PROX) catalyst that is placed between the fuel stream inlet and the anode catalyst. Amongst the above, the use of a PROX catalyst appears to be the lowest cost method for CO clean-up to desired levels with minimal hydrogen consumption. [13], [16]

2.2.3 CO sensors

The problem with the use of PROX catalysts arises either when hydrogen gas is also oxidised because it is wasted or when the CO is inadequately removed leading to CO poisoning. In order for the oxidant (air or oxygen) fed into the PROX reactor to be just enough to oxidise CO and protect the fuel cell without parasitically wasting hydrogen gas, the presence and concentration of CO must be detected to regulate the oxidant supply and activity of the PROX reactor. Thus, a CO sensor must be incorporated into a fuel cell system. Figure 2-2 shows the steps of fuel processing in a fuel stack system equipped with a CO sensor. [19], [9] Commercially available CO sensors were designed to work in the presence of oxygen and thus fail in PEM fuel cells where the environment is highly reducing. As such, infrared spectroscopy (IR) is used to detect CO in fuel cells. IR spectroscopy is based on absorption spectroscopy; it is compatible with a fuel cell environment; it has a high accuracy and has rapid responses. However, IR spectroscopy detection systems are large and expensive, therefore are not ideal for PEM fuel cell applications. Several studies have been conducted in search of a new CO sensor for use in fuel cells. [19], [9]

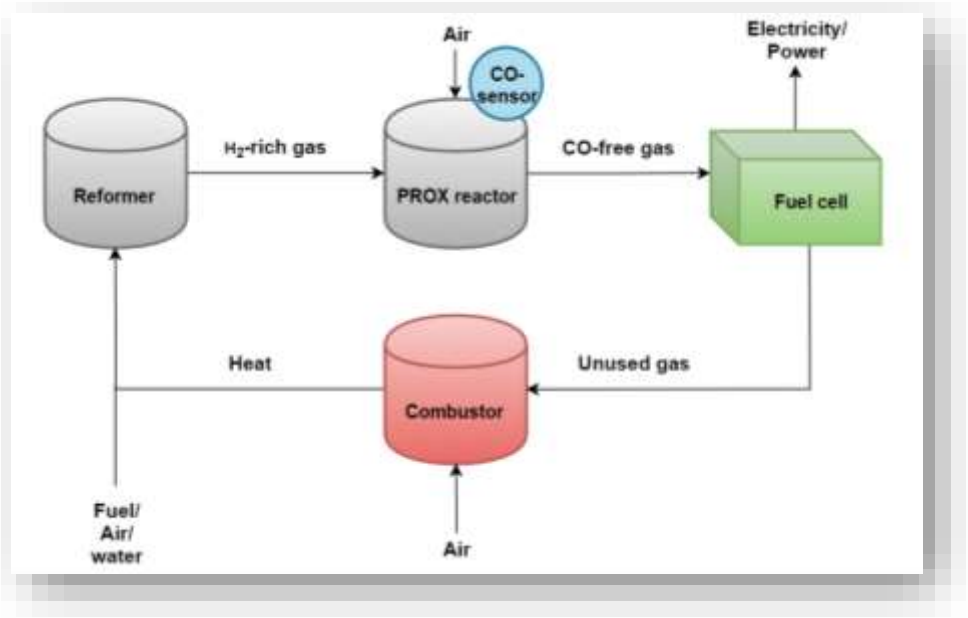

Figure 2-2: A schematic representation of the processing of fuel in a fuel stack system. [20]

Most developed CO sensors are amperometry devices. These sensors are mini-fuel cells (for instance a mini-PEMFC and a mini-SOFC). The mini-PEM fuel cell CO sensors are based on monitoring hydrogen oxidation kinetics at the anode which is inhibited and thus varied by carbon monoxide. [21] On the other hand, the exact mechanism in which CO is detected by a mini-SOFC is not yet fully understood. With that said, a mini-SOFC was used to detect 0 - 4000 ppm of CO by monitoring both the short-circuit current through the cell and the electromotive force (EMF) generated from the cell. These mini-fuel cells are compactible, have low cost and rapid response but they are cross-sensitive to hydrogen. [21], [22], [23]

Another CO sensor type that has been developed is based on chemi-resistance whereby CO is adsorbed on a material and the effected resistance of the material is monitored. With this type of sensor, tin oxide and thin film copper chloride have been explored. A tin oxide CO sensor exhibits similar advantages and disadvantages as does a mini-fuel cell and in addition, tin oxide has a high-power consumption. [19] On the other hand, copper chloride is tolerant to hydrogen. However, the operation of the sensor is compromised in the presence of water vapour. Dynamic response CO sensors which are based on pattern recognition have been developed, they have merits on low cost and tolerance to hydrogen. The major drawback of this CO sensing system is that they have a fixed RH value. [19], [9]

In a nutshell, impressive work has been done in the search for a CO sensor to supplement the PROX reactor and effectively counteract CO poisoning. However, each of the developed CO sensors has serious cons and thus the search for a novel CO sensor continues. A novel CO sensor should meet the following criteria:

- Since PEMFC efficiency deteriorates at small levels of CO, the CO sensor must be highly sensitive to CO (detect from 1-100 ppm). [9]

- The hydrogen-rich inlet stream contains chemicals like CO_2, NO_2 and methane together with the toxic CO, thus the sensor must be highly selective to CO. [19], [9]

- The PEMFC is a proton-exchange membrane which relies on water content to facilitate proton exchange and the fuel cell environment is humid. As such, the CO sensor must be compatible with humidity. [19], [9]

- For the CO sensor to effectively protect a PEMFC, it must have fast response times (approximately 1 min), it must be reversible and give quick feedback on changes of CO levels. [19], [9]

- One of the reasons PEMFCs are suitable for vehicle applications is that they are compact; as such it is necessary for the CO sensor system to be compactible. [19], [9]

2.3 Carbon dots

2.3.1 CDs overview

As relatively new materials, carbon nanodots (CDs) have not been employed in the sensing of CO. CDs are zero-dimensional carbon nanomaterials with sizes that range from 1-10 nm and have indigenous surface functional groups such as hydroxyl, carbonyl, carboxyl and amino groups (see Figure 2-3). [24] Most CDs are generally comprised of the elements carbon, oxygen, hydrogen and nitrogen. [25] They were serendipitously discovered in 2004 as one of the two major by-products during the purification of single-walled carbon nanotubes (SWCNT). [26] During the discovery of CDs, Xu et al., synthesised SWCNT from the oxidative reduction of carbon soot and subsequent surface functionalisation through boiling in nitric acid. Thereafter, the resulting crude of SWCNT were subjected to purification preparative electrophoresis in agarose gel and glass beads matrixes whereby, CDs were separated a major by-product. [27] As such, CDs were etched out from two-dimensional carbon

nanomaterials, SWCNT, of relatively larger particle size (150 nm). To date, CDs have been prepared via various chemical, electrochemical and physical synthetic methods using organic based precursors ranging from carbon soot to milk [28] and apple juice. [29] Moreover, Mandani et al., proved the existence of naturally occurring CDs by extracting them from honey as summarised in Figure 2 - 4. The extraction entailed subjecting honey to diluting, dialysing and precipitation to separate out larger biomolecules, whereby 15 mg CDs from a gram of honey was extracted as depicted in Figure 2 - 4. [30]

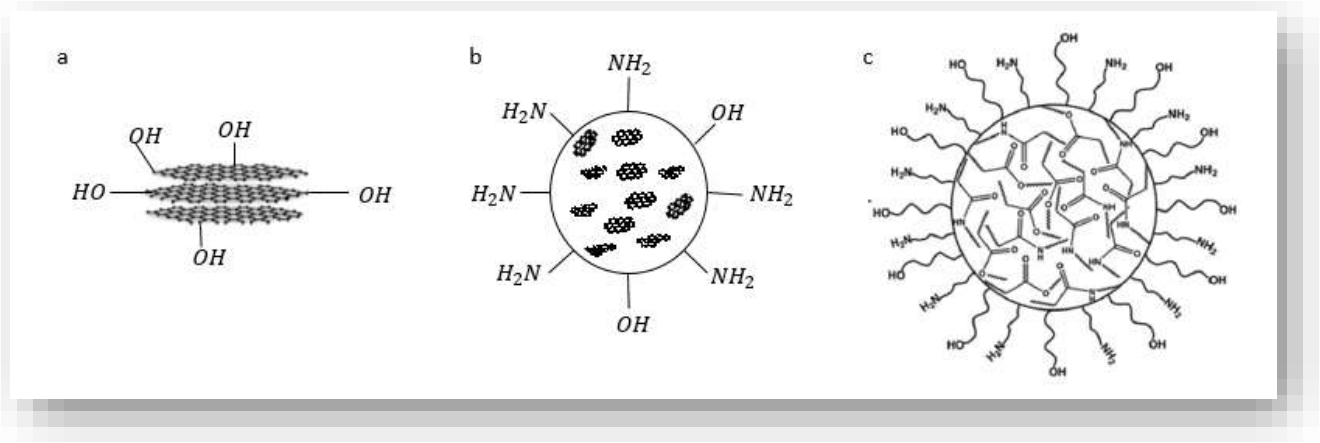

Figure 2-3: The three different types of CDs (a) graphene quantum dots (GQDs), (b) carbon nanodots (CNDs) and (c) polymer dots (PDs) (modified from (Zhu et al., 2015) (Zhu et al., 2013). [31], [32]

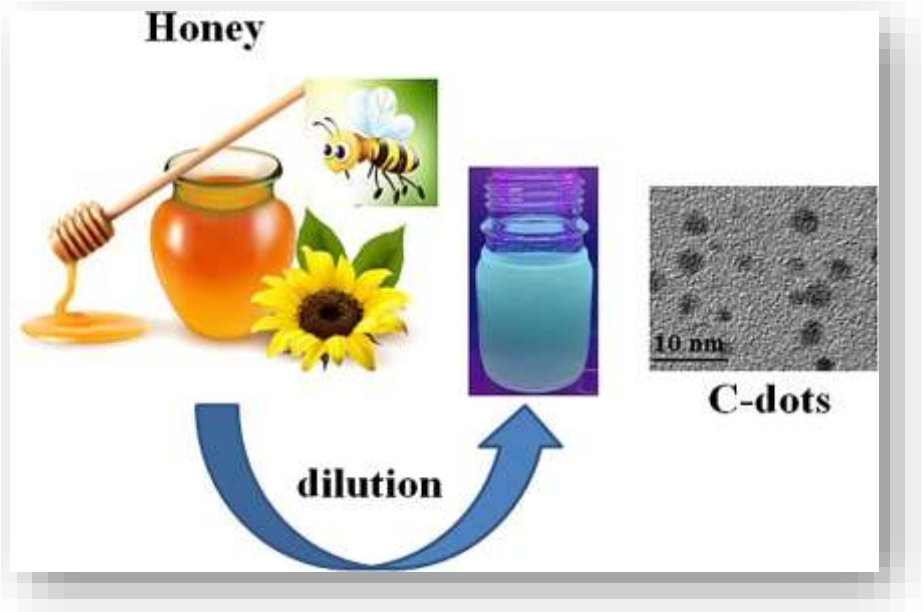

Figure 2-4: Illustrates the attainance of naturally occuring CDs from honey. [30]

As illustrated in Figure 2-3, there are three different types of CDs distinguished based on their intrinsic inner structure and surface functional groups, namely, graphene quantum dots (GQDs), carbon nanodots (CNDs) and polymer dots (PDs). GQDs consist of one or a few layers of graphene stacked together with chemical groups connected at the edges. Thus, GQDs are anisotropic materials with a width larger than height. Their synthesised is favourable when using layered carbonaceous starting material. CNDs are spherical aggregates, with chemical groups connected on the surface (amorphous CNDs are called carbon nanoparticles whereas the crystalline CNDs are called carbon quantum dots). Similarly, PD are spherical aggregates but are grafted with polymer chains connected on the surface of the carbon core. [33]

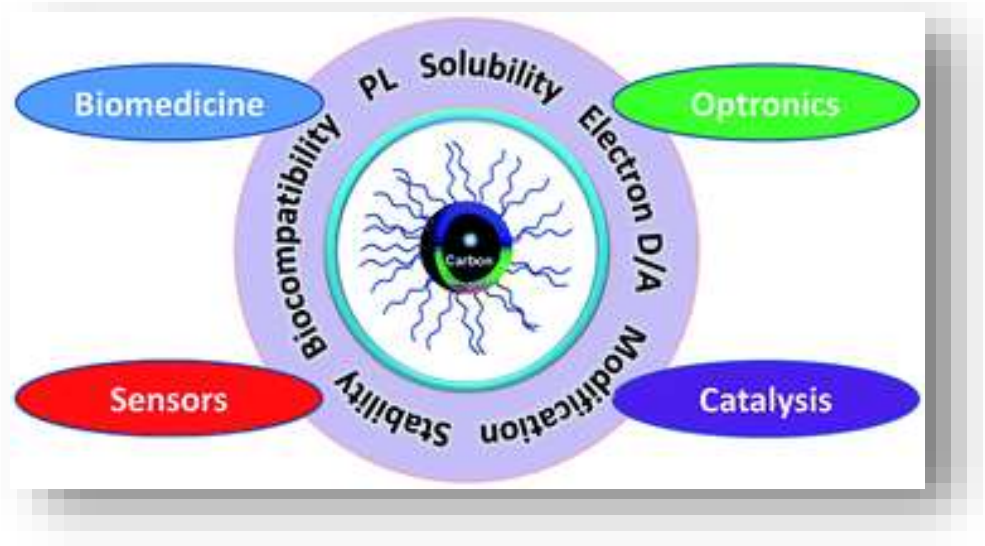

Figure 2-5: Shows CDs in the centre (with a carbon core and functional groups wiggling on the surface), the appealing properties of CDs (PL is photoluminescence and D/A stands for donor/acceptor) and a fields where CDs can be applied. [26]

Since their discovery, CDs have been shown to be good semi-conductors that exhibit a number of appealing optical properties, such as photoluminescence (PL), electrochemiluminescence and photo-induced electron transfer as depicted in Figure 2-5. Similar characteristics are exhibited by inorganic quantum dots. However, CDs are superior to their inorganic counterparts, quantum dots, because CDs are biocompatible, stable and open to modification. [34] The biocompatibility of CDs is bestowed by the fact that CDs are produced from carbon nanomaterials or organic building blocks and as a result CDs are mainly comprised of the element carbon which renders them less toxic to human beings (and other biota) compared to inorganic quantum dots. Inorganic quantum dots are non-carbon based nanomaterials of 1-10

nm; they traditionally made from colloidal synthesis and based on elements of the 2nd and 6th group of the periodic table (e.g. cadmium and zinc) and from the 3rd and fifth group, phosphides and indium arsenide. [35] Inorganic quantum dots were discovered in glass matrix and in colloidal solutions and later named '*inorganic quantum dots*' in 1986. [36] Since then, inorganic quantum dots have been a central theme in nanotechnology, being applied in biomedicine, photovoltaic devices (solar cells), light emitting diodes (LEDs), quantum dots display, photodetector devices and photo-catalysts. Toxicity is the major obstacle of the application of inorganic quantum dots, especially in biomedicine. [37] CDs are a green alternative to inorganic quantum dots, thus they received attention in a vast number of fields (biomedicine, optoelectronics, catalysis, sensing) were inorganic quantum dots largely fell shots due to their toxicity.

CDs (and quantum dots) are artificial clusters of semiconducting atoms that can confine the atoms motion due to their small size. This is just as in an atom, whereby the energy levels are quantised due to the confinement of electrons. [38] One of the most important selling points of the CDs is the feasibility to tune their band gap with ease and therefore control the absorption and emission frequencies; tuning of the bang gap of CDs occurs via varying the size of CDs which in turn is affected by the preparative method and/or post-treatment of the CDs. [26] In this way it is possible for the optical properties of CDs to be adjusted according to their purpose of use without significant cost or without the use of high-end technology. [39]

2.3.2 CDs' optical properties

2.3.2.1 CDs versus bulk semiconductor

As previously mentioned, CDs are 1 - 10 nm sized semi-conductors, and they perform better than bulk semiconductors. Materials are classed into three categories based on their electric conduction, namely conductors, semiconductors and insulators. Semiconductors are comprised of (1) a range occupied lower-energy levels known as the valence band; (2) a range of forbidden range of energy levels well known as the band gap; and (3) a of range unoccupied higher-energy levels known as the conduction band. In bulk semiconductors, the valence and conduction band are continuum bands (the vibrational energy levels are closely packed) and the band gap a is fixed parameter for that material. [40], [41] Conversely, in quantum dots, the valence and conduction band are made up of a manifold of discrete vibrational energy levels and the band gap is a function of size of that material (Figure 2-6).

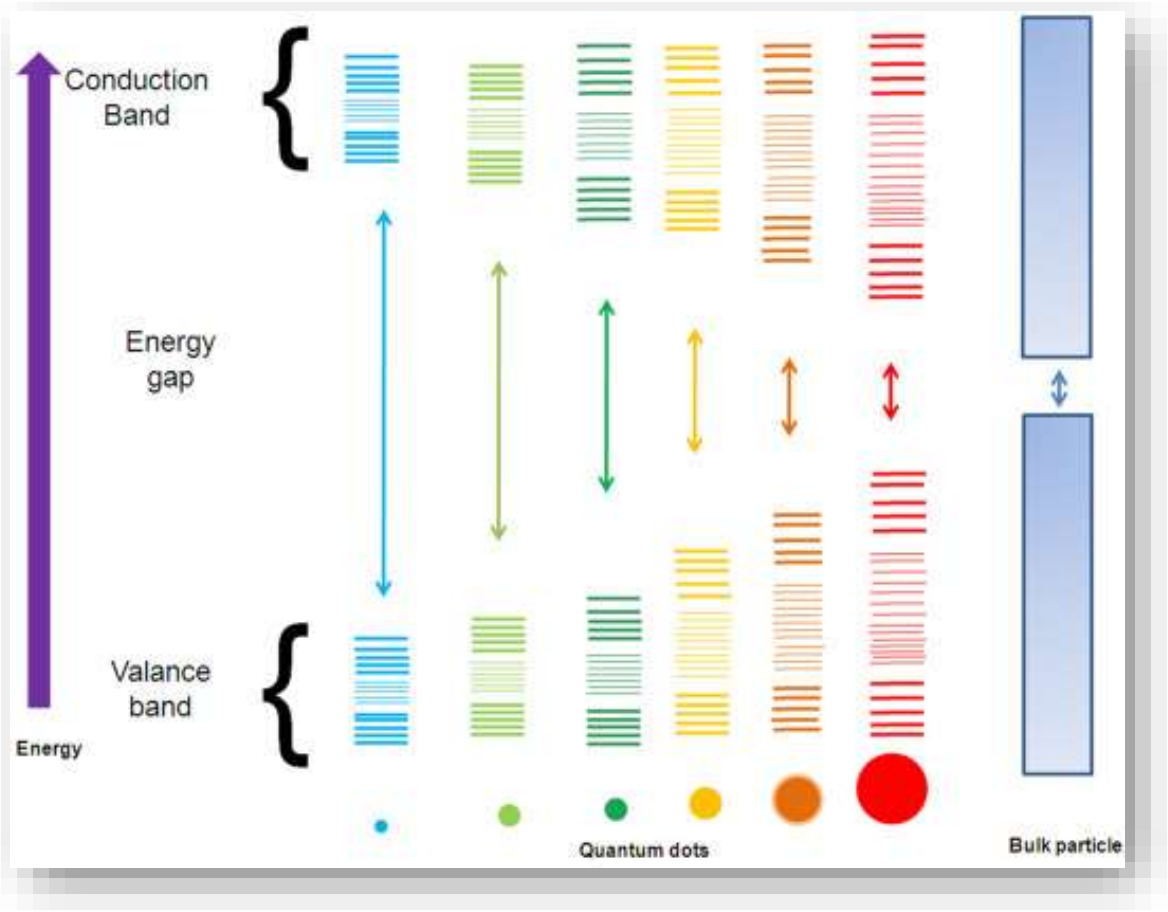

Figure 2-6: Schematic representation of the discrete vibrational energy levels of quantum dots versus the Continuum vibrational energy levels of bulk semi-conductors. Also, illustrates the bag-gap dependency of quantum on their particle and emphasis the blue to red-shift of the emitted light that accompanies the particle size increase of quantum dots. [38]

As illustrated in Figure 2-6, bulk semi-conductors are three-dimensional 3D structures thus the electrons are allowed to flow freely around continuum vibrational levels of the conduction and valence band, respectively. Quantum confinement is a phenomenon where an electron's movement is restricted to a respective discrete vibrational level of the conduction or valence band. Quantum wells express quantum confinement in one of their three dimensions. That is one of the dimensions have a size of 1-100 nm with the electron of confined propagation while, the other two dimensions retain their actual size and allow free movement of electrons. Thus, quantum wells are two-dimensional (2D) structures. The well-known nanotubes, as well as nanowires, nanorods and thin films are all classified as 2D structures. Materials that express confinement in one dimension are known as quantum wires. The one-dimension (1D)

structures, quantum wires confine electrons (or holes) in two special dimensions and allow free propagation in the one dimension. Quantum dots express quantum confinement in all three dimensions. That is, all dimensions of the material have nanoscale size and electrons have confined propagation in all dimensions (Figure 2-7). Thus, quantum dots are zero-dimension (0D) structures.[42]–[44]

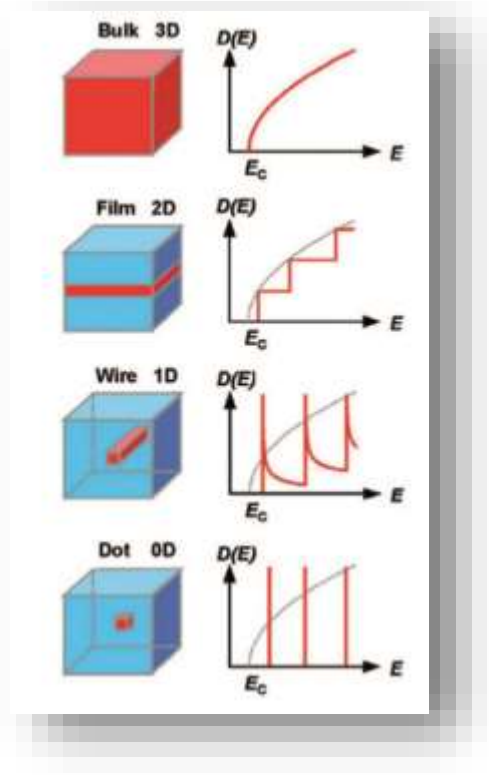

Figure 2-7: Effect of reduced dimensionality. Electrons are confined in a semiconductor (red) with a smaller band gap than the cladding semiconductor (blue). The confinement changes the density of states, depicted as D(E). Ec is the conduction-band edge of a 3D. [44]

By absorbing energy in a form of heat or electromagnetic radiation, the electron of the semi-conductors is *excited* and risen to the conduction band from the valence band. During this action, the electron leaves the atom and leaves behind a hole in the valence band (a hole and an electron pair are called an exciton). The average distance between the hole and the electron is called the exciton Bohr radius. When the size of the semiconductor falls below the Bohr radius the semiconductor is called quantum dots (recall that carbon-based quantum dots are called CDs). The exciton has a limited lifetime and the electron will come back to the valance band and recombine with the hole. The recombination process is normally a radiated process which includes a photon release, a phenomenon called luminescence. [26], [41]

Due to three-dimensional confinement, quantum dots can directly absorb incident light, eliminating the need for special light coupling techniques such as grating. Electrons of quantum dots have longer lifetimes compared to bulk, quantum wells and wires semiconductors because they ideally have density of states that is independent of temperature (Figure 2-7), thus electron distribution is not highly dependent on the temperature. Also, when the band gap energy is higher than the energy of the photon, then the electrons can absorb multiple phonons in attain the excited state. This results in reduced efficiency of scattering mechanism, which in turn counteracts current leakage (also known dark current). [44]

Generally, the smaller the size of the semi-conductor the larger its the band gap. Therefore, high energy is required to excite the CDs (and inorganic quantum dots) and simultaneously higher energy is released when the CDs returns to its resting state. This equates to higher frequencies of light being emitted after excitation of CDs. Moreover, as the semi-conductor grows smaller, the light emitted exhibits colour shift from red to blue (Figure 2-6). [26], [41] In the case of photo-excitation, whereby the electron is excited upon absorbing a photon, the luminescence is referred to as photoluminescence (PL). [38] As anticipated, CDs display excellent photoluminescence. Moreover, CDs can be excited by a chemical reaction, an electrochemical reaction and by an electric current; in which case the luminescence is referred to as chemiluminescence [45], electrochemiluminescence [46], and electroluminescence [47], respectively.

2.3.2.2 Types of luminescence

The relationship between the energy of the absorbed photon and the energy of the photon emitted can be used to classify the types of photoluminescence. In a case where the absorbed and emitted photon has the same energy the photoluminescence is referred to as resonant radiation. Wherein, emission occurs proximately after absorption with the entire process completed in an order of 10^{-9}s and without any significant internal reformation of the photoluminescent material. [48] However, when the photoluminescent material is not in solution or gas phase, an electron band structure may be formed leading to complex secondary emission involving both coherent (elastic modes with zero energy losses) and non-coherent contributions. [49] Also, there is phosphorescence which has a longer lifetime of 10^{-4} - 10^{-2} s. During phosphorescence, the absorbed photon undergoes intersystem crossing into a state with a different spin multiplicity, usually a triplet state. This process is very rare and is referred to as radiative transition. [50] Conversely, fluorescence is the most common type of luminescence

observed [51]; CDs (and quantum dots) generally exhibit fluorescence [1], specifically photoluminescence. [39], [52] During fluorescence the emitted photon has less energy compared to the absorbed photon. This is as a consequence of loss of energy as the photoluminescent material relaxes back to its ground state conformation; process occurs within 10^{-8} to 10^{-4} s. [48]

2.3.2.3 Relation between absorption and emission spectra

Absorption and emission transitions

As mentioned above, the band gap is sandwiched by the valence and conduction band which are made up of vibrational levels. Upon absorbing a photon, the dot is excited from the lowest vibrational level on the valence band to one of the vibrational levels of the conduction band (see Figure 2-8). This transition (T_1) corresponds to the absorption/excitation energy. [26], [41] The potential energy of the excited dot increases with the energy of the absorbed photon. Thus, the dot has more potential to land on a higher vibrational level of the conduction band when the excitation energy higher. Subsequently, the excited dot rearranges to adapt to a conformation that is most favourable in the conduction band. The rearrangement results in loss of energy, thus the excited band drops to a lower vibrational level from the vibrational level it landed on. Eventually, the excited dot drops to the lowest vibrational level of the conduction band before it transits (T_2) back to the conduction. [26], [41] The dot only fluoresces upon transitioning from lowest vibrational level of the conduction band to any of the vibrational levels of the valence band. It is this transition (T_3) that correlates to the emission energy. The dot subsequently goes through rearrangement to adopt to the most favourable conformation of the valence band namely the ground state. Once the dot is completely relaxed, it resides in the lowest vibrational level of the valence band (i.e. ground state). [26], [41] Thus, the fluorescence emission occurs at a lower energy compared to the absorption energy partly due to loss of energy through vibrational relaxation, geometry and solvation rearrangement.

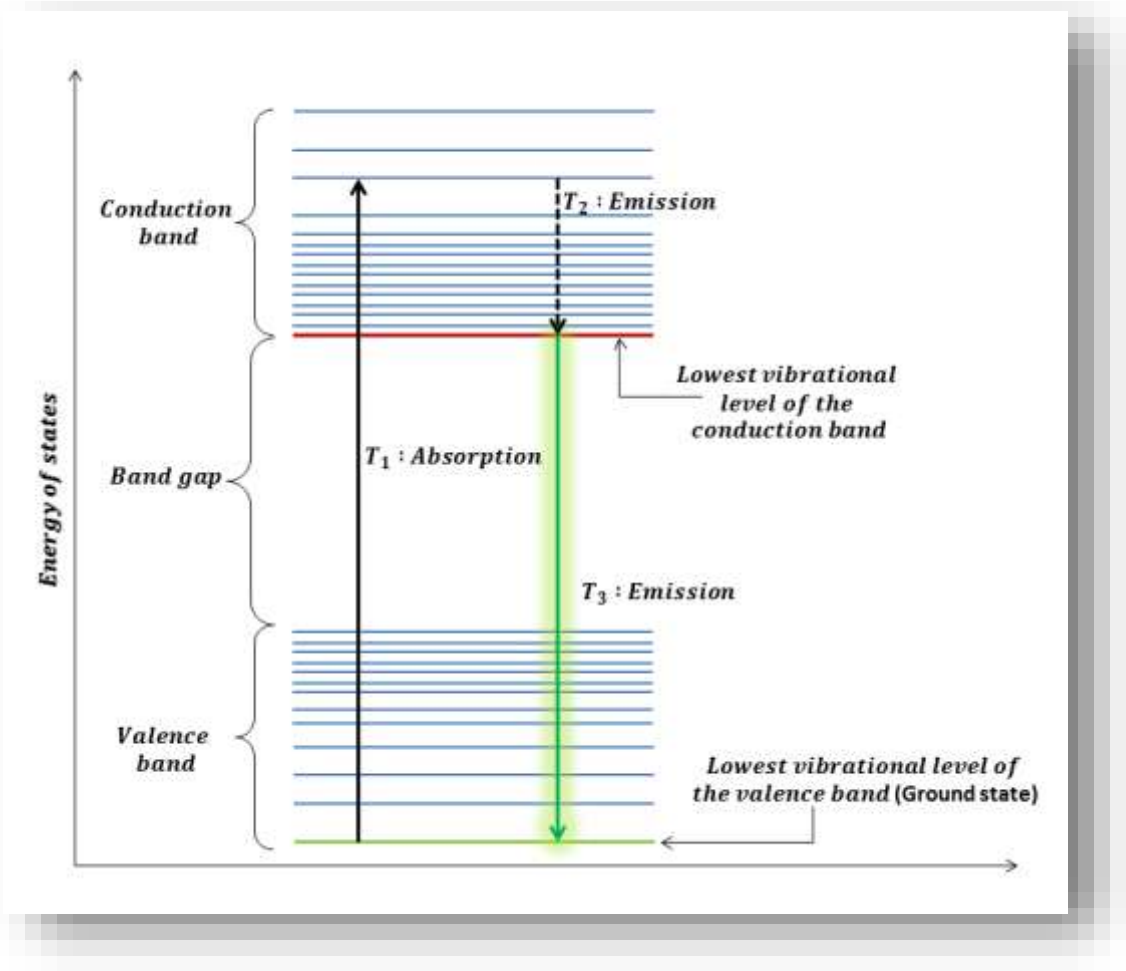

Figure 2-8: Energy diagram of CDs. [53]

Stokes shift

The energy difference between absorption peak and fluorescence emission peak is called Stokes shift. CDs exhibit characteristic large Stokes shift which allow for detection of fluorescence at signal intensity. [38] In bulk semiconductors where energy levels are generally equally spaced, the UV-vis absorption and emission spectra are almost mirror images separated by a small (approximately 10 nm) Stokes shift (Figure 2-9). [54] However, CDs exhibit characteristic large Stokes shift (Figure 2-10) which allow for detection of fluorescence at signal intensity. [38]

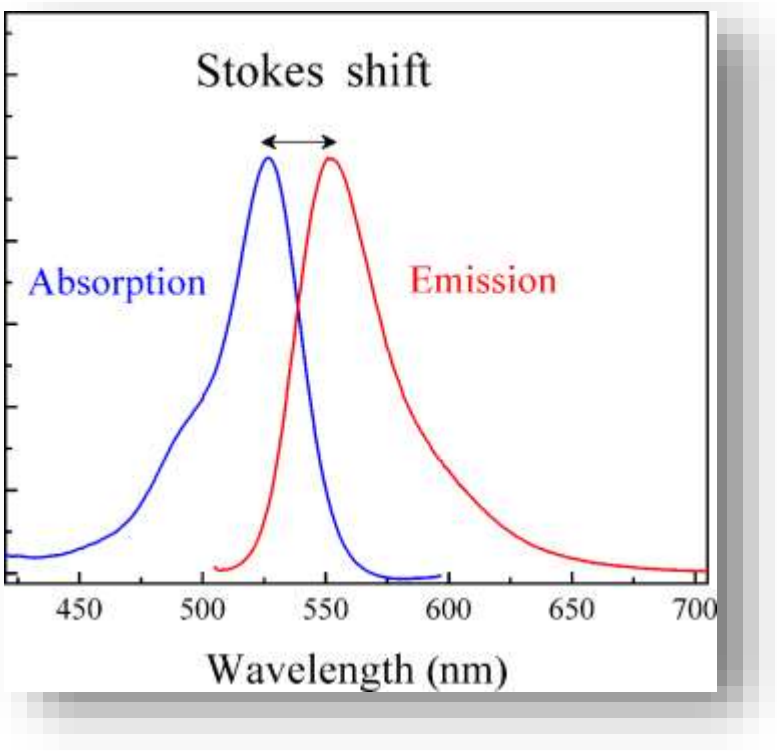

Figure 2-9: Absorption and emission spectra of rhodamine 6G with ~25 nm Stokes shift. [55]

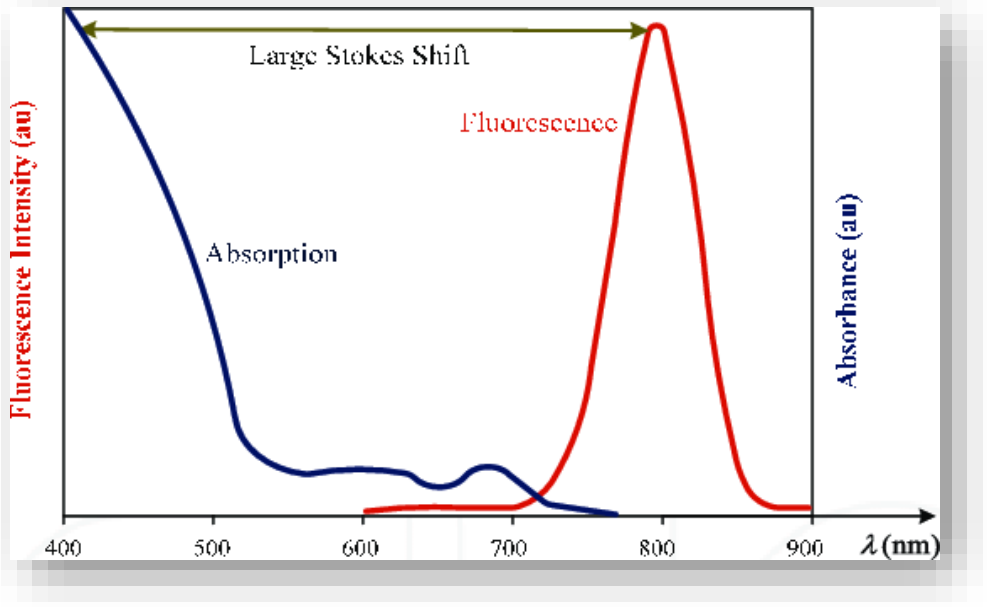

Figure 2-10: Absorption and emission spectra of typical quantum dots with large Stokes shift. [53]

Fluorescence lifetime

As discussed above the distance between an absorption and an emission peak is referred to as Stokes shift and it plays a role in the sensitivity with which CDs can detect an analyte. Another characteristic of CDs that plays a role in the sensitivity feature of CDs sensors is fluorescence lifetime. Fluorescence lifetime is time elapsed between absorption of a photon by a material and its subsequent emission. Longer fluorescence lifetimes are favoured as they aid in easily distinguishing the CDs fluorescence signal and background fluorescence. In general, larger CDs have fluorescence lifetimes because they have more spaced energy levels where the electron-hole pair can be trapped and live longer. [53]

2.3.2.4 Efficiency of fluorescence

Fluorescence quantum yield (QY)

It is critical to evaluation of the optical efficiency of CDs, and other photoluminescence material in general. The optical efficiency of the fluorescence of the semiconductor is quantified as the fluorescence quantum yield (QY). As shown in Equation 2-1, fluorescence QY of a material is the fraction of photons absorbed when the light is shone on material that are emitted as the material luminescence. [53], [56], [57]

$$fluorescence\ QY = \frac{number\ of\ emitted\ photon}{number\ of\ absorbed\ photons} \qquad \text{[Equation 2-1]}$$

In other words, fluorescence QY is a measure of the PL strength of a semiconductor. It is realized that when the fluorescence trait of a material is used for detection of an analyte, then the material should ideally exhibit a high QY for it to have the lowest limit of detection of the analyte. In general, the fluorescence QY of materials can be determined via two approaches namely the absolute and comparative methods. [56], [57] Absolute methods entail either the use optical methods to directly measure a portion of absorbed photons emitted as luminescence or calorimetric methods (photoacoustic, thermal lensing) to directly measure a portion of photons lost by non-radiative recombination. On the other hand, comparative methods are based on comparison of PL measurements of an investigated sample and a luminescence standard under identical conditions. For CDs, the comparative technique based on Equation 2-2 is the most often used method for the determination of fluorescence QY, where a dye with similar properties as the material of interest is as a reference. [56], [57]

$$\mathrm{QY} = \mathrm{QY_{ref}} \frac{\eta^2}{\eta_{ref}^2} \frac{\mathrm{I}}{\mathrm{A}} \frac{\mathrm{A_{ref}}}{\mathrm{I_{ref}}} \qquad \text{[Equation 2-2]}$$

Where, *QY* is quantum yield; η is the refractive index; *I* is integrated emission intensity; *A* is the optical density. The subscript *Ref* refers to the reference fluorophore with known fluorescence QY. [56], [57]

The maximum value of fluorescence QY is 1 however in reality the value is less than 1 for virtually all luminescent materials because there is a larger of number of non-radiative processes that lead to a decrease in the number of emitted photons. The fluorescence QY can be determined in terms of the rate constants of the radiative (k_{rad}) and non-radiative (k_{nr}) processes according to Equation 2-3. [56], [57]

$$QY = \frac{\sum k_{rad}}{\sum k_{rad} + \sum k_{nr}} \quad \text{[Equation 2-3]}$$

The k_{rad} term includes the rate of fluorescence and phosphorescence while the k_{nr} term includes the rate constants of all the non-radiative processes. The lifetimes of the photoluminescence are also related the fluorescence QY of the material. Thus, the fluorescence QY can be expressed in terms of the luminescence lifetimes as shown in Equation 2-4 (provided that lifetime = τf=1/kf). [56], [57]

$$QY = \frac{k_f}{k_f + \sum k_{nr}} = \frac{\tau}{\tau_f} \quad \text{[Equation 2-4]}$$

Photostability and photobleaching

Over time, the fluorescence QY of fluorescent materials may decrease. The leading cause of this is photobleaching. Photobleaching is the photochemical modification (such as cleavage of a covalent bond) of the PL centre of a material that compromises the PL centre's fluoresce ability. CDs are appealing for sensing and other fluorescent spectroscopy because they (and their inorganic counterparts) have been found to be significantly more stable against photobleaching than organic dye molecules. In other words, CDs are photostable. [53]

2.3.2.5 Origin of CDs photoluminescence

The CDs exhibit photoluminescence due to one or more of its inherent features. Firstly, since CDs are 10 nm scale materials, the carbon core of CDs possesses condensed energy levels, and thus exhibit photoluminescence due to quantum confinement. In this case, the PL (in turn the conductivity) of the CDs will be related to the size of the CDs. Secondly, the PL of the CDs may originate from the hybridisation of the carbon backbone and the connected chemical groups i.e. the surface defects introduced by the connections (surface state). This mechanism of the PL can be investigated by studying the PL behaviour of CDs with varying pH and

polarity of solvent; whereby, the PL of CDs may drastically change upon protonation but later be recovered at alkaline conditions. Thirdly, the PL of CDs may rise as a result of the molecule state of CDs (fluorophores on interior of CDs/ of chemical groups connected on the edge or surface of CDs). This mechanism is not ideal because it renders the CDs not photostable. Lastly, PL of CDs may be ascribed to the crosslink-enhanced emission effect (CEE). [31], [58]

To understand the CEE effect, one must appreciate that organic fluorescent materials traditionally have carbon-based pi-electrons as their PL centre building block. These carbon-based pi-electrons are carbon-carbon double or triple bonds. [59], [60] On the other hand, heteroatoms containing double bond (C=O, C=N, N=O, etc.) and single bonds (amino based groups, C-O, etc.) exhibit weak fluorescence but, can show increased PL with suitable immobilisation. The suitable immobilisation can be attained via cross-linking and aggregation. [58], [59] The CEE effect is common in polymer dots (PDs) specifically non-conjugated PDs. That is, there are two main types of PDs, namely conjugated PDs (with carbon pi-electrons in PL centre) and non-conjugated PDs. Figure 2-11 compares the two types of PDs and illustrate the relationship between conjugated PDs and other carbon dots. CEE of non-conjugated PDs can result from formation of covalent bonds, supramolecular interactions and/or rigidity caused be aggregation as illustrated in Figure 2-12. [59], [60]

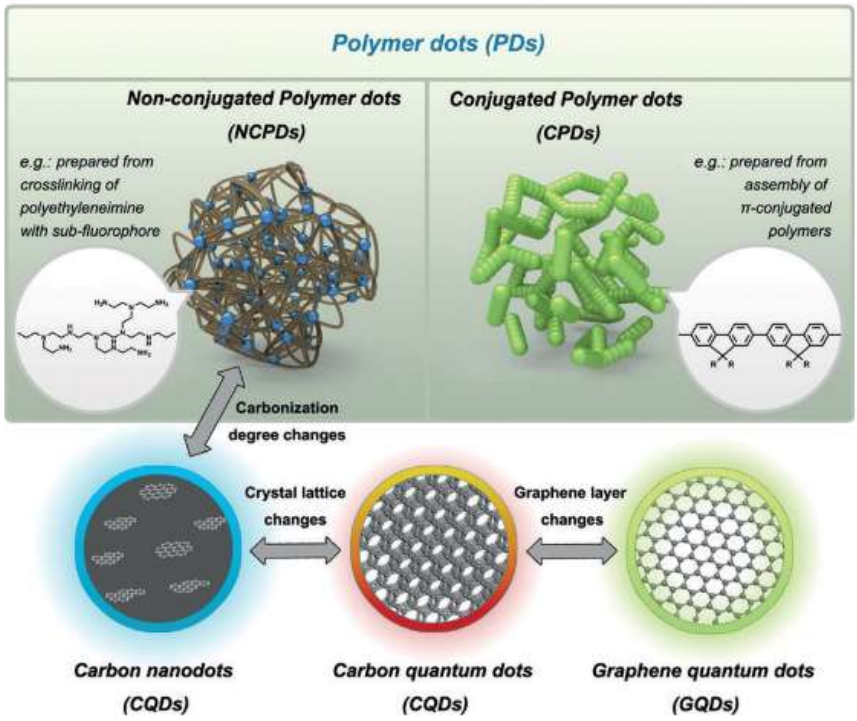

Figure 2-11: Representation of PDs (the PDs always contain CPDs and NCPDs), and the relationship between NCPDs and other CDs. [59]

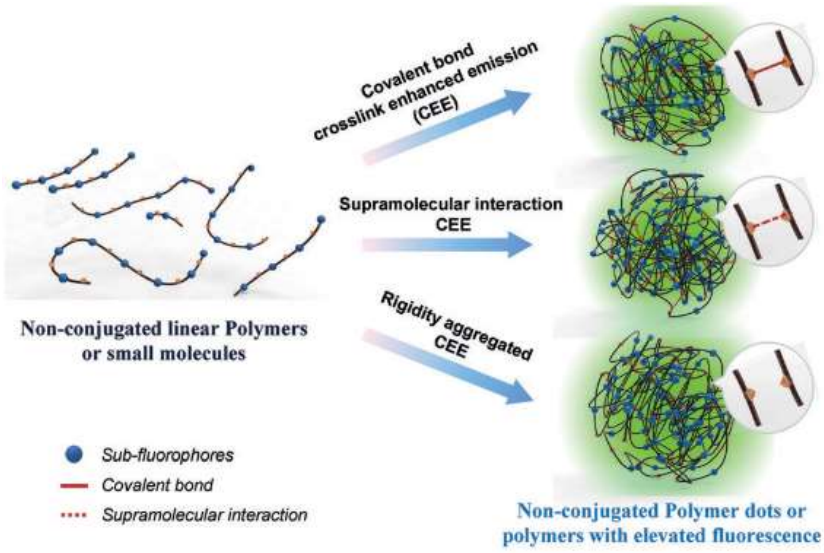

Figure 2-12: Illustration of the three routes that lead CEE effect of the non-conjugated linear polymers. [59]

AIQ and AIE

Aggregation is not only important in enhancing the PL of non-conjugated PDs, but also plays a key role in the PL behaviour of most (if not all) fluorescent materials. This has given rise to

phenomena such as aggregation induced quenching (AIQ) and aggregation induced emission (AIE). [61] AIQ is when fluorescence QY decreases with an increase in the amount of material. It has been studied for over half a century since Föerster's discovery of the concentration quenching effect in 1954. [61] It has been generally observed that materials with aromatic luminophores (PL centres) suffer from AIQ. That is traditional luminophores generally emit significantly strongly in isolation than they do as clusters/aggregates. This is because upon aggregation, the pi-electrons of the individual molecules became in close proximity with each and thus partake in strong pi-pi stacking intermolecular forces. This is particularly observed severely with rod-like or disc like shaped aromatic luminophores. This pi-pi stacking results in formation of non-radioactive channels through which the excited state of such aggregates often uses to decay/relax back to ground state. Consequently, the emission of the aromatic luminophores the aggregated state is extensively quenched. [59], [61]

Often, materials that exhibit AIQ show excellent results at lab scale but fail dismally in application because the aggregated state plays vital roles in sensing, bio-imaging, organic light-emitting diodes, optical waveguide, etc. On the other hand, materials that exhibit aggregation induced emission (AIE) are appropriate for application. These materials may exhibit little or no fluorescence at low concentrations but are very fluorescence in solid state or in high concentrations. The comparison of the AIQ and AIE effect is commonly demonstrated using Perylene and hexaphenylsilole (HPS). As shown in Figure 2-13, Perylene suffers from AIQ while the PL of HPS is enhanced through AIE. In both cases, aggregation is induced by gradually increasing the fraction of water (a poor solvent).[61], [62] As a disc shaped aromatic molecule, upon aggregation perylene forms intense pi-pi interactions resulting in the observed AIQ effect.[61]–[63] On the other hand, HPS show has no emission when well dissolved but emits strongly upon aggregation. [61], [63]

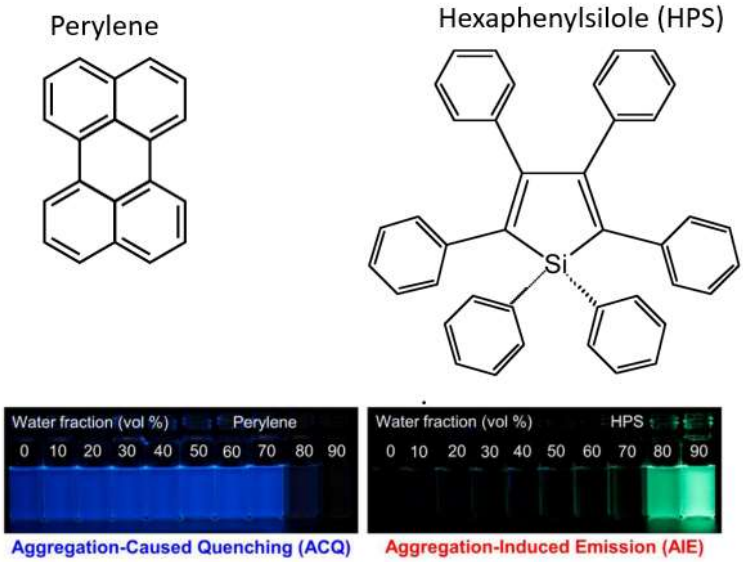

Figure 2-13: The demonstration the AIQ and AIE effects of Pyrelene and hexaphenylsilole, respectively, by gradually increasing the fraction of water (a poor solvent) by Mei et al., [61]

HPS exhibits AIE because in solution sate the active molecular motions along the sigma bonds that join the phenols to the central unit of the HPS act as non-radioactive channels for energetic decay from the excited state to the ground state. However, in aggregated state HPS molecules experience spatial constraints as well as the interact with each other resulting in the restriction of the sigma bonds motions. Thus, the nonradiative decay channels are blocked and emission is cultivated. [63] Researchers have established that the AIE effect is due to the restriction of intramolecular motion which is comprised of the restriction of intramolecular rotations and vibrations.[63], [64] As illustrated in Figure 2- 14, other typical PL centres that exhibit include TPE and THBA. [63], [64]

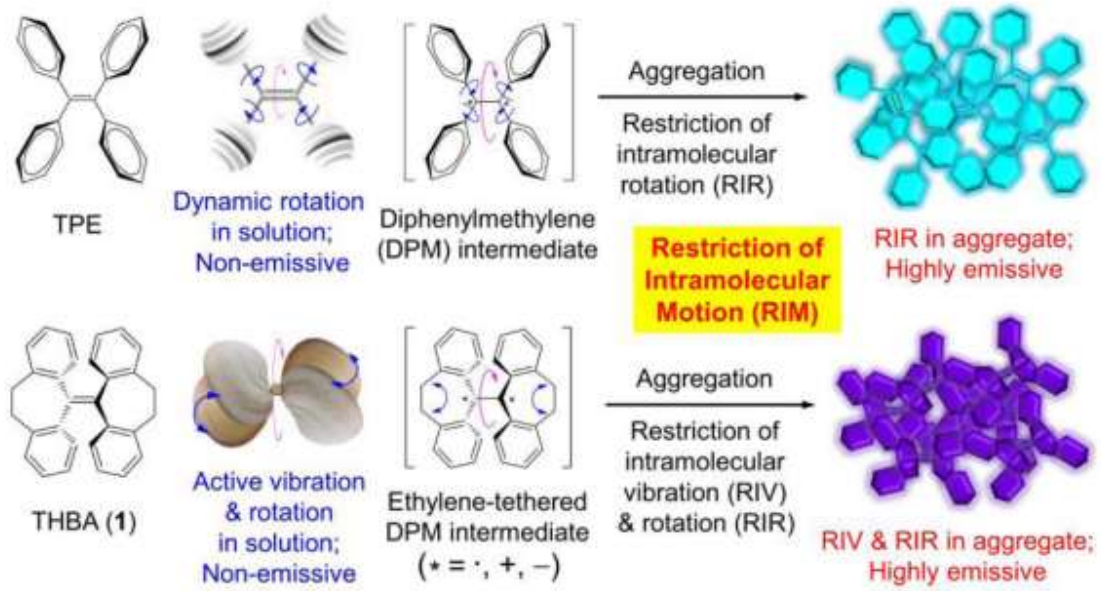

Figure 2-14: Illustration on restriction of intramolecular motion. [64]

2.3.2.6 Synthesis of carbon dots (CDs)

Since their accidental discovery as by-products, the synthesis of CDs has grown in the past decade. As mentioned earlier on, CDs (and any other nanomaterial for that matter), can be synthesised through chemical, electrochemical or physical techniques. These synthetic techniques are essentially achieved through two synthetic approaches, namely bottom-up and top-down procedures which are depicted in Figure 2-15. Moreover, the properties of the CDs obtained can be optimised during preparation or through post-treatment. Post-treatment of CDs essentially the modification of CDs and it is very important because it allows tailoring of CDs for an application.

Figure 2-15: The two approaches for carbon dots synthesis namely top-down and bottom-up approach. [65]

Top-down approach

Top-down essentially entails the etching of CDs crystals from already existing crystals such as carbon nanotubes. In this approach, the synthesis precedes under harsh conditions. The top-down approached proceeds through arc-discharge, laser ablation and electrochemical synthesis methods. [1], [66] During their discovery, CDs were serendipitously synthesised via a top-down approached whereby, the CDs were etched out of carbon nanotubes through an arc-discharge synthesis. [27] In 2006, Sun *et al.*, reported the first synthesis of CDs via laser ablation. They synthesised CDs through mechanical ablation (i.e. hot-pressing) of mixture of graphite powder and cement and annealing argon in argon flow. A Q-switched Nd:YAG laser (1064 nm, 10 Hz) was used for the ablation in the presence of water vapour with argon as carrier gas at 900 °C and 75 kPa. To achieve bright luminescence emissions, the CDs were treated with an aqueous nitric acid solution and subsequently passivated with the $PEG_{1500}N$ and PPEI-EI, respectively. [67]

Then, in 2007 Zhou *et al.*, reported the synthesis of CDs via an electrochemical treatment of multi-wall carbon nanotubes. They synthesised carbon nanotubes with a 30-40 nm diameter on a carbon paper and thereafter subjected them to an electrochemical cell with a degassed acetonitrile solution, 0.1 M tetrabutylammonium perchlorate (TBAP) supporting electrolyte, Pt working electrode, $Ag/AgClO_4$ reference electrode and an applied potential of cycles between -2.0 and 2.0 V at a scan rate of 0.5 V/s. The emergence of CDs was indicated by the colour change of the electrolyte from colourless to brown under day light and to blue under

UV-lamp. Thus, carbon nanotubes were degraded or rather broken down to form CDs with a diameter of 2.8 ± 0.5 nm in diameter as confirmed by high-resolution transmission electron microscopy (HR-TEM). [2] Following this, many researchers synthesised CDs via the top-down approach until they realised the need to implement a greener synthetic method. [68]

Bottom-up approach

Bottom-up approach involves the build-up of CDs crystals from a carbonaceous building block. Herein the carbonaceous material is subjected to external energy such as heating, microwave pyrolysis and ultra-sonication. [1] The bottom-up approach is not only favoured because proceeds via green synthetic procedures but, it also produces nanomaterials with less defects, more homogeneous chemical composition, better long and short-range ordering. Moreover, it precedes via facile synthesis procedures with an abundance of carbon materials to serve as precursors. Thus, the majority of the reported CDs are synthesised through the bottom-up approach via pyrolysis and solvo-thermal synthesis. [1] Pyrolysis synthesis is the chemical decomposition of carbon-based materials through application of heat in the absence (or near absence of oxygen). The synthesis of CDs via pyrolysis normally entails a reflux reaction done under inert atmosphere such as nitrogen [69], [70], hydrogen and argon. Alternatively, CDs can be obtained through pyrolysis by subjecting the carbonaceous starting material to microwave-irradiation; this synthetic process microwave-assisted pyrolysis. [24] Microwave-assisted pyrolysis has an advantage of short synthesis duration. [71]

Solvo-thermal synthesis entails dissolving a carbonaceous material in solvent under high pressure (when the solvent is water, the process is called hydrothermal synthesis). During this process, the carbon source breaks down and upon condensation single nanomaterials are formed through nucleation. Normally, the functional units of the carbon source are retained on the surface of the CDs. Thus, for this project the carbon source with pi-acceptor functional groups will be considered to yield CDs which can interact with the pi-donor analyte, CO. The summary of advantages and disadvantages of the different synthesis procedures are summarized in Table 2-2 below.

Table 2-2: Summary of the advantages and disadvantages of different synthesis methods [71]**.**

Synthesis method	Advantages	Disadvantages
Arc discharge	Easily producible as by-products	Hard to remove impurities Expensive equipment
Laser ablation	Simple experimental setup	Low yield
Electrochemical approach	Low cost, High output, Easy manipulation of reaction parameters	Difficult to dope
Solvo-thermal	Low cost Easy manipulation of reaction parameters	Long synthesis duration
Pyrolysis of precursors (and microwave assisted pyrolysis)	Simple procedure Short synthesis duration	Difficult to scaled Broad size distribution

Modification

One of the appealing properties of CDs is their openness to modification. As mentioned above, CDs properties can be optimised during preparation or post-preparation treatment. The simplest, most trivial post-treatment is physical post-treatment which has to do with subjecting as-synthesised CDs though purification to remove impurities and/or promote a narrow particle size distribution of the CDs. Filtration, centrifugation, gel-electrophoresis and column chromatography have been widely reported in the purification of CDs. [33]

Also, CDs are generally subjected toward chemical post-treatment whereby the chemical structure of CDs is altered. The most widely reported form of CDs chemical post-treatment is surface modification. [1] CDs can be functionalised of passivated depending on type of functional groups that reside on their surface. Functionalised CDs refer to CDs with chemical groups such as hydroxyl, amino groups on the surface. Whereas passivated CDs refers to CDs with polymer chain on the surface. This distinction is necessary because PDs are self-passivated, whereas the CNDs and CQDs are only passivated upon surface modification. Surface modification is necessary for enhancing the photoluminescence of CDs and tuning of

the properties of CDs to make them more suitable for their intended application. For instance, the above mentioned laser ablation as-synthesised CDs were passivated with $PEG_{1500}N$ and PPEI-EI respectively, to enchance/induce their photoluminescence.[67] Then, Tang *et al.*, exploited openness to modification property of the CDs they synthesised to couple an anticancer drug doxorubicin (DOX) as shown in Figure 2-16. [72]

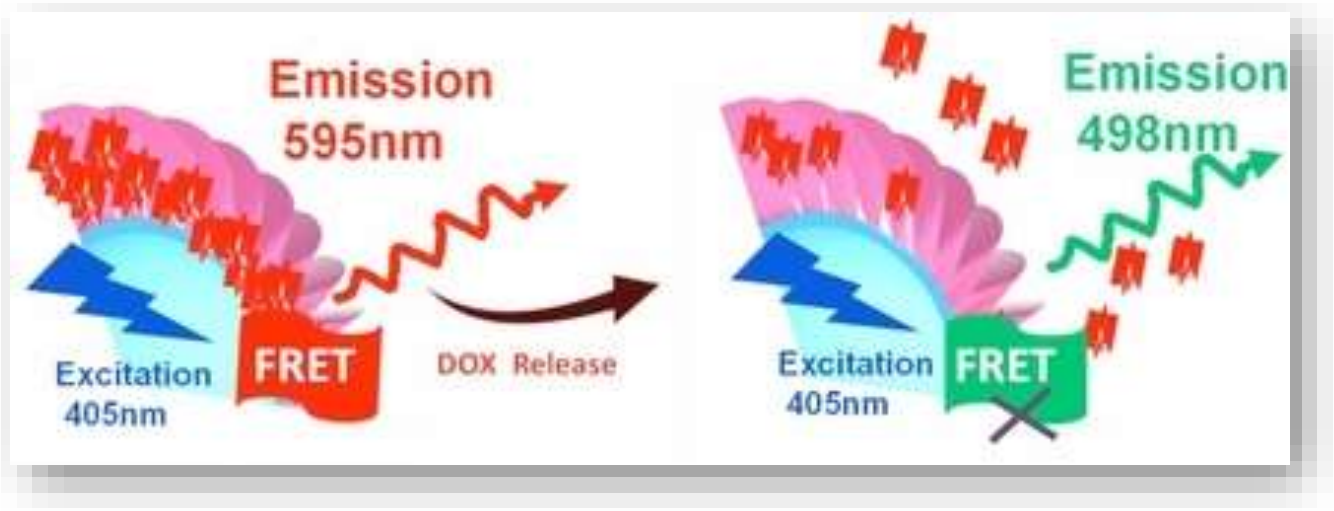

Figure 2-16: A schematic of the CDs/DOX for FRET mechanism for drug tracking and delivery. CDs acts as both a drug carrier and a donor and DOX acts as an acceptor. When DOX is released from the CDs surface, the FRET between CDs and DOX is terminated, recovering the short wavelength [72]

They were able to apply these CDs in drug delivery and monitoring drug release. The drug tracking occurred via fluorescence resonance energy transfer (FRET) between CDs and DOX. In this case, CDs act as a donor chromophore and in their electronic excited state, transfer energy to DOX (an acceptor chromophore) through non-radiative dipole-dipole coupling. This FRET resulted in the shift the PL of CDs to longer wavelength. Upon acid catalysed dissociation of DOX and CDs (drug release) at the target site, the PL of CDs at short wavelength is recovered. [72] Figure 2-17 is a boastful illustration of the incredible modifiability of CDs as it shows a more intricate surface modification of CDs conducted by Cheng *et al.*, [24] They started with NH_2 functionalised CDs, modified them to yield Br functionalised CDs, then exchanged the Br chemical group for polymer 1 and lastly linked polymer 2 forming polymer CDs. [24]

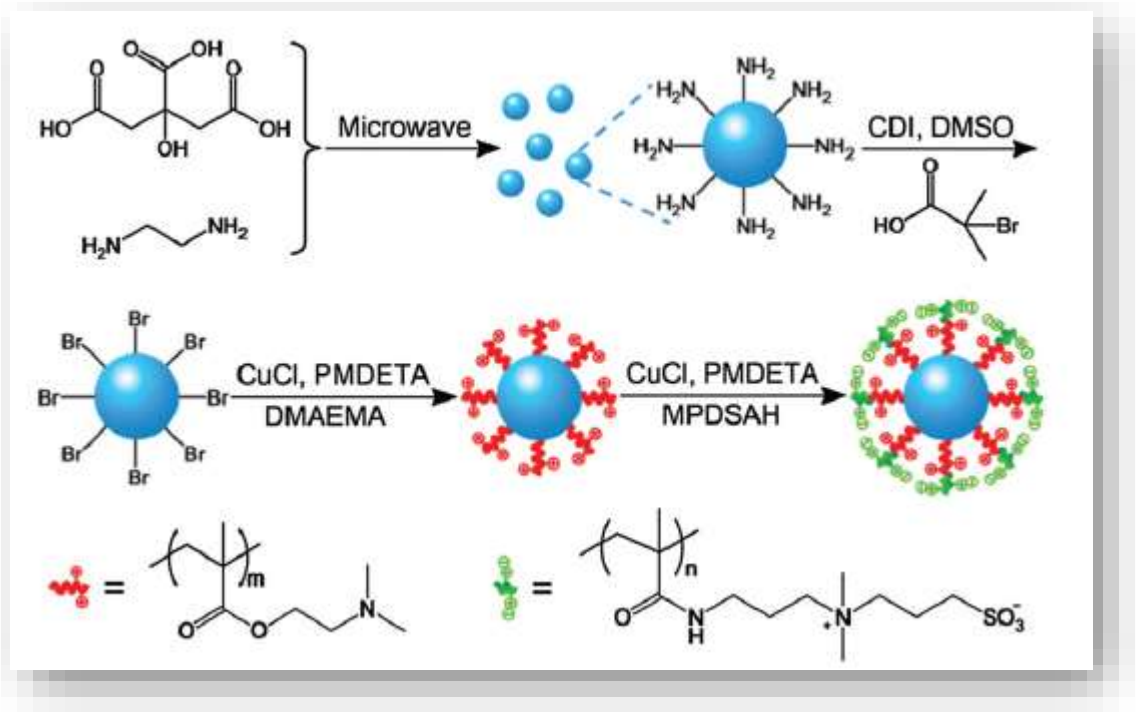

Figure 2-17: A schematic illustration of the synthetic route of NH2-C-dots, Br-coated C-dots, and polymer dots. DMSO and PMDETA dimethyl sulfoxide and penta-methyl-diethyl-enetriamine, respectively, and were used as primers. [24]

2.3.3 CDs in sensing

2.3.3.1 Principle of CDs sensors

The physiochemical property of interest for application of CDs in sensing is PL. PL is the ability of a material to emit light after absorbing electromagnetic radiation. CDs can sense analytes because their PL is highly dependent on their environment. It is proposed that the dependency of the PL of the CDs on their environment is as a result of the surface functional groups of CDs interacting with molecules (or analytes) in the vicinity CDs via non-covalent or ionic bonds. This interaction probably alters the nature of the hybridisation between the carbon backbone and the connected chemical groups of CDs; which would ultimately alter the PL nature of the CDs. As such, sensing of an analyte (molecule of interest) is achieved through monitoring the change of PL of the CDs in response to stimuli; whereby the PL of CDs is either quenched or enhanced in presence of an stimuli (i.e. analyte). [73], [74] In addition, when the amount of analyte is directly related to the change in PL intensity of CDs, the analyte can be both detected and quantified (Figure 2-18). CDs have been proven to sense metal ions and inorganic salts such as Hg^{2+}, Cu^{2+}, Fe^{3+}, Pb^{2+}, Ag^{+}, Cr (VI), $C_2O_4^{2-}$, PO_4^{3-}, CN^{-}, F^{-}, ClO^{-} and I^{-}

. Further, CDs have proved to detect complex molecules such as DNA, methyl parathion and ascorbic acid. [73], [75], [33], [76]

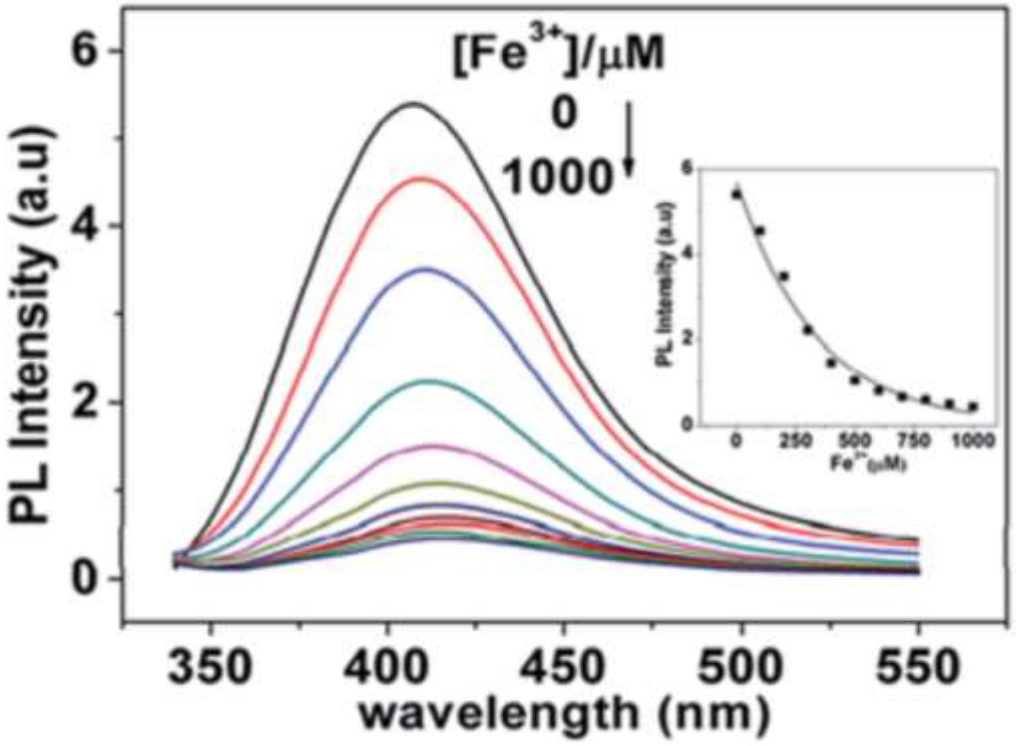

Figure 2-18: Illustrated Fe^{3+} concentration dependent PL quenching of CDs. Whereby CDs PL intensity decreases with increasing Fe^{3+} concentration. [73]

The change in PL nature of the CDs-based fluorescence sensing manifest via one of three major mechanisms, namely photo-induced electron transfer (PET), Forster resonance energy transfer (FRET), and inner filter effect (IFE). PET and FRET are the most common manifestations of PL change of the CDs-based fluorescence sensing, with IFE mostly limited to material with extremely high optical density such as quinine sulphate. PET manifests when the interaction between CDs and the analyte form a complex. Reductive PET is when the CDs acts as an electron acceptor for the electron donor analyte. Whereas, oxidative PET is when the CDs acts as an electron donor for the electron acceptor analyte. PL quenching of CDs occurs during oxidative PET whereby the excited electron on CDs are transferred (along with their energy) from the conduction band of CDs to valence band of the analyte, resulting in reduced fraction of the electromagnetic radiation being emitted when CDs return to the ground state. PL enhancement occurs during reductive PET whereby electron of the analyte are transferred to valence band of the CDs resulting in a higher of electrons excited, which in-turn increase the

ratio of electromagnetic radiation being emitted. It's worth noting that the excited complex can return to the ground state without the release of photons. [71]

Another commonest manifestation of PL change of CD-based fluorescence sensors is FRET. FRET is a non-radiative energy transfer process originating from dipole–dipole interactions between donor and acceptor molecules. As seen in the earlier on discussed CDs/DOX drug tracking and delivery scenario, quenching occurs when CDs act as an electron donor and donate electrons from their conduction band to an analyte. FRET results in reduced fraction of the electromagnetic radiation being emitted when CDs return to the ground state. Conversely, PL enhancement occurs when CDs act as electron acceptors during FRET and gain electron analyte. [71]

PL Quenching can be either be static or dynamic. Dynamic quenching process occurs in the excited state only and thus is not observed in emission spectra of CDs. On the other hand, Static quenching affects the ground-state of CDs and is apparent on the emission spectra of CDs. [71] Also, PL quenching can occur in two ways (1) the PL wavelength can be increased i.e. decrease in energy of photon being emitted, and (2) the PL intensity can be decreased (i.e. decrease in number of photons being emitted. In CDs/DOX, FRET resulted in long wavelength emission by the CDs . [72] Conversely, during detection of Fe^{3+} FRET resulted in reduced PL intensity of the CDs. [73]

2.3.3.2 Sensing mechanism of CDs

The simplest sensing mechanism is when the PL is either turned-off (quenched) or turned-on (enhanced) in the presence of an analyte (Scheme 2-4.a). The sensing mechanism of CDs can be complex as observed with an "off-on" CDs type of sensor. In this system, the PL intensity of the CDs is quenched by one molecule and recovered by the analyte. The off-on CDs sensors were established through the observation that the PL of CDs may be switched off by metals and recovered upon introduction of chelators to the system (Figure 2-19a).

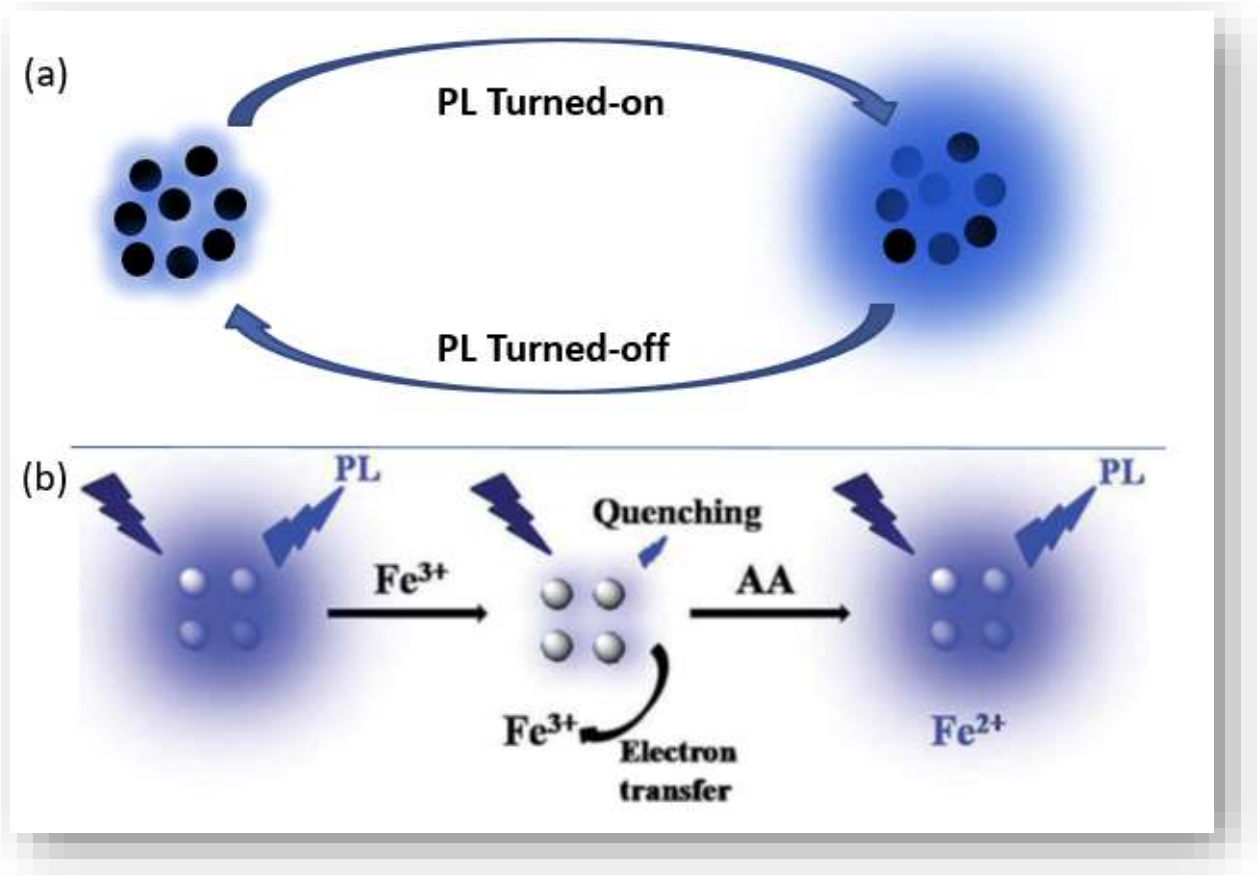

Figure 2-19: Illustration of the AA sensor based on the off–on fluorescent probe of CDs adjusted with Fe^{3+}. [73]

Several molecules have been detected using this system. This includes the detection of glutathione where Ag (III) was the PL off switcher. It has been suggested that the metals quench the PL intensity of CDs by causing the CDs to aggregate and that the chelators recover the PL by forming complexes with the metals. However, the mechanism of sensor functionality is specific to the system. For instance, ascorbic acid has been detected through PL recovery which was earlier quenched by Fe^{3+}, in this system the PL quenching by Fe^{3+} is not through aggregation of the CDs but rather it is attributed to non-radiative electron transfer from an excited state of CDs to the d orbital of the Fe^{3+} ion. However, upon addition of ascorbic acid, the PL of CDs is recovered because Fe^{3+} is reduced to Fe^{2+}. [73]

2.4 Characterisation of carbon nanodots (CDs)

Transmission electron microscopy (TEM) is the primary technique for proving CDs. It gives information on particle morphology, size distribution and crystal organisation. With better resolution, high-resolution TEM (HRTEM) permits the visualisation of graphite lattice planes of the carbon core. *X-ray diffraction* (XRD) evaluates the crystallinity of the crystalline carbon

core of CDs by providing information upon unit cell dimensions and crystal spacing. *Raman spectroscopy* is used to determine the graphitic nature of the carbon nature of CDs carbon core and the relative abundance of the core carbon atoms and surface atoms. This is achieved through assessing the ratio of intensities of the D and G band (D band which arises from disoriented sp^2 carbon whereas G band rises from crystalline graphite carbons, they occur around 1350 and 1600 cm^{-1} respectively. [1]

The nature of the surface of CDs can be studied using *X-ray photoelectron spectroscopy (XPS)* and *Fourier transform infrared (FTIR) spectroscopy*. XPS can be used to determine the atomic units on the surface of CDs. On the other hand, an FTIR spectrum has vibrational band which are characteristic of functional units on the surface the CDs. The optical property of the CDs is probed by *UV-vis spectroscopy and Photoluminescence spectroscopy* the absorption of light and photo excitation-emission properties of the CDs are evaluated. This photoluminescence (PL) property of the CDs is exploited for sensing application, by monitoring it in the presence of an analyte. [15], [25]

The PL strength of the material is measured by *Fluorescence Quantum Yield (%QY)*; which is the ratio of number of photons absorbed to number of photons that are subsequently emitted by a photoluminescent material. The *%QY* of CDs is determined in reference to a dye with known %QY. It is important to note that even though UV-vis and PL spectroscopy measurements are concentration depended, %QY is concentration independent.

3 Experimental procedure

3.1 Introduction

This chapter details the experimental procedure followed to synthesise and characterise CDs in this project. There are two main sections to this work. Firstly, the development of the synthesis method of highly photoluminescent CDs is tackled where CDs are synthesised from three carbon precursors (sucrose, chitosan and PEG_{400}). In this section, the synthesis proceeded via the autoclave, microwave and the reflux method. The second section is a paramedic study of the hydrothermal synthesis of highly photoluminescent CDs using PEG and is comprised of four sub-sections wherein the concentration of PEG, the reaction time, solvent and molecular weight of PEG are respectively varied. All the materials were purchased at Sigma Aldrich, while all the synthesis was done at the Wits University. On the other hand, characterisation of the synthesised CDs was done at Wits University, North-West University (NWU) and Council for Scientific and Industrial Research (CSIR).

3.2 Development of the synthesis method of highly photo luminescent CDs

3.2.1 Sucrose

Three solutions were prepared by dissolving a mass of 20 g of sucrose in a volume of 40 mL oleic acid. The first solution was placed in a Teflon cup, and heated at 215 ℃ in an autoclave for 5 hours. The second solution was subjected to an irradiation treatment in a microwave oven for 20 minutes at 700 W. The third solution was placed in three-neck round bottom flask and refluxed in an oil bath at 215 ℃ under nitrogen protection and vigorous stirring for 5 hours (Figure 3-1). After cooling to room temperature, volumes of 100 mL water were added to the reaction contents in order to disperse CDs in the respective colloidal solutions. Excess oleic acid was extracted by washing solution 3 times with 30 mL fractions of hexane for each of the reaction contents. The resulting respective brick-red CDs solutions were purified by filtering with a micro-filter of 0. 22 μm pore-size and dried in an oven at 60 ℃ to obtain orange-brown and dark brown solid products for the reflux and microwave synthesised CDs respectively. The autoclave synthesised CDs remained suspended in water.

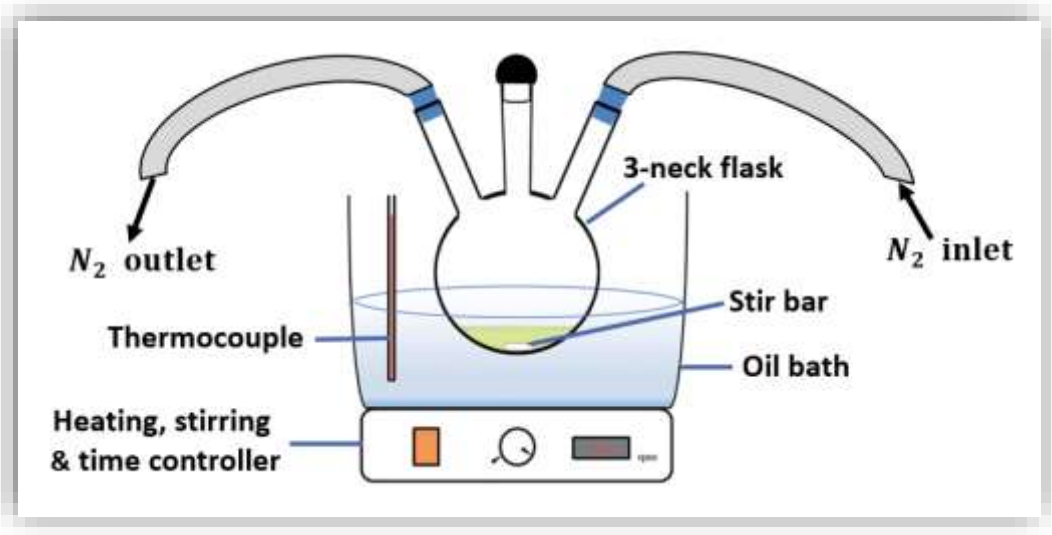

Figure 3-1: Schematic representation of the reflux method set-up.

3.2.2 Chitosan

A mass of 0.3 g of chitosan was added to a volume 30 mL 2% acetic acid solution. The contents were placed in a microwave oven for 18 minutes at 700 W. On the other hand, a mass of 0.7 g of chitosan was dissolved in a volume of 25 mL ethanol placed in a Teflon cup, and the contents were heated at 200 ℃ in an autoclave for 6 hours. After cooling to room temperature, both resulting solutions were respectively centrifuged for 15 minutes at 14000 rpm; the supernatant was filtered through a micro-filter with a pore size of 0.22 µm. The resulting brick red solutions (green under UV light) were heated to boil and evaporate the solution, water. Thereafter, black solid products were obtained. In addition, a mass of 10 g chitosan was added to 150 mL 2% acetic acid solution. The contents placed in three-neck round bottom flask and refluxed in an oil bath at 200 ℃ under nitrogen and vigorous stirring for 6 hours. The produced colloidal solution was cooled to room temperature and filtered with a micro-filter of 0. 22 µm pore size to purify the CDs. The resulting yellow solution was dried in the oven at 60 ℃ for 36 hours to obtain a dark brown gel-like product.

3.2.3 PEG

A 1:1 volume ratio solution of PEG_{400} and water was placed in a Teflon cup, and heated at 215 ℃ in an autoclave for 5 hours. Then, two solutions were prepared by mixing a PEG_{400} and water in a 3:1 volume ratio (9 ml of PEG_{400} and 3ml of water). The first solution was subjected to irradiation treatment in a microwave oven for 5 minutes at 700 W. The second solution was refluxed in an oil bath at 215 ℃ under nitrogen protection and vigorous stirring for 5 hours.

After cooling to room temperature, the resulting respective brick-red CDs solutions were purified by filtering with a micro-filter of 0.22 μm pore size. The resulting, respective brick-red CDs remained dispersed in water after being left to dry in an oven at 60 ℃ for several days.

3.3 Hydrothermal synthesis of highly photo luminescent CDs using PEG: A paramedic study

3.3.1 Variation of volume percentage of PEG_{400} to water

In order to study the effect of the concentration of the precursor on the production of CDs, mixtures of PEG_{400} and water were made at varied volume % PEG_{400} (25 %, 33 %, 50 %, 67 %, 75 % and 100 % PEG_{400}) and respectively subjected to hydrothermal treatment. The mixtures were placed in a Teflon cup, heated in an autoclave at 215 ℃ for 5 hours. Once the reactions were done and had cooled to room temperature, the resulting colloidal solution was filtered with a micro-filter (pore size= 0. 22 μm) to yield purer CDs dispersed in water.

3.3.2 Variation of reaction time

On the other hand, mixtures of 25 % PEG_{400} and water were also placed in a Teflon cup, heated in an autoclave at 215 ℃ for various reaction times (1, 2, 3, 4, 5 and 12 hours) in order to investigate the effect of reaction time on CDs synthesis. Once the reactions were done and had cooled to room temperature, the resulting colloidal solution was filtered with a micro-filter (pore size= 0. 22 μm) to yield pure CDs dispersed in water.

3.3.3 Variation of solvent used during synthesis

Mixtures of 25 volume % PEG_{400} with various solvents (DCM, acetonitrile, ethylene glycol, Chloroform, DMSO, 1-butanol, 2-butanol and ethanol) were prepared and subjected to solvo-thermal treatment in order to probe the role of different solvents on CDs synthesis. The mixtures were placed in a Teflon cup, heated in an autoclave at 215 ℃ for 5 hours. Once the reactions were finished and had cooled to room temperature, water was added on the resulting colloidal solutions. The excess solvent was extracted using hexane fractions to yield CDs dispersed in water. Then the excess water was evaporated with a rota- evaporator and resulting brown contents was left in an oven (set at 70℃) to dry.

3.3.4 Variation of molecular weight of the PEG precursor

A mass of 0.2 g PEG (of varying molecular weight of 1500, 4000, 6000, 10 000, 12 000 and 35 000 respectively) was mixed with a mass of 0.4 g citric acid. It should be noted that these high molecular weight PEGs are in solid phase at room temperature. As such, the mixture was

first ground to yield a uniform powder. The powder was placed in the oven which was ramped to 215℃ for 45 minutes and the reaction was run for 1 hour and 30 minutes at this temperature. Thereafter, the reaction was allowed to naturally cool to room temperature. The resulting brown product was dissolved in water, the bigger particles were separated out using sedimentation, then the excess water was evaporated with a rota- evaporator and resulting viscous liquid was left in an oven (set at 70℃) to dry.

3.4 Characterization

3.4.1 TEM

CDs samples were prepared by dispersing a small amount in a solvent and drop casted onto a carbon coated copper grid, and the grid was dried in ambient air for 45 min before inserting it in the transmission electron microscope (Tecnai Spirit T12 instrument at 120 kV). On the other hand, the solid phase synthesised CDs samples were analysed by high-resolution transmission electron microscopy (HRTEM) using a Tecnai G2 30ST at 200 kV. The captured images were processed and analysed using Image J 1.48v software and the image analysis results were interpreted using the Origin 8.50 software.

3.4.2 PL and UV-vis spectra

The CDs samples were diluted in water and the UV–vis absorption spectrum was measured using the Varian Cary 500 UV-vis NIR spectrophotometer. Subsequently, the photoluminescence emission was measured using Cary Eclipse Photoluminescence spectrometer for each CDs sample, respectively.

3.4.3 FTIR spectra

The FTIR spectrum was measured using the Bruker Vector 22 FT-IR spectrometer. The measurements were done under ambient conditions, scanning the CDs sample 4000 and 500 cm^{-1}. The analysis of the resulting FTIR spectra was done to determine the functional groups of CDs.

3.4.4 Quantum yield measurements

The quantum yield of the CDs was determined using the a|e freeware which calculates QY using following equation [56], [57]:

$$QY = QY_{ref} \frac{\eta^2}{\eta_{ref}^2} \frac{I}{A} \frac{A_{ref}}{I_{ref}}$$

The quinine sulphate was dissolved in 0.1 M H_2SO_4 (refractive index (η) of 1.33) and CDs were dissolved in deionized water (η = 1.33). Where, *QY* is quantum yield; *I* is integrated emission intensity; η is the refractive index; *A* is the optical density. The subscript *R* refers to the reference fluorophore of known QY. At room temperature and 350 nm excitation wavelength, quinine sulphate in 0.1 M H_2SO_4 has a QY of 58%. The a|e freeware is a function that runs on MatLab.

3.4.5 %By-product determination

Since, the TEM images revealed the presence of relatively larger particles, carbon nanospheres (CNS), in CDs samples. The percentage of the by-product in the TEM images was determined using the equation below where #CNS is the number of CNS, #CDs is the number of CDs and k is the ratio of the CNS to CDs particle size. K accounts for the fact that the differently sized particle occupy different areas on the TEM image. An illustration of the determination of the %by-product is shown in Figure 3-2.

$$\frac{\#CNS}{\#CNS+\frac{\#CDs}{k}}$$

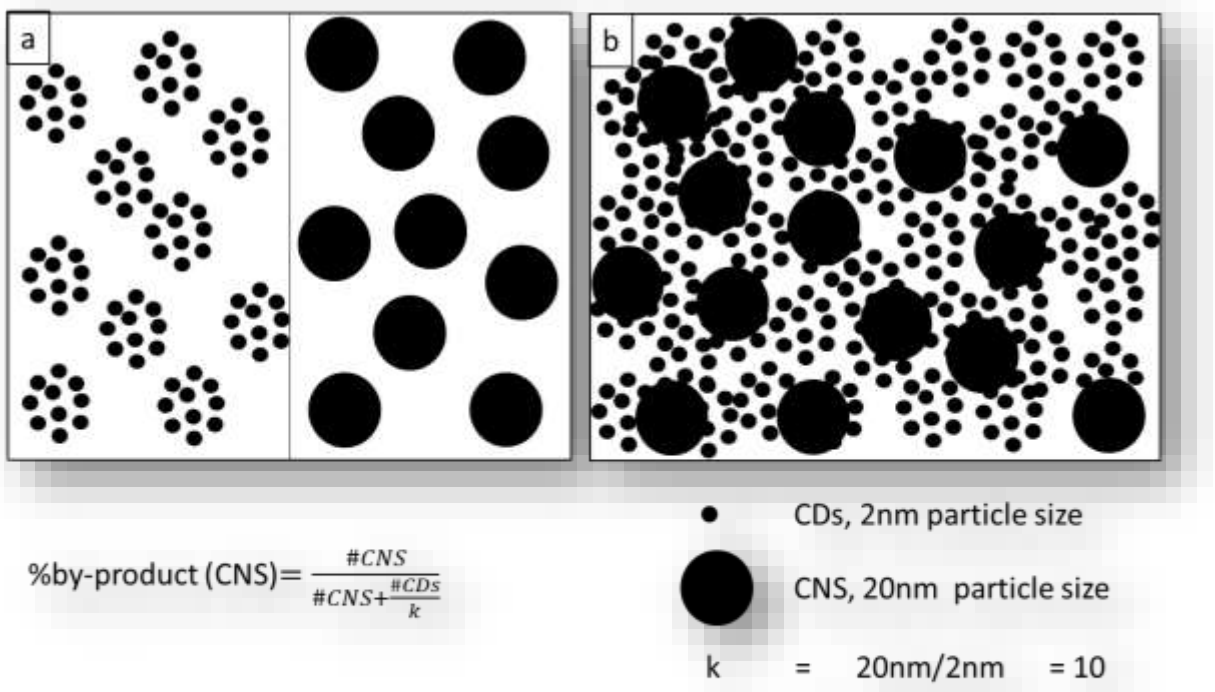

$$\%\text{by-product (CNS)} = \frac{\#CNS}{\#CNS + \frac{\#CDs}{k}}$$

	a	b
Count of particles	CDs = 100, CNS = 10	CDs= 328, CNS= 14
%by-product	50 %	30%

Figure 3-2: Illustration of the %by-product calculation

4 Development of the synthesis method to make highly photoluminescent CDs

4.1 Introduction

It has been realised that the properties of CDs depend on the reaction conditions as well as the purification procedures used post synthesis. [77]–[84] Even though, CDs are relatively new materials, there are many reports on their synthesis in literature. [1], [85] However, there are few reports on the optimisation of the conditions used to achieve the best synthesis conditions. [1], [86] Moreover, there is no well-developed standardised methods for the synthesis and/or modification approach for tuning the properties of CDs. [1], [86] In this study, the synthesis procedure to make CDs was explored by investigating three different preparative methods. These were an autoclave, a microwave and a reflux set-up method. Three different precursors namely, sucrose, chitosan and polyethylene glycol, were also used in the three synthesis procedures. The method-precursor couples that produced CDs with high fluorescence quantum yield and purity were used in further optimisation studies (Chapter 5).

As discussed in the literature review (Chapter 2), the bottom-up synthesis to make carbon dots entails the use carbonaceous precursors to build-up CDs. With the many carbon-based materials that earth offers, researchers have used many different carbon precursors to make CDs. [1], [58], [86], [87] Conjugated carbon precursors, such as saccharides, have been explored extensively for the synthesis photoluminescent CDs since carbon based conjugated chemical groups are well known photophores. [86] Though, the synthesis of CDs from non-conjugated carbon precursors such as citric acid and linear polymers have also been reported. [58]

In an effort of synthesising CDs that can interact and detect CO, the choice of precursor was narrowed down to carbon precursors with pi-acceptor functional groups since CO is a pi-donor. [88], [89] Following this, sucrose, chitosan and poly(ethylene) (PEG) which have -OH as the pi-acceptor functional groups were chosen to be explored as carbon precursors for the synthesis of CDs in this study (Figure 4-1). [89] Sucrose is a commonly found disaccharide consisting of two carbon rings, namely glucose and fructose. [86] CDs synthesised from sucrose have been reported to highly photoluminescent. [70], [86] An important issue relating to CDs is their environmentally friendly nature. [1], [90] As such, it comes as no surprise that reports of CDs

synthesised from waste material is substantial in literature. [90]–[93] Following this trend, chitosan was investigated for CDs synthesis in this study. Chitosan is a polysaccharide made from treating the chitin shell of lobsters, crabs, shrimps and other crustaceans with an alkaline solution. [94] Conversely to sucrose and chitosan, PEG is a linear (polymer) carbon precursor. [95] PEG is commonly used as a capping agent and was chosen to be explored as a carbon precursor for CDs due to its readily availability and the growing interest of using polymers to synthesise self-passivated CDs.[86], [96]

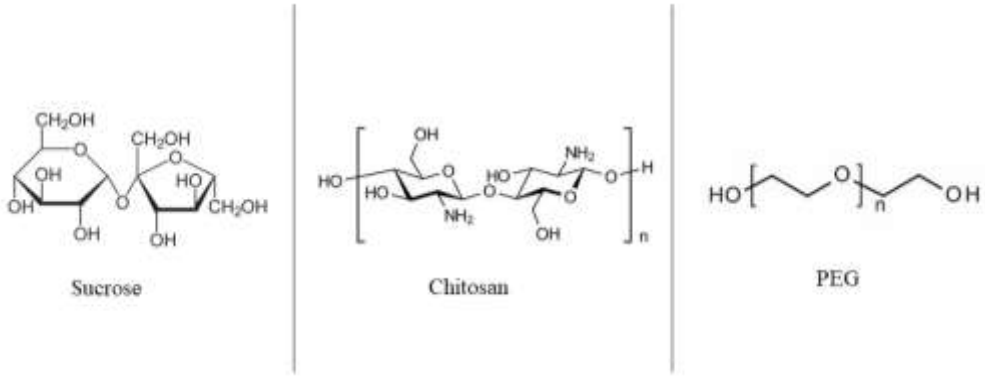

Figure 4-1: The carbon precursors investigated for the synthesis of CDs

The synthesis proceeded via three methods namely, the autoclave method, the microwave and the reflux method. The microwave assisted hydrothermal synthesis is very popular method for synthesising CDs as it involves very short reaction times. [1], [85], [87] The autoclave method has been commonly used in the synthesis of carbon nanoparticles alongside the CVD and reflux method, thus it comes as no surprise that CDs synthesised using the autoclave method are substantially reported in literature. [1], [71], [97]–[99] On the other hand, the CDs synthesised from the reflux method are not commonly reported in literature. [70], [87] Nonetheless, of the chosen methods, the reflux method allows easy adjustment of the gas type/flow under the reaction conditions. See Figure 4-2 below for the reactors used to investigate the synthesis of CDs; the reaction set-ups are described in chapter 3.

Figure 4-2: The reactors investigated for the synthesis of CDs

4.2 Results and discussion

The experimental procedure used to synthesis CDs from sucrose, chitosan and PEG, respectively, using the autoclave method was detailed in chapter 3 and summarised in Figure 4-3. As shown by the schematic diagram in Figure 4-3, the synthesised CDs appeared brick red under day light and milky green under UV light exposure due to their particle size dependent fluorescence. [86], [100]–[102] Crystallising CDs out of solution proved to be a challenge. Thus, majority of the CDs samples were not obtained in solid phase. In cases were the CDs were obtained in solid state, the yields were very low (Table 4-1). Nonetheless, the obtained %yields were comparative with %yields of CDs that are reported in literature. The characterisation of these CDs was thus limited to liquid state characterisation techniques; these techniques could be used to give qualitative data. Ideally, the product is required in solid state as this makes characterisation of the CDs easier and more importantly, this phase is desired for the testing of CO-sensing ability of the CDs.

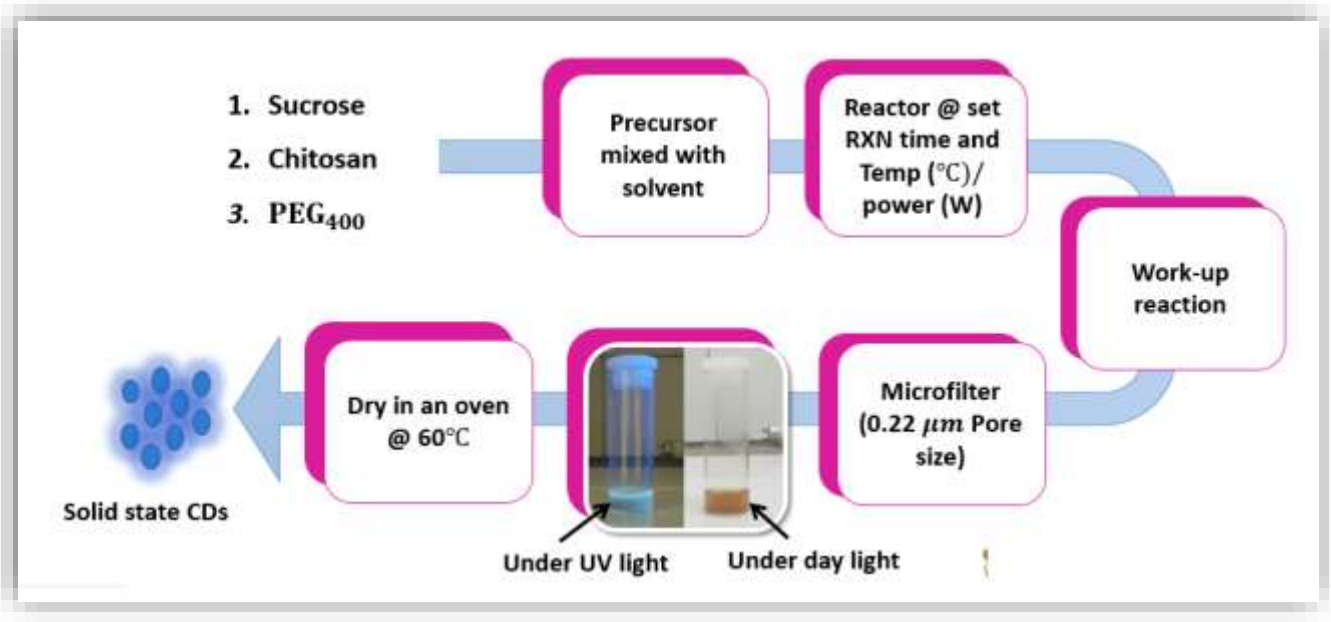

Figure 4-3: Schematic diagram showing the synthesis of CDs from three different precursors.

Table 4-1: The physical state and % yield of the CDs.

method/precursor	Autoclave	Microwave	Reflux
Sucrose	Gel (yield~5 %)	Solid, (yield=10 %)	Solid (yield=7.5 %)
Chitosan	Solid (yield=7.1 %)	Gel (yield~2 %)	Solid (yield=8%)
PEG_{400}	In solution	In solution	In solution

4.1.1 CDs from sucrose

4.1.1.1 Synthesis

As mentioned above, sucrose was used as a precursor to synthesise CDs via the solvothermal reactions which proceeded using three different rectors (autoclave, microwave and reflux). Oleic acid served as a "hot solvent" during the synthesis of CDs similar to reports on caramelisation of sucrose, hydrothermal reactions of glucose, and production of CDs from other sucrose analogues. [70], [103], [104] Other fatty acids can be selectively used as a solvent depending on the melting point of the saccharide precursor. [70] A high concentration of sucrose was used to promote a single burst of nucleation to yield uniformly sized nanoparticles. [70] CDs were produced across all three explored methods at yields of 5, 10 and 7.5% for the autoclave, microwave and the reflux method, respectively. Though these yields are small, they

are comparative with yields most reported for CDs synthesis. [100], [105]–[108] However, they fall short on the CDs yield of 41.8% that is reported by Cheng *et. al.*, where a similar reflux method of the synthesis of CDs from sucrose was conducted [70]. It is not clear why the values obtained in this study were so much lower than those of Cheng *et. al.*, under similar reaction conditions (sucrose as carbon precursor, oleic acid as solvent and refluxing under nitrogen purging). [70]

4.1.1.2 TEM images

The synthesised CDs were visualised under TEM, and the captured micrographs are shown in Figure 4-4 alongside the particle size distribution curves of the synthesised CDs. CDs with particle sizes of 10.41±2.42 nm, 2.83±0.62 nm, and 6.31±1.62 nm were produced using the autoclave, the microwave and the reflux reactors, respectively. TEM images revealed that the autoclave method yielded well-dispersed sucrose synthesised CDs, whereas the CDs synthesised using microwave showed some aggregation. TEM images also revealed that the reflux method yielded CDs that were largely contaminated with an elongated carbon by-product material which has not been described in the similar literature. [109], [110]

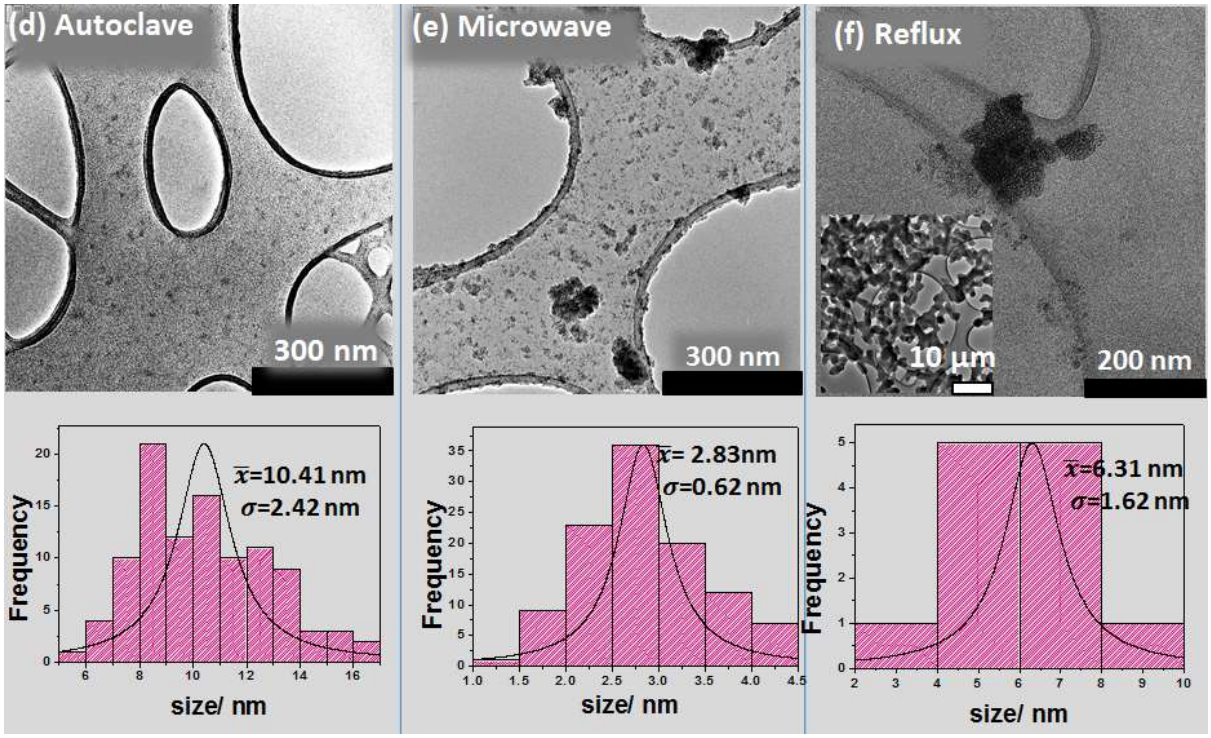

Figure 4-4: TEM images and corresponding particle size distribution curves of Sucrose-CDs synthesised using (a) autoclave, (b) microwave and (c) reflux, respectively.

4.1.1.3 UV-vis absorption and PL emission spectra

The optical properties of the sucrose synthesised CDs were probed with UV-vis spectroscopy. The resulting UV-vis absorption and fluorescence spectra are shown in Figure 4-5. All the sucrose synthesised CDs had similar UV-vis absorption spectra, exhibiting three distinct absorption bands at 200 nm, 230 nm and 280 nm (Figure 4-5a). Table 4-2 shows the summary of the observed UV-vis spectra peaks and their corresponding assignments. The band at 200 nm was attributed to n–σ* transitions of the aromatic C-C bonds while the band at approximately 230 nm is due to the n- π* transition. [31], [31], [111], [111]–[113]The peak around 280 nm was the main peak and is attributed to the π –π* transitions in the –C=C bond of aromatic rings in the CDs. [114]–[116] This confirms the presence of conjugated cyclic carbons in the product. There was also an observable tail in the UV-vis spectrum that extends into the visible region.

All the explored methods yielded photoluminescent products as shown by the manifestation of an emission peak upon excitation of the samples with a wavelength of 350 nm (Figure 4-5a). Like other reports in the literature, these sucrose synthesised CDs emitted at approximately 460 nm when excited at 350 nm. [70] The similarities of the UV-vis absorption and emission data infers that the optical properties of the three samples are of the same nature. [85] Given that the optical properties of the CDs are related to their chemical structures [85], it can be deduced that sucrose gives products with similar chemical structures irrespective of the reactor used for the hydrothermal synthesis. However, the different methods produce products with different size.

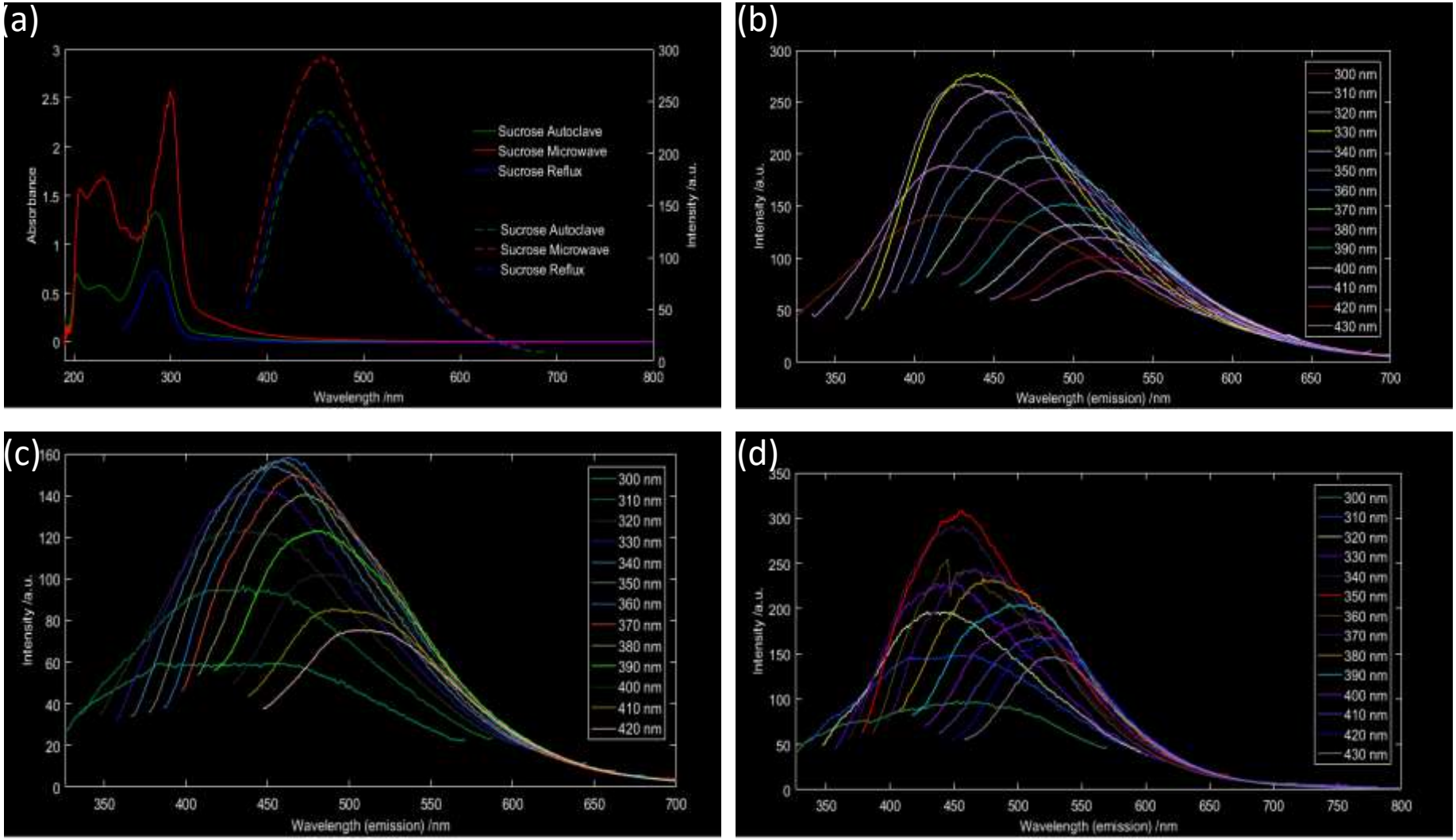

Figure 4-5: (a) UV-Vis absorption and PL spectra of Sucrose-CDs at 350 nm excitation wavelength. PL spectra of (b) autoclave, (c) microwave and (d) reflux synthesised Sucrose--CDs, respectively, at various excitation wavelengths

Table 4-2: UV-Vis and PL emission peaks of Sucrose-CDs, with corresponding spectral assignments and particle size of the CDs.

Sample		**UV-Vis peak/ edge (nm)**			**PL emission peak (nm), at 350 nm excitation λ**	**Size of CDs (nm)**
precursor	method	n–σ*	n–π*	π –π*		
Sucrose	autoclave	191	230	288, 351	458	10.41 ± 2.42
	microwave	200	233	288	454	2.83 ± 0.62
	Reflux	196	231	290; 376	459	6.31 ± 0.62

The optical properties of the sucrose synthesised CDs were probed further by monitoring the PL emission of the CDs at various excitation wavelengths. The sucrose synthesised CDs samples were excited at 300 – 430 nm at 10 nm increments and the resulting spectra are shown in Figure 4-1 a, b and c for the autoclave, microwave and reflux synthesised CDs, respectively. Additionally, the trend of the emission peak with increasing excitation wavelength was plotted and shown below in Figure 4-6 (black curves). An increase in the excitation wavelength was accompanied by a shift of the emission peak of CDs to higher values. This observed blue shift (shift of PL emission peak to longer wavelengths) is an indication of the excitation dependent emission behaviour of CDs that have been frequently reported in the literature. [19], [117]–[122] This feature has been attributed to CDs possessing multiple surface states that are excited at different wavelengths —following that CDs have been dubbed multicolour CDs and deemed as potential candidates for use as inks for inkjet-printing multicolor patterns, sensitizers in solar cells, etc. [123]

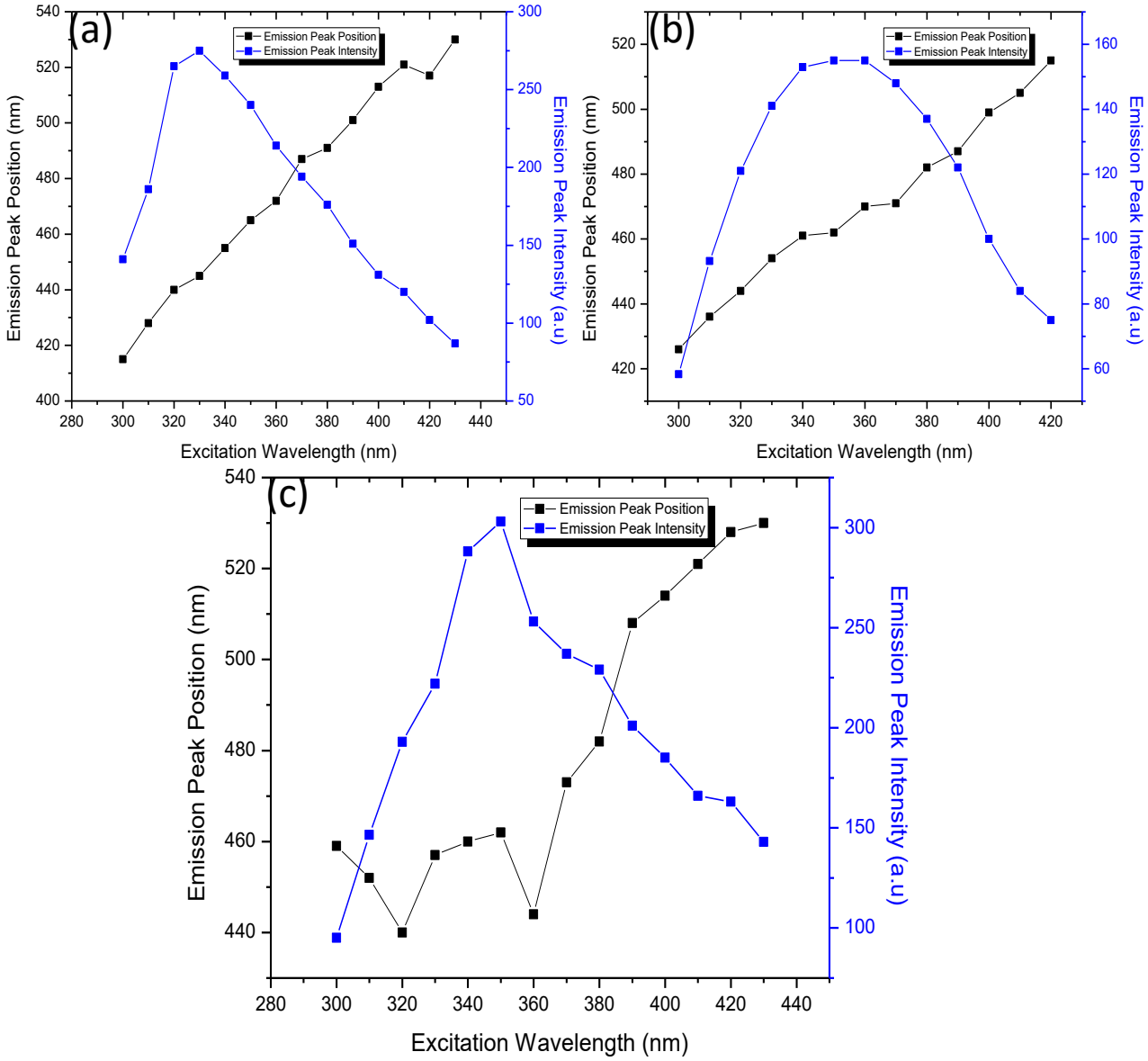

Figure 4-6: The excitation wavelength vs emission peak position (black) and the excitation wavelength vs emission peak intensity(blue) of (a) autoclave, (b) microwave, and (C) reflux synthesised Sucrose-CDs, respectively.

It was noticed that the intensity of the PL emission also varies with the excitation wavelengths. The plots of the intensity of the PL emission against the excitation wavelength yielded inverted U-shaped curves for the sucrose synthesised CDs, as shown in Figure 4-6 (blue curves). It was inferred that the vertex of the curve is the optimal PL emission peak of the respective sucrose synthesised CDs sample. The optimal PL emission peaks of the synthesised CDs occurred at different positions and were yielded by different excitation wavelengths see Table 4-3 below. It was noticed that the position of the optimal PL emission peak and the corresponding

excitation wavelength of the different CDs have a linear relationship that correlated with the particle size of the CDs, respectively (Figure 4-7). For the smaller CDs, the higher excitation wavelengths produced the optimal PL emission peak. Also, the optimal PL emission peak occurs at positions of higher wavelengths for smaller CDs. Following this, it can be inferred that the particle size of the synthesised CDs informs the PL intensity of the sucrose synthesised CDs at a given excitation wavelength, which in turn informs the PL intensity of the %QY of the CDs (see later). In a nutshell, the optimal PL emission peak of smaller sucrose synthesised CDs manifests at longer wavelengths and results from excitation with longer wavelengths. As such, it can be deduced that smaller sucrose synthesised CDs are more suitable for applications where long-wavelength emitting CDs are preferred and vice versa. This is agreement with reports where larger CDs (and higher nitrogen content where applicable) contribute to efficient long-wavelength emissions of CDs. [124], [125]

Table 4-3: The strongest PL emission at varying excitation wavelengths with the corresponding excitation wavelength and size of the sucrose- CDs sample

Sample		**Strongest PL peak**		**CDs size (nm)**
precursor	method	$\lambda_{excitation}$ **(nm)**	$\lambda_{emission}$ **(nm)**	
Sucrose	autoclave	330	430	10.41 ± 2.42
	Reflux	350	450	6.31 ± 0.62
	microwave	360	460	2.83 ± 0.62

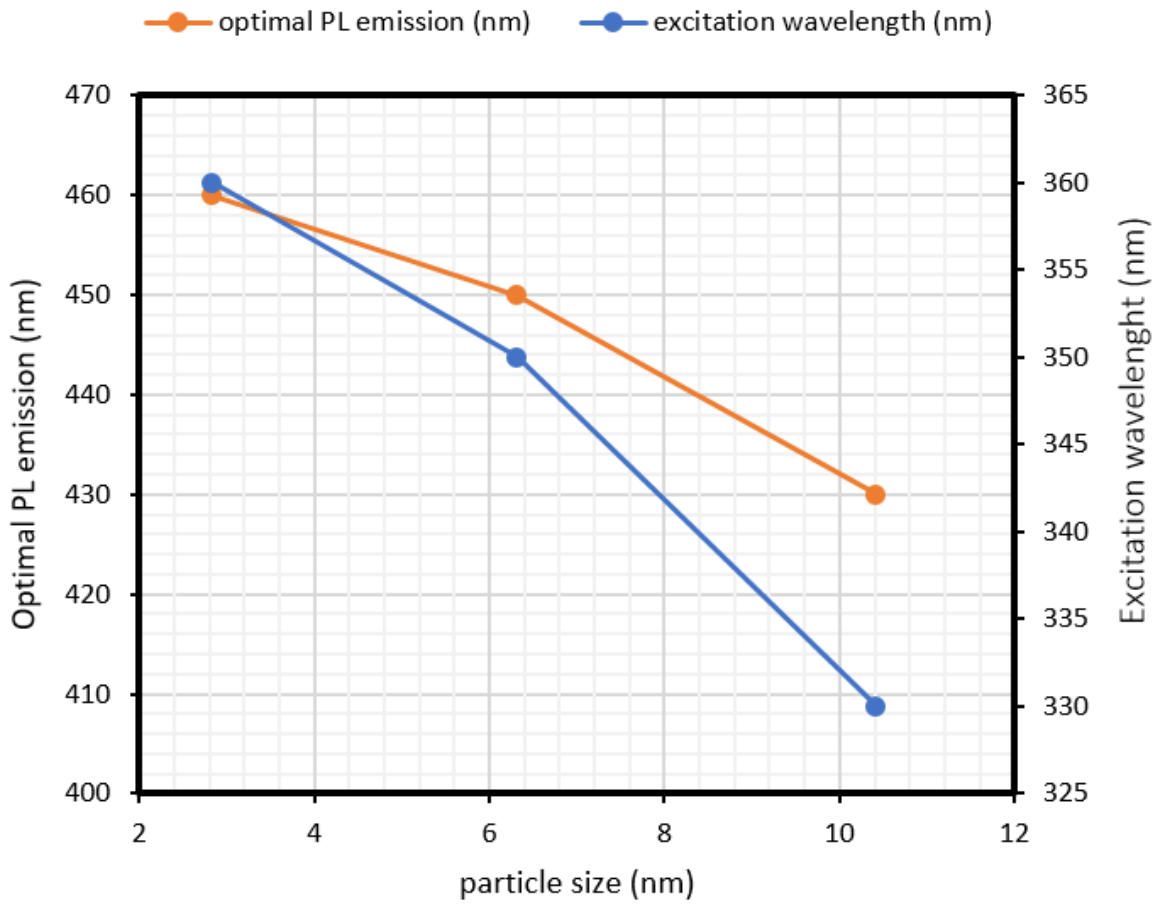

Figure 4-7: Particle size of sucrose synthesised CDs versus their optimal PL emission and the corresponding excitation wavelength

4.1.1.4 FTIR spectra

The chemical structure and the surface functional groups of the synthesised CDs were investigated using FTIR spectroscopy. The recorded spectra are shown in Figure 4-8. The FTIR spectra of the synthesised CDs are similar to one another but are different from the FTIR spectrum of the sucrose precursor. These differences indicate that the solvothermal treatments caused a change in the structure of the sucrose resulting in the formation of CDs. The most significant change is the presence of more pronounced and bigger peaks at 2920 cm^{-1}, and 2820 cm^{-1} for the CDs compared to the raw sucrose where these peaks are smaller. The larger peaks in the CDs indicate that there is more terminal CH_2 and $–CH_3$ groups in the CDs compared to the raw material sucrose. The other notable change is the reduction in the number of FTIR vibrational peaks in the 750 cm^{-1} to 1200 cm^{-1} region in the CDs compared to sucrose. This region is where the sucrose $–CO_2H$, and the –COH vibrational modes reside. [126] Upon

pyrolysis of the sucrose, there is a reduction in the area under the peaks between number 750-1200 cm^{-1}. The peaks in CDs at about 3400 cm^{-1} is due to terminal OH groups. [127]–[130] It is broad due to the hydrogen bonding between the CDs and the solvent used in the synthesis procedure. As mentioned above, the FTIR spectra of the three sucrose synthesised CDs are similar (Figure 4-8). Importantly they all have similar absorptions at ~ 3400 cm-1, 2950 - 2800 cm^{-1} and large peak at 1020 cm^{-1}. This infers that the sucrose synthesised CDs have similar chemical structures which agree with the findings of the UV-vis spectra analysis. The significant changes are observed in the ratio of the 1020 cm^{-1} peak to the peak between 1600 - 1100 cm^{-1}. This suggests that the larger CDs (autoclave method synthesised) contain more OH/COO/CO_2H on their surface than smaller CDs. In other words, larger CDs have more O-related surface defects than smaller CDs. [131]Perhaps, this plays a role in the variation of the optimal PL emission peak position and excitation wavelengths that are observed between sucrose synthesised CDs of various sizes.

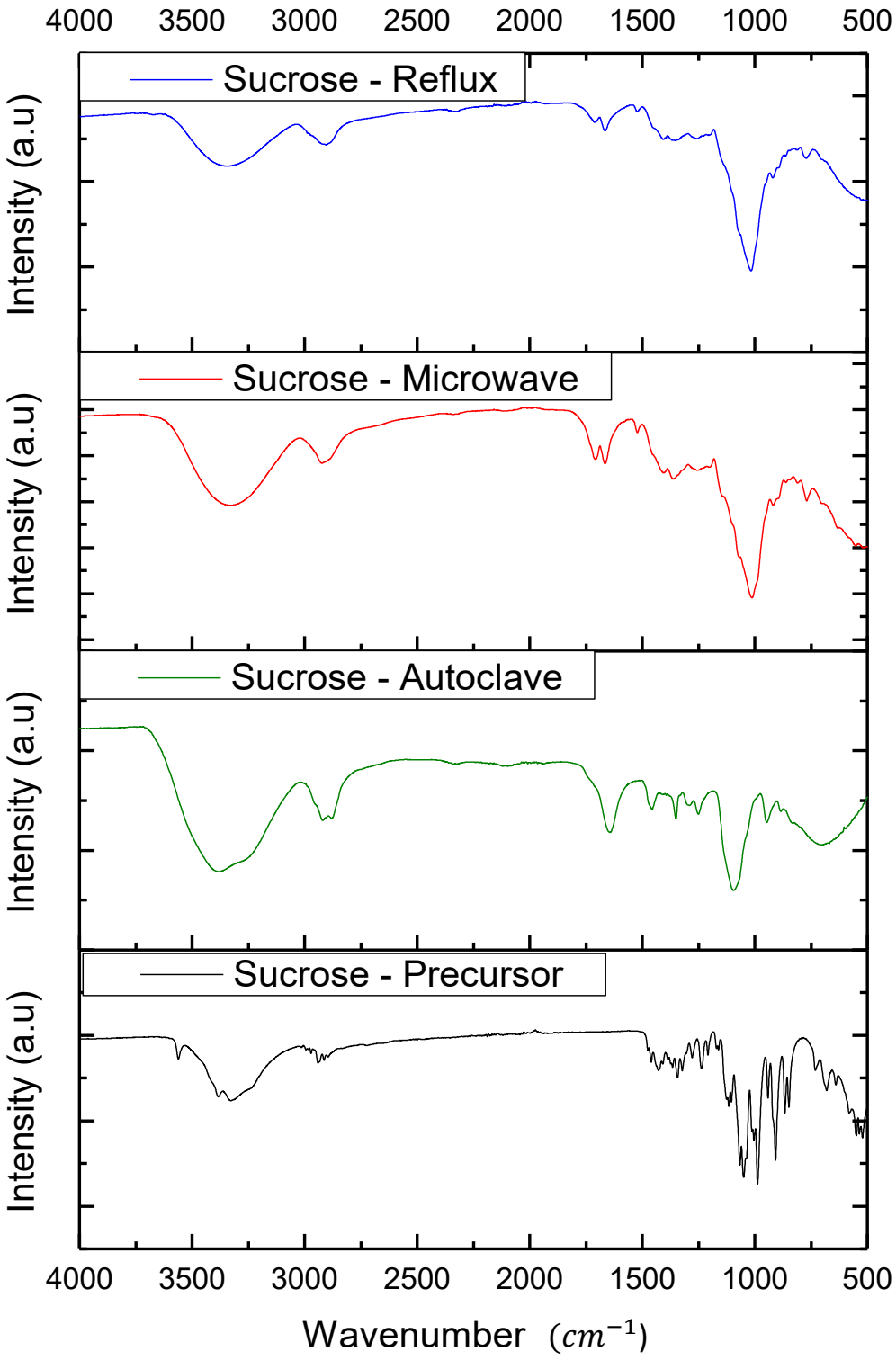

Figure 4-8: FTIR spectra of Sucrose-CDs synthesised via reflux, microwave, autoclave and the FTIR spectra of Sucrose respectively

4.1.1.5 Fluorescence %QY

The UV-vis spectroscopy data were used to determine the %QY of the synthesised CDs. As discussed above, %QY measures the photoluminescence efficiency of the CDs. %QY is a ratio of the emitted photons to the absorbed photons. Additionally, quinine sulphate (QY=58) in 0.1 M sulphuric acid was used as a standard at an excitation wavelength of 350 nm. The %QY of the samples was determined to be 0.4%, 4,3% and 1.0 % for the autoclave, microwave and reflux synthesised CDs, respectively (Table 4-4). The low %QYs of less than 10% are not unexpected for sucrose synthesised CDs as sucrose generally produces bare CDs (without passivation) which often exhibit low %QY. This can be improved significantly through passivation and doping. [100], [105]–[108] With that said, there are several reports of sucrose synthesised CDs that exhibit high %QY of up to 26%. [70] It was also found that the %QY increases with a decrease in particle size (for instance, %QY increasing by 760% following a particle size decrease of 73%). This observed inverse proportionality relationship between the particle size of the sucrose synthesised CDs and the %QY is well reported in the literature. [1], [132] Moreover, it ascribed to the quantum size effects as smaller CDs have bigger band gaps and thus has the potential to exhibit very strong emission. [1], [132]

Table 4-4: Fluorescence %QY of the sucrose synthesised CDs

method	Autoclave	Microwave	Reflux
CDs size (nm)	10.41 ± 2.42	2.83 ± 0.62	6.31 ± 0.62
%QY	0.5%	4.3%	1.0%

4.1.1.6 Summary

Sucrose formed well dispersed CDs when the autoclave method was used. However, the use of a microwave yielded CDs with aggregation, while CDs from the reflux method had severe contamination. Across all three methods, sucrose formed CDs with 5-10 % yield which is much lower that what was expected yield for bulk synthesis using sucrose. The excess oleic acid which served as a solvent for CDs synthesis from sucrose was laborious to separate from the resulting CDs. In summary, it was found that sucrose is not a precursor of choice for CDs synthesis

4.1.2 CDs from Chitosan

4.1.2.1 Synthesis

As a waste product, chitin, is a very appealing carbon precursor. [94] However, as is, chitin is insoluble in conventional solvents due to its crystalline structure with a highly aggregated three-dimensional network held together by strong hydrogen bonds and cohesive forces. [94] Thus, chitosan which is derived from treating chitin with an alkaline solution, was used instead as a carbon precursor for synthesis of CDs using the autoclave, microwave and reflux method, respectively. [94] Similarly, to most reports in literature, a mixture of water and acetic acid were used a solvate chitosan in the microwave and the reflux method [94], [96], [133]–[135]; acetic acid was added to promotes the solubility of chitosan in water. [94] In contrast, ethanol was used as a solvent for the autoclave method since alcohols have also been reported to be good at dissolving chitosan. [136] All the individual work-up reactions of the different methods were relatively laborious as the crude products were a slurry that required intensive sedimentation and decantation. Nevertheless, CDs were obtained across all three methods as confirmed by various characterisation techniques discussed below. The microwave method had the lowest %yield of 2%, while the autoclave and reflux methods had %yields which was comparable to those reported in literature. [1], [134]

4.1.2.2 TEM images

Chitosan was explored as a carbon precursor for the synthesis of CDs via three methods, namely the autoclave, microwave and the reflux method as detailed in chapter 3. The resulting TEM images and corresponding particle size distributions are shown below in Figure 4-9. The autoclave method yielded chitosan synthesised CDs with a small particle size of 6.29 ±1.17 nm. The sample was obtained in solid form at a low yield of 7.1%. Moreover, TEM revealed that the sample comprised mainly of elongated carbon sheets that resemble aggregated onion-like carbons. [137] The synthesis of CDs from chitosan using the microwave method also followed the same trend as the synthesised sample had a low yield of ~2% with most of the sample existing as aggregated and elongated carbon sheets. The measured particle size of the elongated carbon sheets was 57±14nm. Unlike the autoclave method, no Chitosan-CDs were revealed in the TEM images.

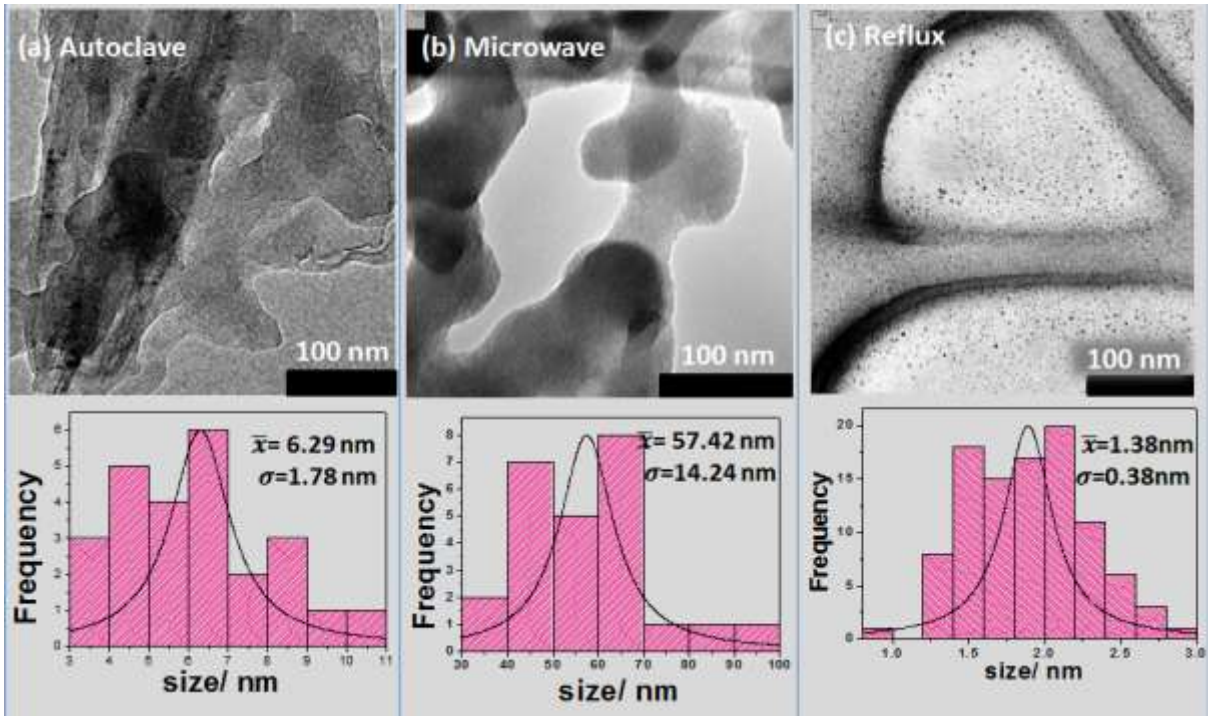

Figure 4-9: TEM images and corresponding particle size distribution curves of Chitosan-CDs synthesised using (a) autoclave, (b) microwave and (c) reflux methods, respectively.

On the other hand, the reflux method yielded chitosan synthesised CDs with good mono-dispersion and spherical morphology as shown in Figure 4-9 (c). The refluxed synthesised CDs were crystallized out of solution forming a small amount of CDs with a yield of 8% which is comparative to yields reported in literature. [134] This method yielded the smallest chitosan synthesised CDs with a particle size of 1.4±0.4 nm. In a nutshell, when chitosan is used as a precursor, the reflux method yielded CDs sample with appealing properties as compared to the autoclave and microwave. Though it is worth mentioning that the reproducibility of this reflux synthesised CDs proved to be challenging (Figure S1).

4.1.2.3 UV-vis absorption and PL emission spectra

UV-Vis absorption and emission spectroscopy were carried out on the synthesised samples, and resulting spectra are shown in Figure 4-10. As seen in Figure 4-10a, the synthesised samples have multiple absorption peaks spanning across 200 – 350 nm and are an indication of the diversity of the sizes and possibly functional groups of the CDs. [102], [138], [139] It was noted that the UV-Vis absorption spectra of the chitosan synthesised CDs were very different from each other. The assignments of the UV-Vis absorption peaks are shown in Table 4-2. The peak at approximately 200 nm is attributed to transitions associated with the C = O

bonds [33], [119], [140], [141] whereas the peak at 240 nm is attributed to n–π* transitions of aromatic sp^2 domains and confirms the existence of aromatic components. [45], [142]–[144] The strong absorption band at about 270 nm can be attributed to the π –π* transitions of the C=C bonds. The absorption peak at about 350 nm is attributable to the weak π aromatic orbitals of Chitosan-CDs. [45], [144]

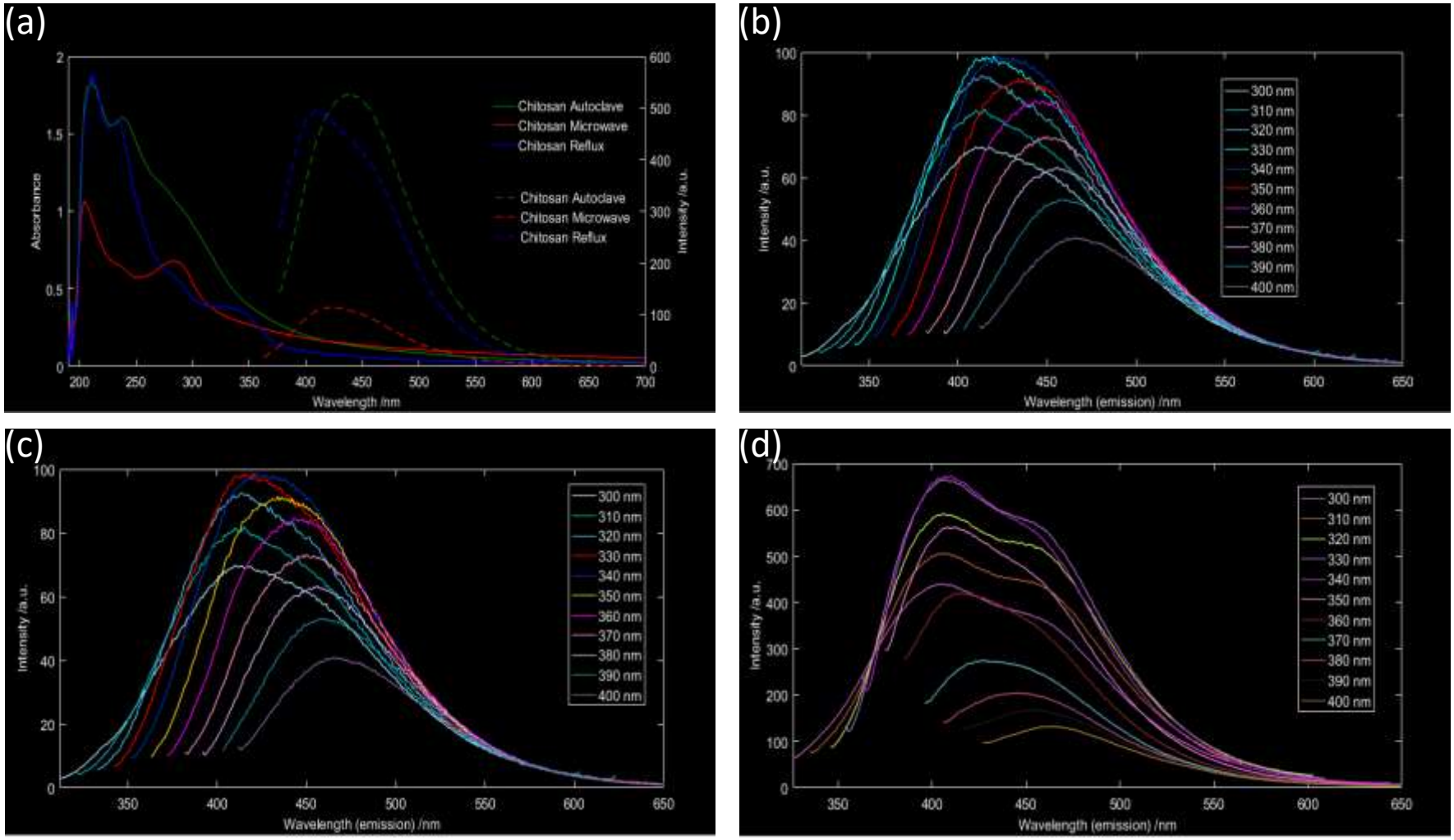

Figure 4-10: (a) UV-Vis absorption and PL spectra of Chitosan-CDs/nanoparticles at 350 nm excitation wavelength. PL spectra of products produced from (b) autoclave, (c) microwave and (d) reflux synthesised Chitosan-CDs/nanoparticles, respectively, at various excitation wavelengths.

Table 4-5: UV-Vis and PL emission peaks of chitosan-CDs, with corresponding spectral assignments and particle size of the CDs.

Sample		**UV-Vis peak/ edge (nm)**			**PL emission peak (nm), at 350 nm excitation λ**	**Size of CDs (nm)**
Precursor	method	n–σ*	n–π*	π –π*		
Chitosan	autoclave	200	240	300	440	6.29 $\pm$1.78
	microwave	200	-	285	418	-
	Reflux	202	238	285,350	408	1.38$\pm$ 0.38

The samples made by the autoclave and the reflux synthesis methods emitted wavelengths of 440 nm and 408 nm, respectively, when excited at a wavelength of 350 nm Figure 4-10 (a). These emission peaks are consistent with literature as the emission peak of CDs generally occurs between 400-600 nm wavelengths. [145] Interestingly, even though the chitosan and microwave synthesised sample had no visible CDs under TEM, the produced sample is also photoluminescent, emitting a wavelength of 418 nm when excited at 350 nm excitation wavelength. Thus, it suggests that they may be buried in the apparent elongated carbon sheets. [1]

The synthesised CDs were subjected to excitation at various excitation wavelengths in order to investigate whether the synthesised CDs exhibit the well-reported excitation-dependent emission CDs. [146]–[152] The resulting spectra of the samples produced by the autoclave, microwave and reflux methods are shown in Figure 4-10 b, c, and d respectively. The reflux synthesised Chitosan-CDs exhibit two PL maxima between the excitation wavelengths of 280-340 nm. The higher wavelengths PL maxima occurred at 330 nm, and the other is found at 420 nm Figure 4-10 (d). This double PL maxima emission indicates that the sample either contains different sizes of CDs or the CDs different functional group. [67], [153][26], [87], [154] Since the TEM data indicated that the CDs are mono-dispersed, the effect is ascribed to CDs bearing varying functional group on their surface (i.e. surface defects). Moreover, the increase of the excitation wavelengths at 280-340 nm is not accompanied by a significant change in the positions of these two PL emission peaks. Thus, it can be inferred that at excitation wavelengths below 340 nm, the regular blue-shift feature of most CDs is not observed. The excitation-independent wavelength behaviour has been reported for nitrogen-doped CDs, where the C-O-

C/C-O-H surface defects are relatively fewer. [124], [155]–[158] It should be noted that chitosan bears nitrogen containing group, and as such, this behaviour could be attributed to nitrogen doping of the CDs. [134] The double PL emission maxima peak converges to one peak at excitation wavelengths beyond 340 nm. Additionally, the PL emission starts to exhibit the excitation-depended emission as indicated by the shifting of the PL emission peak to higher wavelengths as the excitation wavelength was gradually increased to 400 nm. This mixed behaviour of the PL emission infers that the reflux (and chitosan) synthesised CDs exhibited PL emission that arises from various origins (i.e. quantum confinement and surface states). [1], [33]

When the autoclave and the microwave synthesised CDs were respectively excited at wavelengths of 200 nm to 350 nm, the corresponding emission peaks gradually shifted to higher wavelengths exhibiting the well-reported excitation-dependent PL emission of CDs (Figure 4-10 a and b, respectively). [1] The plot of the PL emission peak position against the excitation wavelength is shown in Figure 4-11 (black curves), as seen the plots are exponential curves. The excitation independent-emission nature of the reflux synthesised CDs was manifested a long tail along the growth region of the exponentials curve (Figure 4-11a, black curves).

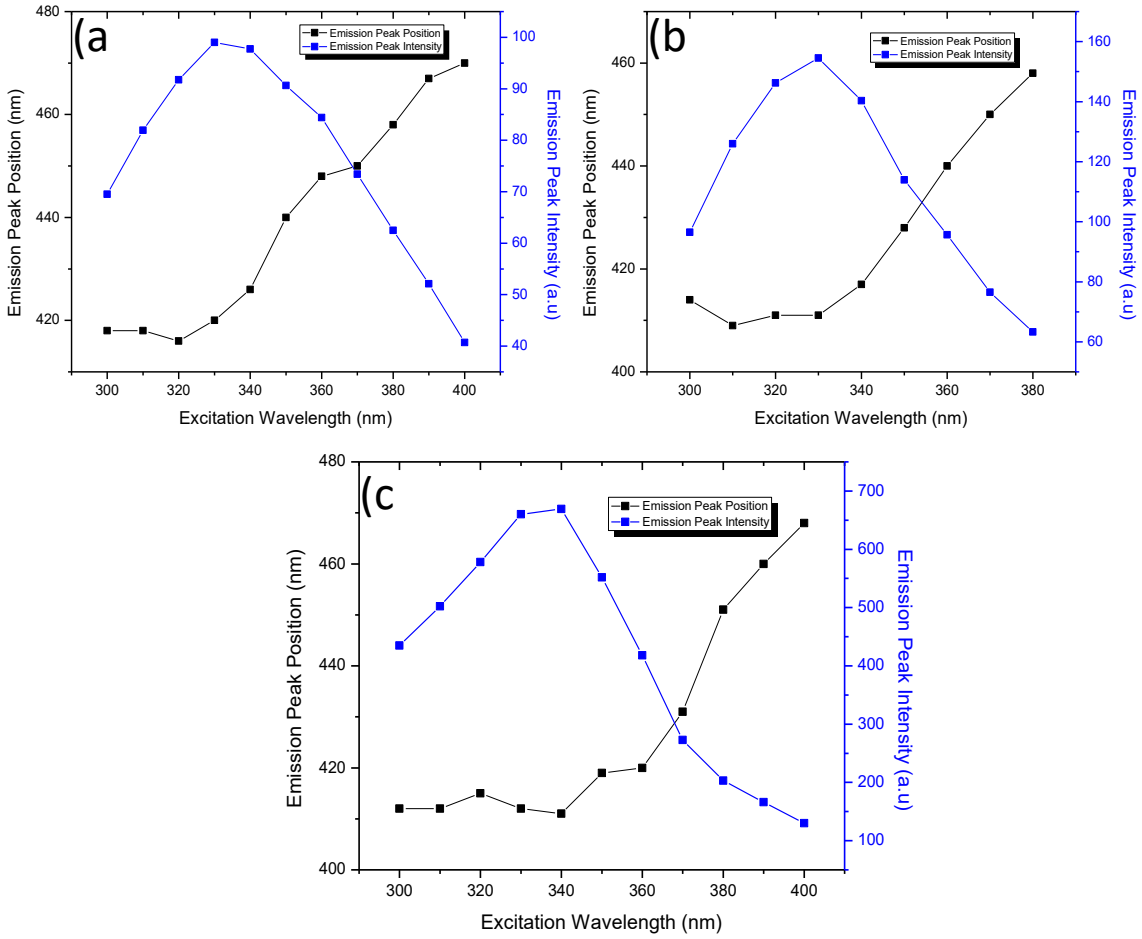

Figure 4-11: The excitation wavelength vs emission peak position (black) and the excitation wavelength vs emission peak intensity(blue) of (a) autoclave, (b) microwave, and (C) reflux synthesised Chitosan-CDs, respectively.

As like in many literature reports, it was noted that the intensity of the PL emission peak also varies as the excitation wavelength was varied. [1] The plots of the intensity of the PL emission peak against the excitation wavelength show an inverted U-shaped curve where the vertex corresponds to the optimal PL emission, as shown in Figure 4-11 (blue curves). The optimal peak of all the synthesised CDs occurred at an excitation wavelength of 330 nm and resides around 410 - 420 nm.

4.1.2.4 FTIR spectra

The FTIR spectra of the synthesised CDs were recorded to elucidate their chemical structure and surface functional groups (Figure 4-5). The broad peak at about 3430 cm^{-1} is assigned to the –OH groups. While peaks at 2900 cm^{-1} and 2820 cm^{-1} originates from the –CH2 and –CH

vibrational modes, respectively. The broad shoulder at about 3200 cm^{-1} is assigned to aromatic C=C vibrational modes. The peak at 1618 cm^{-1} arises from a -C=O stretching mode. The sharp peaks at about 1390 cm^{-1} arise from symmetric carboxylate stretches confirming the existence of –OH, and –CO2H functional groups on the surfaces of the CDs. The sharp bands at about 1020 cm^{-1} originates from -C-O bond vibrations. The bands at about 1060 cm^{-1} are understood to be due to –C-O-C bonds. The sharp peaks at 1441 cm-1 and 1590 cm^{-1} are attributable to the vibrations of the –C=C of aromatic rings. [127]–[130]

The FTIR data of the microwave synthesised CDs suggests that the product is similar to that of the chitosan precursor, which indicates that very small amounts of CDs were produced. On the other hand, autoclave synthesised CDs had a much smaller chitosan peak which resides around 1060 cm^{-1}. [134] In contrast, the refluxed synthesised CDs do not exhibit a chitosan peak at all. Thus, the FTIR spectra data infer that during the reflux method, the chitosan precursor is wholly transformed into CDs, while during the autoclave method has some residual chitosan retained on the CDs sample. These results are in agreement with the TEM data as the reflux synthesised sample was comprised of CDs particles, while the autoclave synthesised sample exhibited very few CDs with the majority of the sample being a by-product.

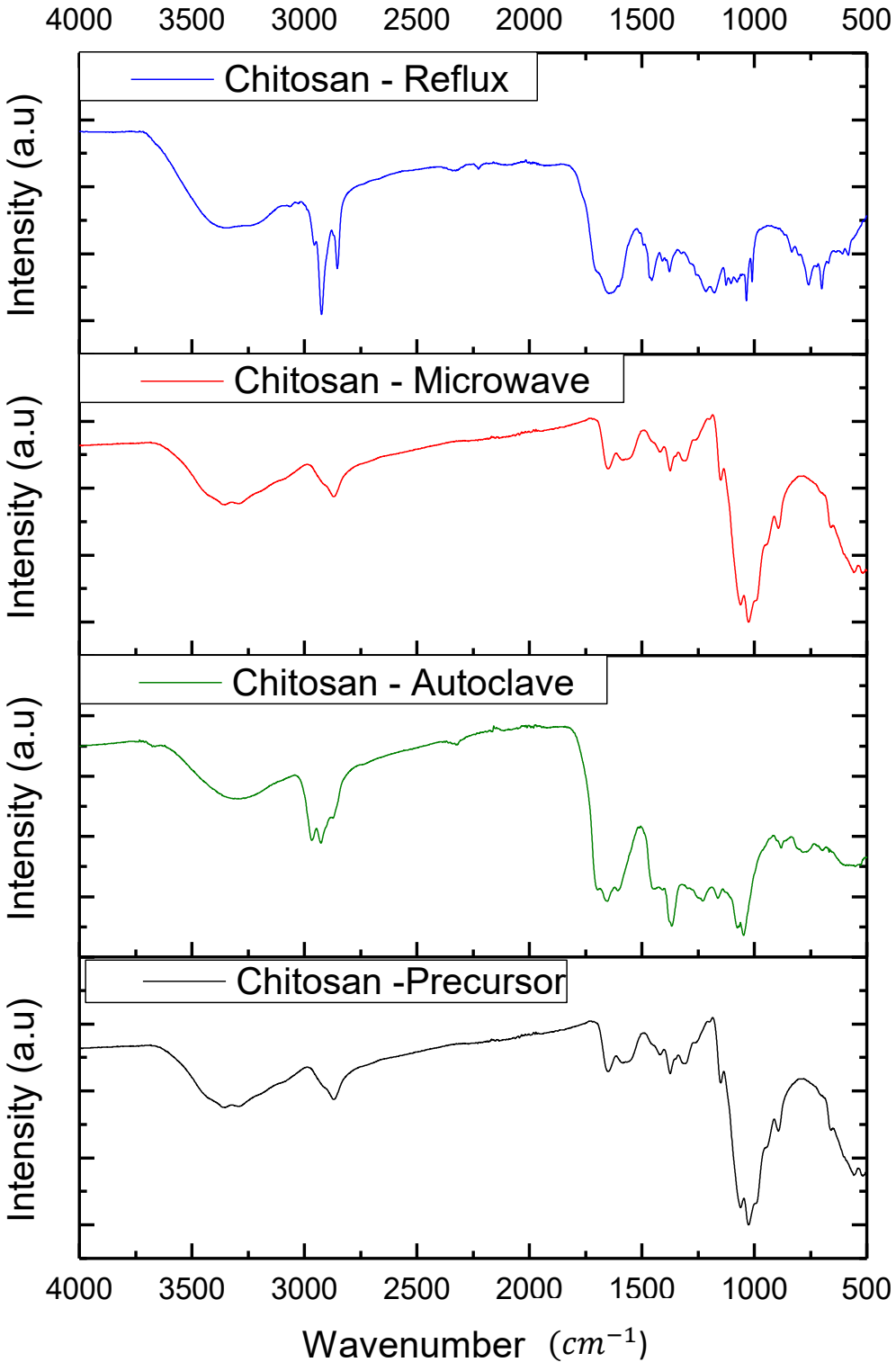

Figure 4-12: FTIR spectra of Chitosan-CDs/nanoparticles synthesised via reflux, microwave, autoclave and the FTIR spectra of Chitosan respectively.

4.1.2.5 Fluorescence %QY

The %QY of the chitosan synthesised was determined using quinone sulphate as a reference dye. The %QY of the autoclave and microwave synthesised CDs was determined to be only 0.4%. This %QY is very low, especially when considering that as a polymer, chitosan is expected to yield highly photoluminescent self-passivated CDs. [1] Nevertheless, the chitosan synthesised CDs follows the inverse proportionality relationship of the particle size and the %QY as the %QY increases from 0.4% to 16 % following particle size decrease from 6.29 nm to 1.38 (Table 4-7). Thus, the high %QY of this reflux synthesised CDs is not only ascribed their small particle size but, is also ascribed to the presence of the nitrogen element in the CDs structure. [132] The main difference between low %QY and the high %QY chitosan synthesised CDs is the quality of the sample, as observed in TEM. Thus, it is inferred that the low %QY is partly due to the non-radiative interactions between the CDs and the majority sample, which is elongated carbon sheets.

Table 4-6: Fluorescence %QY of the chitosan synthesised CDs

Method	Autoclave	Microwave	Reflux
CDs size (nm)	6.29 ±1.78	-	1.38± 0.38
%QY	0.4%	0.4%	16%

4.1.2.6 Summary

When chitosan was used as a carbon precursor, the autoclave and microwave method formed samples that show less or no CDs particles on TEM. The %QY of the produced CDs was also very low. On the other hand, reflux method synthesised well dispersed CDs with a narrow particle size and a high %QY. The high %QY was ascribed to nitrogen-doping since chitosan is both a carbon and a nitrogen source. However, this synthesis of CDs from the reflux method was not reproducible. As such, similarly to sucrose, chitosan was also found to not be an ideal carbon precursor for CDs synthesis.

4.1.3 CDs from PEG_{400}

4.1.3.1 Synthesis

Conversely, to the other precursors (sucrose and chitosan) which are solid, PEG_{400} is a viscous liquid at ambient temperature and pressure. [95] Water was used as a solvent during the hydrothermal treatment of PEG_{400} like other reports in literature where PEG is used for CDs

synthesis [159], [160]. The autoclave, microwave and reflux reactions proceeded with ease and yielded a crude product that required minimal work-up treatment. The evaporation of the solvent through use of a rota-evaporation was not successful, thus the final CDs products were suspended in solution. Following this, the %yield of the CDs could not be determined.

4.1.3.2 TEM

TEM analysis of the synthesised sample revealed that PEG yielded well-dispersed CDs across all three explored synthesis methods (Figure 4-13). The autoclave method yielded the smallest CDs with a particle size of 2.52 ±0.8 nm, followed by the microwave method which yielded CDs of 3.3 ± 1.5 nm, and lastly the reflux method the largest particle CDs size at 4.8 ± 1.0 nm. TEM images also revealed that the CDs synthesised using the microwave and the reflux methods had small carbon nanospheres (CNSs) as a by-product. The CNSs are well dispersed with a particle size of 20-40 nm. This material is not the target product for this study and will thus not be discussed further. However, it has potential for application in a vast number of fields as its size bridges the gap between well-reported carbon nanospheres (50 nm to 1μm^2) and carbon dots. [161], [162] Thus, it is worth being studied further in future.

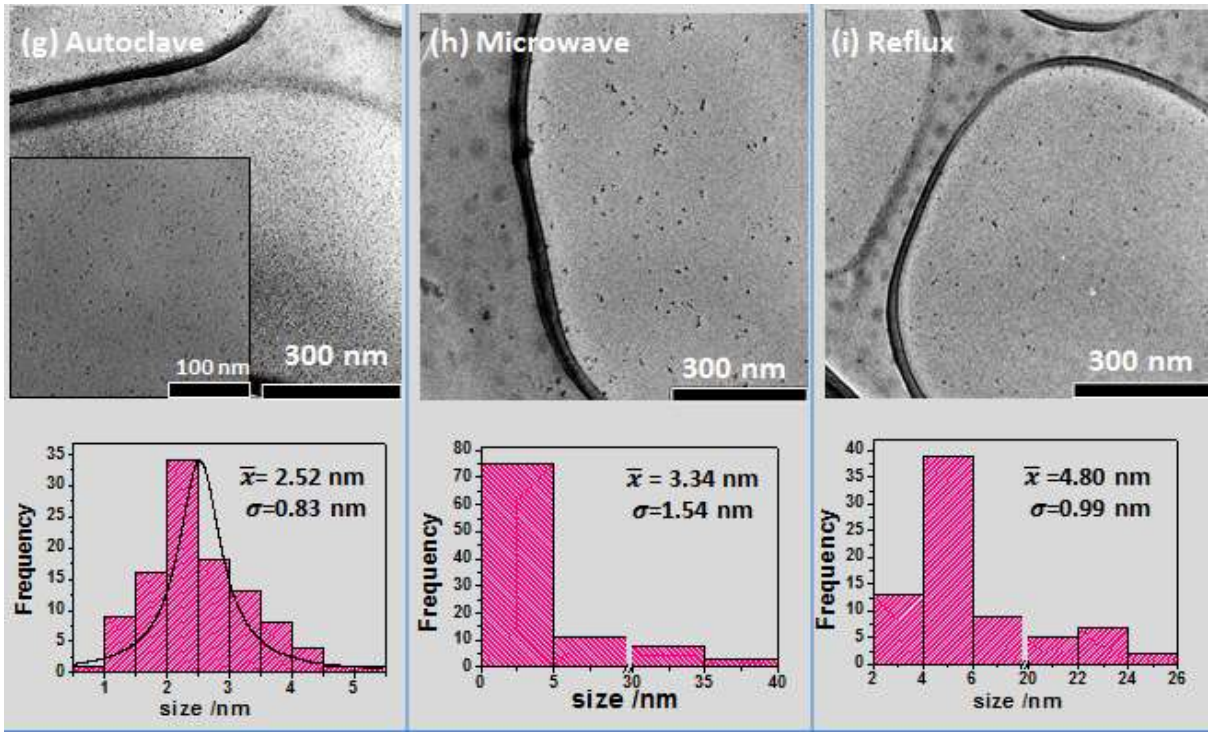

Figure 4-13: TEM images and corresponding particle size distribution curves of PEG-CDs synthesised using (g) autoclave, (h) microwave and (i) reflux, respectively

4.1.3.3 UV-vis absorption and PL emission spectra

The obtained PEG synthesised CDs were characterised using UV-vis absorption and emission spectroscopy. The recorded UV-vis spectra are shown in figure 4-14, and the peak assignments are shown in Table 4-7. The strongest absorption peak of the synthesised CDs was around 200 nm. This peak was attributed to the n–σ* transitions of the aromatic C-C bonds. [31], [31], [111], [111]–[113] After that, the UV-vis absorption spectra have tails that extend to 330 nm for the microwave and reflux synthesised CDs, whereas it extends to 430 nm for the autoclave synthesised CDs. Moreover, there are absorption edges along the tail. The microwave and reflux synthesised CDs have an absorption edge at 285 nm, while the autoclave CDs have an absorption edge at 350 nm. The absorption edges around 285 nm were ascribed to the n –π* transitions of the C=O bonds. [24], [50], [119], [163], [164]While the absorption edge around 350 nm was attributed to the π –π* transitions in the –C=C of the CDs aromatic rings. [114]–[116] The observed absorption spectra are similar to other PEG synthesised CDs [165]. However, in some reports, the UV-vis absorption spectra of the PEG synthesised CDs have two distinctive peaks, one at 200 nm and another 350 nm. [166] Chen et al. found that the peak around 350 nm diminishes with an increased reaction time of the synthesised CDs. [167]

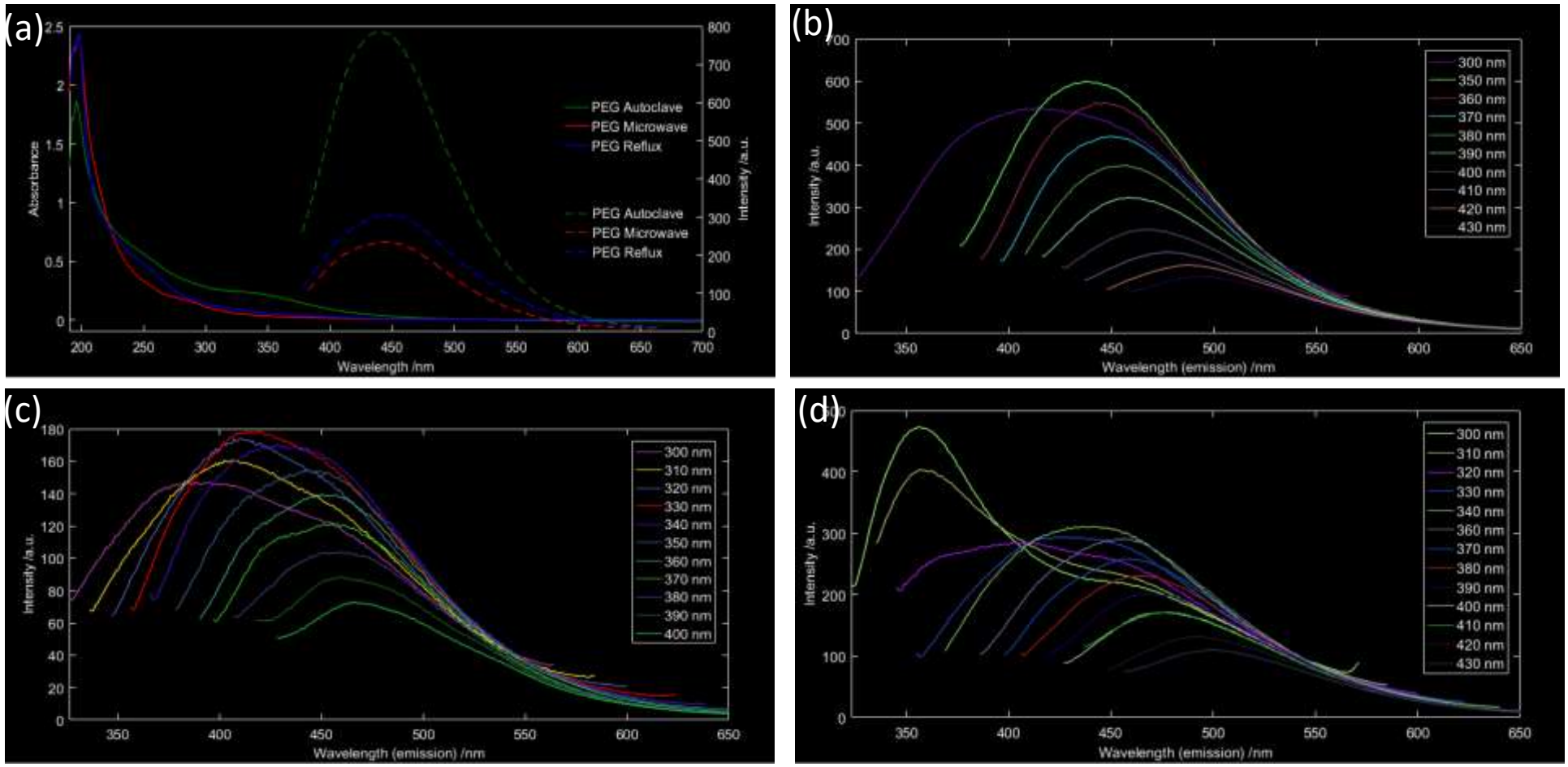

Figure 4-14: A UV-Vis absorption and PL spectra of PEG-CDs at 350nm excitation wavelength. PL spectra of (b) autoclave, (c) microwave and (d) reflux synthesised PEG-CDs, respectively, at various excitation wavelength

Table 4-7: UV-Vis and PL emission peaks of PEG-CDs, with corresponding spectral assignments and particle of the CDs

Sample		UV-Vis peak/ edge (nm)			PL emission peak (nm), at 350 nm excitation λ	Size of CDs (nm)
		n–σ*	n–π*	π –π*		
PEG	autoclave	200	-	350	430	2.52±0.83
	microwave	200	285	-	442	3.34±1.54
	Reflux	200	265	-	448	4.80±0.99

When bearing in mind that the PEG precursor is not photoluminescent, it can be inferred that the PL emission peaks manifested upon excitation of the samples is due to the conversion of PEG precursor to CDs upon synthesis. [168]At 350 nm excitation wavelength, the autoclave, microwave and reflux synthesised CDs emit at 430 nm, 442 nm and 488 nm wavelengths, respectively. This infers that the synthesised CDs have slightly different optical properties among each other, which in turn infers that they have slightly different chemical structures. The reflux synthesised CDs are more conjugated than the other synthesised CDs as displayed by their red-shifted emission peak. [167]

After that, the synthesised CDs were excited at varying excitation wavelengths, and the resulting spectra are shown in Figure 4-14 a, b, and c for the autoclave, microwave and reflux synthesised CDs, respectively. As expected, the excitation-depended photoluminescence was observed across all the synthesised CDs samples. [33], [111], [111], [169]–[171] That means, the PL emission peak changed position and intensity in response to a change in the excitation wavelength. Firstly, there was a noticeable blue shift on the PL emission peak that accompanied the increase of the excitation wavelength (Figure 4-15, black curves). Secondly, as the excitation wavelength was increased, the intensity of the PL emission peak was generally increased, and then gradually decreased. The observed excitation dependent photoluminescence is ascribed to C-O-C/C-O-H surface defects and the presence of aromatic π orbitals from bigger particles will have larger effect than from smaller CDs. [131] Alternatively, the observed blue-shift can be ascribed to size-dependent absorption. [125], [172], [172]–[175] Also, other studies have ascribed the decrease in PL intensity to an increase in the excitation wavelength. [125], [172], [172]–[175] Though, this alternative explanation

may only be applicable where the by-product (small CNS) is also photoluminescent since the CDs are were found to be monodispersed.

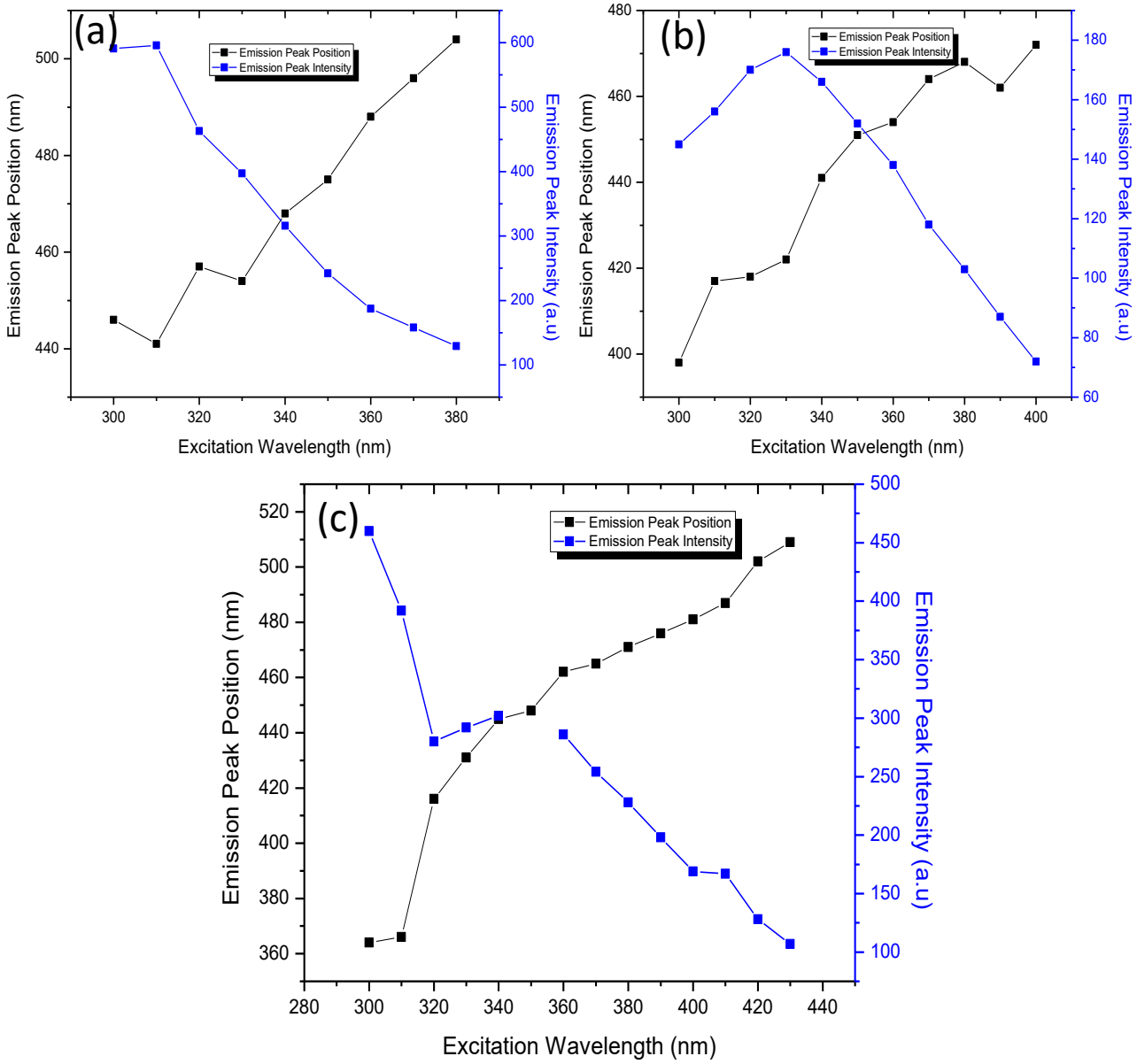

Figure 4-15: The excitation wavelength vs emission peak position (black) and the excitation wavelength vs emission peak intensity (blue) of (a) autoclave, (b) microwave, and (C) reflux synthesised PEG-CDs, respectively.

As depicted in Figure 4-15, over a range of excitation wavelengths the PL emission of the autoclave, microwave and reflux synthesised CDs had a maxima excitation wavelength of 310 nm, 330 nm and 350 nm, respectively. Following this, the optimal PL emission peak was found at wavelengths of 505 nm, 470 nm and 440 nm for the autoclave, microwave and reflux

synthesised CDs, respectively. The results are summarised below in Table 4-8. As illustrated in Figure 4-16 the particle size of the CDs is directly proportional to the excitation wavelength at which the optimal PL emission peak is produced. That is the smaller the PEG synthesised CDs, the lower the wavelength required to yield the optimal PL emission peak and vice versa. This observed linear relationship, is the inverse of the linear relationship that was established for the sucrose synthesised CDs. As such, it can be inferred that the optical nature of the PEG synthesised CDs varies significantly from that of the sucrose synthesised CDs. Furthermore, the particle size of the PEG synthesised CDs is inversely proportional to position of the optimal PL emission peak. That is the optimal PL emission peak occurs at longer wavelengths for smaller CDs and vice versa. A similar relationship was observed for the sucrose synthesised CDs. Thus, for both sucrose and PEG synthesised CDs, smaller CDs are more suitable for long-wavelength emitting CDs applications and vice versa.

Table 4-8: UV-Vis and PL emission peaks of PEG-CDs, with corresponding spectral assignments and particle size of the CDs

Sample		**Strongest PL peak**		**CDs size (nm)**
precursor	method	$\lambda_{excitation}$ **(nm)**	$\lambda_{emission}$ **(nm)**	
Sucrose	autoclave	310	505	2.52 ± 0.83
	microwave	330	470	3.34 ± 1.54
	Reflux	350	440	4.80 ± 0.99

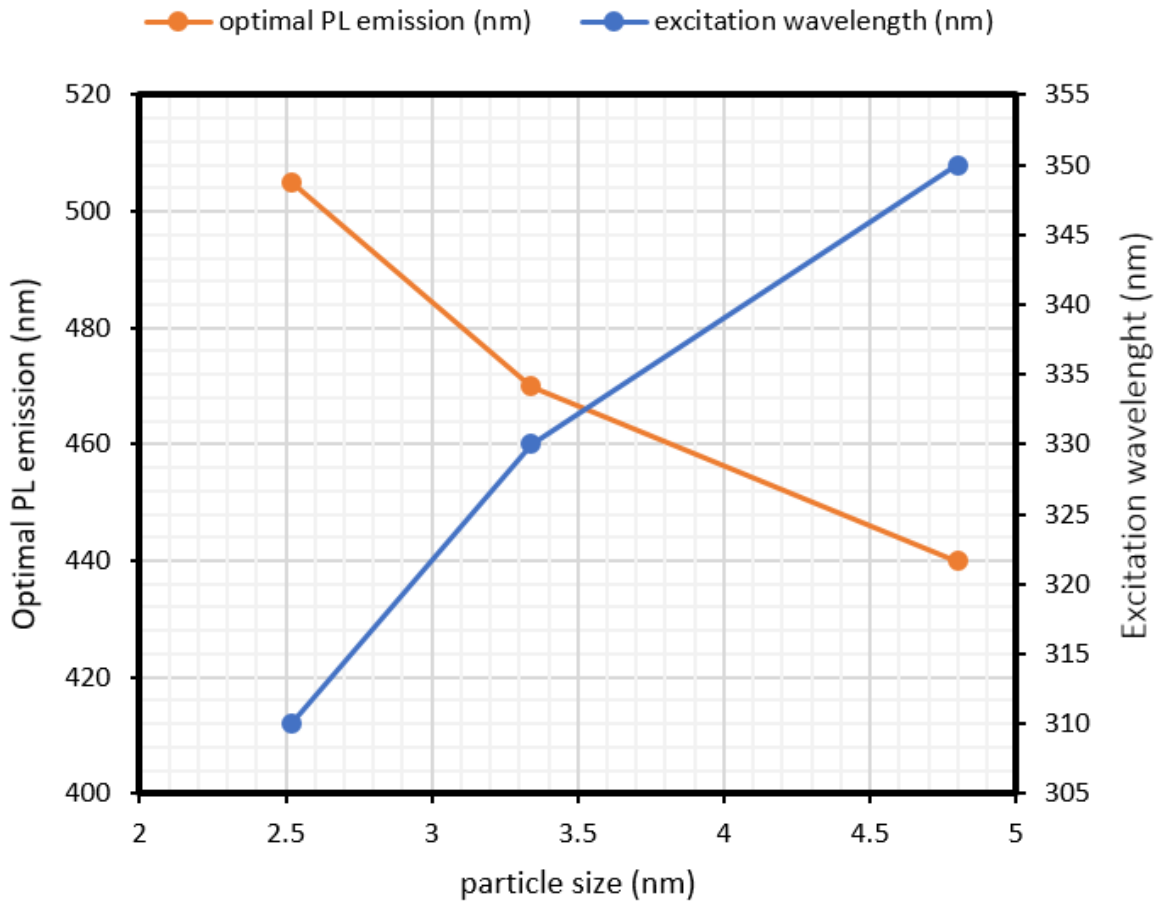

Figure 4-16: Particle size of PEG synthesised CDs versus their optimal PL emission and the corresponding excitation wavelength

4.1.3.4 FTIR

The PEG synthesised CDs were characterized by FTIR spectroscopy and the results are in shown in Figure 4-17. The broad peak at about 3400 cm^{-1} was due to the terminal –OH groups on the surface of the CDs. [52], [176]–[179]The broadening of the peak could be due to the hydrogen bonding occurring between the hydrogens of the CDs, the solvent and some of the unreacted PEG. The Peak with a shoulder at about 2810 cm^{-1} and 2910 cm^{-1} are due to the –CH_2 and –CH stretches. [180] The peaks at about 900 cm^{-1} are due to the aromatic out of plane –CH stretches. [180] The rest of the peak is of similar assignments to those of the Chitosan and Sucrose CDs. There is no observable significant change in the FTIR spectra of the PEG and that of the PEG CDs, an indication that the functionalization of the CDs is not significantly different from that of the precursor.

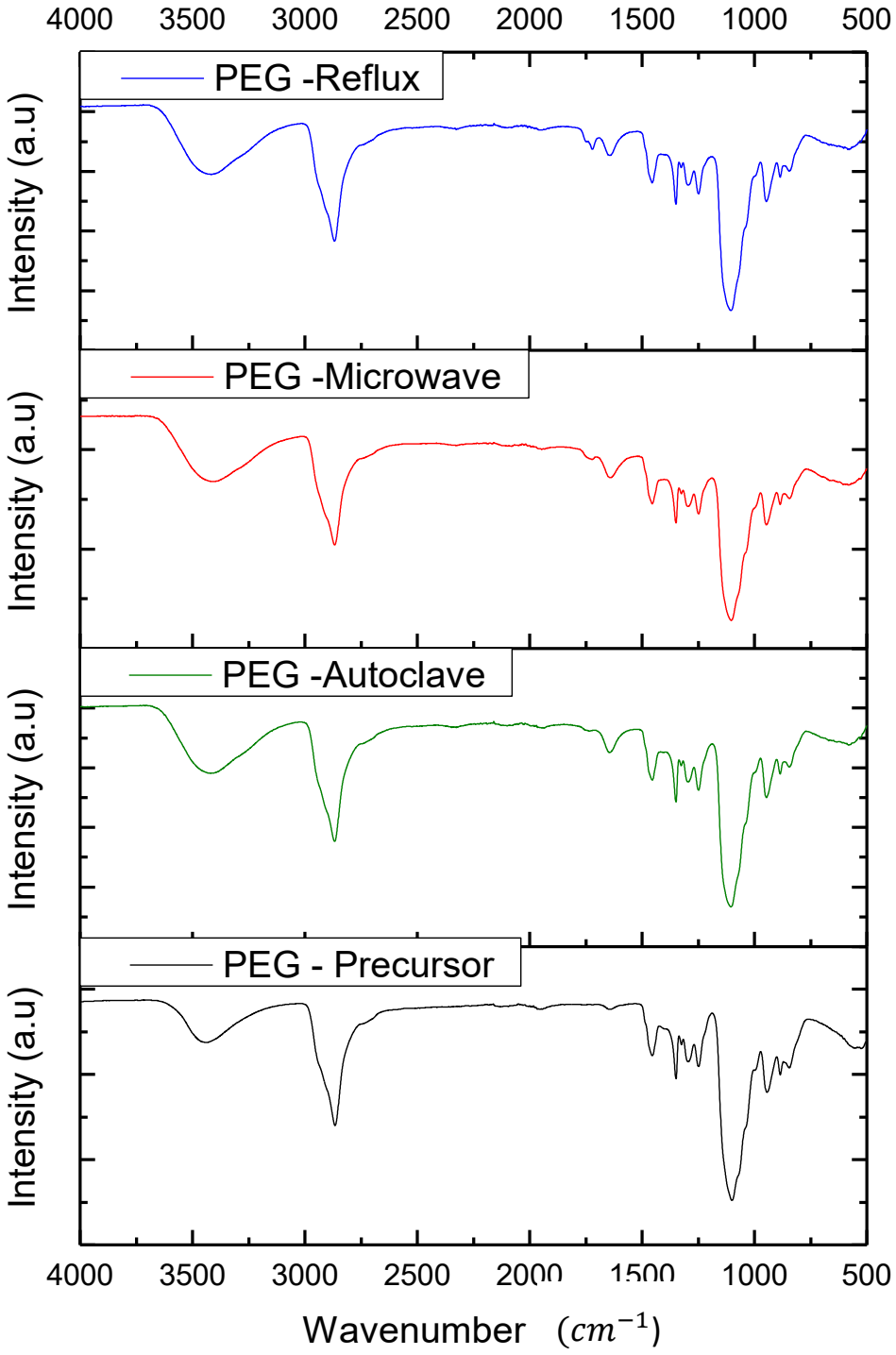

Figure 4-17: FTIR spectra of PEG-CDs synthesised via reflux, microwave, autoclave and the FTIR spectra of Sucrose respectively

4.1.3.5 Fluorescence %QY

The %QY was determined at excitation of 350 nm using quinone sulphate as photoluminescent reference material. The %QY was determined to be 2.8% for the smallest CDs of sizes 2.52 nm, 6.6% for the medium-sized CDs of 3.34 nm in size, and 11.4% for the largest CDs od sizes 4.80 nm (Table 4-11). It is apparent that unlike the sucrose and chitosan synthesised CDs, the PEG synthesised CDs exhibit a direct proportion relationship between the CDs particle size and the %QY. Herein, larger CDs have higher %QY. This suggests that the photoluminescence of the synthesised CDs is mostly generated from surface defects, which more course and larger CDs having more of. Also, as discussed above the study of varying excitation wavelength revealed that the optimal PL emission of the PEG synthesised CDs occurred at 310, 330 and 350 nm excitation wavelength for the autoclave, microwave and reflux synthesised CDs. Following this, it is not unexpected that the reflux synthesised CDs exhibit a superior %QY at an excitation of 350 nm.

Table 4-9: Fluorescence %QY of the sucrose synthesised CDs

method	Autoclave	Microwave	Reflux
CDs size (nm)	2.52±0.83	3.34±1.54	4.80±0.99
%QY	2.8%	6.6%	11.4%

4.1.3.6 Summary

Well-distributed CDs with a narrow particle size distribution and a modest %QY were synthesised across all three methods when PEG was used as a carbon precursor. It was found that CNS were expressed as by-products. Moreover, the synthesised CDs remained in solution. Thus, future studies should entail eliminating the production of by-products as well as obtaining CDs as a solid product. In a nutshell, PEG was chosen as a good carbon precursor for CDs synthesis.

4.2 Conclusion

4.2.1 Methods

Of all the reaction methods explored, the microwave method proved to have the shortest reaction times. However, the reaction was tedious as the pressure fluctuations were challenging to monitor, meaning that the reaction times were difficult to control. Thus, rendering the reaction times challenging to maintain and/or simulate. On the other hand, the reflux method

was easy to set-up and to maintain. However, the reproducibility of the results proved to be poor. The autoclave method yielded reproducible CDs samples at reaction times of 5-6 hours. This was attributed to the ease at which reaction conditions of the autoclave method can be controlled.

4.2.2 Precursors

The use of sucrose yielded CDs sample with either aggregation or severe contamination. At the same time, the use of chitosan yielded CDs samples with CDs particle as a minority. As such, the %QYs of these CDs were found to be less than 1%. However, it is worth highlighting that the synthesis of CDs from chitosan using the autoclave method, yielded the smallest CDs throughout this study with the highest determined %QY of 16%. Though this CDs sample is appealing, attempts to reproduce the sample proved very difficult. Of all the investigated carbon precursors, PEG yielded CDs samples of good quality across the three synthesis methods. That is, all PEG synthesised CDs samples were well-dispersed with a narrow particle size distribution. Thus, it can be deduced that PEG is a robust carbon precursor for the synthesis of CDs. With that said, it was found that the small carbon spheres were expressed as by-products on the PEG synthesised CDs samples. Though the contamination of the PEG synthesised CDs is not as severe as that of the chitosan synthesised CDs, it is still necessary to pursue the synthesise of purer PEG synthesised CDs. In point of fact, it has been substantially argued that the observed PL of most reported CDs may be due to the by-products that present in CDs samples. As such, the synthesis of purer CDs is necessary in order to be able to account for observed %QY.

4.2.3 Summary

In a nutshell, this study showed, that in comparison, PEG is a robust carbon precursor for the synthesis of CDs. The PEG synthesised CDs had %QY of up to 11%. These CDs also had excitation dependent photoluminescence which in turn would enable them to be applied in sensing, imaging and other photo-response dependent applications. More importantly, the CDs were found to be highly functionalised with OH groups which are sought after because it is believed that the OH group will interact with CO and thus play a crucial role in the detection of CO by CDs. However, further studies are necessary in order to obtain pure, solid-state CDs with high %QY. As such, a thorough investigation of the reaction parameters of CDs synthesis from PEG will be investigated in the following chapter in order to map out the feature engineering of CDs. Since the autoclave method proceeds via facile experimental procedures,

the investigation of various reaction parameters will be conducted using the autoclave method. The experiments are discussed in Chapter 5.

5 Hydrothermal synthesis of highly photo luminescent CDs using PEG: A paramedic study

5.1 Introduction

For the successful application of CDs, the synthesis of highly photoluminescent CDs must be reproducible and up scalable. It was noted in chapter 4 that the use of PEG_{400} as a CDs precursor gave CDs with appealing properties using three different synthesis procedures. In this study, the synthesis of CDs from PEG using the autoclave method is investigated further to evaluate the optimal synthesis reaction conditions. The autoclave method was chosen because (1) it uses a simple reaction set-up, and (2) the reaction is relatively easier to monitor, which in turn allows for (3) easy manipulation of reaction parameters. PEG is a non-toxic, non-immunogenic molecule that can be easily conjugated to other molecules through facile chemistry methods. [122], [176]–[179], [181] As a consequence, PEG is often used as a passivation agent [176], [182] or capping agent [183], [184] to enhance the biocompatibility of the synthesised carbon dots and other nanoparticles. The current synthesis trend is to yield passivated CDs in a one-pot synthesis procedure, either through the addition PEG as a passivation agent into the reaction vessel or a one-pot synthesis method where the precursor is both the starting material and source of passivation. [166], [167], [185] As such, there are numerous reports on the use of the one-pot hydrothermal synthesis of PEG surface-passivated CDs in which saccharides were used as the carbon precursor. [29], [52], [186]–[188][189] As discussed in chapter 2, To date, the type of CDs that have been reported to be fabricated with self-passivation from one precursor are the poly dots (PDs) which are synthesised from polymers. PEG is a linear polymer with varying molecular weights depending on the length of the chain. Thus, it has been used as the sole precursor to successfully synthesise surface-passivated CDs (i.e. PDs) in a one-pot method. [149], [166], [190], [191] In this work, we report the effects of various reaction parameters on the synthesis of self-passivated CDs using PEG as a starting material.

The experimental procedure was described in detail in chapter 3 and summarised below in Figure 5-1. Two synthesis routes were explored over four studies to elucidate the optimal conditions needed to synthesise PEG-CDs. The synthesis routes are (i) liquid state synthesis route whereby the starting materials are in a liquid state and (ii) solid-state synthesis reaction route whereby the starting materials are in solid-state. The reaction parameters investigated through these four studies were: (1) the precursor and solvent volume ratios, (2) reaction time, (3) solvent, and (4) molecular weight of PEG precursor. The first three studies were carried out

through the liquid state type of synthesis, and the general reaction conditions were: (1) liquid state PEG precursor with a molecular weight of 400 g/mol^{-1} (denoted as PEG_{400}), (2) the solvent used was water at 1:3 volume ratio of precursor to solvent, (3) the reaction time was 5 hours and (4) reaction temperatures and 200 -215°C was used. As such, with every investigation, only one reaction parameter of interest (i.e. solvent for the solvent study) was varied while the rest remained constant. Further, the study of the variation of molecular weight of the PEG precursor was carried out through solid-state synthesis. Herein, solid-state PEG was used as the carbon precursor. The solid-state reaction was aided by citric acid and was mixed with PEG of various molecular weights in a 2:1 mass ratio.

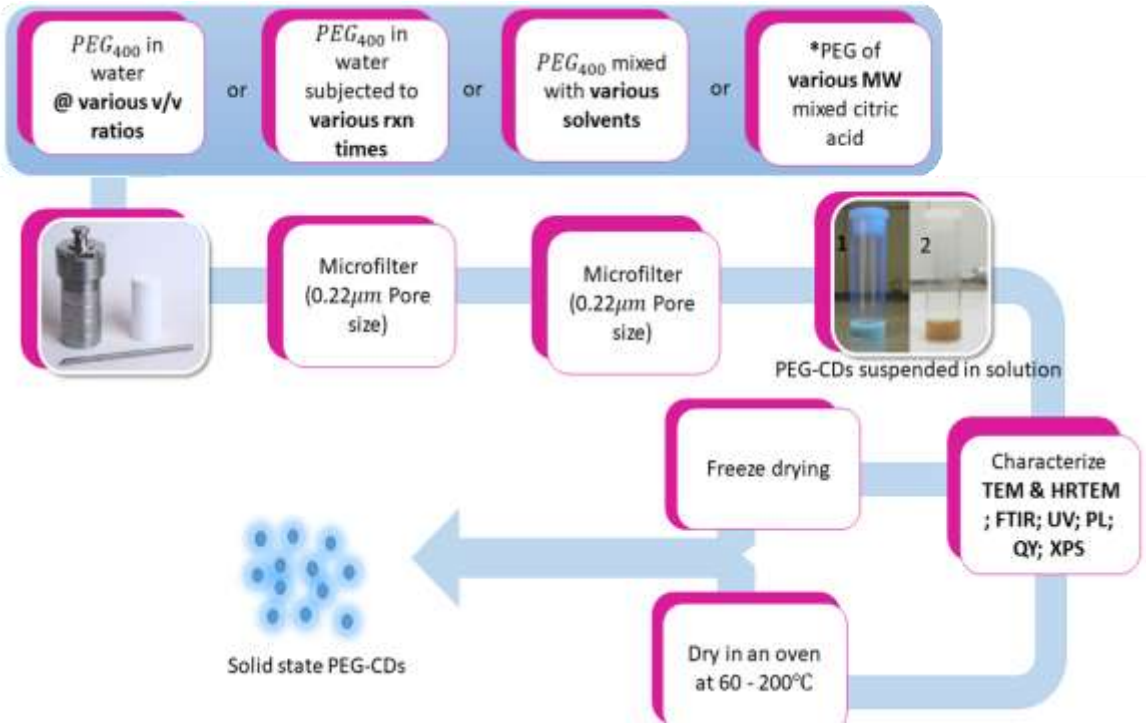

Figure 5-1: Schematic showing how PEG-CDs synthesis using different reaction conditions

The separation of the solid-state CDs from the reactants continued to be a challenge as the synthesised CDs remained suspended in solution. Consequently, the %yield of the products is unknown, and thus, a concentration-dependent analysis could not be done on the prepared CDs. Although a suitable process for the crystallisation of the PEG-CDs out of solution has not been found, various approaches were explored, namely such as dying in an oven, freeze-drying, and solid-state synthesis. Drying in an oven at 60 °C for over three months and freeze-drying resulted in a reduction of the volume of CDs suspension solution, but no solids were obtained. The colour of the CDs solutions increased in intensity upon drying attempts which were

indicative of an increase in the concentration of CDs. The solid-state reaction resulted in CDs that are suspended in a viscous (gel-like) solution. Following that PEG is a well-known capping agent, it is believed that residual PEG chains caps the CDs and force them to stay in solution. To date, obtaining the CDs as a solid-phase product has not been possible. It should be noted that in many studies PEG synthesised CDs are applied whilst suspended in solution, nonetheless, they were reported to have been obtained in solid-state. [29], [52], [186]–[188], [189] The search for a means of obtaining PEG synthesised CDs in the solid-state in our group is still ongoing.

5.2 Results and discussion

5.2.1 Variation of volume percentage of PEG_{400} to water

In chapter 4, it was proven that different carbon precursors yielded CDs with different properties. Herein, an evaluation of whether different concentrations of the carbon precursor yields CDs with different properties is continued. The different concentrations of the PEG precursor were attained by mixing liquid state PEG_{400} with water at different volume ratios. The explored ratios were 25 %, 33%, 50%, 67%, 75% and 100% volume percentage of PEG_{400} to water. As detailed in Chapter 3, the solutions with different volume percentage (vol%) were studied using the autoclave method.

5.2.1.1 TEM images

The synthesised materials were visualised using TEM, and the micrographs are shown in Figure 5-2. All the synthesised CDs are well dispersed with a narrow particle size distribution and a bell-shaped particle size distribution curve. TEM images revealed that at varying vol% of the PEG_{400} precursor mixed with water; the synthesized CDs are approximately 2.7 nm (Table 5-1 and Figure 5-2). These results differ from the work of Lin *et al.,* where larger CDs were formed at a higher concentration of the precursor. [124] TEM images also revealed that the synthesised CDs samples were contaminated by carbon nano-spheres (CNSs) of approximately 22 nm in size, which were described in chapter 4 (the %by-product is shown in Figure S2). However, an exception was observed at 33 vol% of PEG_{400} precursor to water ratio. Wherein two sets of CDs were formed, smaller CDs of 1.69 ± 0.34 nm in size and larger CDs of 10.61 ± 2.81 nm in size (at a 50/50 ratio, see Figure S3). It is important to note that even though the 33vol% PEG_{400}/water sample had a bimodal distribution of CDs particle sizes; both were in the CDs particle size range (Figure 5-2 b). A thorough study of this reaction system was used in a bid to understand the growth mechanism of the CDs. Additionally, CDs were also synthesised from use of solely PEG_{400} as a starting material (i.e. not mixed with water).

The CDs were 4.91 $\pm$ 1.62 nm in size, which is almost double the size of CDs produced with water present (Table 5-1). Also, no contamination or by-product was observed on the TEM images (Figure 5-2 f).

Table 5-1: The volume ratio of PEG_{400} to water used during synthesised and corresponding particle size of the produced CDs

volume ratio of PEG_{400}: water	PEG_{400} %Volume	CDs Particle size (nm)
25:75	25%	2.61 $\pm$ 0.65
33:67	33%	1.69 $\pm$ 0.34
		10.61 $\pm$ 2.81
50:50	50%	2.68 $\pm$ 0.85
67:33	67%	2.69 $\pm$ 0.92
75:25	75%	2.67 $\pm$ 0.43
100:0	100%	4.91 $\pm$ 1.62

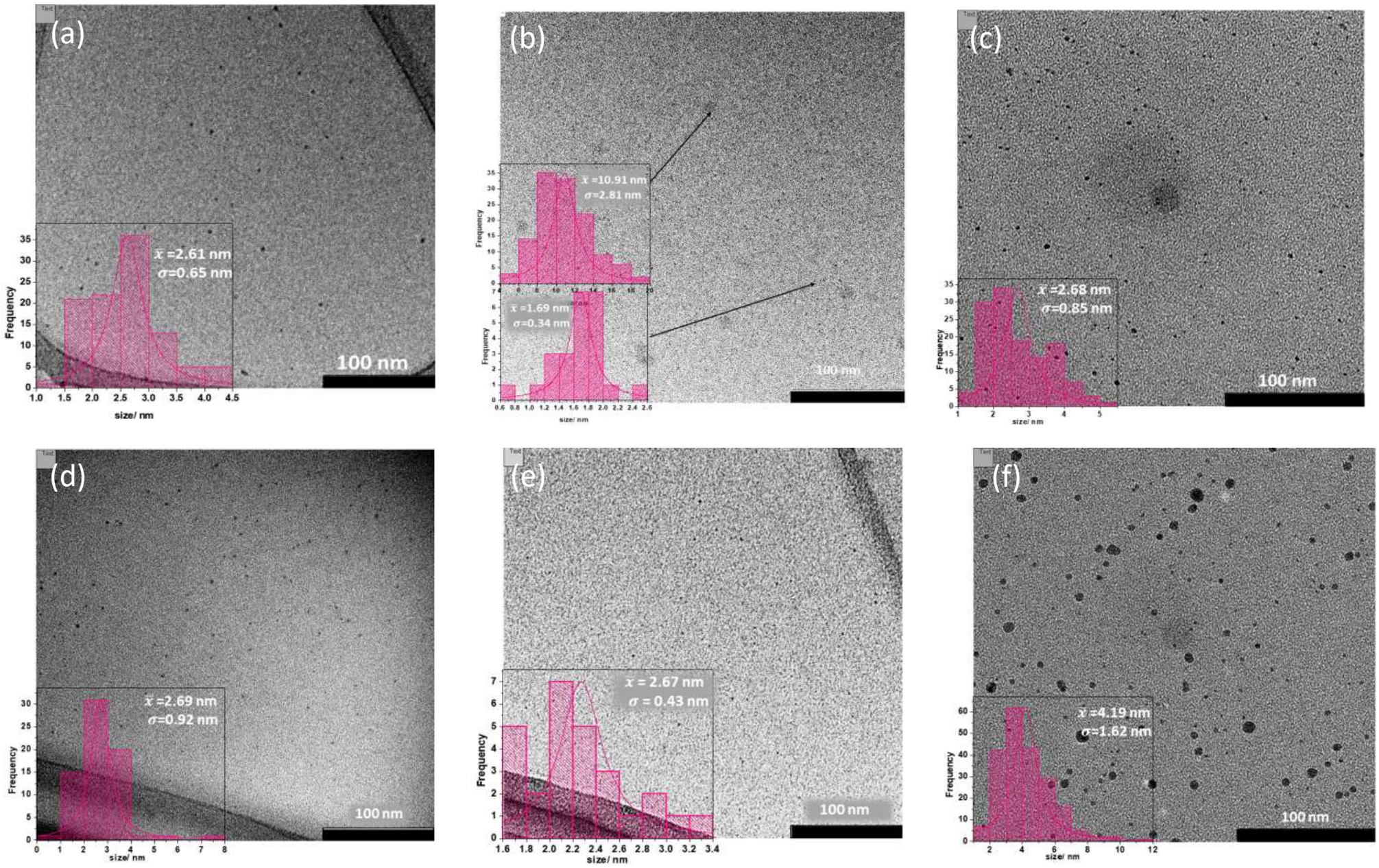

Figure 5-2: TEM images and corresponding particle size distribution curve of PEG-CDs synthesised with (a)25vol%, (b)33vol%, (c)50vol%, (d)67vol%, (e)75vol% and (F)100vol% of the PEG400 precursor was mixed with water, respectively

5.2.1.2 FTIR Spectra

The CDs synthesised from various volume ratio of PEG_{400} to water were subjected to FTIR spectroscopy analysis to determine their chemical structure and the functional groups on their surfaces. The FTIR spectra are shown in Figure 5-3. It was observed that the synthesised CDs had FTIR spectra like that of the PEG_{400} precursor, with differences in the intensities ascribed to dilution effects. A broad peak around 3400 cm^{-1} and a sharp peak around 2950 cm^{-1} n were attributed to the –OH groups [127]–[130] and C-H stretch bonds [180], respectively. Upon transformation from precursor to CDs sample, the ratio of the –O-H/ C-H peaks is significantly increased. This observation is ascribed to decreased exposed CH_2 groups and/or increased -O-H groups on the surface of CDs compared to a polymer chain of PEG_{400} (a long chain with repeating -O-CH_2-CH_2- monomer and terminal -O-H groups).

The peak at about 1021 cm^{-1} is the major peak detected in the samples and was attributed to the vibrational modes of the –C–O bonds. Smaller peaks were also detected on the fingerprint region (below 1500 cm^{-1} wavenumber). The peak at 1441 cm^{-1} and was attributed to aromatic –C=C bands, while the peak at 1200 cm^{-1} was ascribed to the C-O-C bonds. Above the fingerprint region, peaks at 1635 cm^{-1} and 1590 cm^{-1} were attributed to the aromatic C=O carbonyls and the –C-H bond bends, respectively. [180]

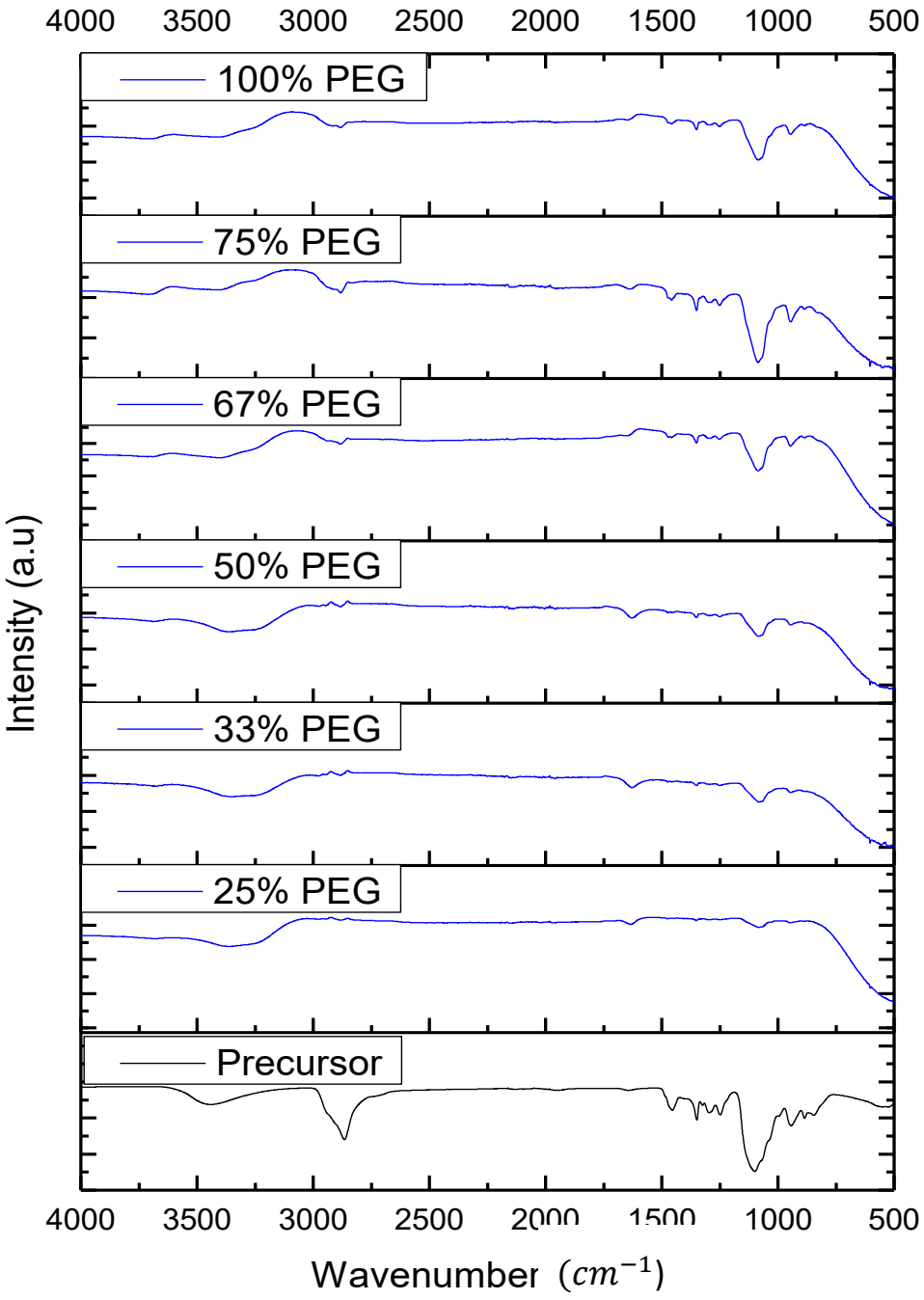

Figure 5-3: FTIR spectra of PEG-CD synthesised using various PEG% starting materials

5.2.1.3 UV-Vis absorption and PL emission spectra

The resulting CDs studied by to UV-vis spectroscopy to determine their absorbance and emission behaviour. The analysed spectra were shown in Figure 5-4. There was an observed absorption peak around 200 nm wavelength for all CDs samples which was attributed to transitions of the C= O bonds. [33], [119], [140], [141] Additionally, the CDs synthesised at

67vol% of PEG_{400} had an absorption peak just above 250 nm wavelength. The peak is attributed to the π –π* transitions of the C=C bonds in the CDs. [114]–[116]

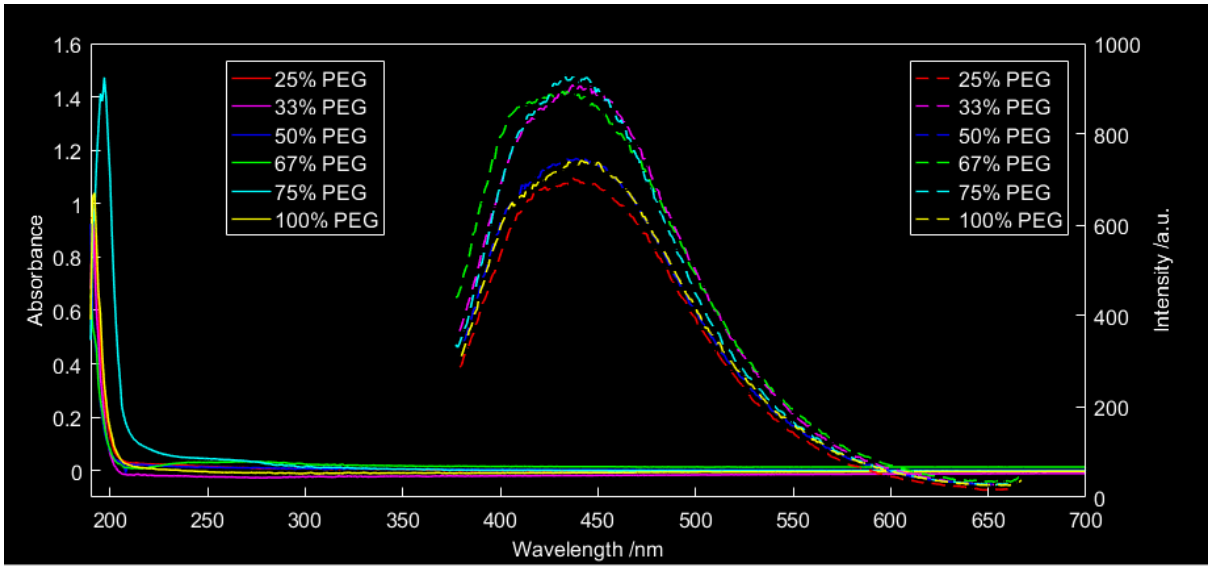

Figure 5-4: UV-Vis absorption and fluorescence spectra of CDs synthesised using various PEG_{400} to water volume ratios at 350 nm excitation wavelength

The synthesised CDs exhibit photoluminescence emission peaks. It is essential to note the PEG_{400} precursor is not photoluminescent. Thus, the observed photoluminescence is ascribed to the CD nanoparticles. When excited at 350 nm, the synthesised CDs emitted at short wavelengths of approximately 425-430 nm. The lack of change in the peak position of the CDs samples synthesised at various vol% of PEG_{400}/water infers that the nature of the PL of PEG synthesised CDs is independent of the concentration of the precursor used during synthesis. [192]–[195] These results are in accordance the findings of Lin *et al.*, where the different concentrations of p-phenylenediamine yielded CDs with similar PL (though, conversely to this study the particle size of their CDs varied). [124]

5.2.1.4 Fluorescence Quantum Yield

Quinine sulphate dissolved in 0.1 M sulfuric acid was used as a reference dye to determine the quantum yield of the synthesised CDs [119], [163], [196], [197] and results are shown in Table 5-2 below. Overall, the QY was determined to be approximately 10 % for CDs synthesised at varying vol% of PEG_{400}/water. Though, it is deduced that the presence of the by-product may enhance the %QY. This is supported by the following findings: The %QY dropped to less than 4% (i) at a low percentage of the by-product (67vol% PEG_{400}/water sample) and (ii) absence of the by-product (33vol% PEG_{400}/water) (Table 5-3 and Figure 5-5). However, further studies that separate the by-product and the CDs and investigate the %QY of the materials

independently are necessary to confirm these findings. In a nutshell, it is deduced that the difficulty in establishing a relation between the vol% PEG_{400}/water of the starting material and the resulting CDs is due to the presence and the lack of consistency in the %yield of the by-product.

Table 5-2: Particle sizes of vol%PEG-CDs and corresponding fluorescence quantum

PEG_{400} %Volume	**25%**	**33%**	**50%**	**67%**	**75%**	**100%**
Particle size (nm)	2.61 ± 0.65	1.69 ± 0.34 & 10.61 ± 2.81	2.68 ± 0.85	2.69 ± 0.92	2.67 ± 0.43	4.91 ± 1.62
%QY	10.4	3.1	9.9	3.5	10.4	7.0

It has been suggested in previous studies that particle size effects play a significant role in the %QY with smaller CDs generally exhibiting higher %QY compared to bigger CDs. [34] Thus, the observed decrease in QY on the 33vol% PEG sample is ascribed to the presence of the bigger CDs particles of the size 10.9 nm at 33vol% PEG. [102], [120], [198]–[200] Also, it is suspected that the dynamic interaction of the differently sized CDs negatively impacts the determined %QY, perhaps due to the quenching effect. [61], [201] On the other hand, the %QY 7% of the CDs synthesised at 100vol% PEG_{400} can be attributed to CDs since no by-products (CNS) were observed on this sample.

Table 5-3: The %by-product observed on TEM images

PEG_{400} %Volume	**The %by-product observed on TEM**
25%	30%
33%	Not applicable
50%	50%
67%	67%
75%	42%
100%	Not applicable

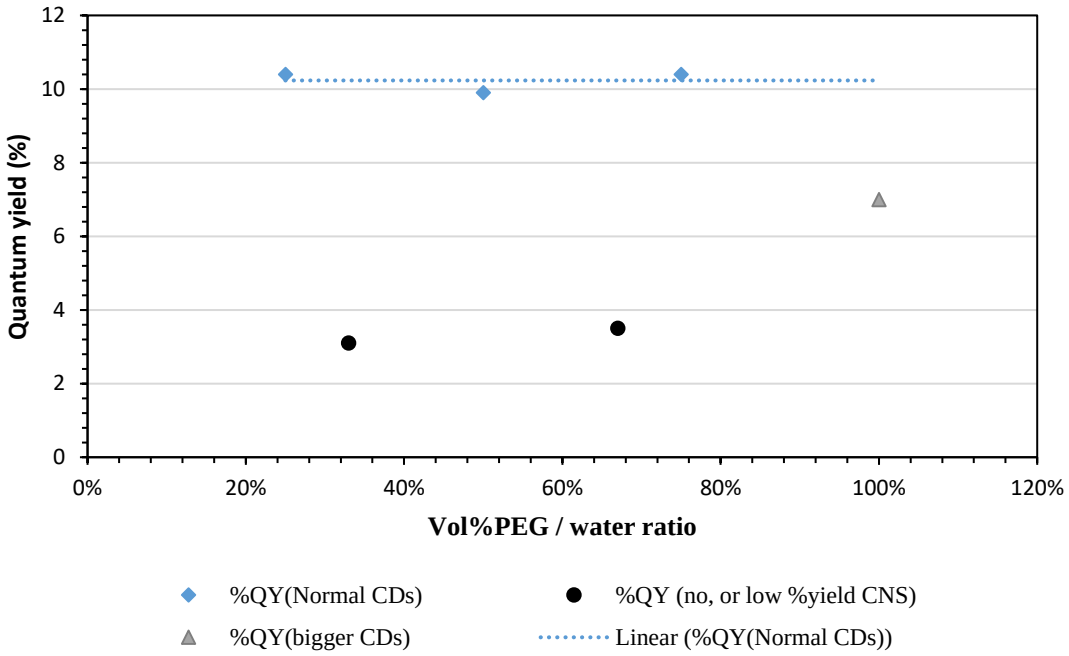

Figure 5-5: Vol%PEG / water ratio of the starting material versus particle size of resulting PEG-CDs

5.2.1.5 Summary

In a nutshell, the use of various volume percentage of PEG_{400} to water yielded CDs of approximately 2.7 nm, which almost doubles to 4.9 nm at 100 vol% of PEG_{400} when no water is present. The spectroscopy analysis of these CDs suggested they have similar chemical structures. The quantum yield of the synthesised CDs was determined to be approximately 10%. However, it drops to 7% accompanying a particle size increase of 45% for CDs synthesised with no water present. This inverse proportional correlation of CDs particle size and quantum yield has been widely reported in the literature. [34] The CDs samples synthesised when water was present had by-products which seem to be partly responsible for the determined %QY though further studies are necessary to confirm this.

Interestingly, CDs sample synthesised with 33 vol% PEG_{400}/water was different from the other CDs samples; it consists of a binomial particle size distribution of CDs of smaller CDs of 1.69 nm and bigger CDs of 10.4 nm in size. The sample exhibited a low quantum yield of 3%. Nevertheless, a careful study of this reaction might give insights into the nucleation and growth mechanism of CDs.

5.2.2 Variation of reaction time

5.2.2.1 TEM images

Herein, the effect of the duration of the synthesis on the properties of the PEG synthesised CDs was investigated. The reaction time was varied from 1 – 12 h and the synthesised CD were visualised using TEM. The captured TEM images and the corresponding particle size distribution are shown in Figure 5-6. The summary of the particle size of the CDs produced after various reaction times is shown in Table 5-4 below. Additionally, the correlation of the particle size of the CDs produced after various reaction times is shown in Figure S4. It was found that there is no significant change in particle size from 1h to 5 h of reaction time and the particles remain at approximately 2.0 nm throughout. However, at t = 12h, a substantial change in CDs size was observed as the CDs size doubled to 4.15 nm. Also, the intensity of the colour of the solutions increased with increasing reaction time, suggesting that the concentration of CDs increased with increasing reaction time.

Table 5-4: The particle of CDs synthesised after various reaction times

Reaction time (h)	CDs Particle size (nm)
1	1.82 ± 0.56
2	2.81 ± 0.50
3	2.04 ± 0.63
4	2.11 ± 0.53
5	2.05 ± 0.45
12	4.15 ± 1.54

All the synthesised CDs samples were well dispersed. However, as detected in the TEM images, when reaction time is higher than 4h, some small CNSs by-product was produced. There is an observed 233% increase in particle size growth between the CDs synthesised after 1 hour compared to those synthesised after 12 hours. Increasing the reaction time to 12 hours is also accompanied by a decrease in the interparticle distance of the CDs due to an increase in the concentration of the CDs. That is nanoparticle aggregation occurs which might be the mechanism of growth of the larger nanoparticles.[202]–[205]

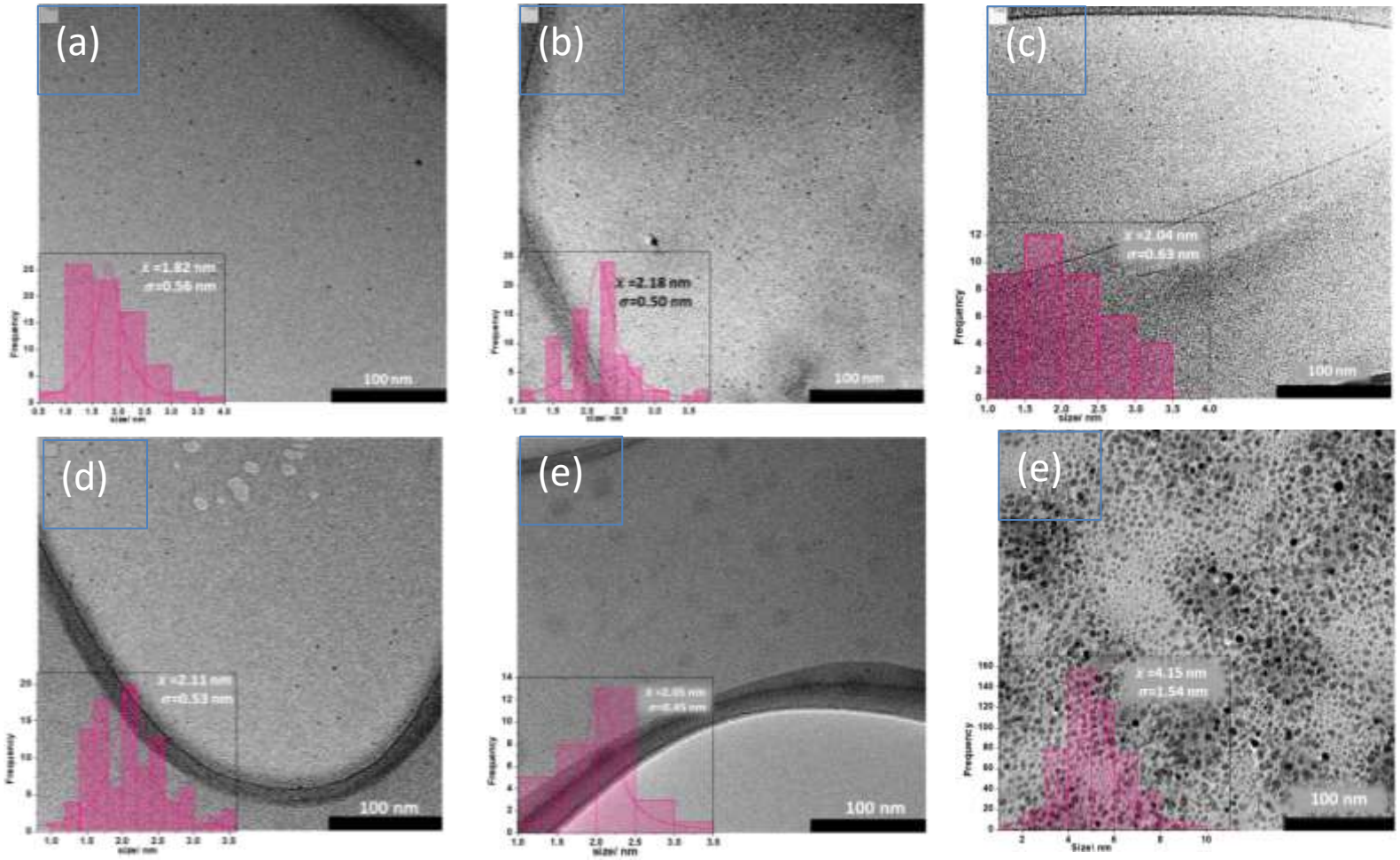

Figure 5-6: TEM images and corresponding particle size distribution curve of PEG-CDs synthesised at (a) 1 h (b) 2 hrs , (c) 3 hrs, (d) 4 hrs, (e) 5 hrs and (F) 12 hrs of reaction time, respectively

5.2.2.2 UV-Vis absorption and PL emission spectra

Figure 5-7 shows the UV absorption of the CDs synthesised after varying reaction times and their corresponding PL emission spectra at 350 nm excitation wavelength. For all the samples synthesised between 1 – 12 hours, there was an observed sharp absorption peak at approximately 200 nm which was assigned to the n–σ* transitions of the aromatic C-C bonds on the CDs [31], [31], [111], [111]–[113]. Weaker absorption bands around 200 nm and 300 nm were also observed. These which could be attributed to a π –π* transition of the –C=C aromatic bonds and an n– π * transition of C=O bonds, respectively. [24], [50], [119], [163], [164] An absorption tail of low intensity that extends into the visible region of the spectrum was observed. The absorption tail is attributed to defects which may arise from the functional group on the surface of CDs. [206]

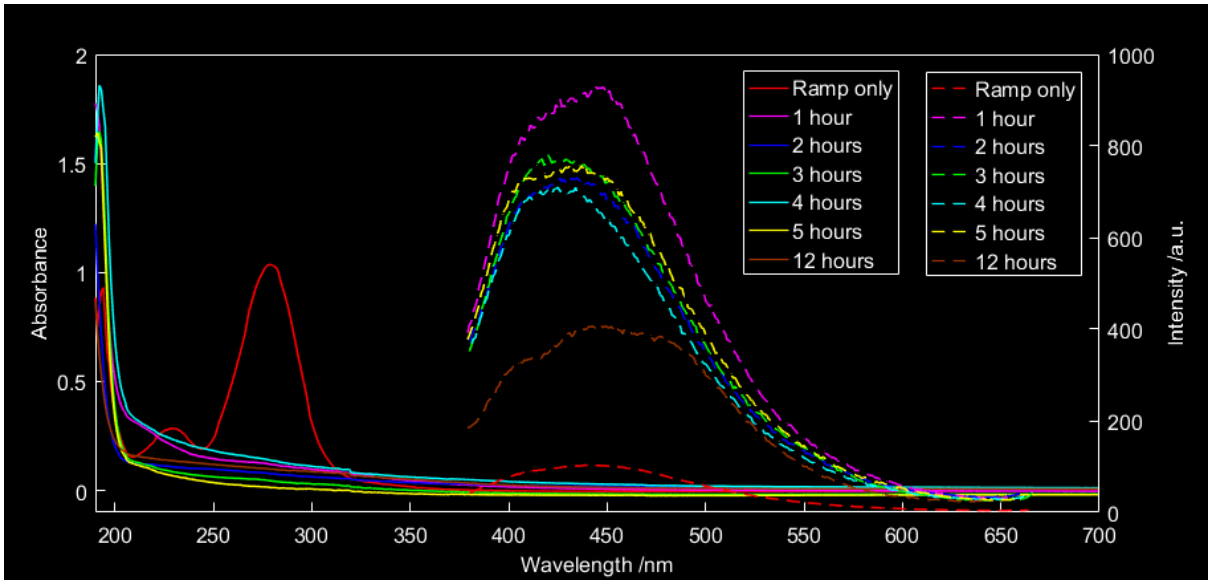

Figure 5-7: UV-Vis absorption and fluorescence spectra of various PEG-CDs synthesised after various reaction time, recorded using 350 nm excitation wavelength.

It is important to state that synthesis of the CDs was done at 200 ℃ and that the synthesis followed a common 3-step route: (step 1) the reaction temperature is achieved to gradual ramping, (step 2) the reaction is run at the reaction temperature and (step 3) the reaction is cooled off to room temperature. Normally, the duration of step 2 is the recorded as the reaction time (Figure 5-8).

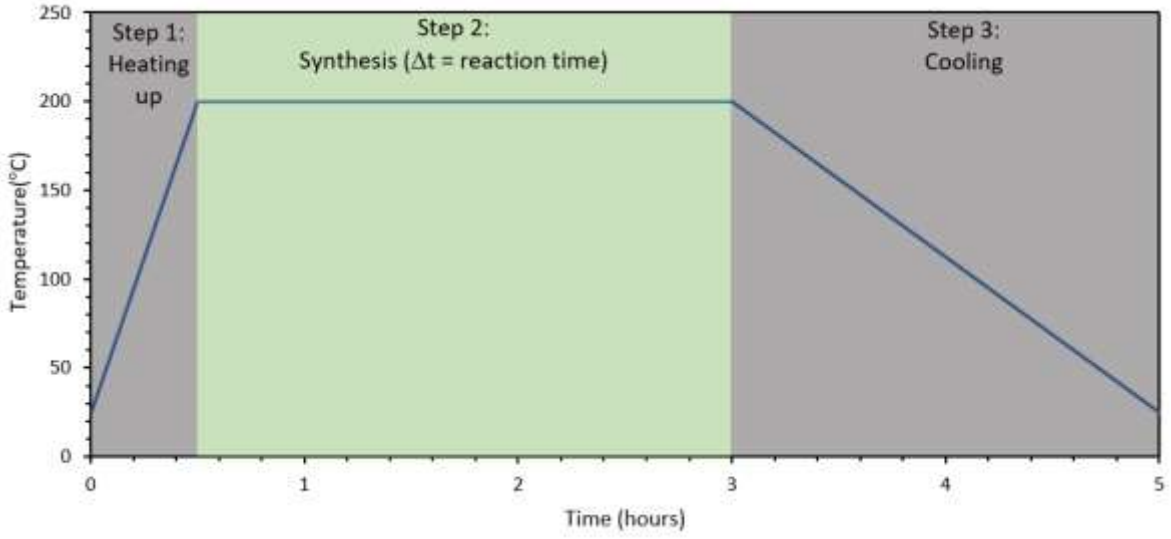

Figure 5-8: General course of reaction: step 1 is the heating up of the reaction to the desired rection temperature, step 2 is the synthesis (the duration of step 2 is generally noted as the reaction time) and lastly step 3 is the cooling of the reaction.

Interestingly, when step 2 was omitted (Figure S5), whereby the reaction vessel was heated to 200 ℃ (at a ramping rate of 10 $℃/min$) subsequently cooled to room temperature without holding the reaction at the set temperature, CDs were still produced (Figure S6 and S7).This experiment shows that the synthesis of CDs from PEG starts at a temperature below 200 ℃ and could influence the autoclave the results from the autoclave method. With that said, it is imported to note that the absorption spectrum of these CDs was different from all other PEG synthesised CDs. This sample exhibited three distinguishable absorption peaks at 200, 240 and 280 nm as opposed one peak around 200nm and a band around 200 – 350 nm.

All the synthesised CDs samples were PL responsive when excited at a 350 nm wavelength. The PL emission maxima all occurred around 425 nm showing no variation in peak position with reaction time. This is not unexpected as the CDs size did not vary as well. However, the results are not in accordance with the results of Chen *et al.,* whereby a reaction of 1h yielded CDs that emit at a significantly different wavelength compared to CDs synthesised after 4h. [131] Chen *et al.,* used p-phenylenediamine as a carbon precursor and formamide as a solvent. [131] It is suspected that the effects of reaction time on the synthesis of CDs are unique to the carbon precursor and/or solvent used. However, further studies are necessary to confirm this.

5.2.2.3 FTIR Spectra

The chemical structure and surface functional groups of the synthesised CDs was investigated using FTIR and the results are shown in Figure 5-9. Similarly to the previously discussed CDs, the synthesised CDs at varying synthesis duration exhibit FTIR peaks at 3400 cm-1, 2950 cm-1, 1600 cm-1 and 1200 cm-1 which are ascribed to –OH, C-H, –C=/–C=O and –C-O bonds, respectively. [127]–[130], [180] The bands around 1600 cm-1 are be ascribed to the –C=C and –C=O vibrational modes of the aromatic rings in the CDs. The FTIR spectra of the synthesised CDs and the carbon precursor are similar, with the majority of the differences ascribed to dilution effects. [180] This finding is ubiquitous in the literature of CDs. It is generally attributed to functional groups of the carbon precursor being retained on the surface of CDs during the hydrothermal synthesis. However, the similarities between the FTIR spectra of the CDs and its carbon precursor may be due to the presence of the residual PEG on the CDs sample since the synthesised CDs remained suspended in solution.

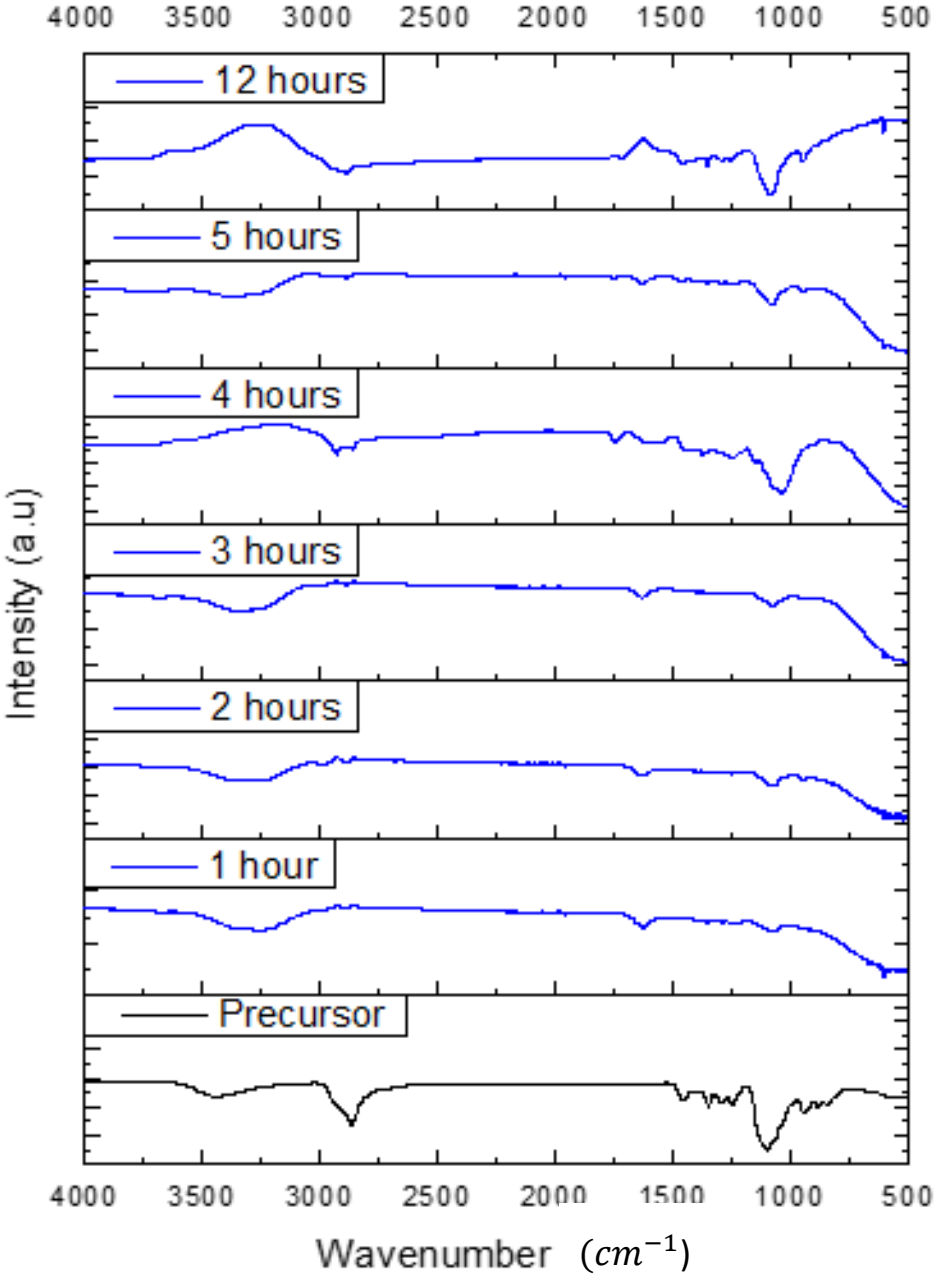

Figure 5-9: FTIR spectra of PEG CDs synthesised at various reaction times

5.2.2.4 Fluorescence Quantum Yield

The quantum yield of the synthesised CDs was determined using quinine sulphate as a reference dye, and the results are shown in Table 5-5. Moreover, the plot of the reaction duration versus the %QY of the resulting CDs is shown in Figure 5-10. As discussed above, the particle sizes of CDs did not significantly change with varying reaction time between of 1 and 5 hours of reaction time. They maintained a particle size of approximately 2 nm throughout. The %QY however was unusual but could relate to uncontrolled experimental artefacts. At 1 h reaction time, the %QY is 1 % which increases as the reaction time is increased and more

particles are formed in the solution. As per the FTIR spectra analysis, the chemical structure of the synthesised CDs has constant across the varying reaction time. It is also inferred that the origin of the PL of the CDs has remained constant across varying reaction times since the UV-vis and PL spectra remained the same. [33] It can be concluded that with regards to samples produced after 1-4 hours what changed was the number of CDs particles in solution. Following this, together with the fact that %QY is not a function time, the observed increase in %QY is attributed to the aggregation-induced emission (AIE) phenomenon. [61], [201] AIE occurs when the photoluminescence of materials is enhanced by increase concentration or density of the material. [61], [201] The %QY then peaks at 3h, reaching a high %QY of 15.1% and after that decreases with increasing reaction time. The %QY decreases by 67% from 3h to 4h reaction time, even though the samples have relatively similar particle size (Figure S8). This behaviour was not expected and requires further studies to be understood.

Table 5-5: Particle sizes PEG-CDs and correponding fluorescence quantum of CDs synthesised after various reaction times

Reaction time(h)	1	2	3	4	5	12
CDs Particle Size (nm)	1.82±0.56	2.18±0.50	2.04 ±0.63	2.11±0.53	2.05±0.45	4.15±1.54
Quantum Yield (%)	1.0	9.0	15.1	6.5	9.0	6.2

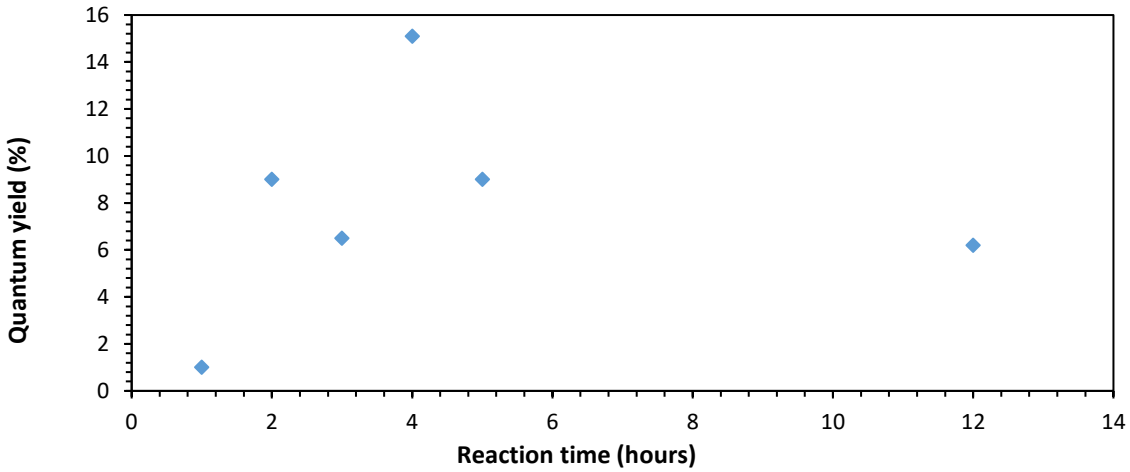

Figure 5-10: The quantum yield of CDs synthesised after reaction times

5.2.2.5 Summary

The synthesised CDs after 1-5 h are approximately 2 nm in size. The particle size of CDs increased by 102% when the reaction time was 12h. At reaction time beyond 4h the synthesised CDs samples have by-product (CNSs) as detected and seen on the TEM images. The %QY of the synthesised CDs did not correlate with their particle size, and further studies are required to understand these findings. The synthesised CDs after 3, had a particle size of 2nm with no detected by-product and a high %QY of 15%

5.2.3 Variation of solvent used during synthesis

It has been reported that different solvents (having various properties) yield CDs with different characteristics. The solvation system during synthesis plays a role in the aggregation, dehydration, carbonisation, core formation, and growth process that occur during CDs synthesis. The properties of the solvent, i.e. boiling point, solubility, polarity and protic/non-protic properties, dehydrating ability contribute to the characteristics of synthesised CDs. [207], [208] Thus, a study of the variation of the solvent used during the synthesis of CDs from PEG_{400} was conducted. The study of varying solvents on the synthesis CDs was done to achieve the following:

(a) To explore the role solvent of the PEG synthesised CDs

(b) To search means for means of yielding more solid CDs

(c) To find a solvent that yielded CDs with less by-product, i.e. CNS

The explored solvents were 2-butanol, acetonitrile, chloroform, dichloromethane and ethylene glycol. The solvents were chosen due to their low boiling points and the degree at which the carbon precursor dissolved PEG_{400}. The boiling point of all the solvents was below 200 °C, and molecular weights were also below 120 g per mol. Low boiling point solvents are easy to work with as they do not require sophisticated equipment for their removal by evaporation. The chosen solvents exhibit a high relative polarity with a minimum of 0.259 and low molecular weight; this is associated with good polarity. In addition to the advantages, PEG_{400} was soluble in the chosen solvents, which exhibits good dissolution and solubility of the carbon precursor reagents in the solvent. A summary of the properties of the solvents is shown below in Table 5.6. PEG-CDs with various properties were produced form the different solvents. However, the products formed were not solids and the PEG-CDs remained suspended in the solvents or formed liquids due to excess PEG.

Table 5-6: Some of the properties of the solvents used in making PEG_{400} CDs. [209]

Solvent	Boiling Point /°C	Molecular weight/g per mole	PEG_{400} solubility	Relative Polarity
Ethylene glycol	197.6	62.1	Soluble	0.790
Dichloromethane	39.6	84.9	Soluble	0.309
2-butanol	100	74.1	Soluble	0.327
Acetonitrile	82	41.1	Soluble	0.460
Chloroform	61.2	119.4	Soluble	0.259
Water*	100	18	Soluble	1.000

5.2.3.1 TEM images

The TEM images of the respective PEG-CDs products and corresponding particle size distribution curves are shown in Figure 5-11. All solvents yielded mono-dispersed PEG-CDs except for dichloromethane, where the CDs were clustered in one area and had a wider particle size distribution. It is worth pointing out that dichloromethane yielded PEG-CDs that were significantly larger than CDs yielded from the use of all the other explored solvents It was also noticed that chloroform yielded CDs that expressed mild aggregation and a small amount fibrous material. The use of ethylene glycol, dichloromethane, 2-butanol, acetonitrile and chloroform, yielded PEG-CDs with particle sizes of 2.35 ±0.48 nm, 5.93 ± 2.48 nm, 1.66 ± 0.57 nm, 2.68 ± 0.89 nm and 2.94 ± 1.18 nm, respectively as shown below in Table 5.7 and Figure S9. For comparison purposes, the use of water in the (a) variation of %PEG study @25%

vol PEG and (b) the variation of reaction time at 5 hours is also included in Table 5.5 and in future discussions.

Table 5-7: The solvent used during synthesis and the particle size of the synthesised CDs

Solvent	Particle size/nm
Ethylene glycol	2.35 ±0.48
Dichloromethane	5.93 ± 2.48
2-butanol	1.66 ± 0.57
Acetonitrile	2.68 ± 0.89
Chloroform	2.94 ± 1.18
Water(a)	2.61 ± 0.65
Water(b)	2.05 ± 0.45

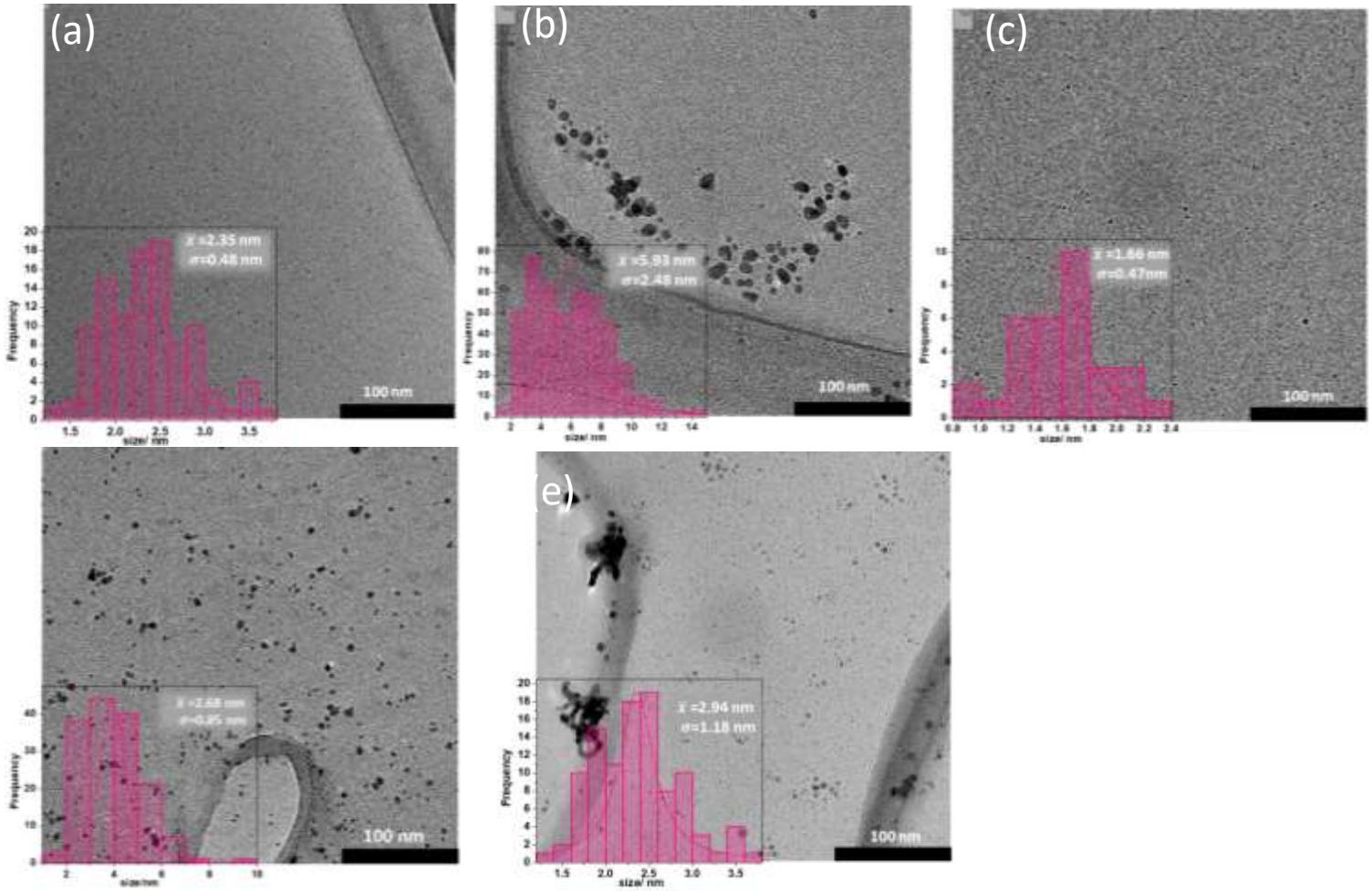

Figure 5-11: TEM images and corresponding particle size distribution curve of PEG-CDs synthesised using different solvent namely (a) ethylene glycol, (b) dichloromethane, (c) 2-butanol, (d) acetonitrile and (e) chloroform, respectively

A correlation matrix was plotted and shown in Table 5.8. A correlation coefficient of 0 suggests that there is no linear relationship between the two variables. [210] A negative sign occurs when one variable increases and the other decreases and a positive sign occurs when one variable increases the other also increases. [210] As shown in Table 5.8, the particle size of the yielded CDs exhibited correlation coefficients of -0.70, 0.15 and -3.9 towards the boiling point, molecular weight and relative polarity of the solvents used during synthesis, respectively. Some correlation between the particle size of the synthesised CDs and the boiling point of the solvent used is seen. As such, the higher the boiling point of the solvent, the smaller the particle size of the synthesised CDs.

Table 5-8: Correlation Matrix of the properties of the solvent used during synthesis and the particle size of the resulting PEG-CDs

	Boiling Point (℃)	Molecular weight (g per mole)	Relative polarity	Particle size (nm)
Boiling Point (℃)	1.00	0.45	0.02	-0.70
Molecular weight (g per mole)	0.45	1.00	-0.72	0.15
Relative polarity	0.02	-0.72	1.00	-0.39
Particle size (nm)	-0.70	0.15	-0.39	1.00

Figure 5-12 is a visual representation of the particle size of the synthesised PEG-CDs against the boiling points of the corresponding solvent that was used during synthesis. The second cluster of data points in Figure 5-12 are of PEG-CDs with particle sizes between 2-3 nm, these CDs were yielded using solvents with a boiling point between 60 – 100 ℃. Meanwhile, the use of 2-butanol, which has a high boiling point of 197.6 ℃ yielded the smallest PEG-CDs of 1.66 ± 0.57 nm size.

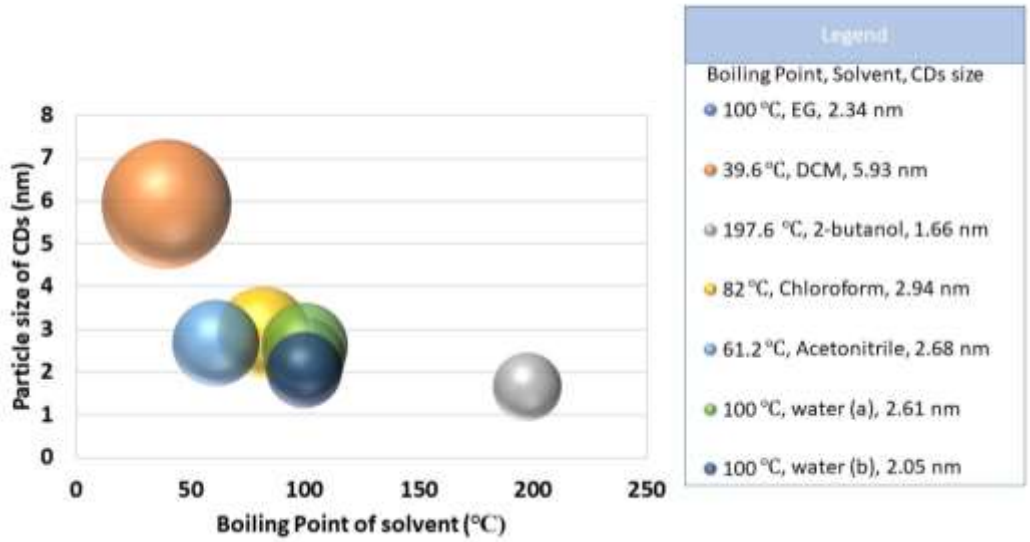

Figure 5-12: Particle size vs boiling point of solvent used. The size of the sphere correlates to the particle size of the CDs

A similar result has been observed by Ding *et al.*, here the smaller CDs size correlated with higher boiling points. [208] Ding *et al.*, explored a 'solvent-engineering' approach through use of formamide, DMF/ formamide, H_2SO_4/H_2O used to produce CDs with tuned optical properties. [208] Formamide which has a high boiling point (210 ℃) compared to all the others used gave the smallest CDs of 1.5 nm in size. [208] A mixture of DMF and formamide gave CDs with d=3-5 nm. DMF had a medium boiling point of 153 ℃. Lastly, H_2SO_4/H_2O which had the lowest boiling point of approximately 100 ℃ yielded the largest CDs of 7 nm. [208] In contrast, Chen *et al.*, obtained no correlation between the boiling point of the solvents used and the particle size of the produced CDs (of sizes 3 -13 nm). [211] Instead, dimethylformamide, methanol and water all formed CDs with extremely similar particle size and particle size distribution even though their boiling points are significantly different (see Figure 5-13 below). [211]

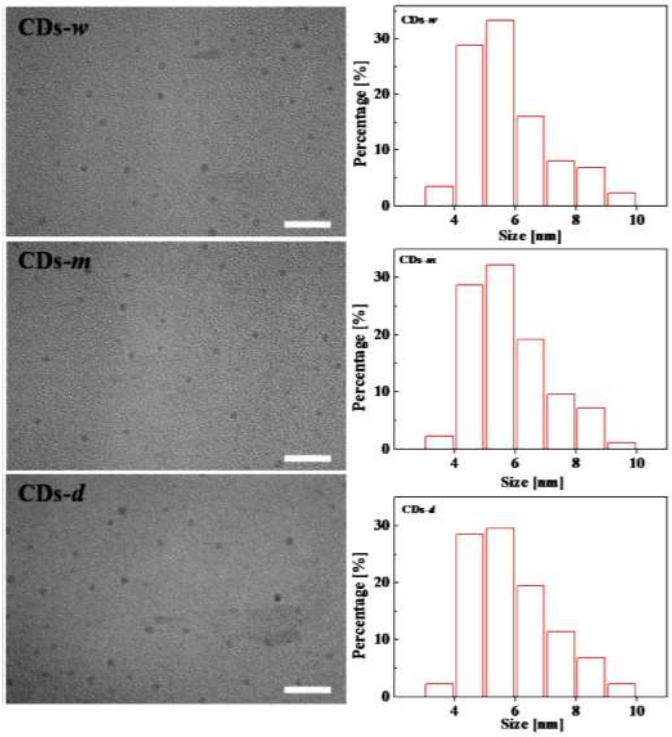

Figure 5-13: TEM image (50 nm scale bar) and corresponding particle size distribution of CDs synthesised by Chen et al., CDs-w, CDs-m, CDs-d were synthesised using water, methanol and dimethylformamide respectively. [211]

5.2.3.2 UV-Vis absorption and PL emission spectra

Figure 5-14 shows the UV-vis absorption and the emission spectroscopy of the PEG-CDs synthesised using various solvents. There was an observed absorption peak below 200 nm in all the synthesised CDs while varying solvent. This peak was ascribed n–σ* transitions. [31], [31], [111], [111]–[113] There was also an absorption seen between 200 nm to 350 nm which was ascribed to the n–π* or π –π* transitions. [24], [50], [119], [163], [164] Conversely, to the varying %PEG and reaction time studies, when the solvent used during the preparation of CDs is varied, the emission peak at 350 nm excitation wavelength changes. The emission peak at 350 nm excitation wavelength is 545 nm, 545 nm, 448, 449 nm, and 480 nm for 2-butanol, acetonitrile, chloroform, dichloromethane and ethylene glycol synthesised PEG-CDs, respectively (see Table 5-9). It worth highlighting that, the used the solvents 2-butanol, and acetonitrile yields CDs has only one absorption peak below 200 nm and exhibited no tail that extended towards 350 nm as seen with other solvents explored under similar reaction conditions. Moreover, with these solvents, 2-butanol and acetonitrile, the produced CDs exhibited emission peaks that are slightly outside the normal range of 400 – 500 nm. It is worth

noting that no established correlation between the particle sizes of the PEG-CDs and the wavelengths of the emitted light at varying solvent was found.

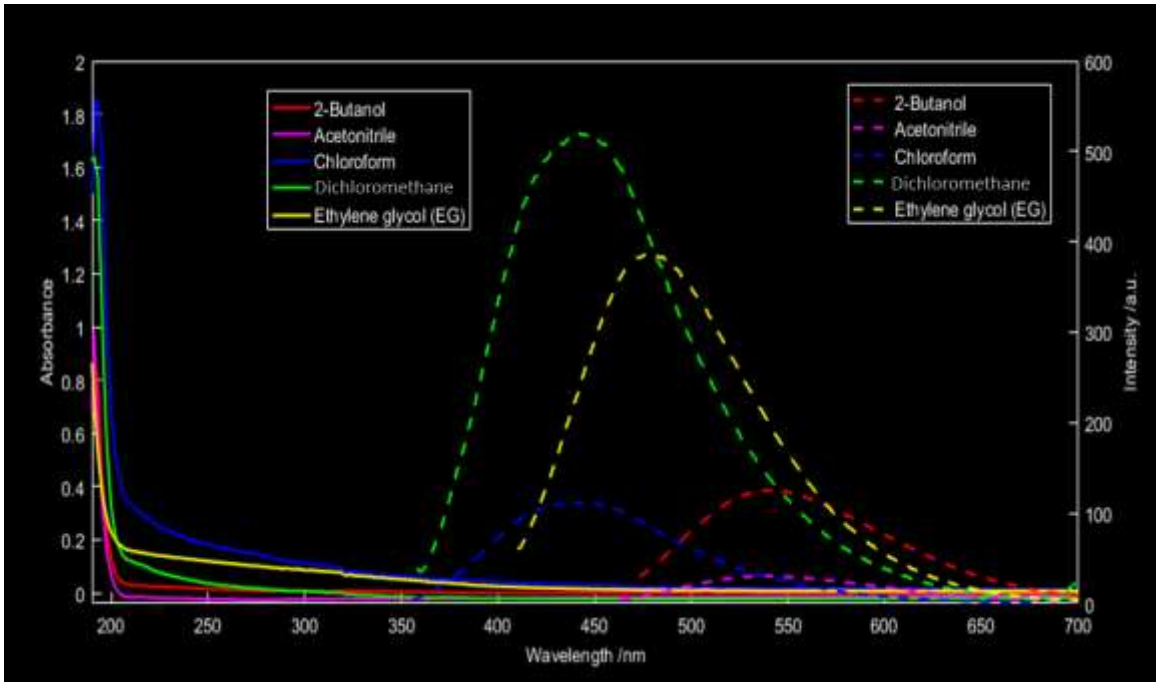

Figure 5-14: UV-Vis absorption and fluorescence spectra of various PEG-CDs synthesised using various solvents, recorded using 350 nm excitation wavelength

Table 5-9: UV-Vis and PL emission peaks of PEG-CDs, with corresponding spectral assignments and particle of the PEG-CDs synthesised using various solvents

Sample	**UV-Vis peak (nm)**	**UV-Vis tail (nm)**	**PL emission peak (nm), at 350 nm excitation λ**	**Size of CDs (nm)**
	n–σ*	n–π* or π – π*		
Ethylene glycol	<200	200 - 350	480	2.35 ±0.48
Dichloromethane	<200	200 - 350	449	5.93 ± 2.48
2-butanol	<200	-	545	1.66 ± 0.57
acetonitrile	<200	-	545	2.68 ± 0.89
Chloroform	<200	200 - 350	448	2.94 ± 1.18
Water [a]	<200	200 - 350	430	2.61 ± 0.65
Water [b]	<200	200 - 350	440	2.05 ± 0.45

In summary, at 350 nm excitation wavelength 2-butanol and acetonitrile synthesised CDs emit at a long-wavelength of 545 nm (green light). On the other hand, EG synthesised CDs emit at a medium wavelength light of 480 nm (blue light), while chloroform, DCM and water synthesised CDs emit at a short-wavelength of 430 - 450 nm (violet light). [212] The synthesised CDs can then be classified as green-CDs, blue-CDs, or violet-CDs based on their PL maxima (Table 5-10). Since the emission of CDs is related to the CDs chemical structure, it can be thus deduced that the type of solvent used plays a significant role in the nucleation and growth of the CDs. Thus, it can be inferred that the solvation nature of DCM and chloroform towards PEG_{400} during the autoclave method are similar to each other and distinctly different to that of 2-butanol, acetonitrile and EG. [207] Additionally, the solvation property of 2-butanol and acetonitrile towards PEG_{400} are similar. [207]

The boiling points of 2-butanol (100 ℃) and acetonitrile (82 ℃) are both low. [207], [208] The polarity does not appear to be important as the polar protic nature of 2-butanol [207], [213] and the nonpolar protic acetonitrile give similar results. [207] Both chloroform (61.2 ℃) and DCM (39.6 ℃) do not give hydrogen bonding. [207], [208] EG is a polar protic solvent with high boiling point (197 ℃) and high polarity and was not expected to form CDs that emitted at a wavelength 480 nm. It is worth noting that the molecular mass of the solvent has a modest correlation (0.51) with the emission peak maxima compared to the boiling point and the relative polarity of the solvent (Table 5-11). Thus, the molecular mass of the solvent plays a minor role during the synthesis of CDs.

Table 5-10: Classification of CDs synthesised using varying solvent based on the PL maxima wavelength they exhibit at an excitation wavelength of 350 nm

CDs Class	Green CDs		blue CDs	Violet CDs			
Solvent	Acetonitrile	2-butanol	EG	DCM	Chloroform	Water (a)	Water (b)
PL emission @350 nm excitation	545	545	480	449	448	440	430

Table 5-11: The correlation matrix of the properties of the solvent used during synthesis and the emission wavelength of the resulting PEG-CDs at 350 nm excitation wavelength

	Boiling Point (℃)	Molecular weight (g per mole)	Relative polarity	Particle size (nm)	Emission peak (nm)
Boiling Point (℃)	1.00	0.45	0.02	-0.70	0.42
Molecular weight (g per mole)	0.45	1.00	-0.72	0.15	0.51
Relative polarity	0.02	-0.72	1.00	-0.39	-0.44
Emission peak (nm)	0.42	0.51	-0.44	-0.33	1.00

5.2.3.3 FTIR Spectra

FTIR spectroscopy was carried out on CDs synthesised from PEG_{400} as a precursor and various solvents using the autoclave method. The resulting FTIR spectra is below shown in Figure 5-15. The FTIR spectra of the synthesised CDs exhibit three distinct pattern and supports the classification of the synthesised CDs into three groups, namely green CDs (EG synthesised), blue CDs (2-butanol and acetonitrile synthesised) and violet CDs (DCM and chloroform synthesised). The transformation of the sample from precursor to CDs can see through formation of a second C-H stretch peak around 2850-3000 cm^{-1} region. [180] That is the PEG_{400} exhibits one C-H stretch peak while CDs have two C-H stretch peaks. These two peaks are less defined on spectra of the DCM and chloroformed synthesised CDs (violet CDs). Similarly, to the precursor, the green (EG synthesised) and violent CDs (DCM and chloroformed synthesised) exhibit broad O-H peak around 3300 cm^{-1} [127]–[130] and C=O stretch peak was observed around 1635 cm^{-1}. [180] The broadening of these O-H peaks reflects H hydrogen bonding. Conversely, the blue CDs (2-butanol and acetonitrile synthesised CDs) exhibited a sharp O-H peak around 3600 cm^{-1} which suggests that they do not partake in hydrogen bonding. [214]–[216] which suggest that the H protons are sterically hindered from freely interchanging and partake in hydrogen bonding. This could have impact on UV-vis absorption tail that extends from 200 nm the towards 350 nm.

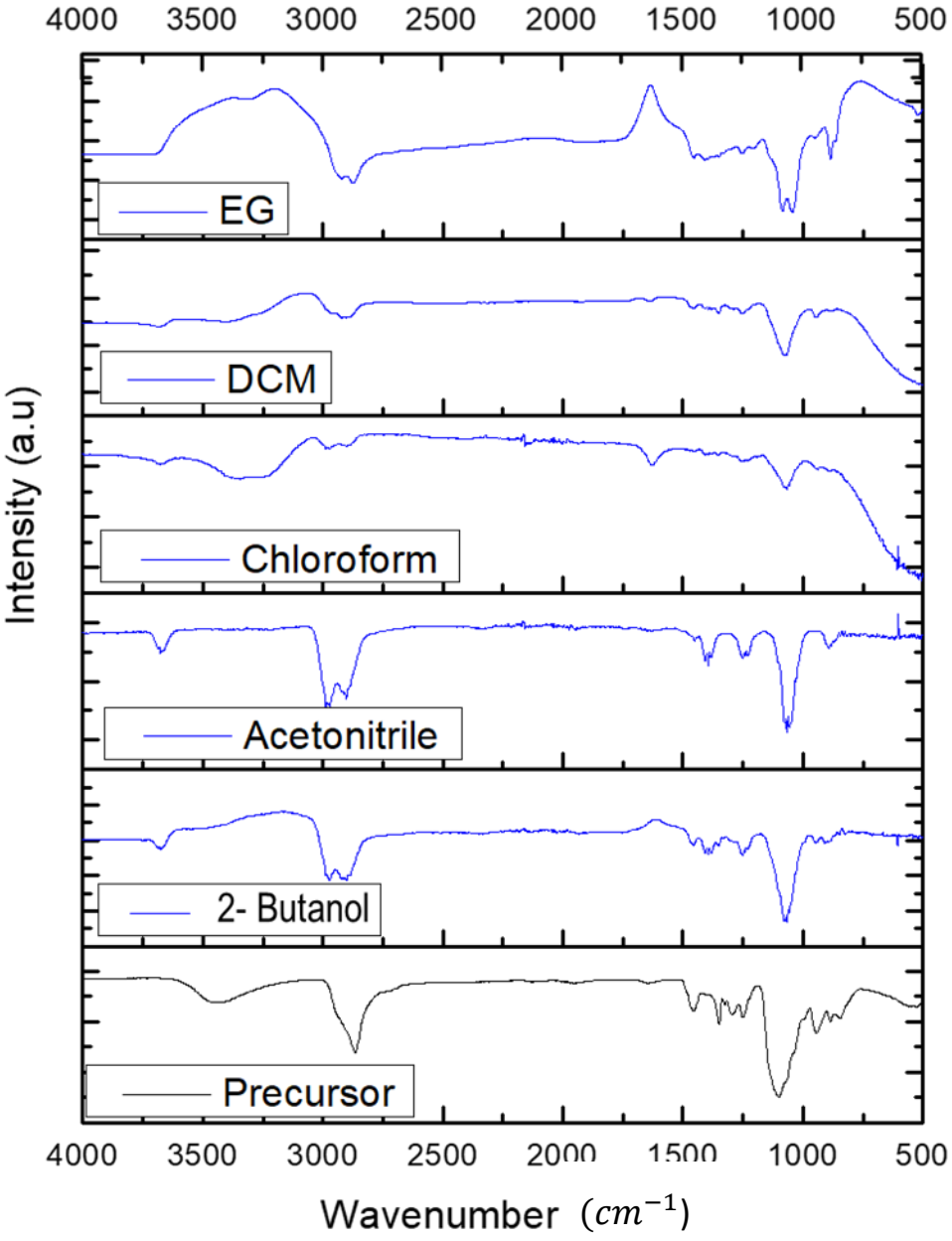

Figure 5-15: FTIR spectra of PEG CDs synthesised using various solvents

The FTIR spectra fingerprint region (>1500 cm^{-1}) of the green, blue and violet dots is also distinguishable. The fingerprint region of the violet CDs (DCM and Chloroform synthesised) is very similar to the fingerprint region of the PEG_{400} precursor with differences ascribed to dilution effects. The blue CDs (EG synthesised), is slightly different in that the C-O peak around 1021 cm-1 is a twin peak as opposed to a singlet peak. Conversely, the fingerprint region of the green CDs (2-butanol and acetonitrile synthesised) is different because (1) the C-O peak around 1021 cm^{-1} is a complex, (2) lacks a broad peak below 750 cm-1 and (3) has two

distinct multiplet peaks at 1250 and 1435 cm^{-1} as opposed to expressing continuous steam of peaks along 1500-1021 cm^{-1} wavenumber. These multiple peaks are assigned to aromatic ring C=C stretch, while the peaks along 1500-1021 cm^{-1} ascribed to C-H and C-O stretches. The FTIR spectra fingerprint region analysis also revealed that the 2-butanol CDs also express some C-H bond bends peaks.

5.2.3.4 Fluorescence Quantum Yield

The UV-vis absorption and emission were used to determine the fluorescence quantum yield (%QY) of CDs synthesised using various solvents. CDs were suspended in water for the spectroscopy analysis, it is worth bearing in mind that the determined %QY is independent of the concentration of CDs. The determined %QY are shown in Table 5-12 and plotted in Figure 5-16.

Table 5-12: Corresponding particle sizes and fluorescence quantum yield % as the synthesis solvent was varied as starting conditions

CDs Class	Blue CDs	Green CDs		Violet CDs			
Solvent	EG	Acetonitrile	2-butanol	DCM	Chloroform	Water (a)	Water (b)
QY	13	2.4	3.8	5.0	4.9	10.4	9.0
Particle size (nm)	2.34	2.68	1.66	5.93	2.94	2.61	2.05

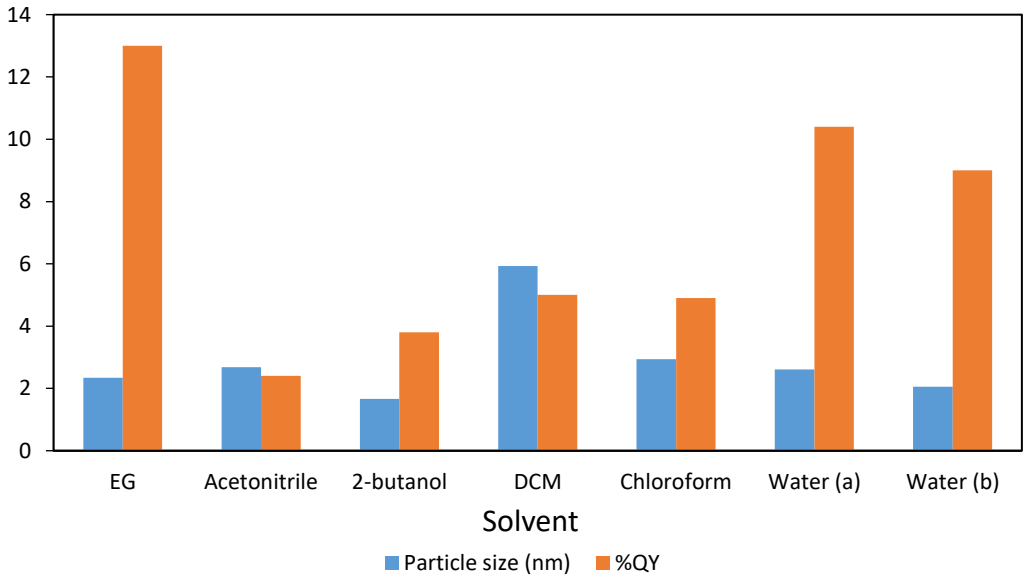

Figure 5-16: Particle size distribution and quantum yield at various reaction times

The use of EG as a solvent produced CDs that exhibit the highest %QY of 13% for the solvent engineering study. As apparent in Table 5-12 and Figure 5-16, when analysed globally, the CDs produced in this study do not exhibit a size-dependent %QY. However, when analysed within their different 'types', the general trend that is reported in literature of smaller CDs exhibiting higher %QY and vice versa is observed. [34]

The correlation coefficient of the particle size of violet CDs and the %QY was determined to be only -0.65 (Table 5-13) which is indicative of a modest inverse correlation. [151] The discrepancies associated with this moderate correlation are seen where the %QY of DCM and chloroform synthesised CDs is similar even though there is a 100% particle size difference between them. Moreover, the water synthesised CDs express a direct correlation instead of an inverse correlation.

Table 5-13: The correlation matrix of the particle size of violet CDs and their %QY

	Particle size of violet CDs (nm)	%QY of violet CDs (%)
Particle size of violet CDs (nm)	1.00	-0.65
%QY of violet CDs (%)	-0.65	1.00

Among all synthesised CDs, the green CDs exhibited the lowest QY despite having the smallest CDs of size 1.66 nm, which were yielded from the use of 2-butanol as a solvent. This low quantum yield may be ascribed to the long emission wavelength expressed by this CDs. [210] This low quantum yield may also be ascribed to lack of expression of n–π* or π –π* transitions as evident on the UV-vis absorption spectra. This low quantum yield may be also ascribed be ascribed to lack of expression of n–π* or π –π* transitions as evident on the UV-vis absorption spectra.

Table 5-14: The correlation matrix of the properties of the solvent used during synthesis and the properties of the resulting PEG-CDs

	Boiling Point (℃)	Molecular weight (g per mole)	Relative polarity	Particle size (nm)	Emission peak (nm)	%QY (%)
Boiling Point (℃)	1.00	0.45	0.02	-0.70	0.42	0.02
Molecular weight (g per mole)	0.45	1.00	-0.72	0.15	0.51	-0.35
Relative polarity	0.02	-0.72	1.00	-0.39	-0.44	0.79
Particle size (nm)	-0.70	0.15	-0.39	1.00	-0.33	-0.22
Emission peak (nm)	0.42	0.51	-0.44	-0.33	1.00	-0.54
%QY (%)	0.02	-0.35	0.79	-0.22	-0.54	1.00

It was also noticed that EG and water produced CDs with highest %QYs. Since these two solvents have high relative polarity, it can be deduced that solvents with high relative polarity yield CDs with high %QYs. The above was further supported by a correlation coefficient of 0.79 (shown in Table 5-14) which is indicative a week relationship between the polarity of the solvent used during synthesis and the %QY of the resulting CDs. [210]

5.2.3.5 Summary

CDs size decreases with increasing boiling point solvent with 2-butanol (boiling point = 197.6 ℃) producing the smallest CDs of 1.66 nm in size and DCM (boiling point = 39.6℃) producing the largest CDs of 5.93 nm in size. The solvent used during synthesis plays major role in the UV-vis absorption and emission nature of the resulting CDs, which in turn suggests that the salvation system during synthesis plays an important role in the nucleation, growth and chemical structure of the resulting CDs.

This was linked to the molecular mass of the solvent (correlation coefficient = 0.51) and supported by the FTIR spectroscopy study. The resulting CDs were classed into three groups

based on the PL maxima wavelength at an excitation wavelength of 350 nm. The groups are green CDs (EG synthesised CDs with $\lambda emission_{max}$= 545 nm), blue CDs (2-butanol and acetonitrile synthesised CDs with $\lambda emission_{max}$= 480 nm) and violet CDs (DCM, chloroform and water synthesised CDs with $\lambda emission_{max}$ of 430 - 450 nm). It was deduced that solvents with high boiling and high relative polarity point yield a long-wavelength emitting PEG synthesised CDs, while solvents with low boiling point and low relative polarity favour a short-wavelength emitting PEG synthesised CDs. Also, polar protic solvents form long-wavelength emitting CDs, where CDs with no hydrogen bonding are observed.

The %QY is inversely correlated to the relative polarity of CDs (correlation coefficient = 0.79) with water (relative polarity = 1.000) and EG (relative polarity = 0.790) producing CDs with the highest %QY of ~10% and 13%, respectively. The blue CDs exhibit the lowest %QY owing to an inverse correlation between the PL maxima wavelength and the %QY of the CDs (correlation coefficient = -0.54). There correlation between the particle size and their corresponding %QY not observed (correlation coefficient = -0.22). However, there is correlation between particle size and %QY of CDs within their groups, i.e. violet CDs have correlation coefficient = -0.65. As such, within a class of CDs (i.e. green, blue or violet CDs), the smaller the CDs, the larger the %QY and vice versa.

5.2.4 Variation of molecular weight of the PEG precursor

The effect of using PEG precursors of various molecular masse s on the synthesis of CDs was investigated. In the previous studies, the synthesis of the CDs proceeded via liquid state hydrothermal reactions where liquid state PEG_{400} (molecular weight of 400 g/mol^{-1}) was mixed with a liquid solvent. However, in this study, the synthesis proceeded via a solid-state reaction with respect to having solid state staring materials. It is important to note that the physical state of PEG is a function of its molecular weight. PEG with less than 1000 g/mol^{-1} molecular weight is a liquid at ambient room temperature and atmospheric pressure while PEG with a molecular weight greater 1000 g/mol-1 is in solid. It was also noticed that as the molecular weight of PEG increases the solid-state PEG the becomes more dense (from lightweight, fluffy flakes to granules).

As such, to ensure that the starting material of the synthesis was in a solid-state, PEGs with a molecular greater than 1000 g/mol^{-1} used the carbon precursor in the presence of citric acid as solid-state co-reagent. The reactants were mixed in a 1:2 of citric acid to PEG. After that, the reactants were ground to powder and subjected to high temperature and high-pressure synthesis

in an autoclave reactor. Citric acid has been reported to be good at aiding the hydrolysis of PEG. [159] Citric acid is generally act as an acid that catalysis the cleavage of chemical bonds during acid hydrolysis. [217]–[219] Herein, PEG with molecular weights of 1500, 4000, 6000, 10000, 12000 and 35000 g/mol-1 were investigated as carbon precursors, respectively.

5.2.4.1 TEM images

An attempt to view the synthesised PEG-CDs under TEM was not possible as the synthesised PEG-CDs have a low Z-contract. After that, the synthesised PEG-CDs were viewed under HR-TEM, and the micrographs are shown in Figure 5-17, while the determined particle sizes are shown in Table 5-15. The synthesised PEG-CDs has a particle size range of 1.00 to 2.88 nm; with the PEG_{12000} precursor yielding smallest PEG-CDs while PEG_{35000} precursor yielding the largest CDs (Table 5-15). As shown in Figure S10, the particle size is slowly increased with increasing molecular mass of the PEG precursor. That is the established linear relationship has a very small slope. It was also noted that the correlation is weak as the error bars are wide and the lightest PEG precursor, PEG_{1500}, did not necessarily yield the smallest CDs (Table 5-15 & Figure S10).

Table 5-15: The molecular weight of the PEG precursor and the particle size of the synthesised CDs

PEG molecular weight (g/mol^{-1})	Particle size/nm
1500	1.70 ±0.53
4000	2.13 ± 0.36
6000	1.83 ± 0.65
10 000	2.88 ± 1.00
12 000	1.00 ± 0.35
35 000	2.47 ± 0.63

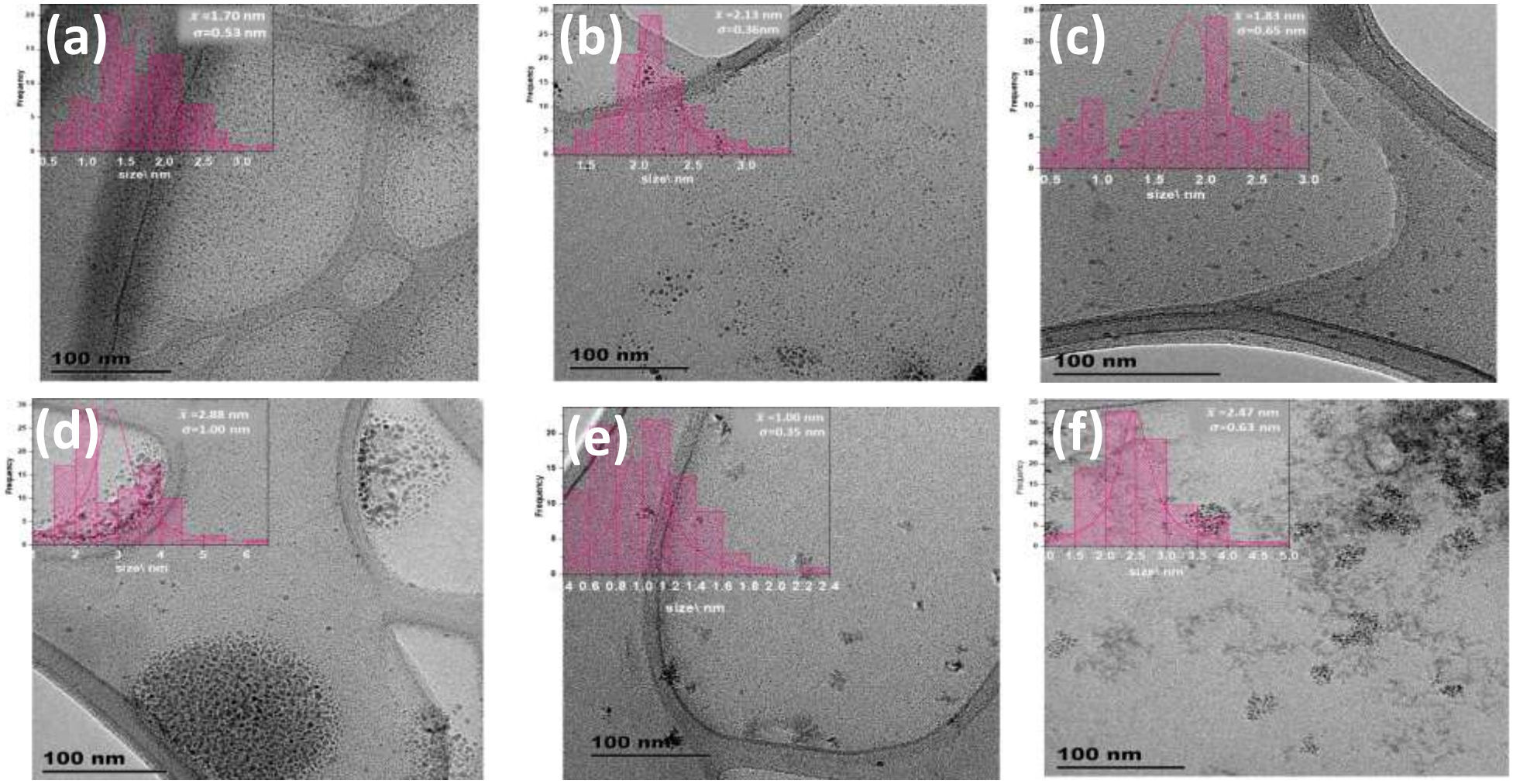

Figure 5-17: HR-TEM images and corresponding particle size distribution curve of PEG-CDs synthesised using PEG of different molecular weights as starting material namely a PEG with MW of (a) 1500 g/mol, (b) 4000 g/mol, (c) 6000 g/mol, (d) 10 000 g/mol, (e) 12 000 g/m, and (f) 35 000 g/mol, respectively

The synthesised PEG-CDs samples show good dispersion, with an exception when the PEG_{10000} and PEG_{35000} were used as PEG precursors see Figure 5-17 d and f, respectively. Moreover, the use of PEG_{35000} yielded CDs samples with mild aggregation. It is also worth pointing that though the majority of the synthesised CDs have a good particle size distribution, the PEG_{6000} and the PEG_{10000} synthesised CDs samples do not exhibit a bell-shaped particle size distribution curve which is an indication of a good particle size distribution. Following that the use of heavier PEG precursors yields CDs with poor dispersion or poor particle size distribution. Furthermore, a high magnification HR-TEM image (Figure S11) revealed that the CDs synthesised from PEG_{12000} are highly crystalline as they exhibit lattice fringes with d-spacing of approximately 0.2 nm, which is ascribed to the 102-diffraction plane of graphitic sp^2 carbon. [159], [220]

5.2.4.2 UV-Vis absorption and PL emission spectra

UV-vis absorption and the emission spectroscopy of the PEG-synthesised using PEG precursors of various molecular shown in Figure 5-18. Like the other synthesised PEG-CDs in this work, all the synthesised PEG-CDs using PEG precursor of varying molecular weight exhibit absorption peaks at a wavelength of approximately 200 nm. The peak is attributed to the π –π* transitions in the –C=C of the aromatic rings in the CDs [114]–[116]. The emission peak at 350 nm excitation wavelength is 450 nm for CDs synthesised from PEG with a molecular weight of 1500, 4000, 6000, 10 000 and 12 000 g/mol-1. Conversely, for the CDs synthesised from PEG of 35 000 g/mol-1, the emission peak is at 460 nm. Following that the emission of CDs is related to its chemical structure, it can be deduced, with a varying molecular weight of PEG, the synthesised CDs have similar chemical structures.

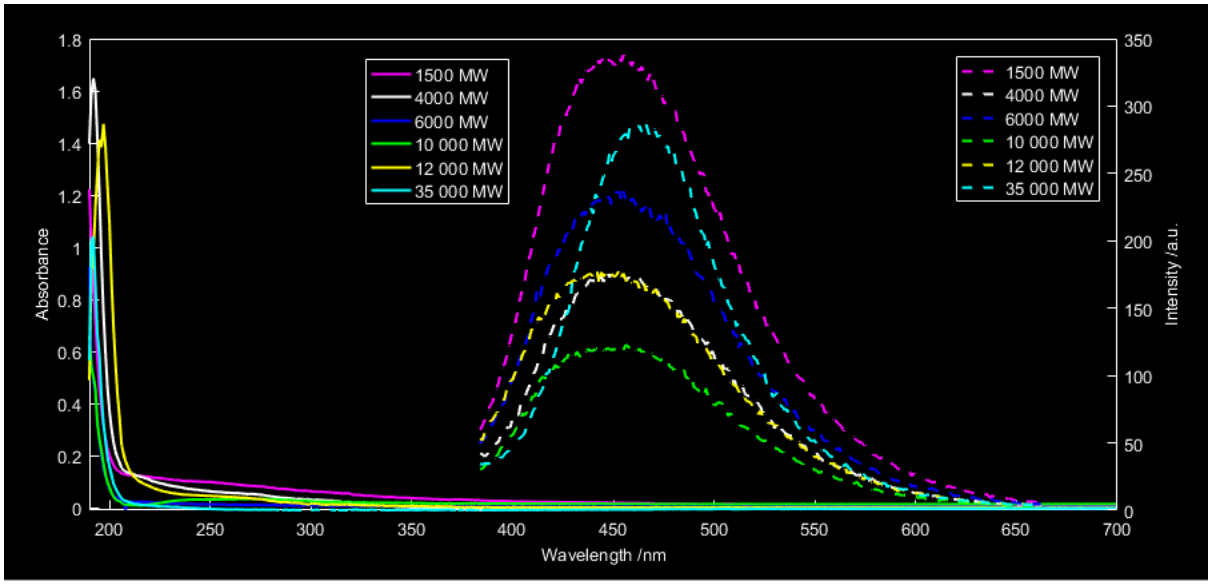

Figure 5-18: UV-Vis absorption and fluorescence spectra of various PEG-CDs synthesised using PEG precursors of various molecular weight

5.2.4.3 FTIR Spectra

The synthesised CDs were subjected to FTIR spectroscopy analysis, and the resulting spectra are plotted in Figure 5-19. The peak at about 3400 cm-1 was ascribed to the vibrational modes of the –OH surface groups of CDs. The peak at 1200 cm-1 was ascribed to the C-O-C bonds. The peaks at about 1600cm-1 were ascribed to the vibrational modes of the aromatic C=C and the carbonyl C=O bonds. [160] The bands at about 2800 cm-1 were assigned as peaks due to the terminal –C-H bonds. The bands at about 2800 cm^{-1} were assigned as peaks due to the terminal –C-H bonds. [221]

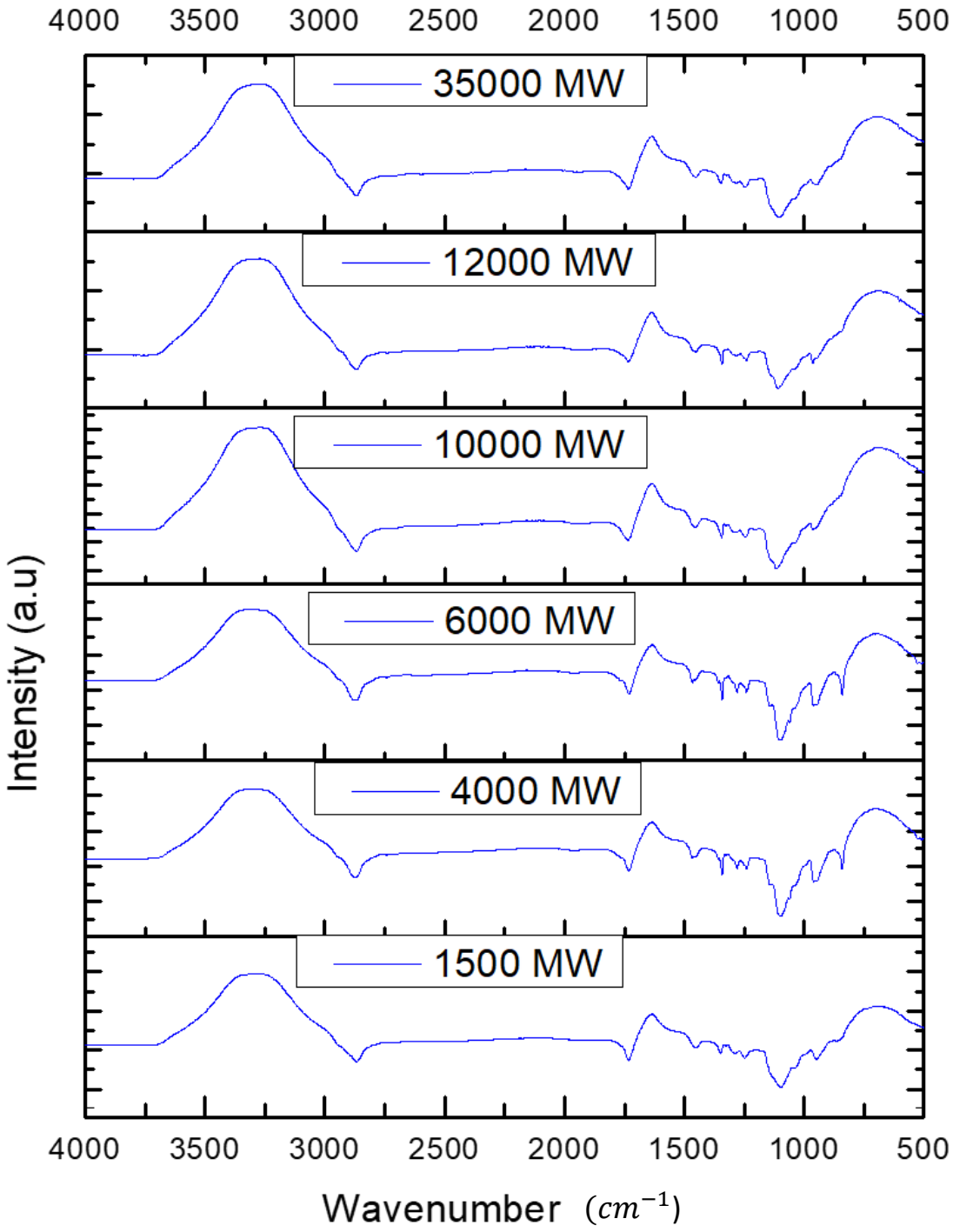

Figure 5-19: FTIR spectra of PEG CDs synthesised using various PEG molecular weights

5.2.4.4 Fluorescence Quantum Yield

As discussed previously, at varying molecular mass of the PEG precursor, the synthesised CDs had particle sizes of 1-3nm. Though the particle size did not vary significantly, the %QY of these synthesised CDs was varied considerably (Table 5-16). As such the determined %QY

showed no correlation to the particle size of CDs. However, a non-linear correlation was established between %QY of the synthesised CDs and the molecular of the PEG precursor. The %QY increased with increasing molecular mass of the PEG precursor, peaked to 18.0% at the use of PEG_{6000} as a precursor, and thereafter decreased (Figure 5-20).

Table 5-16: Corresponding particle sizes and fluorescence quantum yield % as the PEG molecular weight was varied as a starting condition

PEG MW (g/mol^{-1})	1500	4000	6000	10000	12000	35000
Particle Size (nm)	1.70 ±0.53	2.13 ± 0.36	1.83 ± 0.65	2.88 ± 1.00	1.00 ± 0.35	2.47 ± 0.63
Quantum Yield (%)	3.0	8.3	18.0	8.4	4.2	3.3

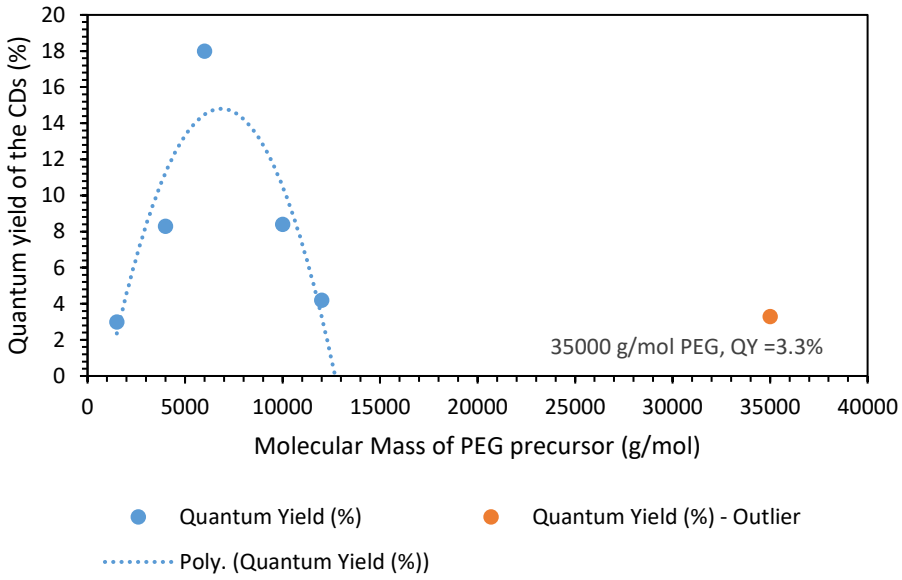

Figure 5-20: The molecular mass of the PEG precursor versus the quantum yield of the resulting CDs

These results are not in agreement with the results of Fan and his research group. [160]When Fan *et al.*, explored the effect of varying the molecular weight of PEG precursor through they yielded CDs where both the particle size and %QY that did not differ significantly (Table 5-17). [160] Perhaps the difference in results of the two studies was brought about by the differences in the synthesis method; Fan *et al.*, used liquid-phase synthesis to synthesise the CDs where they dissolved PEG_{400}, PEG_{1500} and PEG_{6000} in water, respectively. [160] Fan *et al.*, yielded PEG_{1500} synthesised CDs that measured 3.0 nm in size and %QY of 2.5%, while

PEG_{1500} synthesised CDs of 2.13 nm in particle size and a %QY of 8.3% were produced in this study. [160] Additionally, Fan *et al.,* yielded PEG6000 synthesised CDs that measured 3.5 nm in size with a %QY of 2.3%, while CDs of 1.83nm in particle size and %QY of 18% were produced in this study. [160] Thus, it can be deduced that for solid-state PEG precursors, solid-phase synthesis yields CDs with higher %QY. Maybe Zhang *et al.,* synthesised CDs via a solid-phase method similar to this study they obtained CDs with %QY that are comparative to this study and higher than %QY found by Fan *et al.,* where liquid phase synthesis was conducted (see Table 5-18 for comparison of results). [159], [160] Zhang *et al.,* formed CDs with particle size of 2-4 nm and %QY of 9% when using PEG_{2000}. [159]It can be deduced that PEG_{6000} is the optimal PEG precursor of the solid-phase synthesis as the use of PEG_{6000} yielded an optimal %QY of 18%. Though, further optimisation studies are necessary to confirm this. It is also worth noting that, even though 18% is the highest %QY observed for PEG synthesised CDs to date, the record is limited to CDs that are free of doping. Zhang *et al.,* synthesised nitrogen-doped CDs from PEG_{2000}-diamine with a particle of 1.7 nm and %QY of 31%, which was a 244% %QY increase compared to the non-doped CDs which were synthesised from PEG_{2000} . [159]

Table 5-17: Summary of results of Zhang *et al.*, [159] ***and*** **Fan *et al.*,** [155]

Reference	Synthesis Phase	PEG_x precursor (x=molecular weight)	CDs size (nm)	%QY
Fan et. al	Liquid (water used as solved)	PEG_{400}	3	3.5
		PEG_{1500}	3.3	2.5
		PEG_{6000}	3.5	2.3
Zang et al.,	Solid (citric acid used as co-reagent)	PEG_{2000}	1-2	9
		PEG_{2000}-amine	1.7	31

5.2.4.5 Summary

The use PEG precursors of various molecular weights during synthesis yields CDs of approximately 1-3 nm in size. It was found that the dispersion of the synthesised CDs gets compromised as the molecular weight the PEG precursor was increased. The synthesised CDs exhibit similar UV-vis absorption, emission and FTIR spectra which suggest that their chemical structure of the synthesised CDs is similar. Though the CDs synthesised from PEG_{35000} emitted at a slightly longer wavelength. There was no established linear correlation between the %QY of the synthesised CDs and their particle size. However, even though the particle size of the

CDs remains at approximately 2 nm with a varying molecular weight of the PEG precursor, the %QY increased with increasing molecular weight of the PEG precursor, peaks at molecular of 6000 g/mol-1 and then decreases. Thus, PEG_{6000} was identified as the optimal solid-state PEG precursor yielding CDs with a high %QY of 18%.

5.3 Conclusion

The synthesised CDs remained suspended in solution, thus were only characterised using TEM (or HR TEM), UV-vis absorption, UV-vis emission, FTIR spectroscopy and %QY. The FTIR spectra indicated that the PEG CDs were highly functionalised with the terminal –OH groups and the aromatic C=C and C=O being the most prominent bonds present. Most of the synthesised CDs were well dispersed with a narrow particle size distribution.

The variation of vol% PEG_{400}/water, reaction time and molecular weight of PEG precursor do not play a significant role in the particle size and chemical structure engineering of CDs with respect to the use autoclave method. Thus, the average particle size of the synthesised CDs is 2.7 nm, 2.0 nm and 2.0 nm for at varying vol% PEG_{400}/water, reaction time and molecular weight of PEG_{400} precursor, respectively. With that said, it was noted that the particle size of CDs increased significantly to 4.15 nm after 12 h of synthesis. It was also found that the CDs produced after a reaction time of 5h (or above), express small carbon nanospheres of approximately 22 nm as by-products. Thus, to obtained purer CDs, the synthesised CDs must be produced under 5h reaction time when using 25 vol% of PEG_{400} as a precursor and water as a solvent via the autoclave method. It was also found that when water is not present, and PEG_{400} is used as the sole starting material, the particle size of the synthesised CDs increases from 2.7 nm to 4.9 nm.

The %QY of the CDs synthesised at varying volume percentage of PEG_{400} to water was determined to be approximately 10%. However, the %QY of the CDs at varying reaction time and at varying molecular weight of the PEG precursor varied even though the particle size of CDs remained constant. Thus, the CDs particles formed with increasing reaction time showed that %QY is not a function of concentration. It was deduced that the synthesised CDs express aggregation-induced emission at lower concentrations of CDs. However, further studies are necessary to confirm this.

Conversely, varying the solvent used during synthesis plays a significant role in the particle size and chemical structure engineering of the synthesised CDs. It was found that solvents with higher boiling points yield smaller CDs. It was also found that solvents with high relative

polarity yield CDs with high %QY. The molecular weight, boiling point and relative polarity of the solvent were found to be correlated to the emission wavelength of the synthesised CDs, which is in turn related to the chemical structure of the synthesised CDs as confirmed by the FTIR spectra. Long-wavelength emitting PEG synthesised CDs are favoured by synthesis through the use of solvents with the ability to form hydrogen bonds, high boiling point, high relative polarity and high molecular weight. On the other hand, short-wavelength emitting PEG synthesised CDs are favoured by synthesis through the use of solvents with non-hydrogen bonding properties, low boiling point, low relative polarity and low molecular weight. It was also found that for CDs of similar chemical structures and optical behaviour, the %QY has an inverse linear relationship with the particle size of CDs.

6 Sensing ability of CDs: Preliminary testing and proof of concept

6.1 Introduction

Since their discovery in 2010, CDs have been applauded for displaying well-known sensing fluorescent properties such as energy transfer, fluorescence quenching and the sensitivity of fluorescent spectra to molecular environments. [1] As such it is of no surprise that there are numerous reports showing the broad applications of CDs in bio- and chemo-sensing. [1] There are several technical procedures reported in literature on how the sensing ability of CDs is tested. [1], [87] The commonly reported procedure, and probably the simplest procedure, is the monitoring of the PL intensity of CDs upon exposure to an analyte through use of a spectrometer. In general, this testing entails varying the concentration of the analyte to produce a plot illustrating how the PL intensity of the CDs vary with varying concentration of the CDs. [1], [73] Another simple, but less common, testing procedure monitors at the change of the PL peak position on the PL spectra or the fluorescence colour under UV light upon exposure of CDs to an analyte. This method is normally complimented by use of spectroscopy. [1], [222] There are also reports on radiometric fluorescence assays conducted to probe the sensing ability of CDs. These assays look at the change in the relationship of two PL peaks of CDs upon exposure to an analyte. [1] Another testing procedure proceeds via an electrochemical reaction. In this testing procedure, electrodes are made from CDs and the current is monitored following exposure of the electrochemical cell to an analyte. [1]

As discussed in the previous chapters, it was difficult to obtain the synthesised CDs as a solid product in this study. As such, the CO-sensing ability of the synthesised CDs was not investigated in detail because the concentration of the CDs in suspension is unknown. Nevertheless, preliminary testing was done as proof of concept. The testing experiment of choice was one hypothesised to proceed via the ‘on-off-on’ mechanism that had been described in previous chapters whereby the PL of CDs is switched off by first material and recovered by the second material. As such, herein the PL change was monitored by observing the fluorescence of CDs under the UV-lamp irradiation.

6.2 Preliminary results

The step-by-step methodology used in the preliminary testing is outlined in Figure 6-1. To kickstart the procedure, a filter paper was viewed under the UV-lamp to ensure that it did not

show photoluminescence. Thereafter, the filter paper was coated with CDs by inserting the filter paper into a stirred CDs solution under controlled conditions. After stirring for thirty minutes, the filter paper was taken out of the solution and allowed to dry under ambient temperature and pressure. At this point, the filter paper was photoluminescent under the UV-lamp which inferred that the paper/CDs material was successfully produced. The integration of the filter paper and CDs allows for CDs to be probed for sensing in their solid state. Filter paper-based PL sensors are commonly reported in literature.[223]–[226] Patir and Gogoi employed the use of a filter paper based microfluidic device loaded with nitrogen-doped CDs as proof of principle that the CDs they synthesised could be used for parallel detection of Hg^{2+} and Cu^{2+} ions in water. [222] It is important to mention that, the device the fabricated by Patir and Gogoi was more complex and used candle wax channels and other agents to enable the discerning of Hg^{2+} and Cu^{2+} ions. [222] Thereafter, the paper/CDs material was exposed to a Pt solution, upon which the photoluminescence of the paper/CDs was switched off. This behaviour of metal ions switching off the photoluminescence of CDs is not unexpected since it has been well reported in literature. [1], [73], [138] The PL turns off because the metal ion binds to the functional groups of CDs forming non-radiative pathways onto which the CDs' excited state relaxes. [1], [73], [138]

To tie up the preliminary testing, the paper/CDs/Pt material was exposed to CO under ambient temperature and pressure. It was hypothesised that the CO would bind Pt and alter PL of the CDs. However, no PL change was observed under the UV-lamp after exposing the paper/CDs/Pt material to CO. A more appropriate PL monitoring technique could involve a PL spectrometer employed in order to monitor the surface and the changes in PL of the CDs . [1] In further testing, the CO exposure experiment should be conducted at 80 – 120 ℃ to promote the binding of CO to CDs. [4] These would be slightly more favoured testing conditions as they resemble the operating temperature of fuel cells where these CDs are ought to be applied. [4], [13], [15]

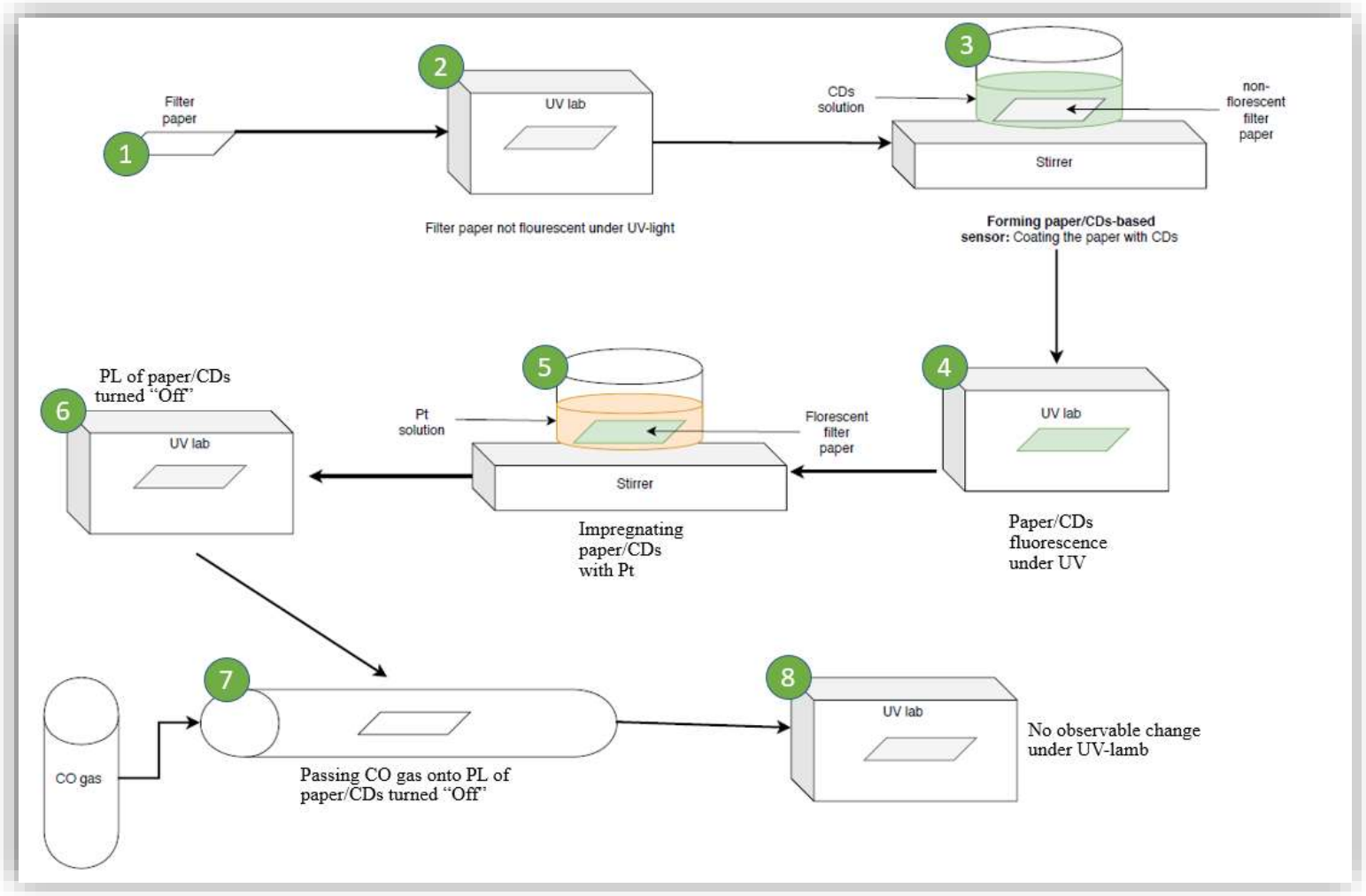

Figure 6-1: Schematic representation of the sensing ability testing of the synthesised CD

6.3 Conclusion

The fabrication of a paper-based sensor from CDs was successful, that is the CDs were incorporated onto the filter paper, as evidenced by the newly acquired photoluminescence of the paper. It was found that the PL of the synthesised CDs is switched off upon exposure to Pt solution. It is deduced that the PL of the synthesised CDs is responsive to Pt and as such can be used a Pt detector. On the other hand, no PL change was observed when the Pt/CDs/paper material was exposed to CO. It is clear that better testing procedures are necessary to show any impact CO may have on the Pt/CDs/paper. In conclusion, these preliminary results indicate a proof of concept approach to produce sensing device using CDs that can be tailored for CO detection. However, thorough testing will be necessary to ensure that the CDs can also be used as CO sensors for application in fuel cells.

7 Conclusion and Future work

7.1 Conclusion

Three methods were explored for the synthesis of CDs from three different carbon precursors. CDs were synthesised using the autoclave, microwave and reflux methods from sucrose, chitosan and PEG as carbon precursors, respectively. The microwave method required short reaction times. However, the equipment pressure fluctuations were difficult to control, making for an unreliable synthesis method. The reflux method was easier to control but difficulties were experienced with reproducing the results. The autoclave method was found to yield good quality, monodispersed CDs samples that were reproducibly produced. Although generally the autoclave method can require long reaction times, it was found that CDs were produced in under 30 minutes using the autoclave method used in this study. As such the autoclave method was chosen as the superior method for synthesising CDs and used in further studies.

The three different carbon precursors (sucrose, chitosan and PEG) all have in common pi-acceptor functional groups. This feature was chosen in order to tailor the resulting CDs for sensing of CO with pi-acceptor functional groups which can interact with a pi-donor analyte i.e. CO. Indeed, all the produced CDs had OH pi-acceptor functional groups. This CD-CO interaction is a very weak interaction and it was anticipated that a metal might be required to assist in the CO detection process. Sucrose yielded aggregated CDs samples, while the chitosan mostly produced samples with CDs as the minority product. Chitosan produced promising CDs when the reflux method was used; the CDs were well-dispersed with a narrow particle size distribution. Moreover, the CDs were highly photoluminescent scoring a high %QY of 16%. However, the method-precursor pair showed lack of reproducibility.

PEG was found to be a robust carbon precursor for synthesising CDs. PEG produced CDs across all three synthesis methods. The PEG synthesised CDs were well-dispersed, with a narrow particle size distribution. The autoclave, microwave and reflux methods yielded PEG synthesised CDs of sizes 2.52 nm, 3.30 nm and 4.8 nm, respectively. It is worth mentioning that the PEG synthesised CDs also gave carbon nanospheres (20 - 40 nm) as by-products. All the PEG synthesised CDs could not be successfully crystallised out of solution.

Nevertheless, the CDs were photoluminescent with %QY of up to 11%. Interestingly, unlike most reports in literature, the bigger CDs had the higher %QY which was attributed to a higher

degree of cross-linking enhanced emission in comparison to smaller CDs. The PL spectra of the CDs was found to be dependent on the excitation wavelength. It was found with PEG synthesised CDs, i.e. smaller CDs had their optimal PL at shorter excitation wavelengths, while larger CDs had their optimal PL at longer excitation wavelengths. Since, PEG was shown to be a more robust precursor for CDs synthesis than sucrose and chitosan, it was the precursor of choice for further studies.

Of the investigated methods and precursors, the autoclave method coupled with the use of PEG as a carbon precursor were selected as the best method for the synthesis of CDs. Following this, the synthesis of CDs from PEG via the autoclave method was investigated further in order to explore the effect of various reaction parameters on the synthesis of CDs as well as to eliminate the production of CNS as by-products and attain CDs in the solid state. The reaction parameters studied were (1) the precursor and solvent volume ratios, (2) reaction time, (3) solvent, and (4) molecular weight of the PEG precursor. Interesting findings were leveraged from this study. Moreover, CDs that were free of CNSs were successfully synthesised. However, obtaining CDs as a solid product remained a challenge.

It was found that varying the ratio of the precursor (PEG), to water did not affect the size of CDs nor did it affect the %QY of the CDs and all the synthesised CDs were approximately 2.7 nm in size and had %QY of approximately 10%. As such, it can be deduced that the variation of the volume ratio of PEG to water has no effect on the chemical structure nor optical properties of the resulting CDs as confirmed by the FTIR and UV-vis spectra analysis. Moreover, varying the volume ratio of PEG to water did not affect the production of CNSs as by-products as CNS were found in all the samples where water was used a solvent. An exception was observed at 33%vol PEG to water, where no by-products were formed but rather two sets of CDs were produced – larger CDs of sizes 10.9 nm and smaller CDs at 1.6 nm. It was deduced that the by-product, CNSs, may enhance %QY of the CDs as it drops to below 4% when less or no by-product is present in the CDs samples.

Variation of the reaction time did not affect the size of CDs but did affect the %QY of the resulting CDs as well as the formation of CNSs. It was inferred that the size of the CDs changed at a very slow rate with varying reaction time as the size of the resulting CDs stayed near constant at 2 nm over 1 – 6 hours reaction time, and only doubled in size after 12 hours reaction time. It was also found that CNSs are only formed after 4 hours reaction time. A U-shaped curve was obtained from the plot %QY of the resulting CDs against reaction time and %QY

peaked to 15% after 3 hours. The increasing part of the peak was ascribed to AIE (aggregation induced emission), while the cause of decreasing part of the peak is unclear.

The synthesised CDs had a similar chemical structures and optical nature as shown by their FTIR, UV-vis and PL spectra. Conversely, the variation of solvent had a significant effect on the particle size of CDs as well as the chemical structures and optical nature of the CDs. Solvents with higher boiling points produced smaller CDs. The molecular weight, boiling point and relative polarity of the solvent were found to be correlated to the emission wavelength of the synthesised CDs, which was in turn related to the chemical structure of the synthesised CDs, as confirmed by the FTIR spectra. The solvents with the ability to form hydrogen bonds, and of high boiling point, high relative polarity and high molecular weight favoured the synthesis of long-wavelength emitting PEG synthesised CDs. On the other hand, the short-wavelength emitting PEG synthesised CDs were favoured by synthesis through the use of solvents with non-hydrogen bonding properties, low boiling point, low relative polarity and low molecular weight. It was also found that for CDs of similar chemical structures and optical behaviour, the %QY showed an inverse linear relationship with the particle size of the CDs. In general, solvents with high relative polarity were found to yield CDs with high %QY.

The variation of the PEG molecular mass study gave similar results as found for both precursor concentration and reaction time variation studies. That is, varying the molecular mass of the precursor also had no effect on the particle size nor the chemical structure of the synthesised CDs. As such, the synthesised CDs were all approximately 1-3 nm in size with similar FTIR, UV-vis and PL spectra. Interestingly, even though the particle size of the CDs remained constant, the %QY increased with increasing molecular weight of the PEG precursor, peaking at 18% at a molecular of 6000 g/mol^{-1}; it then decreased.

It is important to note that the investigation of the effect of the molecular mass of the precursor on the synthesis of CDs proceeded via a solid phase synthesis. For this study, citric acid was used as a co-reagent to the PEGs with a molecular mass greater than 1000 g/mol, to facilitate the hydrolysis of the PEGs. Even using this method, CDs could not be obtained as a solid product but rather were obtained as a brown gel. The search for a means of obtaining CDs in as a solid state is still ongoing.

Preliminary testing of the CO-sensing ability of CDs was done by fabricating a photoluminescent CDs/paper-based sensor. Pt was also added to this paper. It was found that Pt switched the PL of the CDs/paper-based sensor off. The PL of the CDs was expected to be

recovered after CO exposure. However, no PL change was observed upon CO exposure. It was deduced that better testing conditions are necessary to uncover the effect of the CO exposure to the CDs. These preliminary results served as a proof of concept that the synthesised CDs can be used as a sensor. However, tuning of CDs properties and thorough testing will be necessary to ensure that the CDs can also be used as CO sensors for application in fuel cells.

7.2 Future Work

Interestingly, a sample synthesised from 33 vol% PEG_{400}/water (reaction time = 5 h and temperature = 215 ℃) yielded CDs with a binomial particle size of CDs, with smaller CDs at a particle size 1.66 nm size and bigger CDs at a particle size of 10.4 nm. Further studies of this reaction may be necessary to understand the nucleation and growth mechanism of CDs. The study of the variation of the reaction time and molecular weight of the PEG precursor respectively had %QY that did not correlate with the particle size of the CDs. It was suspected that aggregation-induced emission was partly behind the observations. Thus, careful studies of the emission of the PEG synthesised CDs are necessary to uncover both the photoluminescence origin and emission nature of these materials. Furthermore, other studies by numerous authors have shown that N-doping significantly improves the %QY of CDs. Thus, further studies would entail exploring N-doping of CDs using (1) various PEG-amine precursors and (2) using PEG and varying N-doping reagents. With that said, the most pressing quest is the ongoing search of crystallising the PEG synthesised CDs out of the solution. Subsequently, the thorough testing of the CO-sensing ability of the CDs would be done.

Testing in this study was done by fabricating a photoluminescent paper-based device and thereafter monitoring the PL change in response to an analyte using a UV-lamp. This approach offers limitations for instance using the UV-lamp entails use of the naked-eye to observe PL changes which may be inadequate in establishing small PL changes. As such, in further studies a solid-phase photoluminescence spectrometer which programmatically records the PL of specimen will be used instead. To complement this, the resistance of entails paper-based device will be monitored as well. Simultaneously, to promote the binding of Pt to CO as well as simulate operational temperatures of fuel cells, the CO exposure experiment will be done at 80 – 120 ℃. Additionally, further testing will involve CO-sensitivity, CO-selectivity, humidity compatibility studies.

References

[1] R. Jelinek, *Carbon Quantum Dots*. 2017.

[2] J. Zhou *et al.*, "An electrochemical avenue to blue luminescent nanocrystals from multiwalled carbon nanotubes (MWCNTs)," *J. Am. Chem. Soc.*, vol. 129, no. 4, pp. 744–745, 2007, doi: 10.1021/ja0669070.

[3] S. Tao, S. Zhu, T. Feng, C. Xia, Y. Song, and B. Yang, "The polymeric characteristics and photoluminescence mechanism in polymer carbon dots: A review," *Mater. Today Chem.*, vol. 6, pp. 13–25, 2017, doi: 10.1016/j.mtchem.2017.09.001.

[4] X. Cheng *et al.*, "A review of PEM hydrogen fuel cell contamination: Impacts, mechanisms, and mitigation," *J. Power Sources*, vol. 165, no. 2, pp. 739–756, 2007, doi: 10.1016/j.jpowsour.2006.12.012.

[5] J. H. Wee and K. Y. Lee, "Overview of the development of CO-tolerant anode electrocatalysts for proton-exchange membrane fuel cells," *J. Power Sources*, vol. 157, no. 1, pp. 128–135, 2006, doi: 10.1016/j.jpowsour.2005.08.010.

[6] Z. Liu *et al.*, "Pt Alloy Electrocatalysts for Proton Exchange Membrane Fuel Cells : A Review Pt Alloy Electrocatalysts for Proton Exchange Membrane Fuel Cells : A Review," *Catal. Rev. Sci. Eng.*, vol. 4940, 2013, doi: 10.1080/01614940.2013.795455.

[7] X. Ouyang, L. Bednarova, R. S. Besser, and P. Ho, "Preferential oxidation (PrOx) in a thin-film catalytic microreactor: Advantages and limitations," *AIChE J.*, vol. 51, no. 6, pp. 1758–1772, 2005, doi: 10.1002/aic.10438.

[8] A. F. Ghenciu, "Review of fuel processing catalysts for hydrogen production in PEM fuel cell systems," *Curr. Opin. Solid State Mater. Sci.*, 2002, doi: 10.1016/S1359-0286(02)00108-0.

[9] C. T. Holt, A. M. Azad, S. L. Swartz, R. R. Rao, and P. K. Dutta, "Carbon monoxide sensor for PEM fuel cell systems," *Sensors Actuators, B Chem.*, vol. 87, no. 3, pp. 414–420, 2002, doi: 10.1016/S0925-4005(02)00290-3.

[10] J. Wee and K. Lee, "Overview of the development of CO-tolerant anode electrocatalysts for proton-exchange membrane fuel cells," *J. ofPower Sources*, vol. 157, pp. 128–135, 2006, doi: 10.1016/j.jpowsour.2005.08.010.

[11] M. K. Debe, “Electrocatalyst approaches and challenges for automotive fuel cells,” *Nature*, vol. 486, no. 7401, pp. 43–51, 2012, doi: 10.1038/nature11115.

[12] “Fuel Cell Basics,” *Fuel Cell & Hydrogen Energy Association*. https://www.fchea.org/fuelcells.

[13] B. L. Carrette, K. A. Friedrich, and U. Stimming, “Fuel Cells ± Fundamentals and Applications,” *Fuel Cells*, no. 1, pp. 5–39, 2001.

[14] Office of Energy Efficiency of Renewable Energy, “Comparison of Fuel Cell Technologies,” *U.S. Department of Energy*. https://www.energy.gov/eere/fuelcells/comparison-fuel-cell-technologies (accessed Nov. 17, 2020).

[15] J. Wu *et al.*, “A review of PEM fuel cell durability: Degradation mechanisms and mitigation strategies,” *J. Power Sources*, vol. 184, no. 1, pp. 104–119, 2008, doi: 10.1016/j.jpowsour.2008.06.006.

[16] A. Faur Ghenciu, “Review of fuel processing catalysts for hydrogen production in PEM fuel cell systems,” *Curr. Opin. Solid State Mater. Sci.*, vol. 6, no. 5, pp. 389–399, 2002, doi: 10.1016/s1359-0286(02)00108-0.

[17] Z. Liu, L. Ma, J. Zhang, K. Hongsirikarn, and J. G. Goodwin, “Pt alloy electrocatalysts for proton exchange membrane fuel cells: A review,” *Catal. Rev. - Sci. Eng.*, vol. 55, no. 3, pp. 255–288, 2013, doi: 10.1080/01614940.2013.795455.

[18] V. Mehta and J. S. Cooper, “Review and analysis of PEM fuel cell design and manufacturing,” *J. Power Sources*, vol. 114, no. 1, pp. 32–53, 2003, doi: 10.1016/S0378-7753(02)00542-6.

[19] K. S. Bhambare, S. Gupta, M. M. Mench, and A. Ray, “A carbon monoxide sensor in polymer electrolyte fuel cells based on symbolic dynamic filtering,” *Sensors Actuators, B Chem.*, vol. 134, no. 2, pp. 803–815, 2008, doi: 10.1016/j.snb.2008.06.057.

[20] W. Deng and M. Flytzani-Stephanopoulos, “On the issue of the deactivation of Au-ceria and Pt-ceria water-gas shift catalysts in practical fuel-cell applications,” *Angew. Chemie - Int. Ed.*, vol. 45, no. 14, pp. 2285–2289, 2006, doi: 10.1002/anie.200503220.

[21] A. Hashimoto, T. Hibino, and M. Sano, “Solid oxide fuel cells that enable the detection

of CO in reformed gases," *Sensors Actuators, B Chem.*, vol. 86, no. 1, pp. 12–19, 2002, doi: 10.1016/S0925-4005(02)00068-0.

[22] R. Mukundan, E. L. Brosha, and F. H. Garzon, "A low temperature sensor for the detection of carbon monoxide in hydrogen," *Solid State Ionics*, vol. 175, no. 1–4, pp. 497–501, 2004, doi: 10.1016/j.ssi.2004.02.074.

[23] W. G. Planje, G. J. M. Janssen, and M. P. De Heer, "A two-electrode sensor cell for CO detection in a H2-rich gas," *Sensors Actuators, B Chem.*, vol. 99, no. 2–3, pp. 544–555, 2004, doi: 10.1016/j.snb.2004.01.005.

[24] W. Liu *et al.*, "Carbon dots: Surface engineering and applications," *J. Mater. Chem. B*, vol. 4, no. 35, pp. 5772–5788, 2016, doi: 10.1039/c6tb00976j.

[25] M. . Rashid, S.A., Othman, R.N.I.R. and Hussein, *Synthesis, Technology and Applications of Carbon Nanomaterials*. Elsevier, 2018.

[26] Y. Wang and A. Hu, "Carbon quantum dots: Synthesis, properties and applications," *J. Mater. Chem. C*, vol. 2, no. 34, pp. 6921–6939, 2014, doi: 10.1039/c4tc00988f.

[27] X. Xu *et al.*, "Electrophoretic analysis and purification of fluorescent single-walled carbon nanotube fragments," *J. Am. Chem. Soc.*, vol. 126, no. 40, pp. 12736–12737, 2004, doi: 10.1021/ja040082h.

[28] L. Wang and H. S. Zhou, "Green Synthesis of Luminescent Nitrogen-Doped Carbon Dots from Milk and Its Imaging Application," *Anal. Chem.*, vol. 86, no. 18, p. 8902−8905, 2014, doi: 10.1021/ac502646x.

[29] V. A. Online, A. Sachdev, I. Matai, and P. Gopinath, "Implications of surface passivation on physicochemical and bioimaging properties of carbon dots," *RSC Adv.*, vol. 4, no. 40, pp. 20915–20921, 2014, doi: 10.1039/c4ra02017k.

[30] S. Mandani, D. Dey, B. Sharma, and T. K. Sarma, "Natural occurrence of fluorescent carbon dots in honey," *Carbon N. Y.*, vol. 119, pp. 569–572, 2017, doi: 10.1016/j.carbon.2017.04.075.

[31] B. Zhu, S., Song, Y., Zhao, X., Shao, J., Zhang, J. and Yang, "The photoluminescence mechanism in carbon dots (graphene quantum dots, carbon nanodots, and polymer dots): current state and future perspective," *Nano Res.*, vol. 2, no. 8, pp. 355–381, 2015,

Accessed: Dec. 10, 2019. [Online]. Available: https://link.springer.com/article/10.1007/s12274-014-0644-3.

[32] S. Zhu, Q. Meng, L. Wang, … J. Z.-A. C., and undefined 2013, "Highly photoluminescent carbon dots for multicolor patterning, sensors, and bioimaging," *Wiley Online Libr.*, Accessed: Dec. 10, 2019. [Online]. Available: https://onlinelibrary.wiley.com/doi/abs/10.1002/anie.201300519.

[33] S. Zhu, Y. Song, X. Zhao, J. Shao, J. Zhang, and B. Yang, "The photoluminescence mechanism in carbon dots (graphene quantum dots, carbon nanodots, and polymer dots): current state and future perspective," *Nano Res.*, vol. 8, no. 2, pp. 355–381, 2015, doi: 10.1007/s12274-014-0644-3.

[34] R. Jelinek, *Carbon Quantum Dots*. 2017.

[35] B. Li, J. M. Kim, and G. A. J. Amaratunga, "Inorganic Quantum Dot Materials and their Applications in 'Organic' Hybrid Solar Cells," *Isr. J. Chem.*, pp. 1–10, 2019, doi: 10.1002/ijch.201900034.

[36] M. A. Reed, "Spatial quantization in GaAs–AlGaAs multiple quantum dots," *J. Vac. Sci. Technol. B Microelectron. Nanom. Struct.*, vol. 4, no. 1, p. 358, 1986, doi: 10.1116/1.583331.

[37] V. G. Reshma and P. V. Mohanan, "Quantum dots: Applications and safety consequences," *J. Lumin.*, vol. 205, no. September 2018, pp. 287–298, 2019, doi: 10.1016/j.jlumin.2018.09.015.

[38] V. G. Reshma and P. V. Mohanan, "Quantum dots: Applications and safety consequences," *J. Lumin.*, vol. 205, pp. 287–298, 2019, doi: 10.1016/j.jlumin.2018.09.015.

[39] N. Jamaludin, S. A. Rashid, and T. Tan, "Natural Biomass as Carbon Sources for the Synthesis of Photoluminescent Carbon Dots," in *Synthesis, Technology and Applications of Carbon Nanomaterials*, Elsevier, 2018, pp. 109–134.

[40] L. E. Brus, "Electron-electron and electron-hole interactions in small semiconductor crystallites: The size dependence of the lowest excited electronic state," *J. Chem. Phys.*, vol. 80, no. 9, pp. 4403–4409, 1984, doi: 10.1063/1.447218.

[41] H. Zheng, *Ultrafast Electronic Dynamics In Core-Shell Quantum Dots Probed*, no. December. THE UNIVERSITY OF CHICAGO, 2017.

[42] F. Bouzid, F. Pezzimenti, L. Dehimi, F. G. Della Corte, M. Hadjab, and A. Hadj Larbi, "Analytical Modeling of Dual-Junction Tandem Solar Cells Based on an InGaP/GaAs Heterojunction Stacked on a Ge Substrate," *J. Electron. Mater.*, vol. 48, no. 6, pp. 4107–4116, 2019, doi: 10.1007/s11664-019-07180-z.

[43] W. Shockley and H. J. Queisser, "Detailed balance limit of efficiency of p-n junction solar cells," *J. Appl. Phys.*, vol. 32, no. 3, pp. 510–519, 1961, doi: 10.1063/1.1736034.

[44] D. Bimberg and U. W. Pohl, "Quantum dots: Promises and accomplishments," *Mater. Today*, vol. 14, no. 9, pp. 388–397, 2011, doi: 10.1016/S1369-7021(11)70183-3.

[45] P. Teng *et al.*, "Chemiluminescence behavior of the carbon dots and the reduced state carbon dots," *J. Lumin.*, 2014, doi: 10.1016/j.jlumin.2013.09.036.

[46] Y. Dong, C. Chen, J. Lin, N. Zhou, Y. Chi, and G. Chen, "Electrochemiluminescence emission from carbon quantum dot-sulfite coreactant system," *Carbon N. Y.*, vol. 56, pp. 12–17, 2013, doi: 10.1016/j.carbon.2012.12.086.

[47] J. Xu, Y. Miao, J. Zheng, H. Wang, Y. Yang, and X. Liu, "Carbon dot-based white and yellow electroluminescent light emitting diodes with a record-breaking brightness," *Nanoscale*, vol. 10, no. 23, pp. 11211–11221, 2018, doi: 10.1039/c8nr01834k.

[48] R. W. Wood, "The Time Interval between Absorption and Emission of Light in Fluorescence," *Proc. R. Soc. A Math. Phys. Eng. Sci.*, vol. 99, no. 700, pp. 362–371, 1921, doi: 10.1098/rspa.1921.0049.

[49] D. C. Harris, *Quantitative Chemical Analysis, Seventh Edition*. 2006.

[50] M. Anpo, M. Kondo, S. Coluccia, C. Louis, and M. Che, "Application of Dynamic Photoluminescence Spectroscopy to the Study of the Active Surface Sites on Supported Mo/SiO2Catalysts. Features of Anchored and Impregnated Catalysts," *J. Am. Chem. Soc.*, vol. 111, no. 24, pp. 8791–8799, 1989, doi: 10.1021/ja00206a004.

[51] D. C. Harris, *Quantitative Chemical Analysis, Seventh Edition*. 2006.

[52] A. Sachdev, I. Matai, and P. Gopinath, "Implications of surface passivation on

physicochemical and bioimaging properties of carbon dots," *RSC Adv.*, vol. 4, no. 40, pp. 20915–20921, 2014, doi: 10.1039/c4ra02017k.

[53] S. Brkić, "Applicability of Quantum Dots in Biomedical Science," *Ioniz. Radiat. Eff. Appl.*, pp. 21–39, 2018, doi: 10.5772/intechopen.71428.

[54] D. J. Sandman, "A review of: "Primary Photoexcitations in Conjugated Polymers: Molecular Exciton versus Semiconductor Band Model," *Mol. Cryst. Liq. Cryst. Sci. Technol.*, vol. 333, no. 1, pp. 287–288, 2007, doi: 10.1080/10587259908026014.

[55] M. Duteil, "Collective Behaviour : From Cells to Humans," 2018.

[56] J. Valenta, "Determination of absolute quantum yields of luminescing nanomaterials over a broad spectral range: from the integrating sphere theory to the correct methodology," *Nanosci. Methods*, vol. 3, no. 1, pp. 11–27, 2014, doi: 10.1080/21642311.2014.884288.

[57] S. Leyre *et al.*, "Absolute determination of photoluminescence quantum efficiency using an integrating sphere setup," *Rev. Sci. Instrum.*, vol. 85, no. 12, pp. 123115–123119, 2014, doi: 10.1063/1.4903852.

[58] S. Tao, S. Zhu, T. Feng, C. Xia, Y. Song, and B. Yang, "The polymeric characteristics and photoluminescence mechanism in polymer carbon dots : A review," *Mater. Today Chem.*, vol. 6, pp. 13–25, 2017, doi: 10.1016/j.mtchem.2017.09.001.

[59] S. Zhu, Y. Song, J. Shao, X. Zhao, and B. Yang, "Representation of PDs (the PDs always contain CPDs and NCPDs), and the relationship between NCPDs and other CDs.," *Angew. Chemie - Int. Ed.*, vol. 54, no. 49, pp. 14626–14637, 2015, doi: 10.1002/anie.201504951.

[60] S. Tao, Y. Song, S. Zhu, J. Shao, and B. Yang, "A new type of polymer carbon dots with high quantum yield: From synthesis to investigation on fluorescence mechanism," *Polymer (Guildf).*, vol. 116, pp. 472–478, 2017, doi: 10.1016/j.polymer.2017.02.039.

[61] J. Mei, N. L. C. Leung, R. T. K. Kwok, J. W. Y. Lam, and B. Z. Tang, "Aggregation-Induced Emission: Together We Shine, United We Soar!," *Chem. Rev.*, vol. 115, no. 21, pp. 11718–11940, 2015, doi: 10.1021/acs.chemrev.5b00263.

[62] F. Zhang *et al.*, "Self-assembly, optical and electrical properties of perylene diimide

dyes bearing unsymmetrical substituents at bay position," *Sci. Rep.*, vol. 8, no. 1, pp. 1–11, 2018, doi: 10.1038/s41598-018-26502-5.

[63] Z. Zhao, B. He, and B. Z. Tang, "Aggregation-induced emission of siloles," *Chem. Sci.*, vol. 6, no. 10, pp. 5347–5365, 2015, doi: 10.1039/c5sc01946j.

[64] Mei, J., Hong, Y., Lam, J.W., Qin, A., Tang, Y. and Tang, B.Z., "Aggregation-Induced Emission: The Whole Is More Brilliant than the Parts," *Adv. Mater.*, vol. 31, no. 26, pp. 5429–5479, 2014, [Online]. Available: https://onlinelibrary.wiley.com/doi/abs/10.1002/adma.201401356.

[65] A. Sciortino, A. Cannizzo, and F. Messina, "Carbon Nanodots: A Review—From the Current Understanding of the Fundamental Photophysics to the Full Control of the Optical Response," *C*, vol. 4, no. 4, p. 67, 2018, doi: 10.3390/c4040067.

[66] N. J. Coville, S. D. Mhlanga, E. N. Nxumalo, and A. Shaikjee, "A review of shaped carbon nanomaterials," *S. Afr. J. Sci.*, vol. 107, no. 3/4, pp. 1–15, 2011, doi: 10.4102/sajs.v107i3/4.418.

[67] Y. P. Sun *et al.*, "Quantum-sized carbon dots for bright and colorful photoluminescence," *J. Am. Chem. Soc.*, vol. 128, no. 24, pp. 7756–7757, 2006, doi: 10.1021/ja062677d.

[68] K. K. Chan, S. H. K. Yap, and K. T. Yong, *Biogreen Synthesis of Carbon Dots for Biotechnology and Nanomedicine Applications*, vol. 10, no. 4. Springer Berlin Heidelberg, 2018.

[69] Y. Wang *et al.*, "Ratiometric fluorescent paper sensor utilizing hybrid carbon dots-quantum dots for the visual determination of copper ions," *Nanoscale*, vol. 8, no. 11, pp. 5977–5984, 2016, doi: 10.1039/c6nr00430j.

[70] B. Chen *et al.*, "Large scale synthesis of photoluminescent carbon nanodots and their application for bioimaging," *Nanoscale*, vol. 5, no. 5, pp. 1967–1971, 2013, doi: 10.1039/c2nr32675b.

[71] K. K. Chan, S. H. K. Yap, and K. T. Yong, *Biogreen Synthesis of Carbon Dots for Biotechnology and Nanomedicine Applications*, vol. 10, no. 4. Springer Berlin Heidelberg, 2018.

[72] J. Tang *et al.*, “Carbon nanodots featuring efficient FRET for real-time monitoring of drug delivery and two-photon imaging,” *Adv. Mater.*, vol. 25, no. 45, pp. 6569–6574, 2013, doi: 10.1002/adma.201303124.

[73] J. Gong, X. Lu, and X. An, “Carbon dots as fluorescent off-on nanosensors for ascorbic acid detection,” *RSC Adv.*, vol. 5, no. 11, pp. 8533–8536, 2015, doi: 10.1039/c4ra13576h.

[74] J. Gu *et al.*, “Carbon dot cluster as an efficient ‘off-on’ fluorescent probe to detect Au(III) and glutathione,” *Biosens. Bioelectron.*, vol. 68, pp. 27–33, 2015, doi: 10.1016/j.bios.2014.12.027.

[75] J. Hou, J. Dong, H. Zhu, X. Teng, S. Ai, and M. Mang, “A simple and sensitive fluorescent sensor for methyl parathion based on l-tyrosine methyl ester functionalized carbon dots,” *Biosens. Bioelectron.*, vol. 68, pp. 20–26, 2015, doi: 10.1016/j.bios.2014.12.037.

[76] H. M. R. Gonçalves, A. J. Duarte, and J. C. G. Esteves da Silva, “Optical fiber sensor for Hg(II) based on carbon dots,” *Biosens. Bioelectron.*, vol. 26, no. 4, pp. 1302–1306, 2010, doi: 10.1016/j.bios.2010.07.018.

[77] J. Zhou *et al.*, “Facile synthesis of P-doped carbon quantum dots with highly efficient photoluminescence,” *pubs.rsc.org*, Accessed: Dec. 10, 2019. [Online]. Available: https://pubs.rsc.org/en/content/articlehtml/2013/ra/c3ra45294h.

[78] Y. Dong *et al.*, “Carbon-based dots co-doped with nitrogen and sulfur for high quantum yield and excitation-independent emission,” *Angew. Chemie - Int. Ed.*, vol. 52, no. 30, pp. 7800–7804, Jul. 2013, doi: 10.1002/anie.201301114.

[79] Q. Liang, W. Ma, Y. Shi, Z. Li, and X. Yang, “Easy synthesis of highly fluorescent carbon quantum dots from gelatin and their luminescent properties and applications,” *Carbon N. Y.*, vol. 60, pp. 421–428, Aug. 2013, doi: 10.1016/j.carbon.2013.04.055.

[80] Q. Wang, H. Zheng, Y. Long, L. Zhang, M. Gao, and W. Bai, “Microwave-hydrothermal synthesis of fluorescent carbon dots from graphite oxide,” *Carbon N. Y.*, vol. 49, no. 9, pp. 3134–3140, Aug. 2011, doi: 10.1016/j.carbon.2011.03.041.

[81] Q. Shi, L., Yang, J.H., Zeng, H.B., Chen, Y.M., Yang, S.C., Wu, C., Zeng, H., Yoshihito,

O. and Zhang, “Carbon dots with high fluorescence quantum yield: the fluorescence originates from organic fluorophores,” *pubs.rsc.org*, vol. 30, no. 8, pp. 14374–14378, 2016, Accessed: Dec. 10, 2019. [Online]. Available: https://pubs.rsc.org/en/content/articlehtml/2016/nr/c6nr00451b.

[82] C. Zhang *et al.*, “4-Nitrophenol Reduction by a Single Platinum Palladium Nanocube Caged within a Nitrogen-Doped Hollow Carbon Nanosphere,” *ChemCatChem*, vol. 9, no. 6, pp. 980–986, Mar. 2017, doi: 10.1002/cctc.201601364.

[83] S. H. Liu, M. T. Wu, Y. H. Lai, C. C. Chiang, N. Yu, and S. Bin Liu, “Fabrication and electrocatalytic performance of highly stable and active platinum nanoparticles supported on nitrogen-doped ordered mesoporous carbons for oxygen reduction reaction,” *J. Mater. Chem.*, vol. 21, no. 33, pp. 12489–12496, Sep. 2011, doi: 10.1039/c1jm11488c.

[84] X.-Y. Lang *et al.*, “Mesostructured Intermetallic Compounds of Platinum and Non-Transition Metals for Enhanced Electrocatalysis of Oxygen Reduction Reaction,” *Adv. Funct. Mater.*, vol. 25, no. 2, pp. 230–237, Jan. 2015, doi: 10.1002/adfm.201401868.

[85] H. Ehtesabi, Z. Hallaji, S. Najafi Nobar, and Z. Bagheri, “Carbon dots with pH-responsive fluorescence: a review on synthesis and cell biological applications,” *Microchim. Acta*, vol. 187, no. 2, 2020, doi: 10.1007/s00604-019-4091-4.

[86] S. Hill and M. C. Galan, “Fluorescent carbon dots from mono- and polysaccharides: Synthesis, properties and applications,” *Beilstein J. Org. Chem.*, vol. 13, pp. 675–693, 2017, doi: 10.3762/bjoc.13.67.

[87] Y. Wang and A. Hu, “Carbon quantum dots : synthesis , properties and applications,” *R. Soc. Chem.*, pp. 6921–6939, 2014, doi: 10.1039/c4tc00988f.

[88] Y.-W. Chao, “Early transition metal complexes with pi donor ligands and their reaction with alkynes,” *Univ. Arizona - UA Campus Repos.*, 2020.

[89] S. R. Maqsood, N. Islam, S. Bashir, B. Khan, and A. H. Pandith, “Sigma donor and pi acceptor characteristics of certain NN-bidentate ligands: A DFT study,” *J. Coord. Chem.*, vol. 66, no. 13, pp. 2308–2315, 2013, doi: 10.1080/00958972.2013.800866.

[90] W. Meng, X. Bai, B. Wang, Z. Liu, S. Lu, and B. Yang, “Biomass-Derived Carbon Dots

and Their Applications," *Energy Environ. Mater.*, vol. 2, no. 3, pp. 172–192, 2019, doi: 10.1002/eem2.12038.

[91] B. P. de Oliveira and F. O. M. da Silva Abreu, "Carbon quantum dots synthesis from waste and by-products: Perspectives and challenges," *Mater. Lett.*, vol. 282, p. 128764, 2021, doi: 10.1016/j.matlet.2020.128764.

[92] A. L. Himaja, P. S. Karthik, B. Sreedhar, and S. P. Singh, "Synthesis of carbon dots from kitchen waste: Conversion of waste to value added product," *J. Fluoresc.*, vol. 24, no. 6, pp. 1767–1773, 2014, doi: 10.1007/s10895-014-1465-1.

[93] J. Zhu *et al.*, "Waste Utilization of Synthetic Carbon Quantum Dots Based on Tea and Peanut Shell," *J. Nanomater.*, vol. 2019, no. Figure 1, 2019, doi: 10.1155/2019/7965756.

[94] S. G. Jagadish C. Roy, Fabien Salaün, G. C. and J. G. Ada Ferri, and G. C. and J. G. Ada Ferri, "Solubility of Chitin: Solvents, Solution Behaviors and Their Related Mechanisms," *Intech*, no. tourism, p. 13, 2016, [Online]. Available: https://www.intechopen.com/books/advanced-biometric-technologies/liveness-detection-in-biometrics.

[95] T. Y. Ma, D. Hollander, P. Krugliak, and K. Katz, "PEG 400, a hydrophilic molecular probe for measuring intestinal permeability," *Gastroenterology*, vol. 98, no. 1, pp. 39–46, 1990, doi: 10.1016/0016-5085(90)91288-H.

[96] A. Konwar, N. Gogoi, G. Majumdar, and D. Chowdhury, "Green chitosan – carbon dots nanocomposite hydrogel film with superior properties," *Carbohydr. Polym.*, vol. 115, pp. 238–245, 2015, doi: 10.1016/j.carbpol.2014.08.021.

[97] Q. Zhang, J. Su, X. Zhang, J. Li, A. Zhang, and Y. Gao, "Chemical vapor deposition of a PbSe/CdS/nitrogen-doped TiO2 nanorod array photoelectrode and its band-edge level structure," *New J. Chem.*, vol. 36, no. 11, pp. 2302–2307, 2012, doi: 10.1039/c2nj40509a.

[98] D. Xu, Z. Liu, J. Liang, and Y. Qian, "Solvothermal synthesis of CdS nanowires in a mixed solvent of ethylenediamine and dodecanethiol," *J. Phys. Chem. B*, vol. 109, no. 30, pp. 14344–14349, 2005, doi: 10.1021/jp051980i.

[99] K. Hola, Y. Zhang, Y. Wang, E. P. Giannelis, R. Zboril, and A. L. Rogach, “Carbon dots - Emerging light emitters for bioimaging, cancer therapy and optoelectronics,” *Nano Today*, vol. 9, no. 5, pp. 590–603, 2014, doi: 10.1016/j.nantod.2014.09.004.

[100] H. Liu, T. Ye, and C. Mao, “Fluorescent carbon nanoparticles derived from candle soot,” *Angew. Chemie - Int. Ed.*, vol. 46, no. 34, pp. 6473–6475, 2007, doi: 10.1002/anie.200701271.

[101] A. Zhu, Q. Qu, X. Shao, B. Kong, and Y. Tian, “Carbon-dot-based dual-emission nanohybrid produces a ratiometric fluorescent sensor for in vivo imaging of cellular copper ions,” *Angew. Chemie - Int. Ed.*, vol. 51, no. 29, pp. 7185–7189, 2012, doi: 10.1002/anie.201109089.

[102] F. Yuan *et al.*, “Bright Multicolor Bandgap Fluorescent Carbon Quantum Dots for Electroluminescent Light-Emitting Diodes,” *Adv. Mater.*, vol. 29, no. 3, 2017, doi: 10.1002/adma.201604436.

[103] G. A. and K. N., “Unraveling the chemical composition of caramel,” *J. Agric. Food Chem.*, vol. 60, no. 12, pp. 3266–3274, 2012, [Online]. Available: http://ovidsp.ovid.com/ovidweb.cgi?T=JS&PAGE=reference&D=emed10&NEWS=N&AN=22375847.

[104] X. Sun and Y. Li, “Colloidal Carbon Spheres and Their Core/Shell Structures with Noble-Metal Nanoparticles,” *Angew. Chemie - Int. Ed.*, vol. 43, no. 5, pp. 597–601, 2004, doi: 10.1002/anie.200352386.

[105] H. Zhu, X. Wang, Y. Li, Z. Wang, F. Yang, and X. Yang, “Microwave synthesis of fluorescent carbon nanoparticles with electrochemiluminescence properties,” *Chem. Commun.*, no. 34, pp. 5118–5120, 2009, doi: 10.1039/b907612c.

[106] X. Wang, K. Qu, B. Xu, J. Ren, and X. Qu, “Microwave assisted one-step green synthesis of cell-permeable multicolor photoluminescent carbon dots without surface passivation reagents,” *J. Mater. Chem.*, vol. 21, no. 8, pp. 2445–2450, 2011, doi: 10.1039/c0jm02963g.

[107] R. Liu, D. Wu, S. Liu, K. Koynov, W. Knoll, and Q. Li, “An Aqueous Route to Multicolor Photoluminescent Carbon Dots Using Silica Spheres as Carriers **,” *Fluoresc. Nanoparticles*, no. 6 mL, pp. 4598–4601, 2009, doi: 10.1002/anie.200900652.

[108] I. Mihalache, L. M. Veca, M. Kusko, and D. Dragoman, “Memory effect in carbon quantum DOT-PEG1500N composites,” *Curr. Appl. Phys.*, vol. 14, no. 12, pp. 1625–1632, 2014, doi: 10.1016/j.cap.2014.09.020.

[109] F. Wang, Z. Xie, H. Zhang, C. Y. Liu, and Y. G. Zhang, “Highly luminescent organosilane-functionalized carbon dots,” *Adv. Funct. Mater.*, vol. 21, no. 6, pp. 1027–1031, 2011, doi: 10.1002/adfm.201002279.

[110] F. Wang, Z. Xie, H. Zhang, C. Y. Liu, and Y. G. Zhang, “Highly luminescent organosilane-functionalized carbon dots,” *Adv. Funct. Mater.*, vol. 21, no. 6, pp. 1027–1031, Mar. 2011, doi: 10.1002/adfm.201002279.

[111] S. Zhu, Y. Song, X. Zhao, J. Shao, J. Zhang, and B. Yang, “The photoluminescence mechanism in carbon dots (graphene quantum dots, carbon nanodots, and polymer dots): current state and future perspective,” *Nano Research*, vol. 8, no. 2. Tsinghua University Press, pp. 355–381, 2015, doi: 10.1007/s12274-014-0644-3.

[112] S. Zhu, Y. Song, X. Zhao, J. Shao, J. Zhang, and B. Yang, “The photoluminescence mechanism in carbon dots (graphene quantum dots , carbon nanodots , and polymer dots): Current state and future perspective,” *Nano Res.*, vol. 8, no. 2, pp. 355–381, 2015, doi: 10.1007/s12274-014-0644-3.

[113] X. T. Zheng, A. Ananthanarayanan, K. Q. Luo, and P. Chen, “Glowing Graphene Quantum Dots and Carbon Dots : Properties , Syntheses , and Biological Applications,” *Small*, vol. 11, no. 14, pp. 1620–1636, 2015, doi: 10.1002/smll.201402648.

[114] T. N. Phaahlamohlaka *et al.*, “Effects of Co and Ru Intimacy in Fischer–Tropsch Catalysts Using Hollow Carbon Sphere Supports: Assessment of the Hydrogen Spillover Processes,” *ACS Catal.*, vol. 7, no. 3, pp. 1568–1578, Mar. 2017, doi: 10.1021/acscatal.6b03102.

[115] S. D. Knights, K. M. Colbow, J. St-Pierre, and D. P. Wilkinson, “Aging mechanisms and lifetime of PEFC and DMFC,” 2004, doi: 10.1016/j.jpowsour.2003.09.033.

[116] S. D. Knights, K. M. Colbow, J. St-Pierre, and D. P. Wilkinson, “Aging mechanisms and lifetime of PEFC and DMFC,” *J. Power Sources*, vol. 127, no. 1–2, pp. 127–134, Mar. 2004, doi: 10.1016/J.JPOWSOUR.2003.09.033.

[117] H. Li, Z. Kang, Y. Liu, and S. T. Lee, “Carbon nanodots: Synthesis, properties and applications,” *J. Mater. Chem.*, vol. 22, no. 46, pp. 24230–24253, Dec. 2012, doi: 10.1039/c2jm34690g.

[118] L. Cao *et al.*, “Carbon dots for multiphoton bioimaging,” *J. Am. Chem. Soc.*, vol. 129, no. 37, pp. 11318–11319, Sep. 2007, doi: 10.1021/ja073527l.

[119] J. Shen, Y. Zhu, X. Yang, and C. Li, “Graphene quantum dots: Emergent nanolights for bioimaging, sensors, catalysis and photovoltaic devices,” *Chem. Commun.*, vol. 48, no. 31, pp. 3686–3699, Apr. 2012, doi: 10.1039/c2cc00110a.

[120] Y. Zhao, C. Riemersma, F. Pietra, R. Koole, C. De Mello Donegá, and A. Meijerink, “High-temperature luminescence quenching of colloidal quantum dots,” *ACS Nano*, vol. 6, no. 10, pp. 9058–9067, Oct. 2012, doi: 10.1021/nn303217q.

[121] A. Zhu, Q. Qu, X. Shao, B. Kong, and Y. Tian, “Carbon-Dot-Based Dual-Emission Nanohybrid Produces a Ratiometric Fluorescent Sensor for In Vivo Imaging of Cellular Copper Ions,” *Angew. Chemie Int. Ed.*, pp. 7185–7189, 2012, doi: 10.1002/anie.201109089.

[122] H. Wang *et al.*, “Biocompatible PEG-Chitosan @ Carbon Dots Hybrid Nanogels for Two-Photon Fluorescence Imaging , Near-Infrared Light / pH Dual-Responsive Drug Carrier , and Synergistic Therapy,” *Adv. Funct. Mater.*, pp. 5537–5547, 2015, doi: 10.1002/adfm.201501524.

[123] Q. L. Chen, W. Q. Ji, and S. Chen, “Direct Synthesis of Multicolor Fluorescent Hollow Carbon Spheres Encapsulating Enriched Carbon Dots,” *Sci. Rep.*, vol. 6, no. May 2015, pp. 1–8, 2016, doi: 10.1038/srep19382.

[124] S. Lin, Y. Cheng, C. Lin, J. Fang, W. Xiang, and X. Liang, “Carbon nanodots with intense emission from green to red and their multifunctional applications,” *J. Alloys Compd.*, 2018, doi: 10.1016/j.jallcom.2018.01.194.

[125] K. Jiang *et al.*, “Red, green, and blue luminescence by carbon dots: Full-color emission tuning and multicolor cellular imaging,” *Angew. Chemie - Int. Ed.*, vol. 54, no. 18, pp. 5360–5363, 2015, doi: 10.1002/anie.201501193.

[126] J. Wang, M. M. Kliks, S. Jun, M. Jackson, and Q. X. Li, “Rapid Analysis of Glucose,

Fructose, Sucrose, and Maltose in Honeys from Different Geographic Regions using Fourier Transform Infrared Spectroscopy and Multivariate Analysis," *J. Food Sci.*, vol. 75, no. 2, pp. 208–214, 2010, doi: 10.1111/j.1750-3841.2009.01504.x.

[127] "carbon dots ftir - Google Scholar." https://scholar.google.com/scholar?hl=en&as_sdt=0%2C5&q=carbon+dots+ftir+&btnG= (accessed Dec. 10, 2019).

[128] G. H. G. Ahmed, R. B. Laíño, J. A. G. Calzón, and M. E. D. García, "Fluorescent carbon nanodots for sensitive and selective detection of tannic acid in wines," *Talanta*, vol. 132, pp. 252–257, 2015, doi: 10.1016/j.talanta.2014.09.028.

[129] T. Arumugham, M. Alagumuthu, R. G. Amimodu, S. Munusamy, and S. K. Iyer, "A sustainable synthesis of green carbon quantum dot (CQD) from Catharanthus roseus (white flowering plant) leaves and investigation of its dual fluorescence responsive behavior in multi-ion detection and biological applications," *Sustain. Mater. Technol.*, vol. 23, Apr. 2020, doi: 10.1016/j.susmat.2019.e00138.

[130] M. Zhang, Q. Yao, C. Lu, Z. Li, and W. Wang, "Layered double hydroxide-carbon dot composite: High-performance adsorbent for removal of anionic organic dye," *ACS Appl. Mater. Interfaces*, vol. 6, no. 22, pp. 20225–20233, Nov. 2014, doi: 10.1021/am505765e.

[131] D. Chen, H. Gao, X. Chen, G. Fang, S. Yuan, and Y. Yuan, "Excitation-Independent Dual-Color Carbon Dots : Surface-State Controlling and Solid-State Lighting," 2017, doi: 10.1021/acsphotonics.7b00675.

[132] M. L. Mastronardi *et al.*, "Size-dependent absolute quantum yields for size-separated colloidally-stable silicon nanocrystals," *Nano Lett.*, vol. 12, no. 1, pp. 337–342, 2012, doi: 10.1021/nl2036194.

[133] D. Chowdhury, N. Gogoi, and G. Majumdar, "Fluorescent carbon dots obtained from chitosan gel," *RSC Adv.*, vol. 2, no. 32, pp. 12156–12159, 2012, doi: 10.1039/c2ra21705h.

[134] Y. Yang *et al.*, "One-step synthesis of amino-functionalized fluorescent carbon nanoparticles by hydrothermal carbonization of chitosan," *Chem. Commun.*, vol. 48, no. 3, pp. 380–382, 2012, doi: 10.1039/c1cc15678k.

[135] S. A. Mathew, P. Praveena, S. Dhanavel, R. Manikandan, S. Senthilkumar, and A. Stephen, “Luminescent chitosan/carbon dots as an effective nano-drug carrier for neurodegenerative diseases,” *RSC Adv.*, vol. 10, no. 41, pp. 24386–24396, 2020, doi: 10.1039/d0ra04599c.

[136] M. Sano *et al.*, “Relationship between solubility of chitosan in alcoholic solution and its gelation,” *Chem. Pharm. Bull.*, vol. 47, no. 7, pp. 1044–1046, 1999, doi: 10.1248/cpb.47.1044.

[137] I. Y. Y. Bu, “Synthesis of graphitic carbon nano-onions for dye sensitized solar cells,” *Sol. Energy*, vol. 105, pp. 236–242, 2014, doi: 10.1016/j.solener.2014.03.015.

[138] S. Zhu *et al.*, “Highly photoluminescent carbon dots for multicolor patterning, sensors, and bioimaging,” *Angew. Chemie - Int. Ed.*, vol. 52, no. 14, pp. 3953–3957, Apr. 2013, doi: 10.1002/anie.201300519.

[139] S. Zhu *et al.*, “Highly Photoluminescent Carbon Dots for Multicolor Patterning , Sensors , and Bioimaging,” *Angew. Chemie Int. Ed.*, pp. 3953–3957, 2013, doi: 10.1002/anie.201300519.

[140] J. Shen, Y. Zhu, C. Chen, X. Yang, and C. Li, “Facile preparation and upconversion luminescence of graphene quantum dots,” *Chem. Commun.*, vol. 47, no. 9, pp. 2580–2582, 2011, doi: 10.1039/c0cc04812g.

[141] Z. Luo, P. M. Vora, E. J. Mele, A. T. C. Johnson, and J. M. Kikkawa, “Photoluminescence and band gap modulation in graphene oxide,” *Appl. Phys. Lett.*, vol. 94, no. 11, 2009, doi: 10.1063/1.3098358.

[142] V. N. Mehta, S. Jha, H. Basu, R. K. Singhal, and S. K. Kailasa, “One-step hydrothermal approach to fabricate carbon dots from apple juice for imaging of mycobacterium and fungal cells,” *Sensors Actuators, B Chem.*, 2015, doi: 10.1016/j.snb.2015.02.104.

[143] V. N. Mehta, S. Jha, H. Basu, R. K. Singhal, and S. K. Kailasa, “One-step hydrothermal approach to fabricate carbon dots from apple juice for imaging of mycobacterium and fungal cells,” *Sensors Actuators, B Chem.*, vol. 213, pp. 434–443, Jul. 2015, doi: 10.1016/j.snb.2015.02.104.

[144] A. Mewada *et al.*, “Green synthesis of biocompatible carbon dots using aqueous extract

of Trapa bispinosa peel," *Mater. Sci. Eng. C*, vol. 33, no. 5, pp. 2914–2917, Jul. 2013, doi: 10.1016/j.msec.2013.03.018.

[145] M. Mewada, A., Pandey, S., Shinde, S., Mishra, N., Oza, G., Thakur, M., Sharon, M. and Sharon, "Green synthesis of biocompatible carbon dots using aqueous extract of Trapa bispinosa peel," *Mater. Sci. Eng. C*, vol. 5, no. 33, pp. 2914–2917, 2013, Accessed: Dec. 10, 2019. [Online]. Available: https://www.sciencedirect.com/science/article/pii/S092849311300180X.

[146] L. Pan *et al.*, "Truly Fluorescent Excitation-Dependent Carbon Dots and Their Applications in Multicolor Cellular Imaging and Multidimensional Sensing," *Adv. Mater.*, vol. 27, no. 47, pp. 7782–7787, 2015, doi: 10.1002/adma.201503821.

[147] L. Pan *et al.*, "Truly Fluorescent Excitation-Dependent Carbon Dots and Their Applications in Multicolor Cellular Imaging and Multidimensional Sensing," *Adv. Mater.*, vol. 27, pp. 7782–7787, 2015, doi: 10.1002/adma.201503821.

[148] A. Bhattacharya, S. Chatterjee, R. Prajapati, and T. K. Mukherjee, "Size-dependent penetration of carbon dots inside the ferritin nanocages: Evidence for the quantum confinement effect in carbon dots," *Phys. Chem. Chem. Phys.*, vol. 17, no. 19, pp. 12833–12840, May 2015, doi: 10.1039/c5cp00543d.

[149] X. Jia, J. Li, and E. Wang, "One-pot green synthesis of optically pH-sensitive carbon dots with upconversion luminescence," *Nanoscale*, vol. 4, no. 18, pp. 5572–5575, Sep. 2012, doi: 10.1039/c2nr31319g.

[150] R. J. Fan, Q. Sun, L. Zhang, Y. Zhang, and A. H. Lu, "Photoluminescent carbon dots directly derived from polyethylene glycol and their application for cellular imaging," *Carbon N. Y.*, vol. 71, pp. 87–93, May 2014, doi: 10.1016/j.carbon.2014.01.016.

[151] R. J. Fan, Q. Sun, L. Zhang, Y. Zhang, and A. H. Lu, "Photoluminescent carbon dots directly derived from polyethylene glycol and their application for cellular imaging," *Carbon N. Y.*, vol. 71, pp. 87–93, 2014, doi: 10.1016/j.carbon.2014.01.016.

[152] S. Hu, A. Trinchi, P. Atkin, and I. Cole, "Tunable photoluminescence across the entire visible spectrum from carbon dots excited by white light," *Angew. Chemie - Int. Ed.*, vol. 54, no. 10, pp. 2970–2974, 2015, doi: 10.1002/anie.201411004.

[153] W. Kwon and S. W. Rhee, “Facile synthesis of graphitic carbon quantum dots with size tunability and uniformity using reverse micelles,” *Chem. Commun.*, vol. 48, no. 43, pp. 5256–5258, May 2012, doi: 10.1039/c2cc31687k.

[154] S. Hill and M. C. Galan, “Fluorescent carbon dots from mono- and polysaccharides : synthesis , properties and applications,” *Beilstein J. Org. Chem.*, pp. 675–693, 2017, doi: 10.3762/bjoc.13.67.

[155] and X. L. Yongqiang Zhang, Yongsheng Hu, Jie Lin, Yi Fan, Yantao Li, Ying Lv, “Excitation Wavelength Independence : Toward Low-Threshold Amplified Spontaneous Emission from Carbon Nanodots,” 2016, doi: 10.1021/acsami.6b08315.

[156] H. Wang *et al.*, “Excitation wavelength independent visible color emission of carbon dots,” pp. 1909–1915, 2017, doi: 10.1039/c6nr09200d.

[157] H. Yang *et al.*, “Carbon dots synthesized by hydrothermal process via sodium citrate and NH4HCO3 for sensitive detection of temperature and sunset yellow,” *J. Colloid Interface Sci.*, vol. 516, pp. 192–201, 2018, doi: 10.1016/j.jcis.2018.01.054.

[158] Y. Ding *et al.*, “Facile preparation of bright orange fluorescent carbon dots and the constructed biosensing platform for the detection of pH in living cells,” *Talanta*, 2018, doi: 10.1016/j.talanta.2018.06.060.

[159] H. Zhang *et al.*, “Solid-phase synthesis of highly fluorescent nitrogen-doped carbon dots for sensitive and selective probing ferric ions in living cells,” *Anal. Chem.*, vol. 86, no. 19, pp. 9846–9852, 2014, doi: 10.1021/ac502446m.

[160] R. Fan, Q. Sun, L. Zhang, Y. Zhang, and A. Lu, “Photoluminescent carbon dots directly derived from polyethylene glycol and their application for cellular imaging,” *Carbon N. Y.*, vol. 71, pp. 87–93, 2014, doi: 10.1016/j.carbon.2014.01.016.

[161] S. Li, A. Pasc, V. Fierro, and A. Celzard, “Hollow carbon spheres, synthesis and applications-a review,” *J. Mater. Chem. A*, vol. 4, no. 33, pp. 12686–12713, 2016, doi: 10.1039/c6ta03802f.

[162] H. Kristianto, C. D. Putra, A. A. Arie, M. Halim, and J. K. Lee, “Synthesis and Characterization of Carbon Nanospheres Using Cooking Palm Oil as Natural Precursors onto Activated Carbon Support,” *Procedia Chem.*, vol. 16, pp. 328–333, 2015, doi:

10.1016/j.proche.2015.12.060.

[163] J. Zhang, *PEM fuel cell electrocatalysts and catalyst layers: Fundamentals and applications*. 2008.

[164] Z. Wang *et al.*, "Synthesis of strongly green-photoluminescent graphene quantum dots for drug carrier," *Colloids Surfaces B Biointerfaces*, vol. 112, pp. 192–196, 2013, doi: 10.1016/j.colsurfb.2013.07.025.

[165] J. Shen, Y. Zhu, X. Yang, J. Zong, and J. Zhang, "One-pot hydrothermal synthesis of graphene quantum dots surface-passivated by polyethylene glycol and their photoelectric conversion under near-infrared light," *New J. Chem.*, vol. 36, no. 1, pp. 97–101, 2012, doi: 10.1039/c1nj20658c.

[166] L. Yang *et al.*, "One pot synthesis of highly luminescent polyethylene glycol anchored carbon dots functionalized with a nuclear localization signal peptide for cell nucleus imaging," *Nanoscale*, vol. 7, no. 14, pp. 6104–6113, 2015, doi: 10.1039/c5nr01080b.

[167] M. Chen, W. Wang, and X. Wu, "One-pot green synthesis of water-soluble carbon nanodots with multicolor photoluminescence from polyethylene glycol," *J. Mater. Chem. B*, vol. 2, no. 25, pp. 3937–3945, 2014, doi: 10.1039/c4tb00292j.

[168] B. X. Zhang, G. Y. Zhang, H. Gao, S. H. Wu, J. H. Chen, and X. L. Li, "One-step hydrothermal synthesis and optical properties of PEG-passivated nitrogen-doped carbon dots," *RSC Adv.*, vol. 5, no. 10, pp. 7395–7400, 2015, doi: 10.1039/c4ra08869g.

[169] Y. Xu *et al.*, "Nitrogen-doped carbon dots: A facile and general preparation method, photoluminescence investigation, and imaging applications," *Chem. - A Eur. J.*, vol. 19, no. 7, pp. 2276–2283, 2013, doi: 10.1002/chem.201203641.

[170] S. Chandra, S. H. Pathan, S. Mitra, B. H. Modha, A. Goswami, and P. Pramanik, "Tuning of photoluminescence on different surface functionalized carbon quantum dots," *RSC Adv.*, vol. 2, no. 9, pp. 3602–3606, 2012, doi: 10.1039/c2ra00030j.

[171] V. Strauss *et al.*, "Carbon nanodots: Toward a comprehensive understanding of their photoluminescence," *J. Am. Chem. Soc.*, vol. 136, no. 49, pp. 17308–17316, Dec. 2014, doi: 10.1021/ja510183c.

[172] C. W. Lai, Y. H. Hsiao, Y. K. Peng, and P. T. Chou, "Facile synthesis of highly emissive

carbon dots from pyrolysis of glycerol; Gram scale production of carbon dots/mSiO 2 for cell imaging and drug release," *J. Mater. Chem.*, vol. 22, no. 29, pp. 14403–14409, Aug. 2012, doi: 10.1039/c2jm32206d.

[173] A. Amer Ridha, P. Pakravan, A. Hemati Azandaryani, and H. Zhaleh, "Carbon dots; the smallest photoresponsive structure of carbon in advanced drug targeting," *Journal of Drug Delivery Science and Technology*, vol. 55. Editions de Sante, Feb. 01, 2020, doi: 10.1016/j.jddst.2019.101408.

[174] S. Liu *et al.*, "Hydrothermal treatment of grass: A low-cost, green route to nitrogen-doped, carbon-rich, photoluminescent polymer nanodots as an effective fluorescent sensing platform for label-free detection of Cu(II) ions," *Adv. Mater.*, vol. 24, no. 15, pp. 2037–2041, Apr. 2012, doi: 10.1002/adma.201200164.

[175] Y. Z. Yang, N. Xiao, S. G. Liu, L. Han, N. B. Li, and H. Q. Luo, "pH-induced aggregation of hydrophilic carbon dots for fluorescence detection of acidic amino acid and intracellular pH imaging," *Mater. Sci. Eng. C*, vol. 108, Mar. 2020, doi: 10.1016/j.msec.2019.110401.

[176] J. C. G. E. da S. Helena M.R. Gonçalves, "Fluorescent Carbon Dots Capped with PEG200 and Mercaptosuccinic Acid," *Springer*, vol. 20, pp. 1023–1028, 2010, Accessed: Dec. 10, 2019. [Online]. Available: https://link.springer.com/article/10.1007/s10895-010-0652-y.

[177] G. Hong *et al.*, "In vivo fluorescence imaging with Ag2S quantum dots in the second near-infrared region," *Angew. Chemie - Int. Ed.*, vol. 51, no. 39, pp. 9818–9821, Sep. 2012, doi: 10.1002/anie.201206059.

[178] J. Fan, M. Claudel, C. Ronzani, Y. Arezki, L. Lebeau, and F. Pons, "Physicochemical characteristics that affect carbon dot safety: Lessons from a comprehensive study on a nanoparticle library," *Int. J. Pharm.*, vol. 569, Oct. 2019, doi: 10.1016/j.ijpharm.2019.118521.

[179] H. Gonçalves and J. C. G. E. Da Silva, "Fluorescent carbon dots capped with PEG 200 and mercaptosuccinic acid," *J. Fluoresc.*, vol. 20, no. 5, pp. 1023–1028, Sep. 2010, doi: 10.1007/s10895-010-0652-y.

[180] J. Charmi, H. Nosrati, J. Mostafavi Amjad, R. Mohammadkhani, and H. Danafar,

"Polyethylene glycol (PEG) decorated graphene oxide nanosheets for controlled release curcumin delivery," *Heliyon*, vol. 5, no. 4, p. e01466, 2019, doi: 10.1016/j.heliyon.2019.e01466.

[181] H. Wang *et al.*, "Biocompatible PEG-Chitosan@Carbon Dots Hybrid Nanogels for Two-Photon Fluorescence Imaging, Near-Infrared Light/pH Dual-Responsive Drug Carrier, and Synergistic Therapy," *Adv. Funct. Mater.*, vol. 25, no. 34, pp. 5537–5547, 2015, doi: 10.1002/adfm.201501524.

[182] P. Sachdev, A., Matai, I., Kumar, S.U., Bhushan, B., Dubey, P. and Gopinath, "A novel one-step synthesis of PEG passivated multicolour fluorescent carbon dots for potential biolabeling application," *Rsc Adv.*, vol. 38, no. 3, pp. 16958–16961, 2013, doi: 10.1039/C3RA42415D.

[183] H. S. Toh, K. Jurkschat, and R. G. Compton, "The Influence of the Capping Agent on the Oxidation of Silver Nanoparticles : Nano-impacts versus Stripping Voltammetry," pp. 1–8, 2015, doi: 10.1002/chem.201406278.

[184] D. Bartczak and A. G. Kanaras, "Diacetylene-Containing Ligand As a New Capping Agent for the Preparation of Water-Soluble Colloidal Nanoparticles of Remarkable Stability," vol. 26, no. 27, pp. 7072–7077, 2016, doi: 10.1021/la9044013.

[185] J. Shen, Y. Zhu, X. Yang, J. Zong, J. Zhang, and C. Li, "One-pot hydrothermal synthesis of graphene quantum dots surface-passivated by polyethylene glycol and their photoelectric conversion under near-infrared light," *New J. Chem.*, vol. 36, no. 1, pp. 97–101, 2012, doi: 10.1039/c1nj20658c.

[186] X. Li, H. Wang, Y. Shimizu, A. Pyatenko, K. Kawaguchi, and N. Koshizaki, "Preparation of carbon quantum dots with tunable photoluminescence by rapid laser passivation in ordinary organic solvents," *Chem. Commun.*, pp. 932–934, 2011, doi: 10.1039/c0cc03552a.

[187] C. Liu *et al.*, "Nano-carrier for gene delivery and bioimaging based on carbon dots with PEI-passivation enhanced fluorescence," *Biomaterials*, vol. 33, no. 13, pp. 3604–3613, May 2012, doi: 10.1016/j.biomaterials.2012.01.052.

[188] L. Wu *et al.*, "Surface passivation of carbon nanoparticles with branched macromolecules influences near infrared bioimaging," *Theranostics*, vol. 3, no. 9, pp.

677–686, 2013, doi: 10.7150/thno.6535.

[189] S. Sahu, B. Behera, T. K. Maiti, and S. Mohapatra, “Simple one-step synthesis of highly luminescent carbon dots from orange juice: Application as excellent bio-imaging agents,” *Chem. Commun.*, vol. 48, no. 70, pp. 8835–8837, Sep. 2012, doi: 10.1039/c2cc33796g.

[190] Z. Ma, H. Ming, H. Huang, Y. Liu, and Z. Kang, “One-step ultrasonic synthesis of fluorescent N-doped carbon dots from glucose and their visible-light sensitive photocatalytic ability,” *New J. Chem.*, vol. 36, no. 4, pp. 861–864, Apr. 2012, doi: 10.1039/c2nj20942j.

[191] Z. Zhang, J. Hao, J. Zhang, B. Zhang, and J. Tang, “Protein as the source for synthesizing fluorescent carbon dots by a one-pot hydrothermal route,” *RSC Adv.*, vol. 2, no. 23, pp. 8599–8601, 2012, doi: 10.1039/c2ra21217j.

[192] H. A. Gasteiger, S. S. Kocha, B. Sompalli, and F. T. Wagner, “Activity benchmarks and requirements for Pt, Pt-alloy, and non-Pt oxygen reduction catalysts for PEMFCs,” *Appl. Catal. B Environ.*, vol. 56, no. 1–2, pp. 9–35, Mar. 2005, doi: 10.1016/j.apcatb.2004.06.021.

[193] M. K. Debe, “Electrocatalyst approaches and challenges for automotive fuel cells,” *Nature*, vol. 486, no. 7401, pp. 43–51, 2012, doi: 10.1038/nature11115.

[194] H. Yano, M. Kataoka, H. Yamashita, H. Uchida, and M. Watanabe, “Oxygen Reduction Activity of Carbon-Supported Pt−M (M = V, Ni, Cr, Co, and Fe) Alloys Prepared by Nanocapsule Method,” *Langmuir*, vol. 23, no. 11, pp. 6438–6445, May 2007, doi: 10.1021/la070078u.

[195] U. A. Paulus *et al.*, “Oxygen Reduction on Carbon-Supported Pt−Ni and Pt−Co Alloy Catalysts,” *J. Phys. Chem. B*, vol. 106, no. 16, pp. 4181–4191, Apr. 2002, doi: 10.1021/jp013442l.

[196] L. Wang and H. S. Zhou, “Green synthesis of luminescent nitrogen-doped carbon dots from milk and its imaging application,” *Anal. Chem.*, vol. 86, no. 18, pp. 8902–8905, 2014, doi: 10.1021/ac502646x.

[197] X. Zhai *et al.*, “Highly luminescent carbon nanodots by microwave-assisted pyrolysis,”

Chem. Commun., vol. 48, no. 64, pp. 7955–7957, Aug. 2012, doi: 10.1039/c2cc33869f.

[198] L. Hu *et al.*, "Multifunctional carbon dots with high quantum yield for imaging and gene delivery," *Carbon N. Y.*, vol. 67, pp. 508–513, 2014, doi: 10.1016/j.carbon.2013.10.023.

[199] Y. Dong *et al.*, "Polyamine-functionalized carbon quantum dots for chemical sensing," *Carbon N. Y.*, vol. 50, no. 8, pp. 2810–2815, Jul. 2012, doi: 10.1016/j.carbon.2012.02.046.

[200] Y. Dong, H. Pang, H. Yang, … C. G.-A. C., and undefined 2013, "Carbon-based dots co-doped with nitrogen and sulfur for high quantum yield and excitation-independent emission," *Wiley Online Libr.*, Accessed: Dec. 10, 2019. [Online]. Available: https://onlinelibrary.wiley.com/doi/abs/10.1002/anie.201301114.

[201] Z. X. Liu, Z. L. Wu, M. X. Gao, H. Liu, and C. Z. Huang, "Carbon dots with aggregation induced emission enhancement for visual permittivity detection," *Chem. Commun.*, vol. 52, no. 10, pp. 2063–2066, 2016, doi: 10.1039/c5cc08635c.

[202] G. A. Mabbott, "An introduction to cyclic voltammetry," *J. Chem. Educ.*, vol. 60, no. 9, pp. 697–702, 1983, doi: 10.1021/ed060p697.

[203] S. S. Kocha *et al.*, "Best Practices and Testing Protocols for Benchmarking ORR Activities of Fuel Cell Electrocatalysts Using Rotating Disk Electrode," *Electrocatalysis*, vol. 8, no. 4, pp. 366–374, 2017, doi: 10.1007/s12678-017-0378-6.

[204] A. T. Manual, G. Guide, and T. Mode, "Operation Guide 3416 Operation Guide 3416," pp. 8–10, 2000.

[205] S. Zhang *et al.*, "A review of accelerated stress tests of MEA durability in PEM fuel cells," *Int. J. Hydrogen Energy*, vol. 34, no. 1, pp. 388–404, 2009, doi: 10.1016/j.ijhydene.2008.10.012.

[206] J. F. Wager, "Real- and reciprocal-space attributes of band tail states," *AIP Adv.*, vol. 7, no. 12, 2017, doi: 10.1063/1.5008521.

[207] D. Zhao *et al.*, "Synthesis of multicolor carbon dots based on solvent control and its application in the detection of crystal violet," *Nanomaterials*, vol. 9, no. 11, 2019, doi: 10.3390/nano9111556.

[208] H. Ding, J. S. Wei, P. Zhang, Z. Y. Zhou, Q. Y. Gao, and H. M. Xiong, “Solvent-Controlled Synthesis of Highly Luminescent Carbon Dots with a Wide Color Gamut and Narrowed Emission Peak Widths,” *Small*, vol. 14, no. 22, pp. 1–10, 2018, doi: 10.1002/smll.201800612.

[209] MERCK, “Properties of Solvents Chart,” *Sigma Aldrich*. https://www.sigmaaldrich.com/chemistry/stockroom-reagents/learning-center/technical-library/solvent-properties.html (accessed Feb. 11, 2020).

[210] B. Ratner, “The correlation coefficient: Its values range between 1/1, or do they,” *J. Targeting, Meas. Anal. Mark.*, vol. 17, no. 2, pp. 139–142, 2009, doi: 10.1057/jt.2009.5.

[211] L. Chen *et al.*, “Carbon dots prepared in different solvents with controllable structures: Optical properties, cellular imaging and photocatalysis,” *New J. Chem.*, vol. 42, no. 3, pp. 1690–1697, 2018, doi: 10.1039/c7nj03621c.

[212] F. Yan, Z. Sun, H. Zhang, X. Sun, Y. Jiang, and Z. Bai, “The fluorescence mechanism of carbon dots, and methods for tuning their emission color: a review,” *Microchim. Acta*, vol. 186, no. 8, 2019, doi: 10.1007/s00604-019-3688-y.

[213] D. Chao *et al.*, “Solvent-dependent carbon dots and their applications in the detection of water in organic solvents,” *J. Mater. Chem. C*, vol. 6, no. 28, pp. 7527–7532, 2018, doi: 10.1039/c8tc02184h.

[214] W. J. Khudhayer, N. N. Kariuki, X. Wang, D. J. Myers, A. U. Shaikh, and T. Karabacak, “Oxygen Reduction Reaction Electrocatalytic Activity of Glancing Angle Deposited Platinum Nanorod Arrays,” *J. Electrochem. Soc.*, vol. 158, no. 8, p. B1029, 2011, doi: 10.1149/1.3599901.

[215] U. A. Paulus, T. J. Schmidt, H. A. Gasteiger, and R. J. Behm, “Oxygen reduction on a high-surface area Pt/Vulcan carbon catalyst: A thin-film rotating ring-disk electrode study,” *J. Electroanal. Chem.*, vol. 495, no. 2, pp. 134–145, 2001, doi: 10.1016/S0022-0728(00)00407-1.

[216] K. A. Mauritz, C. J. Hora, and A. J. Hopfinger, “Theoretical Model for the Structures of Ionomers: Application To Nafion Materials.,” *Am. Chem. Soc. Polym. Prepr. Div. Polym. Chem.*, vol. 19, no. 2, pp. 324–329, 1978, doi: 10.1021/ba-1980-0187.ch008.

[217] K. J. Nagarajan, A. N. Balaji, S. T. Kasi Rajan, and N. R. Ramanujam, “Preparation of bio-eco based cellulose nanomaterials from used disposal paper cups through citric acid hydrolysis,” *Carbohydr. Polym.*, vol. 235, no. December 2019, p. 115997, 2020, doi: 10.1016/j.carbpol.2020.115997.

[218] E. Olsson, C. Menzel, C. Johansson, R. Andersson, K. Koch, and L. Järnström, “The effect of pH on hydrolysis, cross-linking and barrier properties of starch barriers containing citric acid,” *Carbohydr. Polym.*, vol. 98, no. 2, pp. 1505–1513, 2013, doi: 10.1016/j.carbpol.2013.07.040.

[219] A. Surendra Babu, R. Parimalavalli, and S. G. Rudra, “Effect of citric acid concentration and hydrolysis time on physicochemical properties of sweet potato starches,” *Int. J. Biol. Macromol.*, vol. 80, pp. 557–565, 2015, doi: 10.1016/j.ijbiomac.2015.07.020.

[220] W. Lu *et al.*, “Economical, Green Synthesis of Fluorescent Carbon Nanoparticles and Their Use as Probes for Sensitive and Selective Detection of Mercury(II) Ions,” no. Ii, 2012.

[221] G. Beaune *et al.*, “Luminescence of polyethylene glycol coated CdSeTe/ZnS and InP/ZnS nanoparticles in the presence of copper cations,” *ChemPhysChem*, vol. 12, no. 12, pp. 2247–2254, 2011, doi: 10.1002/cphc.201100266.

[222] K. Patir and S. K. Gogoi, “Nitrogen-doped carbon dots as fluorescence ON-OFF-ON sensor for parallel detection of copper(ii) and mercury(ii) ions in solutions as well as in filter paper-based microfluidic device,” *Nanoscale Adv.*, vol. 1, no. 2, pp. 592–601, 2019, doi: 10.1039/c8na00080h.

[223] V. Christina M. Gonzalez, Muhammad Iqbal, Mita Dasog, Davin Piercey Ross Lockwood, Thomas M. Klapötke, Jonathan G. C, “Detection of High-Energy Compounds Using Photoluminescent Silicon Nanocrystal Based Paper Sensors,” *Nanoscale*, vol. 3, pp. 10715–10722, 2015, doi: 10.1039/b000000x.

[224] H. Wang, S. I. Vagin, B. Rieger, and A. Meldrum, “An Ultrasensitive Fluorescent Paper-Based CO2 Sensor,” *ACS Appl. Mater. Interfaces*, vol. 12, no. 18, pp. 20507–20513, 2020, doi: 10.1021/acsami.0c03405.

[225] A. M. López-Marzo and A. Merkoçi, “Paper-based sensors and assays: A success of the engineering design and the convergence of knowledge areas,” *Lab Chip*, vol. 16, no. 17,

pp. 3150–3176, 2016, doi: 10.1039/c6lc00737f.

[226] C. Sicard *et al.*, “Tools for water quality monitoring and mapping using paper-based sensors and cell phones,” *Water Res.*, vol. 70, pp. 360–369, 2015, doi: 10.1016/j.watres.2014.12.005.

Appendix: Supplementary Information

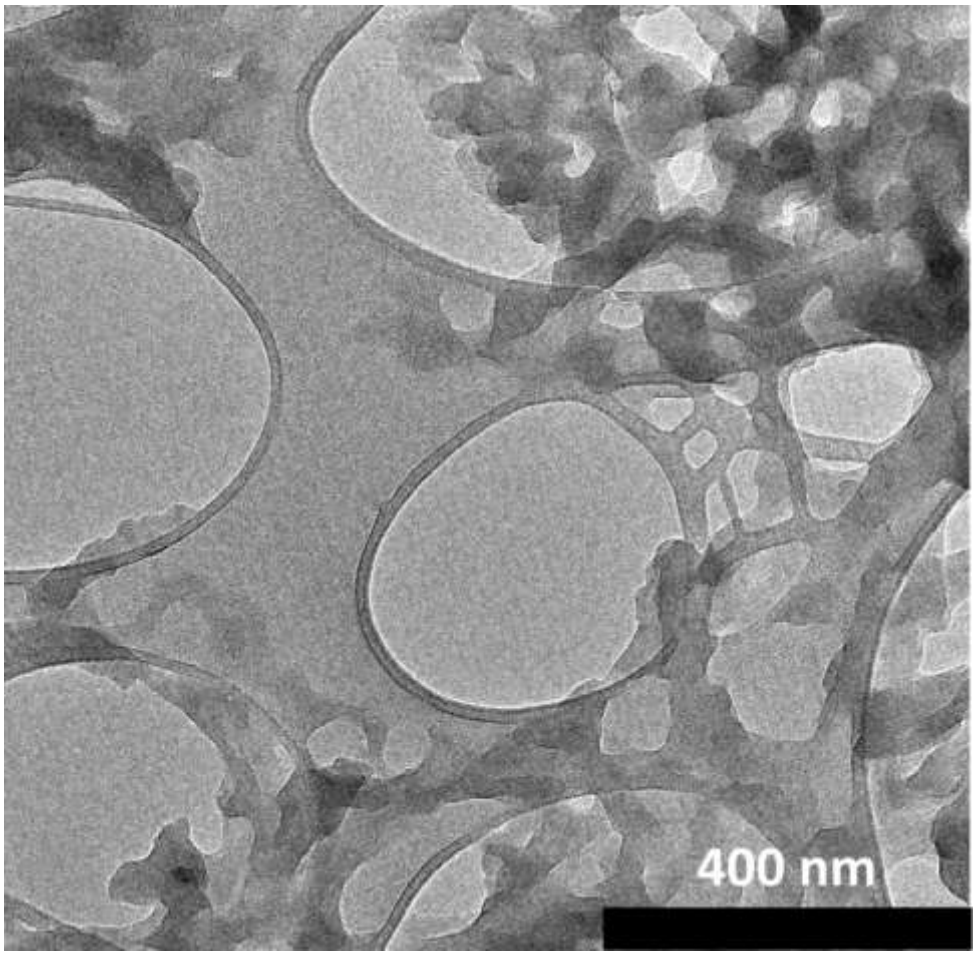

Figure S 1: TEM image of the reflux and chitosan synthesised sample that was not reproducible

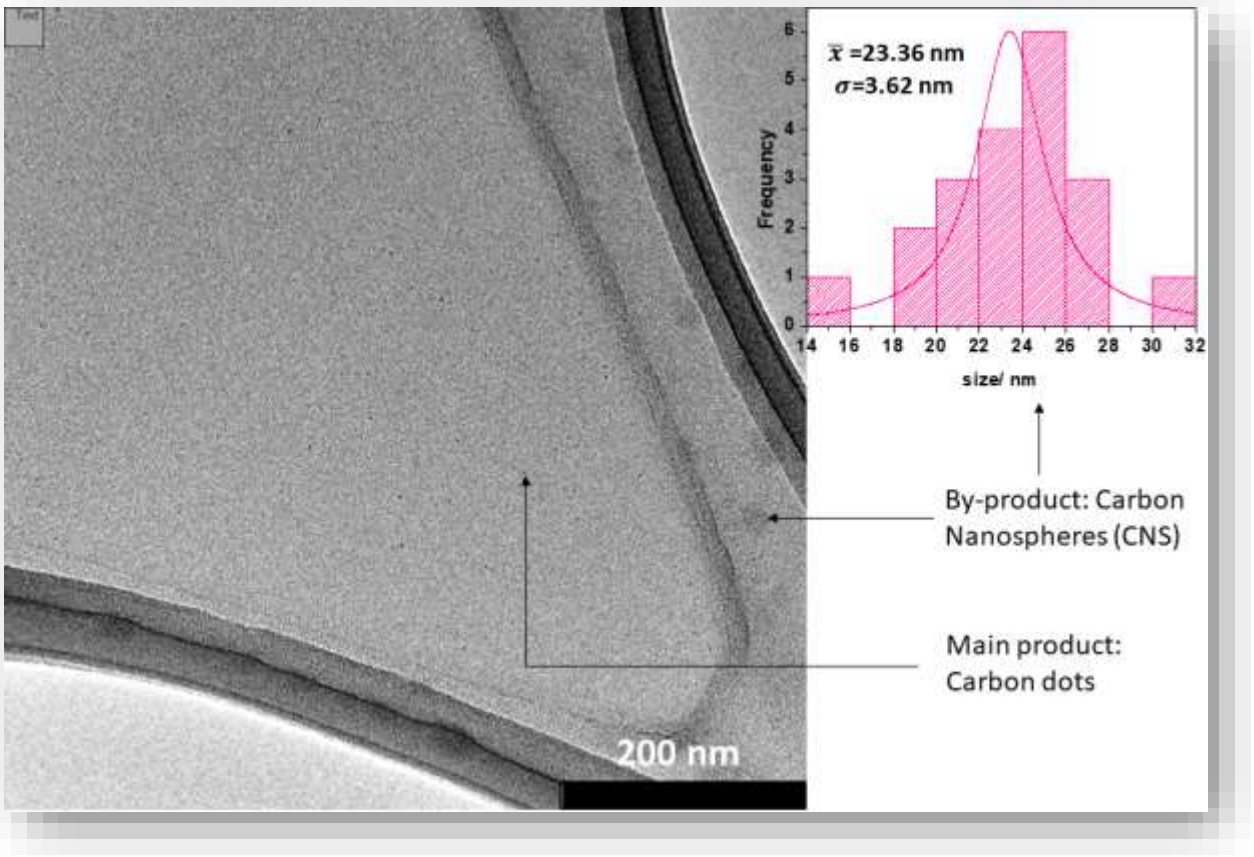

Figure S 2: TEM image of CDs sample with CNS expressed as by-product. CDs have particle sizes of 1-10nm, while the expressed CNS are relatively bigger at 20 – 40 nm

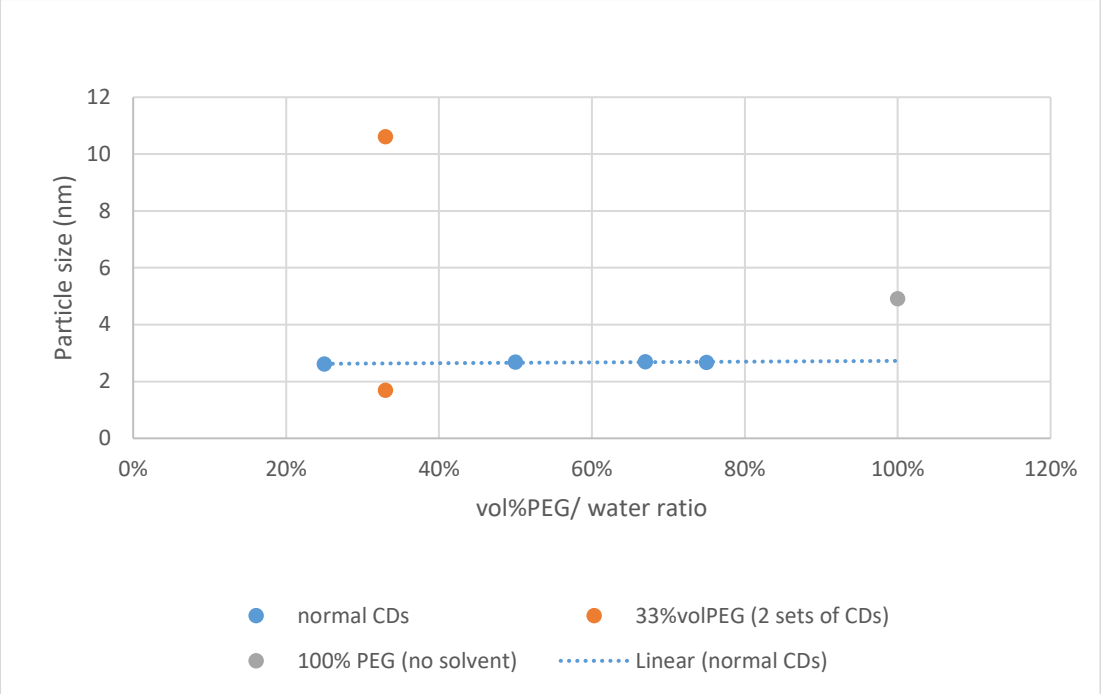

Figure S 3: The vol% of the PEG precursor to water (solvent) ratio versus the particle size of the resulting CDs

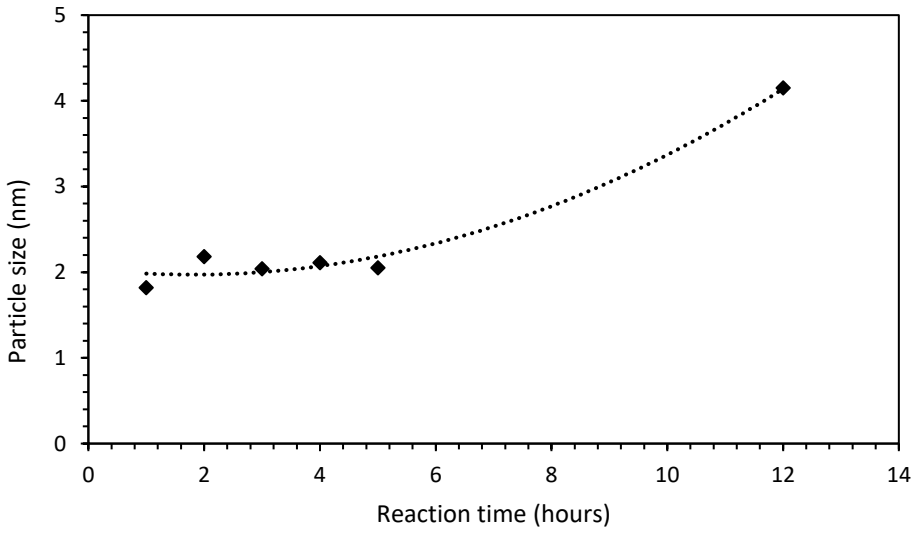

Figure S 4: Particle size of CDs synthesised after various reaction times

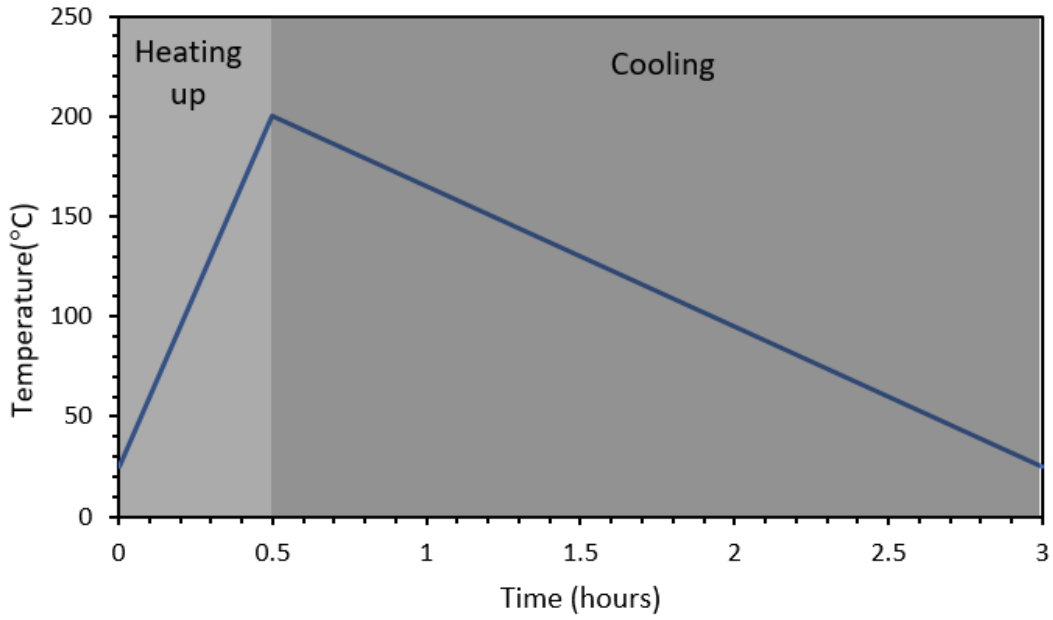

Figure S 5: The course of the 'ramp-only' reaction

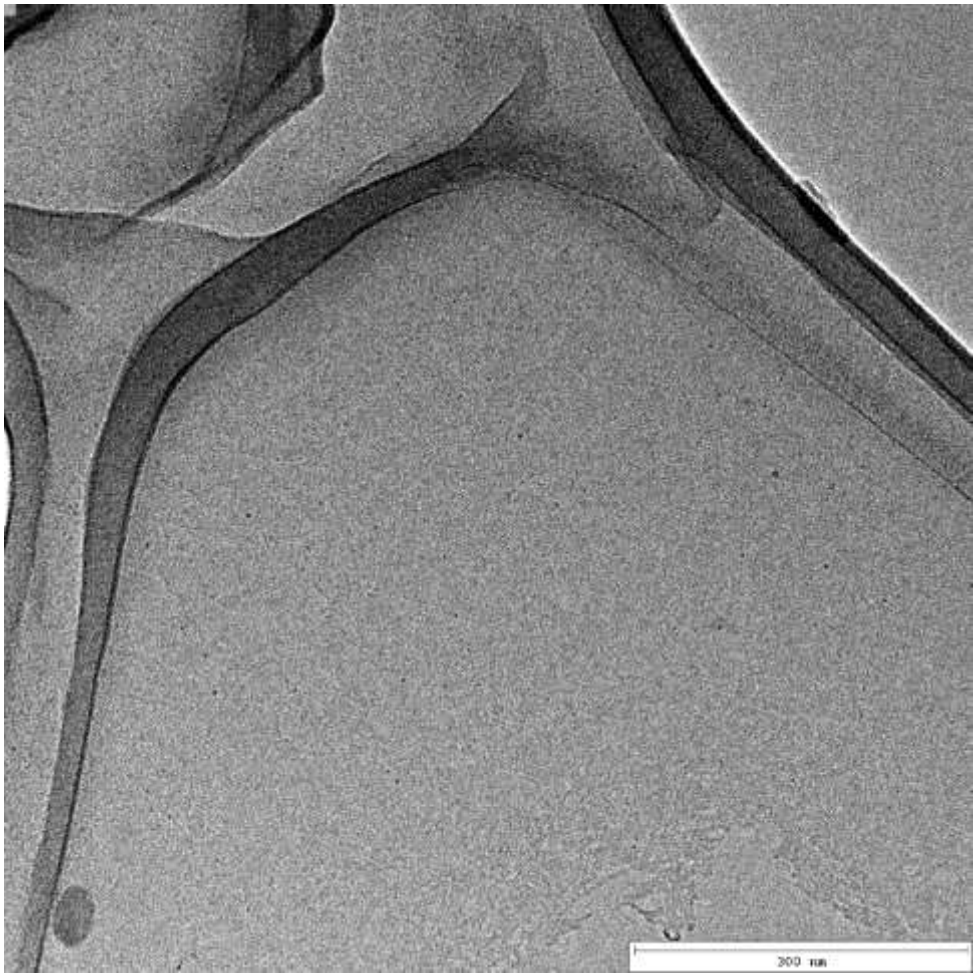

Figure S 6: TEM image of CDs sample synthesised with ramping only

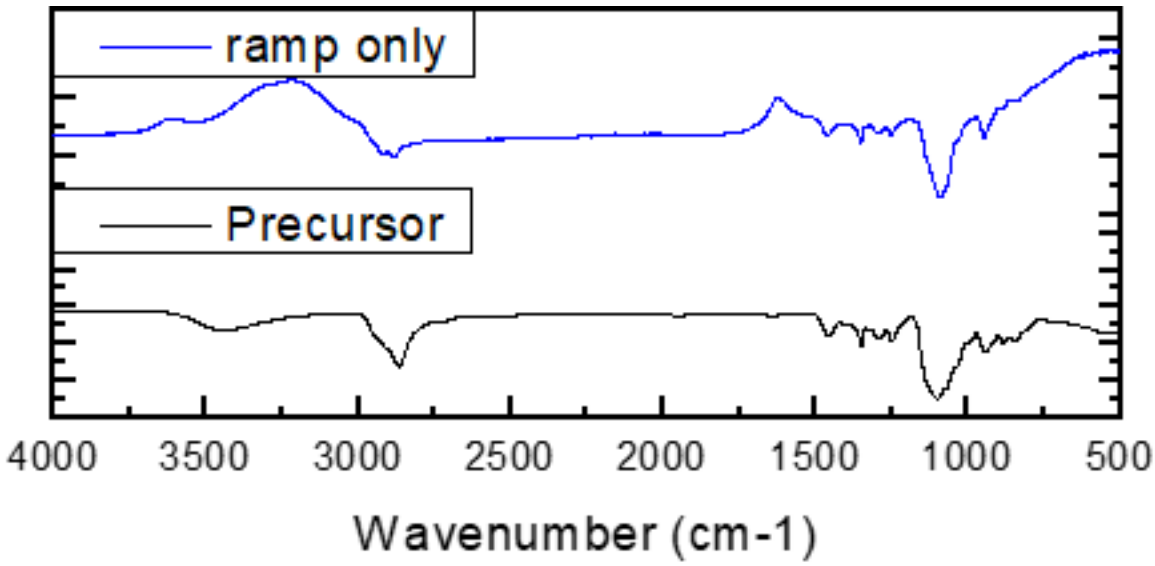

Figure S 7: FTIR spectra the PEG precursor and the CDs sample synthesised after ramping only

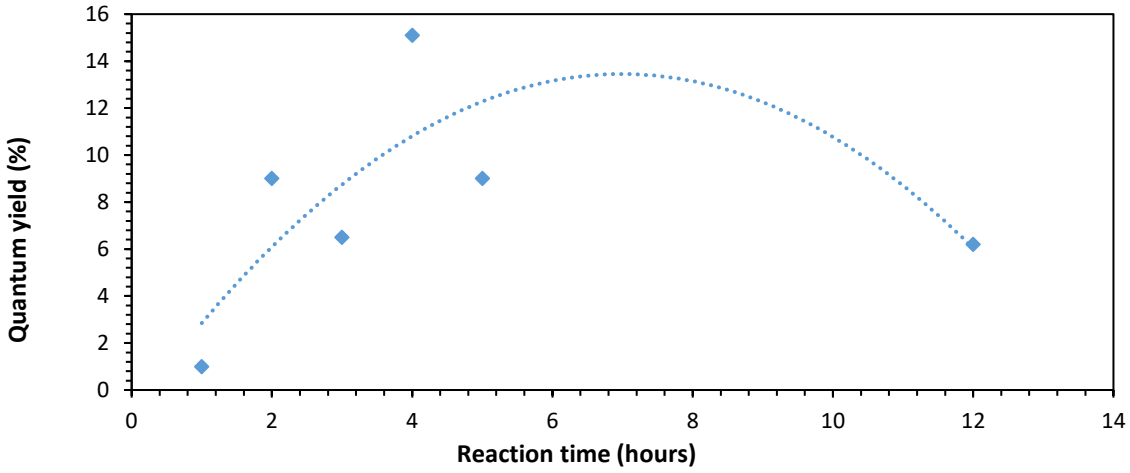

Figure S 8: The quantum yield of CDs synthesised after reaction times with a trend line

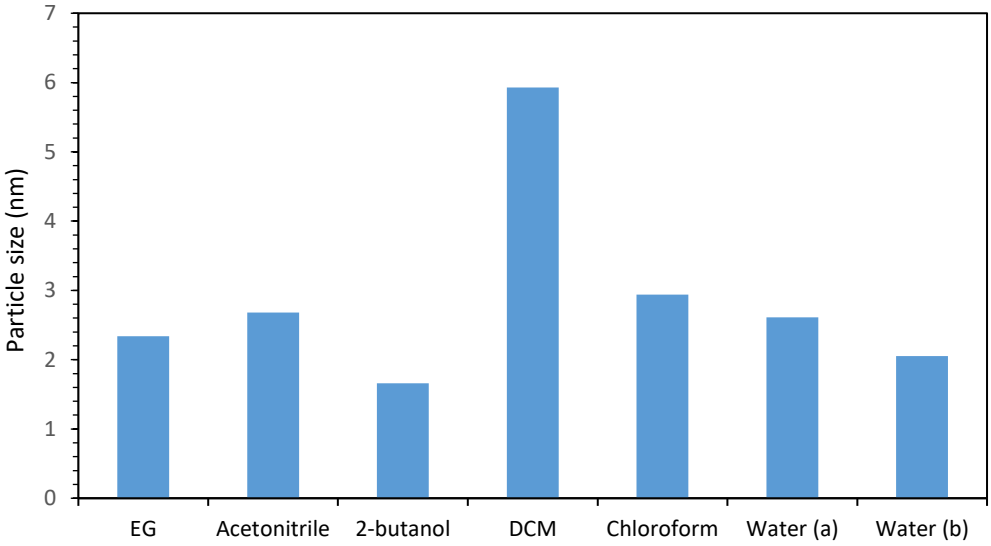

Figure S 9: The particle size of the CDs against solvent used during synthesis

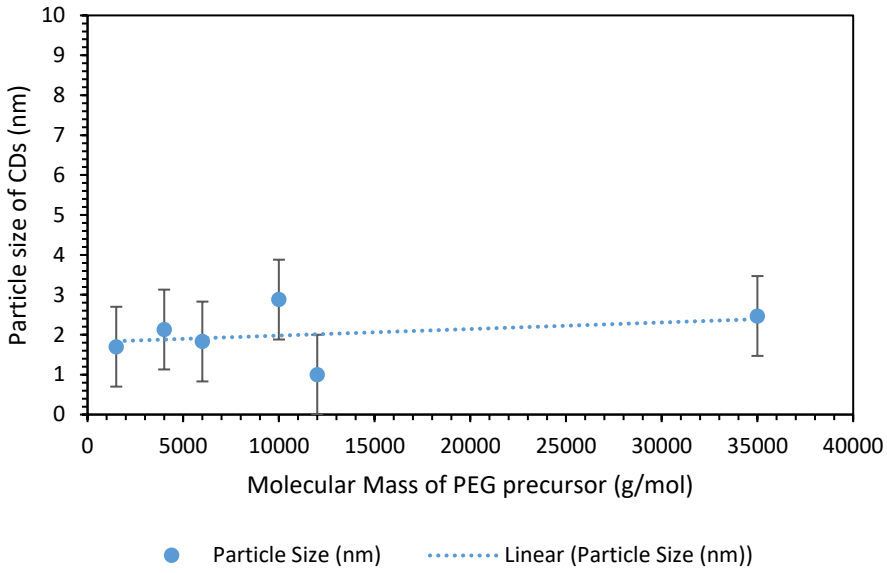

Figure S 10: The molecular mass of the PEG precursor versus the particle size of the resulting CDs

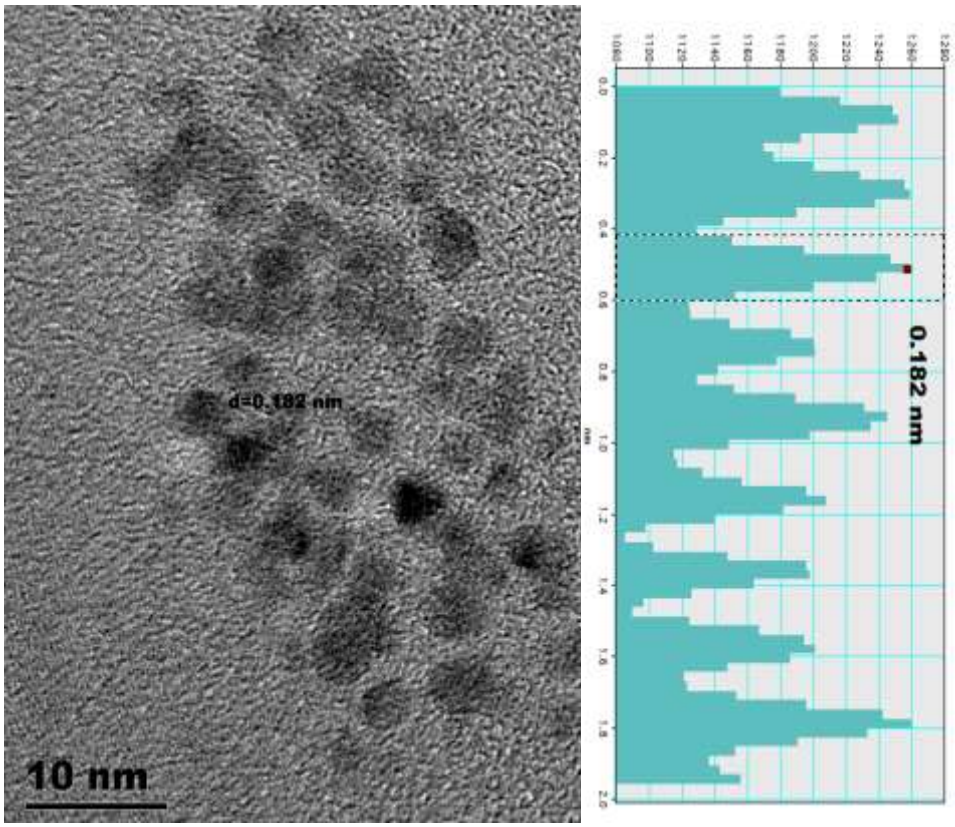

Figure S 11: high magnification HR-TEM image of CDs synthesised from PEG12000 and corresponding d-spacing plot